Experimental and modeling studies of catalytic hydrogenation for conversion of carbon dioxide and hydrogen storage

by

Bagwan Farahanaz Mahammad Rafiq

(20EE20A26017)

A thesis submitted to the

Academy of Scientific & Innovative Research

for the award of the degree of

DOCTOR OF PHILOSOPHY

in

Engineering

Under the supervision of

Dr. Satyam Naidu Vasireddy

CSIR- National Chemical Laboratory, Pune

Academy of Scientific and Innovative Research

AcSIR Headquarters, CSIR-HRDC campus

Sector 19, Kamla Nehru Nagar,

Ghaziabad, U.P. – 201 002, India

January 2025

Certificate

This is to certify that the work incorporated in this Ph.D. thesis entitled, "**Experimental and modeling studies of catalytic hydrogenation for conversion of carbon dioxide and hydrogen storage**" submitted by **Bagwan Farahanaz Mahammad Rafiq** to the Academy of Scientific and Innovative Research (AcSIR) in fulfillment of the requirements for the award of the Degree of **Doctor of Philosophy in Engineering**, embodies original research work carried-out by the student. We, further certify that this work has not been submitted to any other University or Institution in part or full for the award of any degree or diploma. Research material(s) obtained from other source(s) and used in this research work has/have been duly acknowledged in the thesis. Image(s), illustration(s), figure(s), table(s), etc. used in the thesis from other source(s), have also been duly cited and acknowledged.

(Signature of Student)

Bagwan Farahanaz Mahammad Rafiq

Date: 06-01-2025

(Signature of Supervisor)

Dr. Satyam Naidu Vasireddy

Date: 06-01-2025

STATEMENTS OF ACADEMIC INTEGRITY

I, **Bagwan Farahanaz Mahammad Rafiq,** a Ph.D. student of the Academy of Scientific and Innovative Research (AcSIR) with Registration No. **20EE20A26017** hereby undertake that, the thesis entitled "**Experimental and modeling studies of catalytic hydrogenation for conversion of carbon dioxide and hydrogen storage**" has been prepared by me and that the document reports original work carried out by me and is free of any plagiarism in compliance with the UGC Regulations on *"Promotion of Academic Integrity and Prevention of Plagiarism in Higher Educational Institutions (2018)"* and the CSIR Guidelines for "*Ethics in Research and in Governance (2020)".*

Signature of the Student
Date : 06-01-2025
Place : Pune

It is hereby certified that the work done by the student, under my/our supervision, is plagiarism-free in accordance with the UGC Regulations on *"Promotion of Academic Integrity and Prevention of Plagiarism in Higher Educational Institutions (2018)"* and the CSIR Guidelines for "*Ethics in Research and in Governance (2020)".*

NA
Signature of the Co-supervisor
Name :
Date :
Place :

Signature of the Supervisor
Name : Dr. Satyam Naidu Vasireddy
Date : 06-01-2025
Place : Pune

Acknowledgement

Writing this acknowledgment is quite overwhelming as I am grateful to many individuals whose support, guidance, and encouragement have been invaluable to this thesis and there are very few words that can sum up the tremendous contribution they have made to this thesis. First and foremost, I thank God for blessing me with a good life, the strength to persevere, and the ability to succeed in this endeavour. Without this divine support, none of this would have been possible.

The journey of obtaining a doctorate and composing a dissertation is undeniably lengthy and challenging, and it is not undertaken alone. Therefore, I take this moment to extend my heartfelt gratitude to numerous people including my teachers, family members, friends, well-wishers, and colleagues who provided assistance and support throughout the journey of my research and during my testing time. I consider myself ultimately fortunate to have got guidance from many experienced persons during my Ph.D.

First and foremost, I wish to express my heartfelt and sincere gratitude to my research supervisor, **Dr. Satyam Naidu Vasireddy** for granting me the opportunity to pursue my Ph.D. research under his mentorship. His motivation, inspiration, encouragement, and persistent guidance have helped me to make my dreams to reality. I am grateful to him for his valuable advice, and continuous support in terms of fellowship provided during every stage of my research work. I am also thankful to his family for the warm welcome offered to me on the auspicious occasion of “Ganesh Utsav” with Prasad and at the arrival of sweet baby girl.

I am profoundly grateful to **Dr. Amol A. Kulkarni**, whose unwavering support made it possible for me to complete this journey. From day one of my Ph.D., he has been a pillar of support in many ways, starting with something as fundamental as providing a workspace. I consider myself incredibly fortunate to have benefited from his invaluable guidance, technical insights, fellowship, moral support, and encouragement. The saying, 'The toughest times forge the strongest individuals,' resonates deeply with my experience.

I remain profoundly thankful to him and my supervisor for placing their trust in me, recognizing my potential, and guiding me through the most challenging phases of my Ph.D. Their belief in me has been a cornerstone of my growth, and There will forever be a share for both of them in the credit for whatever I achieve in my professional life.

I am extremely thankful to Dr Anil A Kinage for his mentorship, resources and funding at every stage of second part of the work. I would like to express my deepest gratitude to Dr. Anil A.

Acknowledgement

Kinage for his invaluable mentorship, unwavering support, and guidance. His provision of essential resources and financial assistance played a pivotal role in the successful completion of this study, and his encouragement and insights greatly enriched my learning experience.

I am also grateful to the members of Doctoral Advisory Committee (DAC) members, Dr. K. Shanmugnathan, Dr. Amol A Kulkarni, and Dr. Nandini Devi for their sincere comments, suggestions, and constant support.

I extend my heartfelt gratitude to **Dr. Nandini Devi** for providing the experimental facilities that were instrumental in my research work. Her unwavering support, guidance, and encouragement have been truly inspiring throughout my journey. I sincerely thank Dr. Nilesh Mali for providing access to the Aspen facility, which was crucial for my research work. I thank to Mr Anil Palghadmal sir for his constant support and motivation. I am deeply grateful to Dr. Pradip Maity for providing the fellowship that supported my research journey. I thank all my teachers at NCL Dr. Ashish Orpe, Dr. Ram Rup Sarkar, Dr. Nilesh Mali, who once again exposed me to the wonderful subjects of Chemical Engineering. I take this opportunity to thank laboratory members including Dr Kinage Sir's lab members for helping me out in my chemistry . I am grateful to Dr. Ashwini Kumar Nangia and Dr. Ashish Lele, Directors, CSIR-NCL, Pune for allowing me to carry out my research work in India's most prestigious, well-equipped and biggest chemical laboratory. I am grateful for project fellowship provided by DST and CSIR. I am also thankful to the AcSIR coordination office, Student Academic office, PP-I workshop, and the various sections of NCL establishment for their continued support. I am thankful to Mr Mandlik and Mr Mule from CEPD workshop for their immediate technical support when needed. I am thankful to Dr. Sanjay Borikar and Nikita for providing me GC and GCMS facility for my work.

I would like to take this opportunity to express my deep sense of gratitude to my friends cum family for being there in the ups and downs and believing in me while showing me the positive side, thanks to Arshad, Tabrez, Aswini, Bhageyshri, Ashwini, Dr. Shailja, Dr. Vipin, Dr. Tanuja, Dr. Jyoti, Subramaniam, Vishnu, Aviraj, Arunima, Omkar constantly encouraging me to work towards the goal. I am glad to have made wonderful friends with my fellow researchers who helped and supported me at the times including Jayesh, Pavan, Rameshwar, Jayram, Niyati, Pragati, Muzammil, Suman, Mohan, Srilatha, Lavanya, Sadhana, Rani, Minal, Kapil, Kranti, Ravi, Ashish, Amit, Sukhada, Jyoti, Sreejith here at NCL. I am also grateful to many present and past friends at NCL Sarthak, Rajashri, Ranjit, Riya, Srivarshini, Govardhan, Hemant, Mukesh, Pranali, Sriram, Ravindra, Shikha, Abhishek, Jaganath, Nikhil, Preet,

Sudam, Riya, Yagyansh, Dipak, Kameshwar, Aswini, Vidya , Ashwini, Dr. Sadhana, Dr. Sphurti.

I extend my special thanks to **Dr. Rashmi Tamhankar** for her generous support and motivation. She was the driving force for doing PhD here at CSIR-NCL. She is blessing of God in my life.

I wish to express my deepest gratitude to my beloved mother **Bibifatima** and grandfather, **Mr. Chand Bagwan** who now watch over me from heaven. Their unconditional love, values, and unwavering belief in my potential have been my guiding light throughout this journey. Though they are not physically present, their blessings and the principles they instilled in me have provided strength and inspiration during my most challenging moments. I dedicate this achievement to their cherished memories, knowing that everything I accomplish is a testament to their enduring love and support.

My family is always a source of inspiration and great moral support for me in perceiving my education, I am thankful to God for having such a supportive family. Words are insufficient to express my gratitude towards my family. I take this opportunity to express gratitude to my aunty **Ms Shaynaz Bagwan** for tons of love, sacrifice, blessings, unconditional support, and encouragement. I would also like to thank my grandmother **Mrs. Gulzar Bagwan** for her love and blessings. I am deeply indebted to **Vandana Chavan**, **Hardikar uncle** and all my family members my all Mama Mami's who stood up behind me throughout my Ph.D. career and became my strong moral support. Without their constant support and encouragement, I could not stand with this dissertation. I would like to extend my gratitude to my nephew **Subhan** for spreading happiness around me throughout this journey. I also extend my special thanks to my brothers, Bhabhi's and sisters for unconditional support and motivation throughout my Ph.D. journey.

Above all, I owe it all to Almighty God for granting me the wisdom, health, and strength to undertake this research task and enabling me to its completion.

In closing, I'd like to express my gratitude to everyone I've interacted with and who has, consciously or unconsciously, given me the exposure I needed to extend my perspective through conversation, work, encouragement, or other support.

Thank you !

Farahanaz Bagwan

Table of Contents

1 Introduction 1

1.1 Introduction 2

1.2 Direct CO_2 conversion to methanol 5

1.2.1 CO_2 conversion technologies 5

1.2.2 Current status of methanol production 7

1.3 Liquid organic hydrogen carrier (LOHC) 9

1.3.1 Hydrogen storage 11

1.3.2 What Are LOHCs? 13

1.3.3 Key Advantages of LOHC Technology 13

1.3.4 Working Principle of LOHCs 13

1.4 Statement of problem 14

1.5 References 14

2 Design of fixed-bed reactor for direct conversion of CO_2 via hydrogenation to methanol 19

2.1 Introduction 20

2.2 Literature review 21

2.3 Comparison of kinetic models 25

2.4 Reactor model 29

2.5 Adiabatic model development 31

2.5.1 Effect of feed temperature 33

2.5.2 Effect of pressure 34

2.6 Isothermal model development 34

2.6.1 Effect of temperature and pressure 35

2.6.2 Effect of molar H_2/CO_2 ratio 36

2.7 Comparison of adiabatic and isothermal reaction conditions 40

2.8 Sensitivity analysis 41

2.8.1 Sensitivity analysis: Rate constants varied at a time 42

2.8.2 Sensitivity analysis: Rate constants varied seperately 42

2.9 Conclusion 46

2.10 References 47

3 Experimental studies for direct conversion of CO_2 to methanol production in fixed bed reactor (FBR) 51

3.1 Introduction 52

3.2 Literature review 54
3.3 Material and Methods 57
3.3.1 Catalyst 57
3.3.1 Experimental procedure 62
3.3.2 Effect of H_2 to CO_2 molar ratio 70
3.4 Study of mass transfer limitations 72
3.5 Conclusions 73
3.6 References 74
4 Kinetics studies for Quinoline hydrogenation to decahydroquinoline 78
4.1 Introduction 79
4.2 Material and methods 83
4.2.1 Materials 83
4.2.2 Catalyst characterization 83
4.3 Hydrogenation experiments 86
4.3.1 Thermal screening unit (TSU) 86
4.3.2 Hydrogenation in Autoclave reactor 88
4.4 Results and discussion 89
4.4.1 Effect of temperature 89
4.4.2 Effect of hydrogen pressure 91
4.4.3 Effect of catalyst loading 95
4.4.4 Effect of Solvent 96
4.5 Reaction mechanism 98
4.6 Kinetic model development and validation 99
4.6.1 Power law kinetic model 99
4.6.2 Kinetic study and validation with model 100
4.6.3 Parameter estimation 103
4.7 Conclusions 103
4.8 References 104
..... 109
5 Reaction kinetic studies for dehydrogenation of decahydroquinoline for hydrogen generation 109
5.1 Introduction 110
5.1 Materials 115
5.2 Experimental setup and procedure 115

5.3 Result and Discussion 116
5.3.1 Degree of dehydrogenation (DoD) 116
5.3.2 Effect of temperature 116
5.3.3 Effect of stirring speed 117
5.3.4 Effect of catalyst loading 119
5.4 Development of reaction kinetic model 120
5.4.1 Reaction kinetics study 120
5.4.2 Reaction mechanism 121
5.4.3 Development of Power law 122
5.4.4 Reaction kinetics validation with model 122
5.5 Parameter estimation 125
5.6 Study of mass transfer limitations 125
5.6.1 External mass transfer effects 125
5.6.2 Internal mass transfer effects 126
5.7 Conclusions 127
5.8 References 130
..... 135
6 Mass and energy balance for 1 ton of DHQ per day 135
6.1 Introduction 136
6.2 Process for hydrogenation 138
6.3 Simulation Methodology 142
6.4 Process simulations using reaction kinetics 142
Figure 6.3 Simulation Flowsheet for hydrogenation process 145
6.5 Process flowsheet description 146
6.6 Result and discussion 147
6.6.1 Mass and energy balance 147
6.6.2 Sensitivity analysis 153
6.7 Conclusions 157
6.8 References 158
..... 161
7 Conclusions 161
Appendix 165

List of Figures

Figure 2.1 a) Effect of feed temperature on CO_2 conversion, MeOH selectivity, and yield b) Temperature profile at different feed temperatures at 50 bar pressure; c) Effect of pressure on CO_2 conversion, MeOH selectivity, and yield d) Temperature profile at different Inlet pressures from 10 to 50 bar at H_2: CO_2 = 3; GHSV = 720 h^{-1} 33
Figure 2.2 Effect of temperature on (a) CO_2 conversion (b) Methanol selectivity (c) Methanol yield for H_2: CO_2 = 3; GHSV = 720 h^{-1} at P = 50 bar..... 36
Figure 2.3 Effect of temperature on (a) Outlet molar flowrate (b) Rate of reaction for H_2 to CO_2=3; GHSV = 720 h^{-1} at P = 50 bar..... 38
Figure 2.4 a) CO_2 conversion b) CH_3OH selectivity c) CH_3OH yield d) Space-time yield (STY) of methanol as a function of H_2 to CO_2 molar ratios on CuZA catalyst at T=230°C... 39
Figure 2.5 Effect of feed temperature on outlet molar flowrate of methanol along the length of a) Adiabatic and b) Isothermal reactor c) Comparison among adiabatic and isothermal reactor..... 40
Figure 2.6 Sensitivity analysis with all the rate constants varied by a fixed change (-10 to 10%) at 210°C, 230°C, and 250°C for 10 bar, 30 bar, and 50 bar pressure..... 42
Figure 2.7 Sensitivity analysis of rate constants at 230°C at various pressures a) 10 bar b) 30 bar and c) 50 bar 46
Figure 3.1 Commercial Cu/ZnO/Al_2O_3 catalyst from ThermoFischer Scientific a) Pellet form and b) Crushed form..... 58
Figure 3.2 XRD pattern..... 59
Figure 3.3 (a) BET adsorption – desorption isotherm and (b) pore size distribution of CuZA catalyst..... 60
Figure 3.4 (a) Actual reactor set-up (b)Process flow diagram for conversion of CO_2 to methanol production using fixed bed reactor 62
Figure 3.5 Amount of total product for different temperatures at 40 bar..... 65
Figure 3.6 Comparison of the effect of temperature on a) Methanol yield and b) STY of MeOH with reported literature 66
Figure 3.7 Case -2 Comparison of the effect of temperature on yield and STY of MeOH with reported literature..... 67
Figure 3.8 Error analysis for case I at 40 bar (a)At 210°C (b) At 230°C and (c)At 250°C..... 70
Figure 3.9 Samples collected for 50 bar experiments for H_2 to CO_2 ratios of 3, 6 and 9 for 3g and 6 g catalyst (Samples 1-3 → W cat = 3g; Samples 4-6 → W cat = 6g) 71
Figure 3.10 Space-time yield (STY) of methanol for different H_2:CO_2 molar ratio at 50 bar & 250°C..... 72
Figure 4.1 Reaction scheme for Quinoline hydrogenation..... 82
Figure 4.2 XRD analysis of the Pd/Al_2O_3 catalyst (● – PdO;▼ – Al_2O_3)..... 84
Figure 4.3 (a) BET adsorption-desorption isotherm (b) Pore size distribution 85
Figure 4.4 (a) HRTEM image, (b) SAED pattern, (c) particle size distribution (d) Overall energy dispersive X-ray spectroscopy (EDX) mapping image (e)-(g) EDS mapping images of a representative part of the sample containing palladium, aluminum, and oxygen..... 86
Figure 4.5 Thermal screening test for (a) temperature variation and (b) differential thermal analysis of quinoline with IPA in isothermal mode..... 87
Figure 4.6(a)Actual reactor setup (b) Schematic of the autoclave batch reactor for Quinoline hydrogenation 89

Figure 4.7 Effect of temperature at 50 bar a) on yield b) hydrogen uptake of py-THQ, bz-THQ, DHQ 90
Figure 4.8 Effect of pressure on yield of (a) py-THQ (b) bz-THQ, and (c) DHQ at different reaction temperatures ranging from 75^{o}C to 175^{o}C 93
Figure 4.9 Effect of Pressure on hydrogen uptake of (a) py-THQ (b)bz-THQ, and (c) DHQ at different reaction temperature range from 75 to 175^{o}C 94
Figure 4.10 Effect of catalyst loading at 175^{o}C and 50 bar on (a) Yield of products and (b) Hydrogen uptake 96
Figure 4.11 Effect of solvent reaction temperature of 175^{o}C and 50 bar on a) Yield of DHQ b) Hydrogen uptake 98
Figure 4.12 Possible reaction mechanism for hydrogenation of Quinoline to DHQ 99
Figure 4.13 Concentration profile at 50 bar hydrogen pressure for different temperatures (a)125 ^{o}C (b) 150 ^{o}C and (c) 175 ^{o}C (d) Rate constants at different temperatures 102
Figure 5.1 Reaction mechanism 113
Figure 5.2 Experimental setup for dehydrogenation experiments 116
Figure 5.3 Effect of temperature on a) Degree of dehydrogenation and b) DHQ conversion 117
Figure 5.4 Effect of stirring speed on the degree of dehydrogenation and DHQ conversion at 240^{o}C for 5h 118
Figure 5.5 Effect of catalyst loading for 240^{o}C and reaction time of 5 h 119
Figure 5.6 Concentration profile at 50 bar hydrogen pressure at 240 ^{o}C 120
Figure 5.7 Possible reaction mechanism for dehydrogenation of DHQ to Quinoline formation 121
Figure 5.8 Concentration profile at 50 bar hydrogen pressure for different temperatures (a)200 ^{o}C (b) 220 ^{o}C and (c) 240 ^{o}C (d) Rate constants at different temperatures 124
Figure 6.1 Block diagram for hydrogenation 139
Figure 6.2 Process flow diagram for hydrogenation of quinoline to DHQ production 141
Figure 6.3 Effect of reactor pressure on energy requirement 151
Figure 6.4 Effect of Temperature on Energy Required 152
Figure 6.5 Effect of temperature on conversion, selectivity and yield at 40 bar 153
Figure 6.6 Effect of temperature on conversion, selectivity and yield at 50 bar 154
Figure 6.7 Effect of temperature on conversion, selectivity and iyeld at 60 bar 155
Figure 6.8 Effect of pressure on conversion, selectivity and yield at 125 ^{o}C 156
Figure 6.9 Effect of pressure on conversion, selectivity and yield at 150^{o}C 156
Figure 6.10 Effect of pressure on conversion, selectivity and yield at 175^{o}C 157

List of Tables

Table 1.1 Physical properties of methanol [39] 9
Table 2.1 Kinetic models based on the selection of carbon sources and reaction mechanisms 26
Table 2.2 Kinetic models based on different assumptions about reaction mechanisms and reaction parameters 27
Table 2.3 Driving force terms of rate expressions for reactions 31
Table 2.4 Comparison of inlet conditions and performance parameters for adiabatic and isothermal reactor models for H_2: CO_2 = 3 and P = 50 bar 37
Table 3.1: Summary of the literature study of Catalyst, coprecipitation method and reaction parameters on the conversion of CO_2, methanol selectivity and yield. 55
Table 3.2 Reaction conditions and the performance results of the CuZA catalyst 63
Table 3.3 Case-1 Experimental data validation with reported literature 65
Table 3.4 Case-2 Experimental data validation with reported literature 67
Table 3.5 Input conditions for simulation for experimental data validation 68
Table 3.6 Performance analysis for different H_2: CO_2 molar ratios of 3, 6 and 9 at 50 bar and 250^oC 71
Table 4.1 Physicochemical properties of Quinoline and its hydrogenated products 82
Table 4.2 Estimated rate constants and Arrhenius Parameters 103
Table 5.1 Literature on the recent dehydrogenation of LOHC molecules 114
Table 5.2 Estimated rate constants and Arrhenius parameters for dehydrogenation of DHQ to Quinoline formation 125
Table 5.3 Carberry number and Weisz Prater criteria for mass transfer limitations 126
Table 6.1 Mass Balance for hydrogenation process 140
Table 6.2 Mass balance of the complete hydrogenation process in terms of mass flow 148
Table 6.3 Mass balance of the complete hydrogenation process in terms of mass fractions 148
Table 6.4 Energy data in the flowsheet at 175 ^oC and 50 bar 150

Chapter 1

Introduction

1.1 Introduction

The present principal energy source for the globe, which began with non-renewable and limited fossil fuels, has enabled a tremendous period of wealth and growth for human civilization during the past few centuries. The depletion of these finite resources is a result of the constant increase in energy consumption to support industrialization and growth. They don't regenerate on a human timescale after being devoured[1]. But because of their irreversible use, carbon dioxide (CO_2) accumulated in the atmosphere, changing the climate[2]. Recent studies showed that CO_2 is being released abundantly from power plants, cement industries, steel plants, petroleum, oil & gas, and petrochemical plants. The atmospheric CO_2 concentration is now predicted to rise to 417.2 ppm in 2022, which is 51% higher than pre-industrial levels. During the 2012–2021 decade, atmospheric CO_2 increase was 5.2 ± 0.02 GtC yr−1 (48 % of global CO_2 emissions), and the preliminary growth rate estimate for 2022 is around 5.3 GtC yr−1 (2.5 ppm) (Global carbon budget 2022).Given that greenhouse gases cause major issues like global warming, humanity must address the growing concentration of these gases in the atmosphere[1]. The International Panel on Climate Change (IPCC) predicted that by 2100, the CO_2 level will rise to 570 parts per million[3]. Reducing CO_2 emissions is an extensive and difficult task[4]. Thus, the recycling of CO_2 as a feedstock to produce hydrocarbons presents great economic and environmental interests([5]. Utilizing CO_2 provides a different carbon-neutral method for producing useful chemicals and fuels [6]. In an effort to combat climate change and advance sustainable energy alternatives, businesses and governments throughout the world are accelerating the development of CO_2-to-methanol conversion technology. Globally, several organizations are leading this innovative field by converting industrial CO_2 emissions into methanol, a versatile chemical and fuel. Carbon Recycling International (CRI), based in Iceland, pioneered this technology with their George Olah environmental methanol plant and, in 2022, expanded operations with a 110,000-ton capacity plant, demonstrating the scalability of CO_2 utilization Global Leader in Carbon Capture and Utilization & Emethanol [7]. Similarly, LanzaTech, headquartered in the U.S., employs gas fermentation to transform industrial waste gases into methanol and other valuable products[8]. In Denmark, European Energy is constructing one of the largest e-methanol plants, harnessing renewable energy to drive CO_2 conversion. Innovators like Syzygy Plasmonics in the U.S. are employing photocatalysis, a light-driven process, for methanol production[9], while Dimensional Energy focuses on converting CO_2 and water into syngas, a precursor to methanol[10]. Meanwhile, the U.S.-based Air Company specializes in producing carbon-negative fuels by transforming CO_2

into alcohols[11], and the UK's Carbon Clean Solutions integrates CO_2 capture with industrial processes to generate methanol and other chemicals. These companies exemplify the worldwide initiative to reduce carbon emissions by developing innovative solutions, opening the door to a more sustainable future. India, too, has emerged as a significant player in the CO_2 to methanol conversion sector, showcasing its commitment to sustainable energy and carbon neutrality[12]. The National Thermal Power Corporation (NTPC) has launched their CO_2 to methanol plant at its Vindhyachal facility. This plant, equipped with indigenously developed technology, converts captured CO_2 into methanol with an impressive purity of 99.9%, marking a major advancement in carbon utilization[13]. Another notable initiative is the CO_2 to methanol pilot plant in Pune, established through a public-private partnership between the Indian Institute of Technology Delhi (IIT Delhi) and Thermax [14]. This facility, with a capacity of 1.4 tons per day, highlights India's focus on developing indigenous carbon capture and utilization (CCU) technologies, contributing to a circular carbon economy. Furthermore, the Jawaharlal Nehru Centre for Advanced Scientific Research (JNCASR), in collaboration with the Telangana government, is planning to set up India's first large-scale CO_2 to methanol plant. This project aims to transform industrial CO_2 emissions into methanol sustainably. These pioneering efforts are bolstered by research and development programs across India's academic and industrial sectors[15]. Institutions like the Indian Institute of Science (IISc) and the Council of Scientific and Industrial Research (CSIR) are actively working to develop scalable CO_2 conversion technologies. Such initiatives address the dual challenge of mitigating carbon emissions and meeting the growing demand for methanol in industrial applications, including alternative fuels, pharmaceuticals, and chemicals[15].

Liquid Organic Hydrogen Carriers (LOHCs) are a transformative technology in the quest for a sustainable energy future. These innovative compounds provide a safe, efficient, and scalable solution for hydrogen storage and transportation, addressing key challenges associated with traditional methods such as cryogenic liquefaction and compression. LOHCs work by reversibly binding hydrogen molecules through hydrogenation and dehydrogenation cycles, allowing hydrogen to be stored and transported in a liquid state under ambient conditions. This capability mitigates risks related to high-pressure hydrogen handling and eliminates the need for costly infrastructure, making LOHCs a promising enabler of the hydrogen economy. The importance of LOHC technology lies in its ability to unlock The potential of hydrogen as a clean energy vector, capable of decarbonizing hard-to-abate sectors such as transportation, heavy industry, and power generation. By facilitating the seamless transport of hydrogen across

regions and countries, LOHCs pave the way for energy-rich regions to export hydrogen globally, bolstering energy security and supporting the transition to a low-carbon economy.

Globally, several companies are at the forefront of advancing LOHC technology, driving innovation and commercial adoption. Hydrogenious LOHC Technologies, based in Germany, is a recognized leader in this domain. The company has developed advanced LOHC systems that are already being deployed for industrial-scale hydrogen storage and transport. Hydrogenious's solutions, such as their StorageBOX and ReleaseBOX, offer high safety standards and efficiency, making them a reliable choice for hydrogen logistics[16]. Another major player is Chiyoda Corporation, headquartered in Japan, which has developed the SPERA Hydrogen™ technology. This innovative system enables the transportation of hydrogen using methylcyclohexane (MCH) as an LOHC. Chiyoda has successfully demonstrated the commercial viability of its technology by transporting hydrogen from overseas production sites to Japan [17]. Honeywell, a global leader in energy technologies, is exploring LOHC solutions to support hydrogen storage and transport as part of its broader energy transition strategy[18]. Similarly, Axens, a French company specializing in sustainable chemistry, has been actively developing LOHC technologies to optimize hydrogen logistics for industrial applications[19]. In India, the LOHC landscape is evolving rapidly as the country accelerates its hydrogen economy roadmap under initiatives like the National Hydrogen Mission. In order to design, integrate, and develop a Liquid Organic Hydrogen Carrier (LOHC) solution and an e-Bus powered by a 9-M hydrogen fuel cell, Oil India Limited (OIL) has signed an incubation agreement with Ohm Clean Tech Private Limited. IIT-Guwahati would provide mentorship and support to the start-up[20]. The growing adoption of LOHC technology by these companies illustrates the global and national commitment to making hydrogen a fundamental component of the energy transition. LOHCs not only address technical challenges but also enable scalable hydrogen deployment, ensuring the viability of using hydrogen as an eco-friendly and adaptable energy carrier. By leveraging LOHCs, hydrogen can be efficiently stored and transported over long distances, facilitating cross-border energy trade and fostering international cooperation. This capability is particularly significant for countries like India, which can leverage LOHCs to import hydrogen from energy-rich nations while simultaneously exporting its domestically produced hydrogen to global markets. Moreover, LOHC systems align with global sustainability goals by minimizing greenhouse gas emissions and reducing the environmental footprint of hydrogen logistics. Unlike traditional hydrogen storage methods, LOHCs provide a closed-loop system with minimal energy loss, enhancing overall

efficiency and cost-effectiveness. LOHC technology represents a breakthrough in hydrogen storage and transportation, addressing key barriers to hydrogen's widespread adoption. With leading companies driving innovation, LOHC systems are poised to revolutionize the global hydrogen economy. These advancements not only support decarbonization efforts but also foster energy security and international collaboration, making LOHCs a cornerstone of the sustainable energy transition. By embracing LOHC technology, countries and companies worldwide are laying the foundation for a cleaner, greener, and more resilient energy future.

1.2 Direct CO_2 conversion to methanol

1.2.1 CO_2 conversion technologies

The continuous increase in anthropogenic carbon dioxide concentrations necessitates significant climate mitigation strategies to avoid adverse greenhouse consequences. A new school of thinking has emerged as a result of technological developments in the diverse spectrum of CO_2 consumption, with the goal of valuing atmospheric CO_2 as a raw material for useful and reasonably priced commodities. As scalable and market-driven pathways for the CO_2 commodity market, these innovative CO_2 conversion technologies—which include electrolysis, photocatalysis, biohybrid, nanoporous confinement, and chain insertion—outperform traditional carbon capture techniques.

1.2.1.1 Electrocatalysis

In most cases, electrochemistry and catalysis work together to generate electrocatalysis. According to a basic understanding, electrochemistry contributes to the conversion of chemical and electrical energy, while catalysis speeds up the system's chemical reactions. Since this conversion technique allows reactants and electrocatalysts to communicate and share, and Electrocatalysis can be considered a distinct form of heterogeneous catalysis since the electrocatalyst may act as an electrode element[21].

1.2.1.2 Photocatalysis

According to Adamu et al.,2020, a photocatalyst is often classified as a semiconductor with a lower bandgap energy than an insulator. If the energy in the electromagnetic radiation is equal to or higher than the energy in the bandgap, the material's valence electrons will actively permitting the positively charged holes to reside in the valence band while migrating in the conduction band. The generated charge carrier's electrode potential facilitates a photocatalyst's redox thermodynamics. Meanwhile, the photocatalyst's kinetic properties are controlled by both light-driven processes and redox chemistry.

There are several disadvantages to photocatalysis, despite the fact that it is regarded as an appealing alternative for a thermocatalytic process that operates at high temperatures and pressures[22]. Low yield [23], poor light absorption [24], and photocorrosion[22] are the disadvantages. High charge recombination [25], incompatible bandgaps[26], and slow electron transport [23] are all linked to low yield. In the meantime, low UV light energy and a wide variety of bandgaps are associated with poor light absorption. The photocatalysis cannot proceed as planned because of the photocorrosion[26].

1.2.1.3 Biohybrid

Biohybrid systems essentially include both organic (living organisms) and inorganic (semiconductors and/or photocatalysts) components to mimic natural photosynthesis, which converts CO2 into chemicals and building blocks. Currently, biohybrid systems that efficiently convert CO_2 into chemicals or fuels by combining artificial and biological methods are made up of two components: (1) microbial electrosynthesis systems and (2) photosynthetic semiconductor biohybrid systems. Therefore, living things like bacteria or microalgae are crucial to the effectiveness of CO_2 conversion. Both systems, however, operate differently from one another.

1.2.1.4 Electroreduction of CO+ in metal–organic framework

In aqueous solutions such as monoethanolamine and diethanolamine, which are utilized in the majority of industrial sectors' widely used CO_2 separation methods, amine solvents readily react and neutralize acidic CO_2 gasses. But it's also well known that amine absorption technology has drawbacks, such as corrosion, oxidative adsorbent corrosion, sorbent flow fluctuations, and high energy consumption[27] . As active electrocatalysts, tunable nanoporous solid adsorbents electrochemically convert CO_2 into possible C1-based fuels and building blocks, is one of the developing solutions to the barriers. To this end, metal–organic frameworks (MOFs) have become a distinct class of crystalline materials featuring unique three-dimensional (3D) microporous and crystallographic structures. Moreover, MOFs may be readily synthesized to enable minor modifications to their characteristics to accommodate particular uses[28]. Depending on the synthetic pore sizes, MOFs may easily adsorb various gases through a molecular sieving action. The use of MOFs to selectively adsorb and extract CO_2 from gas mixtures is therefore extremely feasible[29]. Nevertheless, the high implementation costs and high temperature adsorption capabilities of this technology are often associated with its disadvantage.

1.2.2 Current status of methanol production

Methanol is a component used in the industrial manufacturing of various added-value chemicals, like formaldehyde [30,31], olefins [32][33], and biodiesel[34,35]. Methanol is used extensively in the plastics industry, as a solvent in the pharmaceutical industry, and in the extraction of animal and plant products as in the preparation of vitamins, cholesterol, and hormones[36]. In addition to this, Methanol is used to make a wide range of intermediates used in the production of several everyday items, including paints, resins, silicones, adhesives, antifreeze, and more. In addition to gasoline, methanol is utilized as a fuel for transportation[37]. Methanol consumed in 2018 was 140 million metric tons. In 2030, it is predicted to be 280 million metric tons.

Valuing CO_2, lowering CO_2 emissions, and meeting the demand for the aforementioned compounds are the objectives. It is desirable to develop a kinetic equation that quantitatively characterizes the effects of carbon dioxide and includes temperature distribution in industrial reactors that can be anticipated in order to accomplish this aim in addition to mechanistic elucidation of the impacts. Although such equations have been developed previously, none of them adequately capture the synthesis patterns across various catalysts. The process by which CO_2 hydrogenates to methanol was not entirely understood in previous decades. This is because the competing reverse water-gas shift (RWGS) process (Eq. 2)[6] places significant thermodynamic constraints on the conversion. The effectiveness of the process determines whether a technology is adopted in the industrial setting. At the moment, there is a lot of room to comprehend the emerging technologies associated with methanol synthesis by carefully examining the reaction mechanism and its associated kinetics. For the synthesis of methanol, lower temperatures and greater pressures are the ideal thermodynamic parameters. Because the RWGS reaction is endothermic and so repressed at low temperatures, this permits great methanol selectivity. Methanol is produced primarily by the carbon monoxide catalytic hydrogenation which makes for 10% of the world's H_2 consumption. The industrial procedure is conducted at 250^{o}C and 50–100 bar. In addition to H_2, renewable methanol has been suggested as a carbon-neutral energy vector for liquid fuel [38].

In order to keep the methanol formation process cost-competitive, process intensification techniques are employed in larger-scale production, which is the focus of future methanol reactor research. As was previously noted, the synthesis of methanol is an exothermic process, which means that fewer moles of methanol are produced in the system in relation to the amount of gaseous reactant mixtures that are introduced into it. This property suggests that the

methanol synthesis process as a whole is economical and effective at using low temperature and high pressure reaction conditions. A commercial plant process's main issue is that heat removal from the reaction system be effective for more cost-effective and efficient plant operation, as excess heat inside the reactor might impact reaction rate and selectivity. This extra heat causes a number of unwanted byproducts to be produced, which further increases the required recycling rate. Because the WGS process, CO, and CO_2 hydrogenation reactions are exothermic among the processes involved in methanol synthesis, a high reactor temperature results in a lower methanol conversion. Therefore, to get a higher methanol production, the recycling ratio needs to be increased, which necessitates recycling the unreacted gas more often than at lower reactor temperatures. Condensing the methanol product requires cooling the gas before recycling. The reacting gas mixtures are then supplemented with fresh gaseous reactants. The raw material in methanol production facilities consists of methanol, water, and a few impurities. Byproducts of the production of methanol include formaldehyde, formic acid, dimethyl ether (DME), and ketones [39].

Methanol Uses

Ethylene, formaldehyde, acetic acid, aromatics, methyl tertiary butyl ether (MTBE), dimethyl carbonate (DMC), biodiesel, and other compounds are all produced industrially using methanol as a building block. One of the most valued new technologies in the field of producing gasoline from renewable resources is the "methanol to gasoline (MTG)" method. Solid acid catalysts such as zeolites and SAPO have proved effective in catalyzing the conversion of methanol into aromatic and olefinic hydrocarbons. In order to provide a more selective spectrum of alkenes for the synthesis of gasoline, these catalysts are constantly being improved. Consequently, from the standpoint of the global economy, investment in critical methanol technologies is crucial. Because of the enormous accumulation of greenhouse gases in the atmosphere brought about by centuries of fossil fuel consumption, the UNFCCC members reached the Paris Agreement in 2015. By establishing two long-term temperature targets, this agreement seeks to mitigate the risk and effects of global warming: (i) limiting the increase in global temperatures to well below 2 °C over pre-industrial levels, and (ii) taking more proactive measures to limit the increase to 1.5 °C over pre-industrial levels. A 20/20/20 approach was used to accomplish these objectives, which include a 20% reduction in CO_2 emissions, a 20% increase in the market share of renewable energy, and a 20% improvement in the efficiency of existing equipment[39].

Table 1.1 Physical properties of methanol [39]

Properties	**Value**
Boiling point (^oC)	64.70
Critical temperature (^oC)	239.43
Critical pressure (kPa)	8096
Critical volume (ml/mol)	118
Critical value of compressibility factor	0.224
Heat of formation at 25 ^oC (kJ/mol)	-239.03
Free energy of formation (liquid) at 25^oC (kJ/mol)	-166.81
Heat of fusion (J/g)	103
Heat of vaporization at boiling point (J/g)	1129
Heat of combustion(gross) at 25^oC (J/g)	22662
Autoignition temperature (^oC)	464
Flash point (^oC)	11
Surface tension at 25^oC (mN/m)	22.1
Specific heat of vapour at 25^oC (J/gK)	1.370
Specific heat of liquid at 25^oC (J/gK)	2.533
Vapour pressure at 25^oC (kPa)	16.96
Solubility in water	Miscible
Density at 25^oC (g/ml)	0.7866
Refractive index	1.3284
Liquid viscosity at 25^oC (mPa)	0.541
Dielectric constant at 25^oC	32.7
Thermal conductivity at 25^oC (W/mK)	0.202

1.3 Liquid organic hydrogen carrier (LOHC)

Fossil fuel supplies will survive for hundreds of years if energy use keeps on its current pace [40]. However, the fear of climate change may terminate the fossil fuel era before the fossil fuel reserves run out. Hydroelectric power (17.8%) and traditional biomass used for cooking and heating in developing countries (73.4%) accounted for 13.5% of the world's total primary energy supply (TPES), or 13 555 Mtoe (570 EJ), in 2013. The International Energy Agency's (IEA) "New Policies Scenario" predicts that by 2035, the share of renewable energy in primary

energy would reach 18% due to the growth of hydropower, biofuels, wind, and solar photovoltaic (PV). By 2050, it is predicted that 100–400 EJ of global energy output would come from renewable sources [40]. The disparities in the production and use of renewable energy between areas, as well as the fluxionality of its creation, necessitate the development of innovative energy storage medium. For instance, the areas that are most areas that are most suitable for producing renewable energy are frequently located distant from areas with the highest demand. As a result, energy must be transported over vast distances and internationally. The summer months, when energy demand is at its lowest, offer the greatest potential for solar energy generation in the northern latitudes. Wind conditions are subject to sudden changes. All things considered; the erratic generation of renewable energy presents difficulties. Even the hydroelectric capacity is not used to its full potential during periods of low usage. Practical energy storage devices are required to eliminate the constraints of Large-scale renewable energy deployment is necessary to balance energy prices and enhance energy security. Excellent energy storage options include coal, oil, and gas. Other energy storage technologies offer advantages and disadvantages, including variations in size classes, storage period lengths, and energy transmission capacities. For instance, compressed air and pumped hydro energy storage systems have brief discharge periods. Although batteries range in capacity from kW to more than 100 MW, they have a poor gravimetric energy density and are unable to store electricity for long periods of time. Not every application calls for the same kind of energy storage. For instance, long-distance land transportation and aircraft rely on premium liquid fuels, while the shipping and power and heating industries can handle more difficult fuels.

With its high energy density and zero carbon emissions when used, hydrogen is a viable energy carrier for a clean and sustainable energy future. However, because hydrogen is a low-density gas under normal circumstances, storage and transportation are one of the biggest obstacles to its widespread use. Hydrogen can be stored under high pressure at ambient temperature or below, or it can be preserved as a cryogenic liquid at its normal boiling point of 20 K. However, the traditional mechanical ways of storing hydrogen (compression or liquefaction) are expensive in terms of money and energy. One alternative method of storage that has been investigated is Cryocompression of hydrogen. Moreover, hydrogen may be kept in solution in metals, adsorbed as a diatomic molecule in porous materials, or combined with other elements to form hydrogen compounds [42–44].

1.3.1 Hydrogen storage

1.3.1.1 Mechanical storage of hydrogen

1.3.1.1.1 Compression

An efficient compressed hydrogen storage system typically requires a working pressure of 700 bar and a capacity of 220 L to store 5 kg of hydrogen gas. The mass of the cylinder, which is usually made of steel, is one major drawback. To get around this, composite cylinders were developed, which significantly decreased operating pressures and reservoir masses. A type IV vessel, a lightweight composite cylinder with a polymer liner akin to high density polyethylene HDPE, was developed to prevent gas diffusion and load-bearing composite overwrap. This device achieves a gravimetric hydrogen uptake capacity of 1.7 kWh.kg-1 and a volumetric hydrogen absorption capacity of 0.9 kWh.L-1, according to the Department of Energy (2015). This storage method is used in the upcoming Toyota Mihai hydrogen fuel cell vehicle. The storage tank's volume is enough for onboard usage, despite the high pressure being a major safety risk [45].

1.3.1.1.2 Liquification

An substantial hydrogen infrastructure enables the delivery and storage of large quantities of hydrogen as a liquid at around 20 K (-253°C). The current global capacity is just around 50 tons per day, which is insufficient to power a largely hydrogen-based mobility system. On the other hand, hydrogen liquefiers are an established technology that can process up to 30 tons of hydrogen per day and consume 30 to 45 MJ of energy per kilogram of liquefied hydrogen. Nonetheless, a number of studies indicate that liquefier capacities of up to 900 tons per day-1 and energy requirements as low as 18–25 MJ.kg-1 could be achievable. One benefit of liquid hydrogen is that it has a large volumetric storage capacity. At -253 °C and 1 atm, liquid hydrogen has a volumetric energy density of 70.8 g.L-1, which is significantly greater than that of compressed gas. However, the process of liquefying hydrogen is highly expensive and energy-intensive. According to Ekins and Bellaby (2008), Hydrogen liquefaction was estimated to cost between $1 and 1.5 kg-1, whereas the cost of compressions at 700 bar was 0.15-0.6 $.kg^{-1}[41]. A double-walled container or a cryostat can be used to hold liquid hydrogen. But the boil-off effect, which results in leaks, is the issue. The boil-off phenomena happens when liquid hydrogen absorbs heat from its surroundings or when it is delivered and refuelled, since it easily evaporates.

To avoid costly and hazardous boil-off loss, the tank has to be vented every three to five days when it is not in use.

1.3.1.1.3 Cryocompression

Compression and cryogenic hydrogen storage are combined in the most recent hydrogen storage methods. In the head space, pressurized liquid hydrogen vessels can produce a mixture of high pressure and liquid hydrogen [42]. The density of hydrogen in liquid form reaches 87 $g.L^{-1}$ at 237 atm, up from 70 $g.L^{-1}$ at 1 atm [43]. These scientists claim that because the hydrogen inside the cryocompressed vessel may be released at a greater temperature, the vessels can tolerate heat. To maintain the hydrogen density at 30% of the original liquid hydrogen density, the venting is stopped once the tank reaches room temperature and the internal pressure of the vessel is maintained at a constant level. When not in use, this enhances tank safety and facilitates better storage. Furthermore, at pressures greater than 13 atm, compressed hydrogen turns into a supercritical fluid, which can free up container space and raise the volumetric energy density.

1.3.1.2 Chemical storage of hydrogen

1.3.1.2.1 Hydrogen storage by chemical reaction with water

Hydrogen may be produced by a chemical reaction between water and other materials, such sodium metal, which can be produced by reducing NaOH in a solar furnace. Calculations show that the gravimetric density of hydrogen kept with sodium is 3.0 weight percent; the gravimetric density increases to 6.3 weight percent when lithium is used in place of sodium. For on-board hydrogen storage applications, this storage method is no longer utilized because of several problems, chief among them being the control of chemical compound reduction to produce original metal [44].

1.3.1.2.2 Hydrogen storage in covalent hydrides

Additionally, hydrides such as organic compounds and ammonia are studied.

For example, methylcyclohexane dehydrogenation/toluene hydrogenation, tetralin dehydrogenation/naphthalene hydrogenation, and decalin dehydrogenation/naphthalene hydrogenation are examples of reversible catalysis pairings that have been used to create organic chemical hydrides [49]. The dehydrogenation process is the key component of non-metallic hydrides. For instance, cyclohexane must be dehydrogenated at 300°C to produce benzene[44], and ammonia must be broken down and hydrogen produced at temperatures more than 400°C in the presence of Ni or Ru catalysts. The kinetics of hydride absorption and

desorption are extremely slow, even though the production and regeneration of hydrides need a high temperature [45].

One creative way to deal with these issues is using Liquid Organic Hydrogen Carriers (LOHCs).

1.3.2 What Are LOHCs?

LOHCs are organic compounds capable of reversibly binding hydrogen through catalytic hydrogenation and dehydrogenation reactions. In their hydrogen-rich form (hydrogenated), they serve as hydrogen carriers, and in their hydrogen-lean form (dehydrogenated), they are ready for reuse. Examples of widely studied LOHC systems include:

- **Toluene/Methylcyclohexane:** Toluene is hydrogenated to methylcyclohexane for hydrogen storage and dehydrogenated back to toluene for hydrogen release.
- **Dibenzyltoluene/ Perhydrodibenzyltoluene:** A high-performing LOHC system with a high hydrogen storage capacity.

1.3.3 Key Advantages of LOHC Technology

1. **High Hydrogen Storage Density**: LOHC systems provide a hydrogen storage capacity comparable to or better than conventional methods such as pressurized tanks or cryogenic liquefaction.
2. **Safe and Stable**: LOHCs are liquids under ambient conditions, reducing the risks associated with hydrogen storage under high pressure or at extremely low temperatures.
3. **Infrastructure Compatibility**: They can be stored and transported using existing liquid fuel infrastructure, making them economically viable for large-scale implementation.
4. **Reusability**: LOHC compounds are chemically stable and can undergo numerous hydrogenation and dehydrogenation cycles without significant degradation.

1.3.4 Working Principle of LOHCs

The LOHC cycle involves two primary steps:

1. **Hydrogenation**: The hydrogen-lean LOHC absorbs hydrogen in the presence of a catalyst converting to its hydrogen-rich form. This reaction is typically exothermic.
2. **Dehydrogenation**: The hydrogen-rich LOHC releases hydrogen through a catalytic process, regenerating its hydrogen-lean form. This reaction is endothermic and requires external energy input.

1.4 Statement of problem

There is a significant scope to intensify the processes for conversion of CO_2 to methanol production. Also, hydrogen storage and transportation are facing challenges as the technologies are not well matured. In view of these challenges, the objectives are formulated as follows:

Part 1: Direct conversion of CO_2 to methanol production

i. Development of fixed-bed reactor model for isothermal and adiabatic reactor conditions
ii. Experimental investigation for higher H_2 to CO_2 ratios to study the performance of the isothermal reactor under optimal conditions
iii. Comparative analysis of adiabatic and isothermal model simulations to obtain the performance of the reactor

Part 2: Development of versatile Liquid organic hydrogen carrier (VLOHC)

iv. To establish optimal conditions for hydrogenation of quinoline to Decahydroquinoline (DHQ)formation under pressurized conditions with heterogeneous catalyst (Pd/Al_2O_3)
v. Selection of suitable solvents for hydrogenation of quinoline
vi. Study of hydrogen uptake capacity for Quinoline under optimal conditions
vii. To identify the hydrogen release capacity of Decahydroquinoline using Pd/Al_2O_3 catalyst
viii. Energy analysis for hydrogenation and dehydrogenation processes

Thesis is organized into six chapters as follows:

Chapter 1 Discusses the introduction on direct conversion of CO_2 to methanol and liquid organic hydrogen carriers with current status of industrial plants

Chapter 2 Design of fixed-bed reactor for direct conversion of CO_2 hydrogenation to methanol

Chapter 3 Experimental studies for direct conversion of CO_2 to methanol production in FBR

Chapter 4 Kinetics studies for Quinoline hydrogenation to decahydroquinoline

Chapter 5 Dehydrogenation studies for decahydroquinoline for hydrogen generation

Chapter 6 Mass and energy analysis for 1 ton per day of DHQ production

Chapter 7 Conclusions

1.5 References

[1] Olah GA, Goeppert A, Prakash GKS. Chemical recycling of carbon dioxide to methanol and dimethyl ether: From greenhouse gas to renewable, environmentally carbon neutral fuels and synthetic hydrocarbons. J Org Chem 2009;74:487–98. https://doi.org/10.1021/jo801260f.

[2] Gaikwad R, Bansode A, Urakawa A. High-pressure advantages in stoichiometric hydrogenation of carbon dioxide to methanol. J Catalysis 2016;343:127–32. https://doi.org/10.1016/j.jcat.2016.02.005.

[3] Younas M, Loong Kong L, Bashir MJK, Nadeem H, Shehzad A, Sethupathi S. Recent Advancements, Fundamental Challenges, and Opportunities in Catalytic Methanation of CO_2. Energy and Fuels 2016;30:8815–31 https://doi.org/10.1021/acs.energyfuels.6b01723.

[4] Wang W, Wang S, Ma X, Gong J. Recent advances in catalytic hydrogenation of carbon dioxide. Chem Soc Rev 2011;40:3703–27. https://doi.org/10.1039/c1cs15008a.

[5] Van-Dal ÉS, Bouallou C. Design and simulation of a methanol production plant from CO_2hydrogenation. J Clean Prod 2013;57:38–45. https://doi.org/10.1016/j.jclepro.2013.06.008.

[6] Stangeland K, Li H, Yu Z. CO_2 hydrogenation to methanol: the structure–activity relationships of different catalyst systems. Energy, Ecol Environ 2020;5:272–85. https://doi.org/10.1007/s40974-020-00156-4.

[7] https://www.carbonrecycling.is/.

[8] https://www.lanzatech.com.

[9] https://plasmonics.tech/decarbonization/.

[10] https://www.dimensionalenergy.com/.

[11] https://www.aircompany.com/.

[12] https://www.carbonclean.com/.

[13] https://ddnews.gov.in/en/ntpc-launches-worlds-first-co%E2%82%82-to-methanol-plant/.

[14] https://carbonherald.com/india-unveils-first-CO_2 -to-methanol-pilot-plant/

[15] https://timesofindia.indiatimes.com/business/india-business/lab2market-jncasr-to-set-up-indias-first- CO_2 -to-methanol-plant-in-telangana/articleshow/105541212.cms.

[16] https://www.hydrogenious.net.

[17] https://www.chiyodacorp.com/en/service/spera-hydrogen/.

[18] https://ess.honeywell.com/us/en/solutions/sustainability/hydrogen-solutions/liquid-organic-hydrogen-carrier.

[19] https://www.axens.net/markets/hydrogen/lohc-compelling-hydrogen-transport-and-storage-solution.

[20] https://renewablewatch.in/2022/04/12/oil-signs-incubation-agreement-with-a-start-up-for-promoting-hydrogen-mobility-solutions/.

[21] White re. modern aspects of electrochemistry.

[22] Chen S, Huang D, Xu P, Xue W, Lei L, Cheng M, et al. photocatalytic and photoelectrochemical water splitting : will we stop with photo corrosion ? Royal Society of Chemistry; 2020. https://doi.org/10.1039/c9ta12799b.

[23] kovačič , photocatalytic-CO_2 -reduction-a-review-of-ab-initio-mechanism-kinetics-and-multiscale-modeling,2020.

[24] Wang, Full-Spectrum Solar-Light-Activated Photocatalysts for Light Chemical Energy, Advanced Energy Materials ,2017.

[25] Yang N, Zhai J, Wang D, Chen Y, Jiang L. Two-Dimensional Graphene Bridges Enhanced Photoinduced Charge Transport in Dye-Sensitized Solar Cells 2010;4:887–94.

[26] Kumar SG, Devi LG. Review on Modified TiO_2 Photocatalysis under UV / Visible Light : Selected Results and Related Mechanisms on Interfacial Charge Carrier Transfer Dynamics 2011:13211–41.

[27] Chen X, Huang G, An C, Yao Y, Zhao S. Emerging N- nitrosamines and N- nitramines from amine-based post- combustion CO_2 capture – A review. Chem Eng J 2018;335:921–35. https://doi.org/10.1016/j.cej.2017.11.032.

[28] Sneddon G, Greenaway A, Yiu HHP. The Potential Applications of Nanoporous Materials for the Adsorption , Separation , and Catalytic Conversion of Carbon Dioxide 2014:1–19. https://doi.org/10.1002/aenm.201301873.

[29] Elhenawy SEM, Khraisheh M, Almomani F, Walker G. Metal-organic frameworks as a platform for CO_2 capture and chemical processes: Adsorption, membrane separation, catalytic-conversion, and electrochemical reduction of CO_2 . Catalysts 2020;10:1–33. https://doi.org/10.3390/catal10111293.

[30] Kropp T, Paier J, Sauer J. Oxidative dehydrogenation of methanol at ceria-supported vanadia oligomers. J Catal 2017;352:382–7. https://doi.org/10.1016/j.jcat.2017.06.011.

[31] Gribovskii AG, Ovchinnikova E V., Vernikovskaya N V., Andreev D V.,Chumachenko VA, Makarshin LL. Microchannel reactor for intensifying oxidation of methanol to formaldehyde over Fe-Mo catalyst. Chem Eng J 2017;308:135–41. https://doi.org/10.1016/j.cej.2016.09.058.

[32] Losch P, Pinar AB, Willinger MG, Soukup K, Chavan S, Vincent B, et al. H-ZSM-5 zeolite model crystals: Structure-diffusion-activity relationship in methanol-to-olefins catalysis. J Catal 2017;345:11–23. https://doi.org/10.1016/j.jcat.2016.11.005.

[33] Zhang T, Wang Z, Zhao Q, Li F, Xue W. Partial hydrogenation of benzene to

cyclohexene over Ru-Zn/MCM-41. J Nanomater 2015;2015. https://doi.org/10.1155/2015/670896.

[34] Pirola C, Manenti F, Galli F, Bianchi CL, Boffito DC, Corbetta M. Heterogeneously catalyzed free fatty acids esterification in (monophasic liquid)/solid packed bed reactors (PBR). Chem Eng Trans 2014;37:553–8. https://doi.org/10.3303/CET1437093.

[35] Boffito DC, Galli F, Martinez PR, Pirola C, Bianchi CL, Patience GS. Transesterification of triglycerides in a new ultrasonic-assisted mixing device. Chem Eng Trans 2015;43:427–32. https://doi.org/10.3303/CET1543072.

[36] Machado CFR, Medeiros JL De, Araújo OFQ, Alves RMB. A comparative analysis of methanol production routes : synthesis gas versus CO_2 hydrogenation. 2014 Int Conf Ind Eng Oper Manag 2014:2981–90.

[37] Bozzano G, Manenti F. Efficient methanol synthesis: Perspectives, technologies and optimization strategies. Prog Energy Combust Sci 2016;56:71–105. https://doi.org/10.1016/j.pecs.2016.06.001.

[38] Dalena F, Senatore A, Basile M, Knani S, Basile A, Iulianelli A. Advances in methanol production and utilization, with particular emphasis toward hydrogen generation via membrane reactor technology. Membranes (Basel) 2018;8. https://doi.org/10.3390/membranes8040098.

[39] Mondal U, Yadav GD. Methanol economy and net zero emissions: Critical analysis of catalytic processes, reactors and technologies. Green Chem 2021;23:8361–405. https://doi.org/10.1039/d1gc02078a.

[40] Aakko-Saksa PT, Cook C, Kiviaho J, Repo T. Liquid organic hydrogen carriers for transportation and storing of renewable energy – Review and discussion. J Power Sources 2018;396:803–23. https://doi.org/10.1016/j.jpowsour.2018.04.011.

[41] Aakko-Saksa PT, Cook C, Kiviaho J, Repo T. Liquid organic hydrogen carriers for transportation and storing of renewable energy – Review and discussion. J Power Sources 2018;396:803–23. https://doi.org/10.1016/j.jpowsour.2018.04.011.

[42] Durbin DJ, Malardier-Jugroot C. Review of hydrogen storage techniques for on board vehicle applications. Int J Hydrogen Energy 2013;38:14595–617. https://doi.org/10.1016/j.ijhydene.2013.07.058.

[43] Friedlingstein P, O'Sullivan M, Jones MW, Andrew RM, Gregor L, Hauck J, et al. NASA Says 2022 Fifth Warmest Year on Record, Warming Trend Continues. Earth Syst Sci Data 2023;14:4811–900.

[44] Züttel A. Hydrogen storage methods. Naturwissenschaften 2004;91:157–72. https://doi.org/10.1007/s00114-004-0516-x.

[45] Yu Z. Equilibrium and kinetics studies of hydrogen storage onto hybrid activated carbon-metal organic framework adsorbents produced by mild syntheses 2016.

[46] Ekins P, Bellaby P. Hydrogen futures: Emerging technologies for hydrogen storage and transport. Solid-State Hydrog Storage Mater Chem 2008:18–50. https://doi.org/10.1533/9781845694944.1.18.

[47] Satyapal S, Petrovic J, Read C, Thomas G, Ordaz G. The U.S. Department of Energy's National Hydrogen Storage Project: Progress towards meeting hydrogen-powered vehicle requirements. Catal Today 2007;120:246–56. https://doi.org/10.1016/j.cattod.2006.09.022.

[48] Hua TQ, Ahluwalia RK, Peng JK, Kromer M, Lasher S, McKenney K, et al. Technical assessment of compressed hydrogen storage tank systems for automotive applications. Int J Hydrogen Energy 2011;36:3037–49. https://doi.org/10.1016/j.ijhydene.2010.11.090.

[49] Hodoshima S, Arai H, Takaiwa S, Saito Y. Catalytic decalin dehydrogenation/naphthalene hydrogenation pair as a hydrogen source for fuel-cell vehicle. Int J Hydrogen Energy 2003;28:1255–62. https://doi.org/10.1016/S0360-3199(02)00250-1.

[50] Biniwale RB, Kariya N, Ichikawa M. Dehydrogenation of cyclohexane over Ni based catalysts supported on activated carbon using spray-pulsed reactor and enhancement in activity by addition of a small amount of Pt. Catal Letters 2005;105:83–7. https://doi.org/10.1007/s10562-005-8009-x.

[51] Sakintuna B, Lamari-Darkrim F, Hirscher M. Metal hydride materials for solid hydrogen storage: A review. Int J Hydrogen Energy 2007;32:1121–40. https://doi.org/10.1016/j.ijhydene.2006.11.022.

Chapter 2

Design of fixed-bed reactor for direct conversion of CO_2 via hydrogenation to methanol

2.1 Introduction

Direct conversion of CO_2 via hydrogenation to value-added chemicals is a vital approach for utilizing CO_2 emitted in the atmosphere from various fossil sources. A wide range of kinetic models with appropriate assumptions regarding the reaction mechanisms and their parameters have been suggested by researchers over the last few decades[1–3]. The rate expressions are developed based on a dual-site LHHW mechanism[4–10]. Although various kinetic models have developed, the CO_2 hydrogenation to methanol reaction mechanism was relatively unclear. This is due to the major thermodynamic limitations on conversion due to competing reverse water–gas shift (RWGS) reactions[11]**.** Industrially, it depends on various performance parameters such as efficiency, safety and CO_2 mitigation, etc. to adopt technology. There is a wide variety of opportunities for understanding how methanol synthesis technologies are developed by studying the reaction mechanism and its associated kinetics. Kinetic modelling is largely used in techno-economic assessment (TEA) studies[12,13].

To study mechanistic approaches for the conversion of CO_2 to useful products, it is necessary to develop a kinetic equation that describes the effects and predict the temperature distribution quantitatively in industrial reactors[14]. Methanol production through the conversion of carbon dioxide route is obtained via a catalytic process using three reversible reactions: (a) carbon monoxide hydrogenation reaction, (b) reverse water-gas shift (RWGS) reaction, and (c) carbon dioxide hydrogenation.

$CO + 2H_2 \leftrightarrows CH_3OH$ $\Delta H_r°(298\ K) = -90.5$ kJ/mol *(a)*

$CO_2 + H_2 \leftrightarrows CO + H_2O$ $\Delta H_r°(298\ K) = +41.1$ kJ/mol *(b)*

$CO_2 + 3H_2 \leftrightarrows CH_3OH + H_2O$ $\Delta H_r°(298\ K) = -49.4$ kJ/mol *(c)*

The preferred thermodynamic conditions for methanol synthesis are low temperatures and higher pressures. This allows high methanol selectivity as the RWGS reaction is endothermic and therefore, suppressed at low temperatures. In order to fully describe, analyze, and forecast the dynamics of many systems or events under various circumstances, mathematical models offer a potent set of tools. Kinetic modelling is one of the most important mathematical frameworks among chemical engineering prediction approaches, with many uses, especially in reactor design and optimization research[15].

Kinetic models were developed based on the rate expressions of all the elementary reactions and their reaction parameters. Many studies have considered Langmuir– Hinshelwood – Hougen – Watson (LHHW) or Eley – Riedel mechanisms and one or more rate-limiting steps (RDS) for the development of kinetic modeling. In the case of the LHHW reaction,

participating reactants will get adsorbed first on the catalyst surface, and then react to form products. The Eley–Rideal mechanism, begins with the adsorption of the reactant on the catalyst active site, while one of the other reactants remains in the bulk phase, and after colliding with each other form products[16].

2.2 Literature review

In the last few decades, researchers have proposed many kinetic models based on different assumptions about reaction mechanisms and reaction parameters.

Natta et al.(1955), developed a kinetic model for the ZnO/Cr_2O_3 catalyst assuming only the hydrogenation of CO, in which it is proposed that the trimolecular reaction of CO and molecular hydrogen to be a rate-determining step. The proposed rate equation at temperatures of 300-360°C is shown in equation 2.1 [17].

$$r = \frac{\gamma_{CO} P_{CO} \gamma_{H_2}^2 P_{H_2}^2 - \frac{\gamma_{CH_3OH}}{K_{eq}}}{\left(A + B\gamma_{CO} P_{CO} + C\gamma_{H_2} P_{H_2} + D\gamma_{CH_3OH} P_{CH_3OH}\right)^3} \qquad (2.1)$$

r is the rate of methanol formation,

γ_i is the fugacity coefficient of species i,

P_i is the partial pressure of species,

K_{eq} is the equilibrium constant of carbon monoxide hydrogenation to methanol

A, B, C, and D are empirical constants

Considering methanol synthesis with carbon dioxide-rich synthesis gas, Bakemeier et al. (1970) observed a mismatch in the comparison of measured rates with those calculated using kinetic equations. Then it was realized that carbon dioxide-dependent terms must be incorporated so that the kinetic equations would be useful for process design. A new rate equation for the ZnO/Cr_2O_3 catalyst assuming the methanol desorption to be rate determining step is obtained. This rate equation predicts that the methanol yield would decrease as the CO_2 partial pressure is increased [17].

$$r = Ae^{\frac{-E}{RT}} * \frac{P_{CO}^n P_{H_2}^m \left(1 - P_{CH_3OH}/(P_{CO} P_{H_2}^2 K_{eq})\right)}{\left(1 + \frac{De^{\frac{-E}{RT}} P_{CO_2}}{P_{H_2}}\right)} \qquad (2.2)$$

In the above equation, A, E, n, m, D, and F are semiempirical parameters. Leonov et al. (1973) is the first researcher to model methanol synthesis kinetics over a $Cu/ZnO/Al_2O_3$ catalyst for temperatures between 220 and 260°C and pressures in the range of 40-55 atm. Their model assumed CO is the source of carbon in methanol and neglected the effect of CO_2 in the feed, the rate-determining step is methanol desorption. The examination

was limited to a narrow pressure range and did not consider the presence of any reaction considering the utilization of carbon dioxide [12]. The rate equation is as below,

$$r = k\left(\frac{P_{CO}^{0.5}P_{H2}}{P_{CH3OH}^{0.66}} - \frac{P_{CH3OH}^{0.34}}{P_{CO}^{0.5}P_{H2}K_{eq}}\right) \qquad (2.3)$$

where,

k is the rate constant for the forward reaction

K_{eq} is the equilibrium constant

Denny and Whan et al. (1978), also reviewed various contradictory reports on the effects of CO_2 on the synthesis and emphasized the partial pressure of carbon dioxide term in the kinetic expression[17]. Klier et al.(1982), developed taking into account the partial pressure of CO_2 without considering its role as a reactant[17]. The rate expression for the temperature range of 225-250°C and pressure of 75 atm is represented as follows,

$$r = k * \frac{K_{redox}^3 * \left(\frac{P_{CO2}}{P_{CO}}\right)^3 * \left(P_{CO}P_{H2}^2 - \frac{P_{CH3OH}}{K_2^*}\right)}{\left(1 + K_{redox}\left(\frac{P_{CO2}}{P_{CO}}\right)\right)^3 * (F + K_{CO2}\,P_{CO2})^n} + k'(P_{CO2} - 1/K_1^*\,(P_{CH3OH}P_{H2O}/P_{H2}^3) \qquad (2.4)$$

where,

k is the rate constant, F is a linear function of pressures of H_2, and CO, and the exponent n ranges from 1 to 3. Villa et al.**(**1985) studied the kinetics of the low-pressure synthesis of methanol from carbon monoxide and hydrogen along with the reverse shift reaction of carbon dioxide over a commercial $Cu/ZnO/Al_2O_3$ catalyst[1]. The model developed by Villa et al.(1985) considered CO as the only reactant and incorporated the CO_2 adsorption term in the model as high concentrations of CO_2 gets strongly adsorbed on the catalyst surface[1]. Following kinetic models were derived as given in equation (2.5),

$$r_1 = \frac{f_{CO}f_{H2}^2 - f_{CH3OH}/K_{eq,1}}{(C_1 + C_2 f_{CO} + C_3 f_{CO2} + C_4 f_{H2})^3} \qquad (2.5)$$

Where at $\overline{T}$= 506K

$$C_1 = \exp(3.49 + 4883(1/T - 1/\overline{T}))$$
$$C_2 = \exp(2.53 + 39060(1/T - 1/\overline{T}))$$
$$C_3 = \exp(3.70 + 15948(1/T - 1/\overline{T}))$$
$$C_4 = \exp(1.54 + 8229(1/T - 1/\overline{T}))$$

$$C_6 = \exp\left(5.18 + 9380(1/T - 1/\overline{T})\right)$$

Graaf et al. (1986,1988,1990) have developed kinetic model based on an LHHW mechanism, taking into account hydrogenation of CO and CO_2 as well as water-gas shift reactions (reactions (a), (b), and (c)) over a commercial $CuO/ZnO/Al_2O_3$ MK-101 Haldor Topsoe catalyst. They considered the rate laws are based on a dual-site LHHW mechanism. Operating conditions are in the range of 210 to 245°C at 15-50 bar[5,18,19].

$$r'_{CH3OH} = k_1 b_{CO}\left\{\frac{f_{CO}\, f_{H2}^{1.5} - (f_{CH3OH}/(f_{H2}^{0.5} * K_1))}{(1 + b_{CO}f_{CO} + b_{CO2}f_{CO2})(f_{H2}^{0.5} + (b_{H2O}/b_{H2}^{0.5})f_{H2O})}\right\} \quad (2.7)$$

$$r_{H2O} = k_2 b_{CO2}\left\{\frac{f_{CO\,2} f_{H2} - (f_{CO} f_{H2O}/K_2)}{(1 + b_{CO}f_{CO} + b_{CO2}f_{CO2})(f_{H2}^{0.5} + (b_{H2O}/b_{H2}^{0.5})f_{H2O})}\right\} \quad (2.8)$$

$$r_{CH3OH} = k_3 b_{CO2}\left\{\frac{f_{CO} f_{H2}^{1.5} - (f_{CH3OH} f_{H2O}/(f_{H2}^{1.5} K_3))}{(1 + b_{CO}f_{CO} + b_{CO2}f_{CO2})(f_{H2}^{0.5} + (b_{H2O}/b_{H2}^{0.5})f_{H2O})}\right\} \quad (2.9)$$

McNeil et al.(1989) developed a rate expression for CO_2 hydrogenation based on the available information on reaction mechanisms in the literature in contrast to empirical models based on experimental results for the operating conditions in the temperature range of 210-240°C and pressures from 2.89 to 4.38MPa [10]. The overall rate expression is as given below,

$$r = \frac{k'_f K_{CH} K_{H2}^2 K_H^2 K_{CO}\left(P_{CO}P_{H2}^2 - \frac{P_{CH3OH}}{Keq}\right)}{K_{CH}K_{H2}^{1.5}K_H^{1.5}K_{CO}P_{CO}P_{H2}^{1.5} + K_{CO2}P_{CO2} + K'_{H2}P_{H2}} + \frac{k''_f K_{H2} K_H K_{CO2} K_{CHO2}\left(P_{CO2}P_{H2} - \frac{P_{CH3OH}P_{H2O}}{K''eqP_{H2}^2}\right)}{K_{H2}^{0.5}K_H^{0.5}K_{CO2}K_{CHO2}P_{CO2}P_{H2}^{0.5} + K''_{CO2}P_{CO2}^2 + K_{H2O}P_{H2O}^3} \quad (2.10)$$

J Skrzypek et al.(1991) concluded that CO_2 is necessary for the process to start and proceed rather than CO. They considered only 2 reactions viz CO_2 hydrogenation and RWGS reaction. [8]. Following are the rate expressions,

$$r_1 = k_1 K_{H2}^2 K_{CO2}\left(\frac{(P_{CO2}P_{H2}^2) - (1/K_{p1})(P_{CH3OH}P_{H2O}/P_{H2})}{(1 + K_{H2}P_{H2} + K_{CO2}P_{CO2} + K_{CH3OH}P_{CH3OH} + K_{H2O}P_{H2O} + K_{CO}P_{CO})^3}\right) \quad (2.11)$$

$$r_2 = k_2 K_{H2} K_{CO2}\left(\frac{(P_{CO2}P_{H2}^2) - (1/K_{p2})(P_{CO}P_{H2O})}{(1 + K_{H2}P_{H2} + K_{CO2}P_{CO2} + K_{CH3OH}P_{CH3OH} + K_{H2O}P_{H2O} + K_{CO}P_{CO})^2}\right) \quad (2.12)$$

Vanden Bussche et al.(1996) developed a unique steady-state kinetic model for methanol synthesis and the water gas shift reaction on a commercial $Cu/ZnO/Al_2O_3$ catalyst. It effectively couples the rate of both overall reactions through the common surface oxygen intermediate. In addition to it, kinetic equations describe the influence of inlet temperature,

pressure, and feed composition[9]. The most relevant kinetic model considering a single-site adsorption mechanism is the one developed by Bussche and Froment in 1996[20]. A steady-state kinetic model was developed for methanol synthesis and the water gas shift reaction. The experiments used to determine the kinetic parameters were performed on an industrial $Cu/ZnO/Al_2O_3$ catalyst at pressures between 15 and 51 bar and for temperatures varying between 180 and 280°C.

$$r_{MeOH} = \frac{k'_{5a}K'_2K_3K_4K_{H2}P_{CO2}P_{H2}\left[1 - \frac{(1/K^*)(P_{CH3OH}P_{H2O})}{P_{CO2}P_{H2}^3}\right]}{\left(1 + (K_{H2O}/K_8K_9K_{H2})(P_{H2O}/P_{H2}) + \sqrt{K_{H2}P_{H2}} + K_{H2O}P_{H2O}\right)^3} \quad (2.13)$$

$$r_{RWGS} = \frac{k'_1P_{CO2}[1 - K_3^*(P_{H2O}P_{CO}/P_{CO2}P_{H2})]}{\left(1 + (K_{H2O}/K_8K_9K_{H2})(P_{H2O}/P_{H2}) + \sqrt{K_{H2}P_{H2}} + K_{H2O}P_{H2O}\right)^3} \quad (2.14)$$

A microkinetic model by Grabow and Mavrikakis (2011) has 49 elementary steps that represent the different intermediates involved in the methanol synthesis. An interesting result is that, under typical conditions, their study showed majorly CO_2 hydrogenation leads to the production of methanol. As concluded by the authors, further studies are required to determine more quantitative results[21]. As stated in the paper of Kunkes et al.(2014), one of the major mechanistic questions is related to whether methanol synthesis and RWGS are parallel pathways, whether methanol synthesis and RWGS share a common intermediate, or whether methanol formation proceeds by sequential RWGS and CO hydrogenation is discussed[22].

In the work done by Park et al.(2014), the kinetic model for the synthesis of MeOH and the corresponding reaction rates were developed assuming the adsorption of CO and CO_2 on various types of active sites of the commercial catalysts and using the rate-determining steps reported in the literature. Observations showed the negative effects of space velocity due to the reduced residence time, and the positive effects of the pressure by the increased concentration of the reactants. The developed model also showed the correlation between CO_2 hydrogenation and WGS reaction, and the maximum MeOH production could be determined by the optimal temperature and CO fraction. Additional experiments regarding various particle sizes confirmed the change in the effectiveness factor as a result of the internal diffusion limitation. By combining the kinetic model with the information regarding the effectiveness factor, it can be easily applied to the design of large-scale reactors for the synthesis of MeOH[6].

$$r_{CO} = \frac{k'_A K_{CO}(f_{CO}\, {f_{H2}}^{1.5} - f_{CH3OH}/(K_{PA}{f_{H2}}^{0.5}))}{(1 + K_{CO}f_{CO})(1 + K_{H2}^{0.5}{f_{H2}}^{0.5} + K_{H2O}f_{H2O})} \quad (2.15)$$

$$r_{RWGS} = \frac{k'_B K_{CO2}(f_{CO2}f_{H2} - f_{CO}f_{H2O}/K_{PB})}{(1+K_{CO2}f_{CO2})(1+K_{H2}^{0.5}{f_{H2}}^{0.5}+K_{H2O}f_{H2O})} \quad (2.16)$$

$$r_{CO2} = \frac{k'_C K_{CO2}(f_{CO2}{f_{H2}}^{1.5} - f_{CH3OH}f_{H2O}/(K_{PC}{f_{H2}}^{1.5}))}{(1+K_{CO2}f_{CO2})\left(1+K_{H2}^{0.5}{f_{H2}}^{0.5}+K_{H2O}f_{H2O}\right)} \quad (2.17)$$

Portha et al.(2017) developed kinetic expressions for methanol synthesis from a CO_2 /H_2 mixture based on a dual-site LHHW mechanism adopted from Graaf et al.,(1988). They found a good agreement between the model-predicted values and the experimental values in the range of operational parameters[7]. Bisotti et al.(2021) stated that the Graaf and the Vanden Bussche − Froment models are not fully adequate in characterizing conditions. The refitted Graaf model is proposed to be more flexible on the operating conditions and feed compositions than conventional models[4]. Over the years, the reaction pathway towards methanol using a Cu-based catalyst has been widely investigated due to Copper's highly active nature, and naturally available element of the earth's crust which makes it sustainable and economical [23,24]. It has been detailed investigated as a model catalyst for CO_2 to methanol reaction [25] and it is the only catalyst we are going to analyze and use for detailed simulation studies. In this chapter, detailed modeling studies are performed using reported models for high molar H_2 to CO_2 ratios to improve the performance characteristics for conversion of CO_2 to methanol over CuZA catalyst to have proper temperature control, most importantly to increase methanol yield per unit catalyst weight.

2.3 Comparison of kinetic models

All of the established kinetic models published in the literature can be classified into four categories according to the choice of carbon sources and reaction processes as given inTable 2.1 Kinetic models based on the selection of carbon sources and reaction mechanismsKinetic models based on different assumptions about reaction mechanisms and reaction parameters is given in Table 2.2.

Table 2.1 Kinetic models based on the selection of carbon sources and reaction mechanisms

Groups	Author	Source	Observations/ Findings	Reference
I	Takagawa et al.(1987)	CO & CO_2	1. Both CO and CO_2 were regarded as carbon sources	[2,18,26]
	Graaf et al.(1988)		2. RWGS was included in the model	
	Seidel et al.(2018)			
II	Klier et al.(1982)	CO & CO_2	1. Considered the CO and CO_2 hydrogenation reactions for kinetic modelling	[10,17]
	McNeil et al.(1989)		2. However, they did not include the RWGS reaction, as they assumed that the CO_2 could not directly be converted into CO during methanol synthesis	
III	Villa et al.(1985)	CO	1. The mechanism adopted proposed that methanol is produced from CO only	[1]
IV	Skrzypek et al.(1991)	CO_2	1. Considered the CO_2 hydrogenation reaction and the RWGS reaction	[7–9,15,27,28]
	Askgaard et al.(1995)		2. Through the RWGS reaction CO can be produced but may or may not take part in the methanol synthesis	
	Vanden Bussche and Froment.(1996)			
	Kubota et al.(2001)			
	Portha et al.(2017)			
	Kouzehli et al.(2024)			

Table 2.2 Kinetic models based on different assumptions about reaction mechanisms and reaction parameters

Sr. No.	Author	Observations/ Findings	References
1	Leonov et al.(1973)	1. First to present a kinetic model of methanol synthesis catalysed by a CuZA catalyst	[1]
		2. They did not include the effect of CO_2 in the reaction feed	
2	Villa et al.(1985)	1. Developed model including the partial pressure of CO_2, but the role of CO_2 as a reactant was also omitted	[1]
		2. Considered CO as a sole reactant and included a CO_2 adsorption term in the model as CO_2 gets strongly adsorbed on the catalyst surface at high concentrations	
3	Dybkjaer et al.(1986)	1. Developed a rate expression for methanol synthesis based on the LHHW mechanism, where H_2 is dissociated and adsorbed on one site on the catalyst surface and then reacts with adsorbed CO_2 on a nearby active site of the catalyst to form methanol	[29]
		2. According to this model, H_2 and H_2O are competing for the same active sites, and the carbonaceous gases (CO and CO_2) are adsorbed on different active sites	
4	Takagawa and Ohsugi.,(1987)	Derived empirical rate expressions for all three methanol synthesis models (3 equations) under a wide scale of operation parameters and included them in their kinetic model	[2]
5	Graaf et al.(1988)	1. Included CO and CO_2 hydrogenation reactions and WGS reactions into the model	[18]

		2. A total of 48 reaction schemes were derived from the various elementary reactions and then the model was statistically scrutinized for the best possible kinetic modeling	
		3. In 1990, they updated the set of reaction parameters for the kinetic model using their experiments carried out in a spinning basket reactor	
6	McNeil et al.(1989)	Developed a rate expression for CO_2 hydrogenation based on the available information on reaction mechanisms in the literature in contrast to empirical models based on experimental results	[10]
7	Skrzypek et al.(1991)	Experimentally observed that only CO_2 is the dominant carbon source during methanol synthesis and included CO_2 hydrogenation and the WGS reaction in their kinetic model.	[8]
8	Vanden Bussche and Froment.(1996)	1. A kinetic model of methanol synthesis was developed by assuming CO_2 as the main reactant, and all the reactions were carried out in a fixed bed reactor catalyzed by ICI 51-2 commercial catalyst	[9]
		2. In their proposed reaction mechanism, carbonate species were formed on the active site of the catalyst	
		3. They showed that the developed model successfully described the methanol formation rate at a wide range of temperature, pressure, feed gas composition	
9	Kubota et al.(2001)	1. Developed a kinetic model by assuming CO_2 hydrogenation as a dominant reaction in methanol synthesis	[30]

		2. They also compared their experimental yield data generated in the pilot plant study with the model-predicted data and found both were in good agreement	
10	Portha et al.(2017)	CO produced during RWGS reaction is considered in the kinetic modeling	[7]
11	Poto et al.(2022)	In this work, single-site, dual-site, and three adsorption-site kinetic models are used to study the kinetics of CO_2 hydrogenation to methanol over a $Cu/CeO_2/ZrO_2$ catalyst.	[31]
12	Kouzehli et al.(2024)	A new kinetic model based on a single active site LHHW mechanism was created after a thorough kinetic analysis of the synthesis of methanol from CO_2 hydrogenation over commercial $Cu/ZnO/Al_2O_3$ catalysts was presented.	[32]

2.4 Reactor model

Modelling of reactions

Various kinetic models are reported to describe methanol synthesis using copper-based catalysts. The modelling and simulation studies are performed for different reaction conditions, i.e., temperature, pressure, feedstock composition, and catalysts. Different kinetic rate expressions are deduced based on the rate-determining step. Generally, the LHHW kinetic model is constituted by the kinetic factor (mostly rate constant), driving force expression (depending on the reactants available in the reaction medium), and adsorption term. The rate of reaction is expressed as follows:

$$\text{Rate of reaction} = \left[\frac{\text{Kinetic factor} * \text{driving force}}{\text{Adsorption term}}\right]$$

The following three reactions are the basis for kinetic rate expressions:

$CO + 2H_2 \rightleftharpoons CH_3OH$ (A)

$CO_2 + H_2 \rightleftharpoons CO + H_2O$ (B)

$CO_2 + 3H_2 \rightleftharpoons CH_3OH + H_2O$ (C)

The elementary reactions for the above three reactions are represented for each species on the catalyst site as follows:

Reaction (A)

$COs1 + Hs2 \rightleftharpoons HCOs1 + s2$ (A1)

$HCOs1 + Hs2 \rightleftharpoons H_2COs1 + s2$ (A2)

$H_2COs1 + Hs2 \rightleftharpoons H_3COs1 + s2$ (A3)

$H_3COs1 + H\ s2 \rightleftharpoons CH_3OH + s1 + s2$ (A4)

Reaction (B)

$CO_2s1 + Hs2 \rightleftharpoons HCO_2s1 + s2$ (B1)

$H\ CO_2s1 + Hs2 \rightleftharpoons COs1 + H_2Os2$ (B2)

Reaction (C)

$CO_2s1 + Hs2 \rightleftharpoons HCO_2s1 + s2$ (C1)

$HCO_2s1 + Hs2 \rightleftharpoons H_2CO_2s1 + s2$ (C2)

$H_2CO_2s1 + Hs2 \rightleftharpoons H_3CO_2s1 + s2$ (C3)

$H_3CO_2s1 + Hs2 \rightleftharpoons H_2COs1 + H_2Os2$ (C4)

$H_2COs1 + Hs2 \rightleftharpoons H_3COs1 + s2$ (C5)

$H_3COs1 + Hs2 \rightleftharpoons CH_3OH + s1 + s2$ (C6)

There are 48 combinations of different kinetic rate expressions that can be derived, with the corresponding reaction rates of elementary reactions. This is predicated on the idea that only the surface reaction is the rate-controlling step and all other elementary reactions are in equilibrium. The driving-force groups are the sole variations among the kinetic rate expressions. Table 2.1 lists these driving-force categories. Here, we have considered all 48 combinations of the kinetic models those could be used for simulation studies. The Kinetic parameters, adsorption, and equilibrium constants are taken from Portha et al.(2017). The rate of reaction for each reaction is based on the dual-site Langmuir−Hinshelwood-Hougen-Watson (LHHW) mechanism with dissociative hydrogen adsorption. The A3B2C3 model rate expressions for three reactions are expressed as follows[7]

$$r_1 = k_1 b_{CO} \left\{ \frac{P_{CO} P_{H_2}^{1.5} - (P_{CH_3OH} / (P_{H_2}^{0.5} * K_1))}{(1 + b_{CO} P_{CO} + b_{CO_2} P_{CO_2})(P_{H_2}^{0.5} + (b_{H_2O} / b_{H_2}^{0.5}) P_{H_2O})} \right\} \quad (2.18)$$

$$r_2 = k_2 b_{CO2} \left\{ \frac{P_{CO\ 2} P_{H_2} - (P_{CO} P_{H_2O} / K_2)}{(1 + b_{CO} P_{CO} + b_{CO_2} P_{CO_2})(P_{H_2}^{0.5} + (b_{H_2O} / b_{H_2}^{0.5}) P_{H_2O})} \right\} \quad (2.19)$$

$$r_3 = k_3 b_{CO2} \left\{ \frac{P_{CO} P_{H_2}^{1.5} - (P_{CH_3OH} P_{H_2O} / (P_{H_2}^{1.5} K_3))}{(1 + b_{CO} P_{CO} + b_{CO_2} P_{CO_2})(P_{H_2}^{0.5} + (b_{H_2O} / b_{H_2}^{0.5}) P_{H_2O})} \right\} \quad (2.20)$$

In addition to the following rates, further simulations are performed using driving force terms as given in Table 2.3 for all the 48 model combinations to verify the best model fit for the experimental data.

Table 2.3 Driving force terms of rate expressions for reactions

Rate controlling step	Driving force group
A1	$P_{CO}\ {P_{H2}}^{0.5} - (P_{CH3OH}/{P_{H2}}^{1.5}K_1)$
A2	$P_{CO}\ P_{H2} - (P_{CH3OH}/P_{H2}K_1)$
A3	$P_{CO}{P_{H2}}^{1.5} - (P_{CH3OH}/{P_{H2}}^{0.5}K_1)$
A4	$P_{CO}\ {P_{H2}}^{2} - (P_{CH3OH}/K_1)$
B1	$P_{CO2}\ {P_{H2}}^{0.5} - P_{CO}P_{H2O}/({P_{H2}}^{0.5}K_2)$
B2	$P_{CO2}P_{H2} - P_{CO}P_{H2O}/K_2$
C1	$P_{CO2}{P_{H2}}^{0.5} - P_{CH3OH}P_{H2O}/({P_{H2}}^{2.5}K_3)$
C2	$P_{CO2}P_{H2} - P_{CH3OH}P_{H2O}/({P_{H2}}^{2}K_3)$
C3	$P_{CO2}{P_{H2}}^{1.5} - P_{CH3OH}P_{H2O}/({P_{H2}}^{1.5}K_3)$
C4	$P_{CO2}{P_{H2}}^{2} - P_{CH3OH}P_{H2O}/(P_{H2}K_3)$
C5	$P_{CO2}{P_{H2}}^{2.5}/P_{H2O} - P_{CH3OH}/({P_{H2}}^{0.5}K_3)$
C6	$P_{CO2}{P_{H2}}^{3}/P_{H2O} - P_{CH3OH}/K_3$

2.5 Adiabatic model development

An adiabatic system is described as no substantial loss or gain of heat with the surroundings taking place during the reaction. A detailed mathematical model is developed to assess the effectiveness of the catalyst in one single tubular adiabatic reactor. The following assumptions are considered to simplify the mathematical model.

i) Steady-state conditions

ii) Ideal gas behavior

iii) Radial heat and mass transfer effects are negligible

iv) No mass transfer limitations

A one-dimensional pseudo-homogeneous model is assumed since the particles in the two phases are so tiny, that gradients between them are not taken into account. Steady-state conditions are considered because the time scales of the processes involved are much larger than the time scale of any transient effects. For adiabatic fixed-bed reactors, steady-state conditions are commonly assumed because the system reaches a stable operating condition

over time, and the variations in temperature, pressure, and concentration along the reactor bed become negligible compared to the overall operating conditions. In this process, gas molecules behave closely to the predictions of the ideal gas law. This assumption is justified as the compressibility factor Z for the gas mixture at high pressure and temperature is estimated using the Soave–Redlich–Kwong equation of state (SRK) and is found to be nearly unity [33,34]. Assuming no mass transfer limitations, the reactor model is simplified to focus solely on the kinetics of the catalytic reaction[20,24].

The steady-state energy balance for the adiabatic catalytic reactor is given by the following equation,

$$\Delta Q - W_s + \sum_{i=1}^{3} F_i H_i|_{in} - \sum_{i=1}^{3} F_i H_i|_{out} = 0 \quad (2.21)$$

As there is no shaft work involved in the process, work done (W_s) = 0;

Heat removed or generated due to cooling,

$$\Delta Q = U\,\Delta A\,(Ta - T) = \frac{Ua}{\rho_b}\Delta W(Ta - T) \quad (2.22)$$

The final expression for differential element in a packed-bed reactor can be represented as,

$$\frac{dT}{dW} = \frac{\frac{Ua}{\rho_b}\Delta W(T_a - T) - \sum_{i=1}^{3} r_i \Delta H_{ri}}{\sum_{i=1}^{n} F_i\, C_{pi}} \quad (2.23)$$

For adiabatic reactor operation, (T_a-T) = 0,

$$\frac{dT}{dW} = \frac{\sum_{i=1}^{3} r_i \Delta H_{ri}}{\sum_{j=1}^{5} F_j\, C_{pj}} \quad (2.24)$$

Where,

T is the reactor temperature, K

T_a is ambient temperature, K

W is the weight of the catalyst, g

ΔH_{ri} is the heat of reaction in J/mol of i^{th} reaction, J/(mol.K)

F_j is the molar flow rate of species, j, mol/h.

C_{pj} is the specific heat capacity of species j, J/ (mol. K)[35]

The reactor simulations are performed using MATLAB® by varying inlet temperature in an adiabatic fixed-bed catalytic reactor and the effect of parameters on CO_2

conversion, methanol selectivity, methanol yield, and rate of reactions are studied. Inlet conditions along with feed composition and catalyst are specified in Table 2.3.

2.5.1 Effect of feed temperature

The effect of feed temperature on CO_2 conversion, methanol selectivity, and yield are simulated for a reactor pressure of 50 bar. The increase in feed temperature influences these parameters for the reactor shown in Figure 2a. The CO_2 conversion was minimal (<1%) at 100°C, and it reached a maximum of 24.54%, with a methanol yield of 16.42% at 200 °C and thereafter remained constant with an increase in feed temperatures (210 °C, 230 °C, 250 °C, and 300 °C). The rate of CO_2 hydrogenation favors the yield of methanol formation over CO hydrogenation as the reverse water gas shift reaction(RWGS) reaches its thermodynamic equilibrium condition to proceed with the reaction. As CO and CO_2 hydrogenation reactions are highly exothermic in nature, temperature inside the reactor increases for an adiabatic reactor. Therefore, the temperature profile shows increase in temperature for different inlet feed temperatures along the length of the catalyst bed as shown in in Figure 2b.

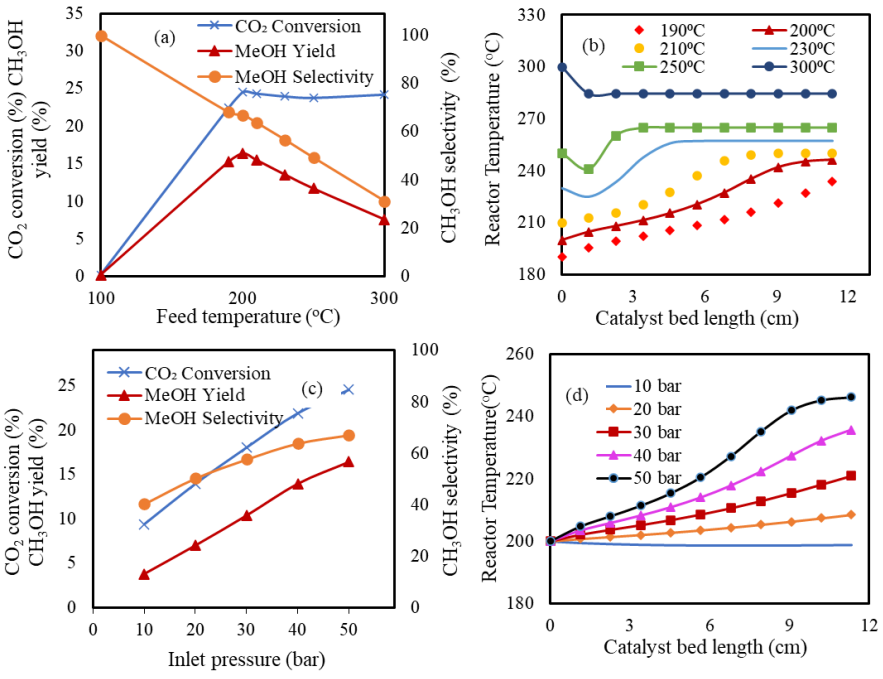

Figure 2.1 a) Effect of feed temperature on CO_2 conversion, MeOH selectivity, and yield b) Temperature profile at different feed temperatures at 50 bar pressure; c) Effect of pressure on CO_2 conversion, MeOH selectivity, and yield d) Temperature profile at different Inlet pressures from 10 to 50 bar at H_2: CO_2 = 3; GHSV = 720 h^{-1}

The optimum feed temperature to operate the reactor is 200°C to limit the reactor temperature to 250°C as the increase in reactor temperature may favour reverse water gas shift reaction. The effect of feed temperature showed an increase in conversion from 0.17% at 100°C to 24.23% at 200°C. However, selectivity towards methanol decreased with increase in temperature from 99.80% to 31.18%, hence, the maximum methanol yield of 16.42% is obtained for the feed temperature of 200°C.

2.5.2 Effect of pressure

The effect of pressure is studied to predict the performance parameters of the adiabatic reactor model in the range from 10 to 50 bar. The performance parameters with respect to the effect of temperature and pressure are represented in Supplementary information for an optimum feed temperature of 200 °C. The CO_2 conversion increased from 9.38% to 24.53% with decrease in rate from 10 bar to 50 bar. The selectivity towards methanol increased from 40.26% to 66.93%, eventually, the yield of methanol increased from 3.78% to 16.42%. It is observed that high-pressure reaction conditions are favourable to achieve increase in CO_2 conversion, methanol selectivity, and yield. The maximum CO_2 conversion of 24.53% and methanol yield of 16.42% are observed at a pressure of 50 bar as shown in in Figure 2c. The rise in reactor outlet temperature with respect to pressure is modelled along the catalyst bed length as shown in in Figure 2d. The maximum temperature of 246°C is obtained for a pressure of 50 bar and approaches plateau along the bed length.

2.6 Isothermal model development

A one-dimensional pseudo-homogenous model for an isothermal fixed-bed reactor is developed with mass balance, momentum balance, and Ergun equation to predict concentration and pressure profiles. The models are simulated using MATLAB considering three chemical reactions that involve the LHHW kinetic model. The model is represented with a pseudo-homogeneous plug-flow model with the following assumptions:

i. Steady-state regime
ii. No axial dispersion
iii. No mass transfer limitations

This leads to a one-dimensional model based on mole balance for multi-component species involving parallel reactions,

$F_{jo} - F_j + (V_{ij} * r_i) * \Delta W = 0$ (2.1)

For a differential element in a packed bed reactor,

$$\frac{dF_j}{dW} = \sum_{\substack{i=1-3 \\ j=1-5}} V_{ij} r_i \qquad (2.26)$$

Where,

Fj = molar flowrate of species

W = weight of the catalyst

V_{ij} = stoichiometric coefficient of species j in reaction i

r_i = rate of reaction for the species i

As the fluid passes through a packed bed of catalyst, it experiences pressure loss in the reactor. Specifically, when the size of catalyst particles is small, the pressure drop in the catalyst bed has to be considered. In this work, we have assumed that catalyst particles are of uniform size. The reactor simulations are performed using MATLAB® by varying inlet temperature in an adiabatic fixed bed catalytic reactor and the effect of parameters on CO_2 conversion, methanol selectivity, methanol yield, and the rate of reactions are studied. Inlet conditions along with feed composition and catalyst are specified in Table 2.3.

2.6.1 Effect of temperature and pressure

The isothermal model simulations are performed in the temperature range from 180 to 300°C for different pressures of 10, 30, and 50 bar. It is observed that CO_2 conversion increases with an increase in temperature until optimum and then attains a plateau to attain thermodynamic equilibrium as shown in Figure 2.2a. The maximum CO_2 conversion is attained in the temperature range from 230 to 250°C for 50 bar to achieve maximum methanol yield. The CH_3OH and CO selectivity as a function of temperature are shown in Figure 2.2b and Figure 2.2c. The CH_3OH selectivity increases to its maximum and decreases gradually with increase in temperature. On the contrary, CO selectivity decreases under optimal CO_2 conversion and increases further with increase in temperature. This may be due to favouring reverse water gas shift reaction at high temperatures leading to high CO formation whereas CO_2 and CO hydrogenation favours in the temperature range from 200 to 230°C. The yield of methanol is calculated based on CO_2 conversion and methanol selectivity. Hence, the optimal conditions for methanol yield were chosen to be 230-250°C as shown in Figure 2.2(d). These conditions form the basis for the operation of the reactor isothermally. The outlet product flow

rates are obtained for optimal conditions at a pressure of 50 bar, H_2-to-CO_2 ratio of 3 and GHSV of 720 h^{-1} as shown in Figure 2.3a. The product composition comprises CO, CO_2, CH_3OH and water formation. As evident from Figure 2.3, the optimal methanol formation is at 230-250°C due to CO and CO_2 hydrogenation at this temperature and a further increase in temperature favours reverse water gas shift reaction for CO and water formation. The individual reaction rates are simulated for a better understanding of in-situ reaction rates that contribute to methanol, CO, and water formation. As shown in Figure 2.3b, the reaction rate for reverse water gas shift reaction is much faster in comparison to CO and CO_2 hydrogenation. Therefore, the increase in CO contribution to methanol formation is further illustrated for different H_2 to CO_2 ratios to study with respect to relative reaction rates. It was clear that methanol formation increased with an increase in the H_2 to CO_2 ratio as reported in the literature[25]. Hence, the simulations are carried out to demonstrate the relative rates for three reactions with increased H_2 to CO_2 ratios.

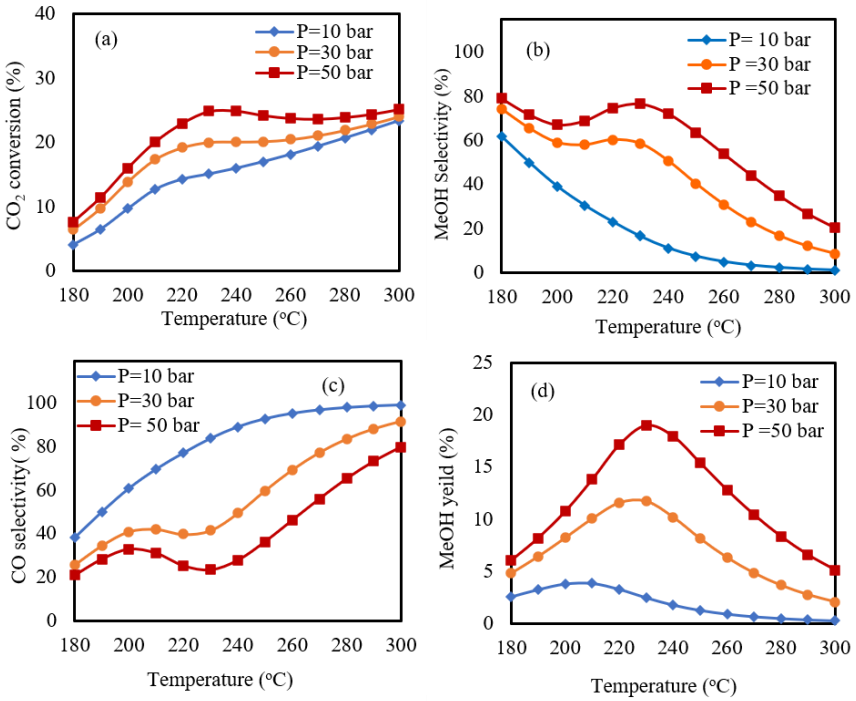

Figure 2.2 Effect of temperature on (a) CO_2 conversion (b) Methanol selectivity (c) Methanol yield for H_2: CO_2 = 3; GHSV = 720 h^{-1} at P = 50 bar

2.6.2 Effect of molar H_2/CO_2 ratio

The variation in H_2 to CO_2 molar ratio has significant effect on the rate of reactions as reported in the literature[25]. The effect of H_2 to CO_2 molar ratios of 3, 6, and 9 are simulated in the pressure range of 10 to 50 bar at an optimal temperature of 230 °C for different GHSV of 720 to 1800 h^{-1}. As shown in Figure 2.4(a-d), CO_2 conversion,

methanol selectivity, yield, and space-time yield have a direct influence with increase in H_2 to CO_2 ratio. The effect of pressure also has a direct influence on the performance parameters of the reactor model under similar conditions. Therefore, the present simulations are performed from 10 to 50 bar pressure and the maximum CO_2 conversion of 44.02%, selectivity of 81.18%, yield of 35.74%, and the space-time yield of 140.28 mg/g_{cat} .h is obtained at 1800 h^{-1} for H_2 to CO_2 ratio of 9. Although CO_2 conversion, methanol yield, and space-time of methanol yield are increased by a significant margin, the selectivity of methanol reaches thermodynamic equilibrium beyond the H_2 to CO_2 ratio of 6 as shown in Figure 2.4. Therefore, it is recommended to operate the reactor at high flow rates of H_2 to CO_2 ratio beyond stoichiometric quantities to improve the reactor performance.

Table 2.3 Comparison of inlet conditions and performance parameters for adiabatic and isothermal reactor models for H_2: CO_2 = 3 and P = 50 bar

Parameter	**Adiabatic model**	**Isothermal model**
CO_2 inflow (ml/min)	15	15, 30, 45
H_2 inflow (ml/min)	45	45, 90, 135
Total flow rate (ml/min)	60	60, 120, 180
H_2: CO_2 molar ratio	3	3, 6, 9
CuZA catalyst (g)	3	3
Particle size (µm)	400	400
GHSV (h^{-1})	720	720, 1260, 1800
CO_2 conversion (%)	24.54	25.02
Temperature (^oC)	190-300	180-300
Pressure (bar)	10-50	10-50
Performance parameters at 230^oC, 50 bar, WHSV = 720 h^{-1}; H_2/CO_2 = 3		
Methanol selectivity (%)	66.93	76.66
CO selectivity (%)	33.07	23.34
Methanol yield (%)	16.42	19.18
STY_{CH3OH} (mg/g_{cat}.h)	64.47	75.30

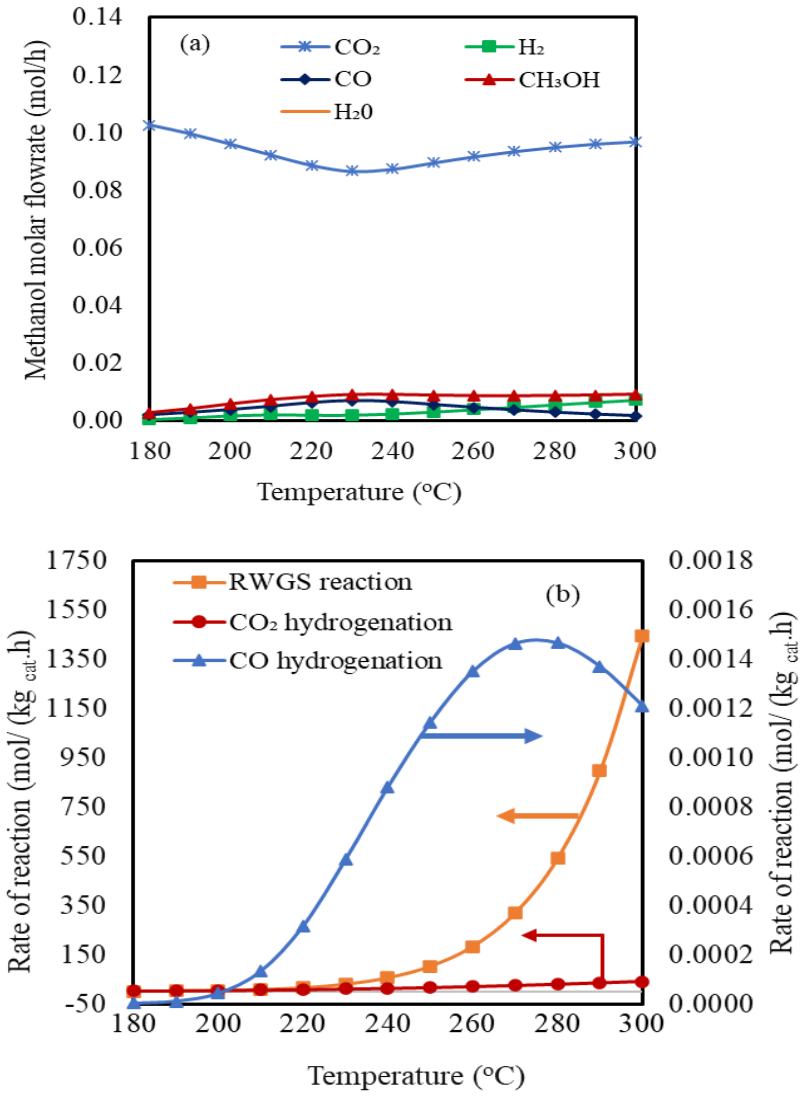

Figure 2.3 Effect of temperature on (a) Outlet molar flowrate (b) Rate of reaction for H_2 to CO_2=3; GHSV = 720 h^{-1} at P = 50 bar

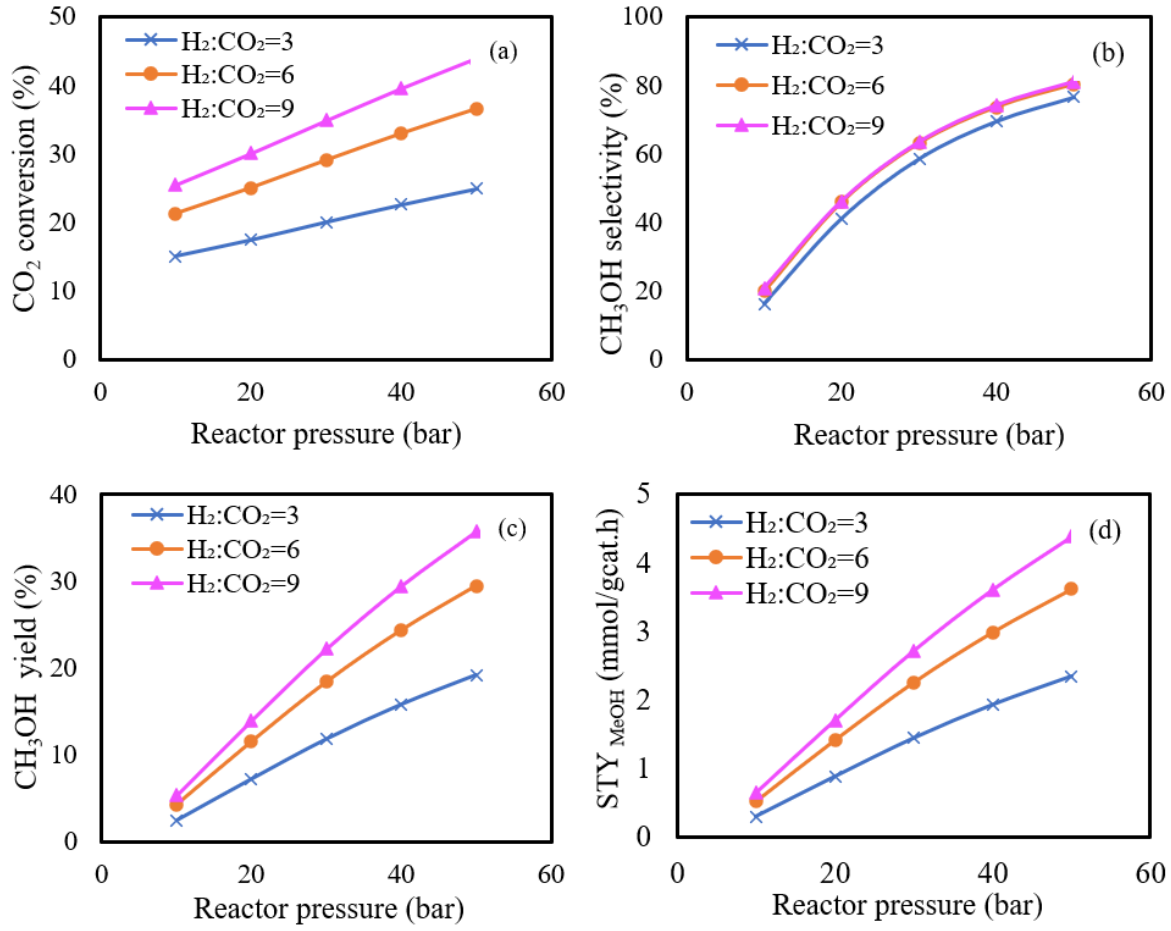

Figure 2.4 a) CO_2 conversion b) CH_3OH selectivity c) CH_3OH yield d) Space-time yield (STY) of methanol as a function of H_2 to CO_2 molar ratios on CuZA catalyst at T=230^oC

The model predictions compare very well with the experimental data for the H_2 to CO_2 ratio of 3, 6, and 9 for 10 bar pressure as reported in the literature[25]. Therefore, the simulations are extended up to 50 bar under optimal conditions and the performance parameters are compared for different ratios. The rate of enhancement in the performance parameters drastically improved for the H_2 to CO_2 ratio of 3 to 9 from 19.03% to 36.41%. Further simulations are analysed for different reaction rates to identify the reaction dominance that contributes to methanol production. The detailed simulation results are plotted for one-to-one comparison as given in Appendix A.

2.7 Comparison of adiabatic and isothermal reaction conditions

The comparative performance analysis for methanol production in adiabatic and isothermal reactors with respect to feed temperature is shown in Figure 2.5(b) and 2.5(c). It clearly indicates that as the feed temperature increases beyond 200°C, the methanol production decreases and the reaction rate drops at a shorter reactor length in the adiabatic reactor. Since

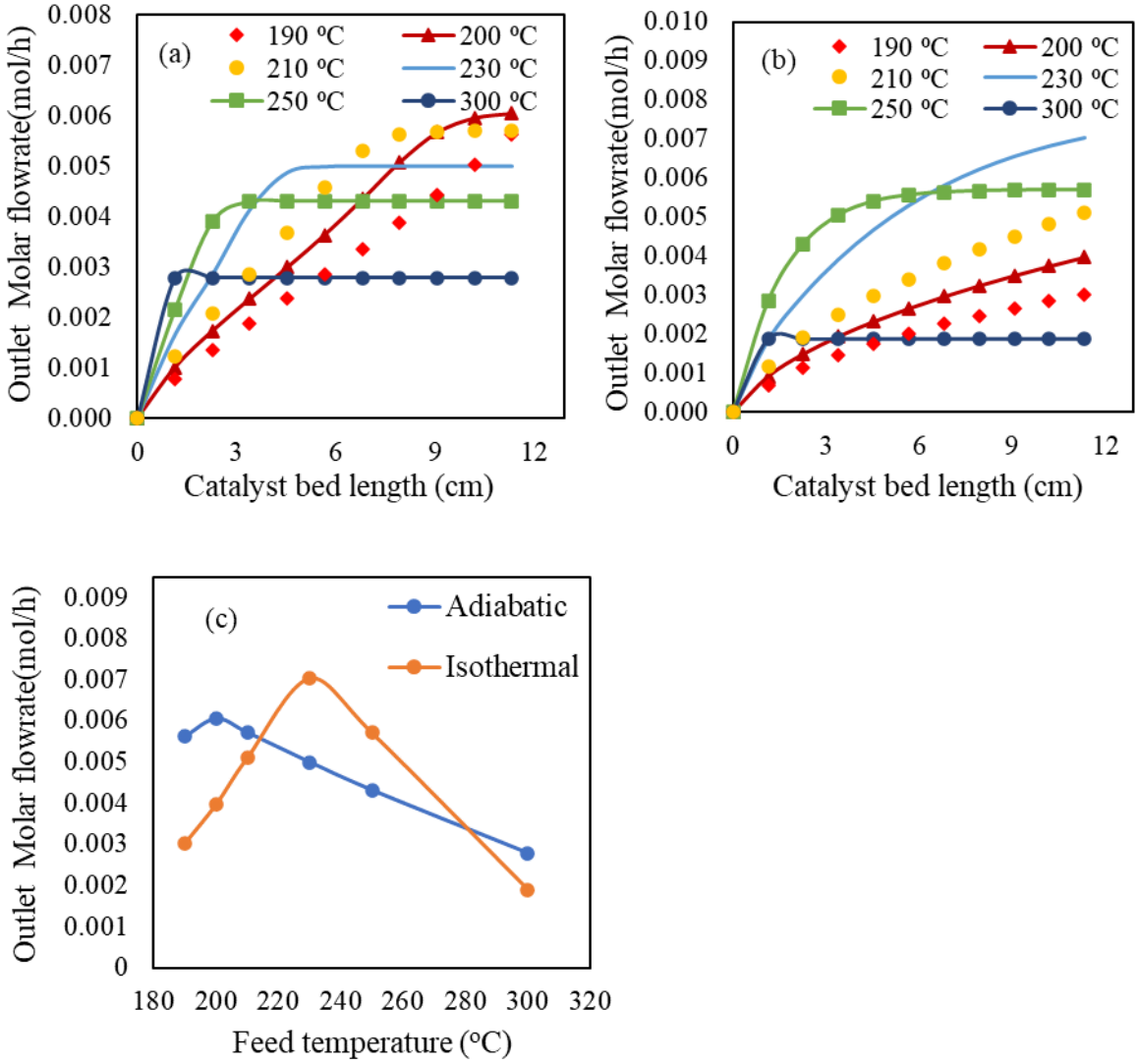

Figure 2.5 Effect of feed temperature on outlet molar flowrate of methanol along the length of a) Adiabatic and b) Isothermal reactor c) Comparison among adiabatic and isothermal reactor

the adiabatic reactor does not remove any heat generated during the reaction, a higher feed temperature raises the temperature throughout the reactor, moving the equilibrium to the left and hastening the rate at which the generation of methanol declines. In the isothermal reactor, as shown in Figure 2.7(b), the effect of the temperature rise is quite the opposite: although high temperature shifts the methanol production equilibrium to the left, it is compensated by the

increase of methanol production rate. Moreover, the reaction equilibrium can be maintained along the reactor as the cooling system keeps the temperature constant. However, when the feed temperature increases above 230°C, the higher reaction rate can no longer compensate for the shifted equilibrium, causing the methanol production to drop. The simulations are carried out for both adiabatic and isothermal reactor models to understand the behavior resulting in methanol formation in each case. The temperature profile is a significant factor contributing to the operation of a methanol synthesis reactor. Methanol is generated via reversible exothermic reactions (a) and (c), which benefit from low temperatures. In the adiabatic configuration, heat released inside the reactor accumulates and there is no cooling system available to take the heat out of the reactor. Consequently, the increase in temperature inhibits the exothermic reactions and eventually suppresses the methanol production. Contrary to the adiabatic case, the constant temperature can be achieved by providing a cooling system that takes out the heat produced from the exothermic reaction, while keeping the temperature constant. This maintains the reaction equilibrium in favour of the methanol production, eventually leading to a higher methanol yield at the end of the isothermal reactor. It is also worth noting that methanol production in an isothermal reactor does not level off until the end of the reactor length, indicating the possibility of obtaining an even higher methanol yield along the length of the reactor. The comparison between adiabatic and isothermal reactor operation can also be explained using equilibrium constants data. It is evident that equilibrium rate constants favour isothermal conditions with an increase in feed temperature for RWGS and CO, CO_2 hydrogenation reactions.

2.8 Sensitivity analysis

The studies on adiabatic and isothermal reactor conditions present a detailed examination of reaction kinetic modelling for a fixed bed reactor aimed at enhancing methanol production. Simulations were conducted over a temperature range of 180°C to 300°C and pressures of 10, 30, and 50 bar to evaluate reactor performance in terms of CO_2 conversion, CO and methanol selectivity and methanol yield. The optimal conditions at the pressure of 50 bar and temperature of 230°C were identified. A comprehensive sensitivity analysis was performed to assess the impact of variations in kinetic constants (k_1, k_2, k_3) within ±5 % range on CO_2 conversion, methanol selectivity, and methanol yield.

2.8.1 Sensitivity analysis: Rate constants varied at a time

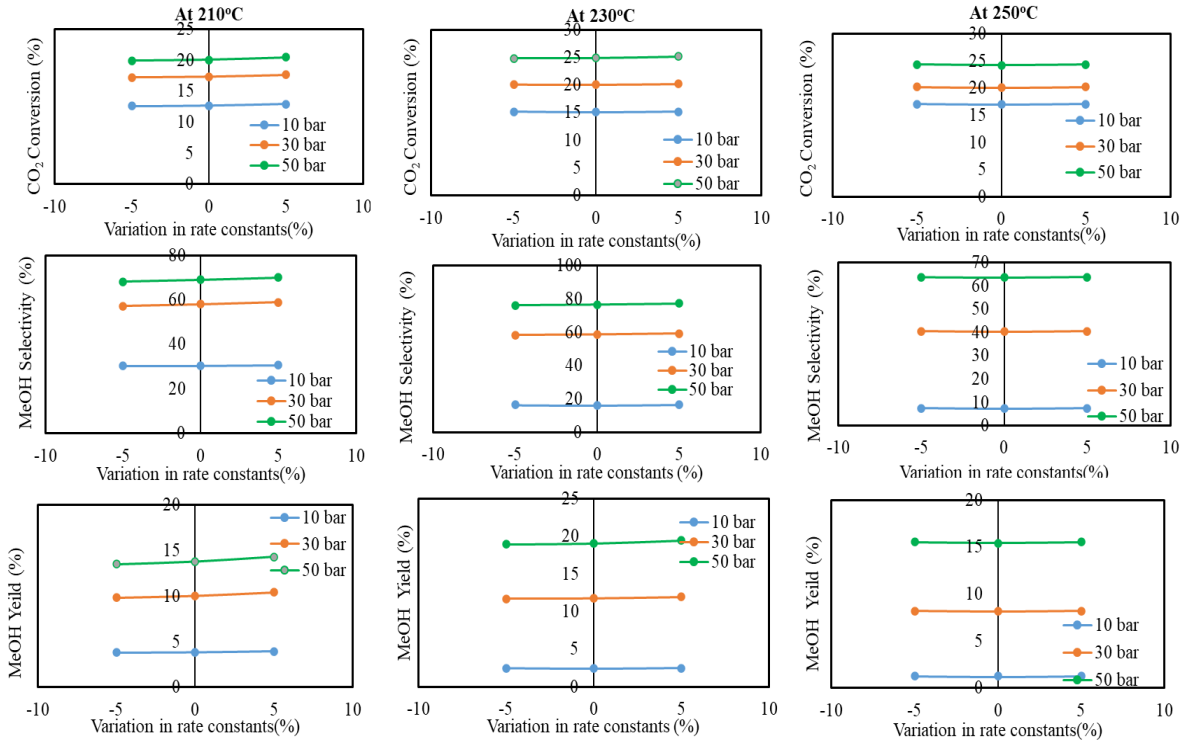

Figure 2.6 Sensitivity analysis with all the rate constants varied by a fixed change (-5 to +5%) at 210°C, 230°C, and 250°C for 10 bar, 30 bar, and 50 bar pressure.

There is not significant effect on the performance parameters observed when the values of rate constants varied at a time. It shows the robustness of the rate constant values as can be seen in Figure 2.6.

2.8.2 Sensitivity analysis: Rate constants varied seperately

CO_2 conversion remains stable with variation in all the rate constants showing minimal sensitivity whereas methanol selectivity and methanol yield remain fairly constant as k_1 shows little sensitivity at 10 bar as can be seen in Figure 2.7(a). Both decrease with Positive variation in k_2 and increase with negative variation in k_2. Both are more sensitive to change in k_3. The increase with Positive variation in k_3 and decrease with negative variation in k_3. At 30 bar, as shown in Figure 2.7(b). CO_2 conversion, methanol selectivity, and methanol yield remain nearly constant, indicating low sensitivity to k_1 and k_2. Positive variations in k_3 lead to increase in all values, while negative variations result in a decrease in all values. CO_2 conversion, methanol selectivity, and methanol yield remain nearly constant, indicating low sensitivity to k_1 and k_2 at 50 bar, as shown in Figure 2.7c. Positive variations in k_3 lead to an increase in all values, while negative variations result in a decrease in all values.

The analysis revealed that changes in kinetic constants have minimal effect on the reaction outcomes with the importance of accurate kinetic parameter estimation for process optimization. The sensitivity analysis offers valuable insights into enhancing the robustness and reliability of reaction models with implications for the design and optimization of industrial processes involving CO_2 conversion and methanol synthesis. The research advances the understanding of how variations in kinetic parameters influence catalytic reactions, providing practical guidance for improving the efficiency and reliability of CO_2 conversion and methanol production processes, thus supporting the broader objective of optimizing catalytic systems for better environmental and economic performance.

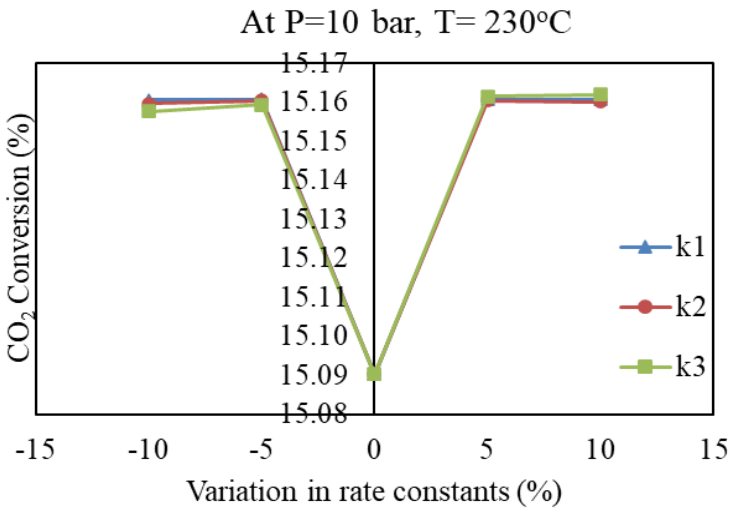

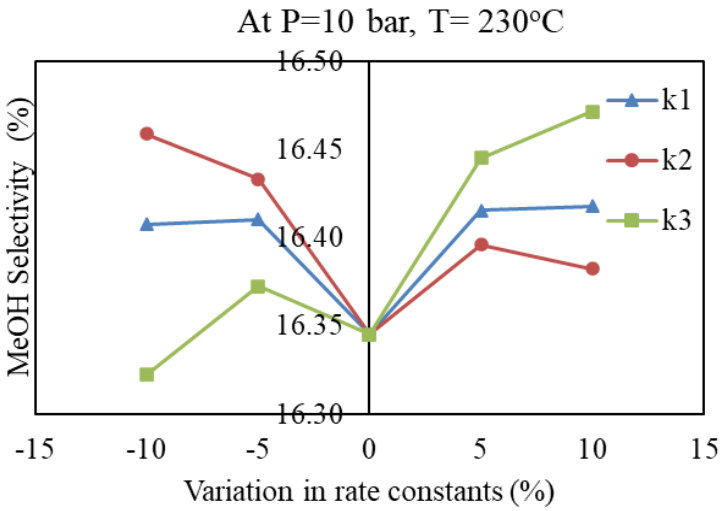

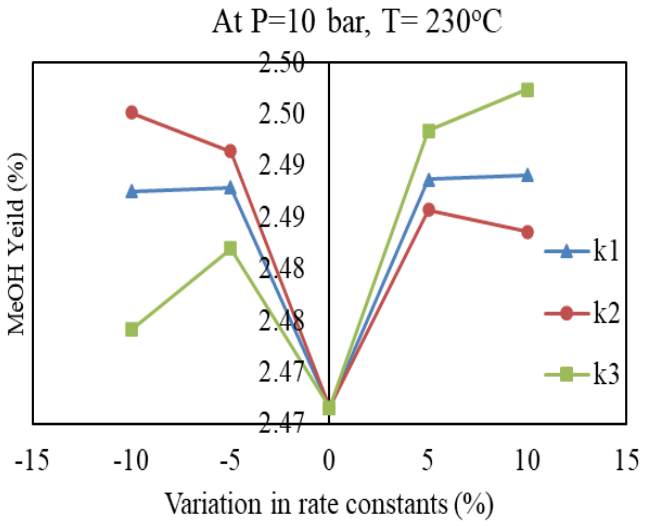
At P=10 bar, T= 230°C
MeOH Yeild (%)
2.50
2.50
2.49
2.49
2.48
2.48
2.47
2.47
-15
-10
-5
0
5
10
15
Variation in rate constants (%)
k1
k2
k3

(a)

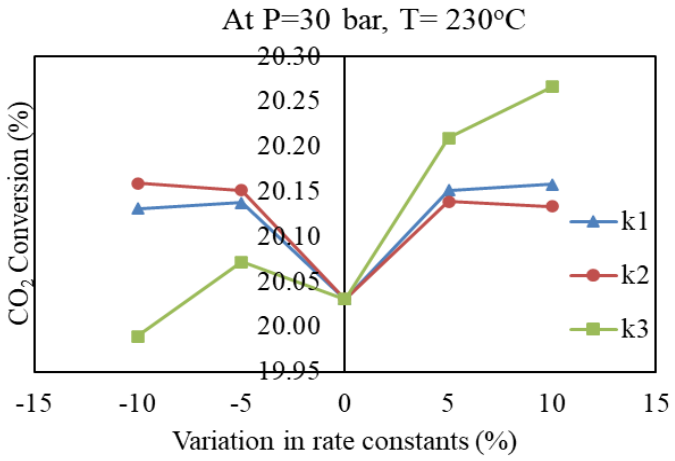
At P=30 bar, T= 230°C
CO2 Conversion (%)
20.30
20.25
20.20
20.15
20.10
20.05
20.00
19.95
-15
-10
-5
0
5
10
15
Variation in rate constants (%)
k1
k2
k3

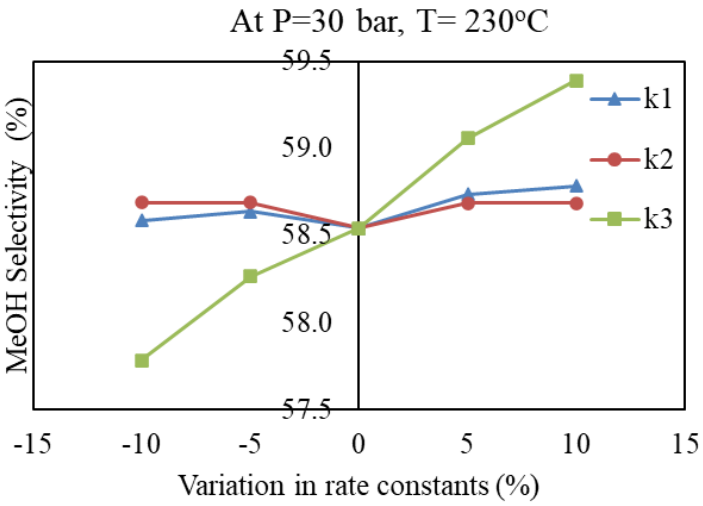
At P=30 bar, T= 230°C
MeOH Selectivity (%)
59.5
59.0
58.5
58.0
57.5
-15
-10
-5
0
5
10
15
Variation in rate constants (%)
k1
k2
k3

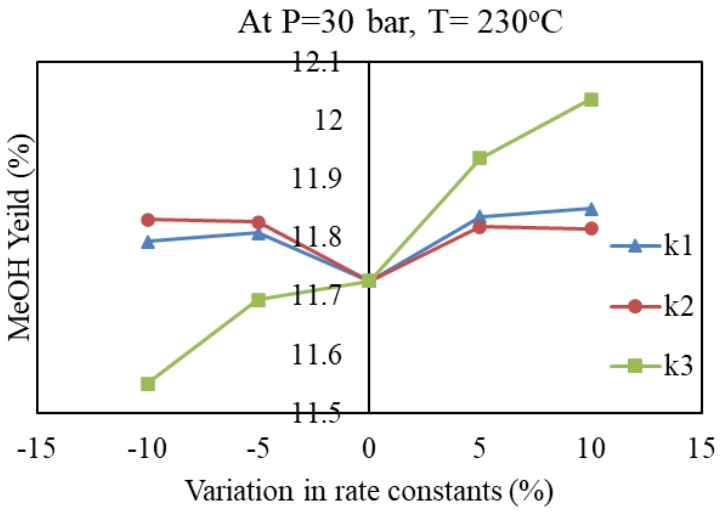
At P=30 bar, T= 230°C
MeOH Yeild (%)
12.1
12
11.9
11.8
11.7
11.6
11.5
-15
-10
-5
0
5
10
15
Variation in rate constants (%)
k1
k2
k3

(b)

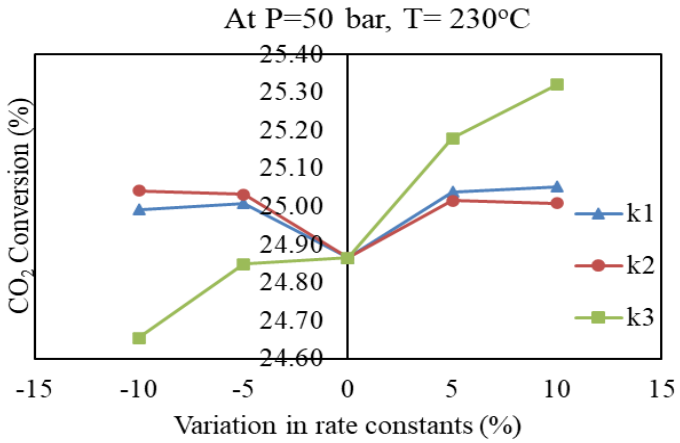
At P=50 bar, T= 230°C
CO2 Conversion (%)
25.40
25.30
25.20
25.10
25.00
24.90
24.80
24.70
24.60
-15
-10
-5
0
5
10
15
Variation in rate constants (%)
k1
k2
k3

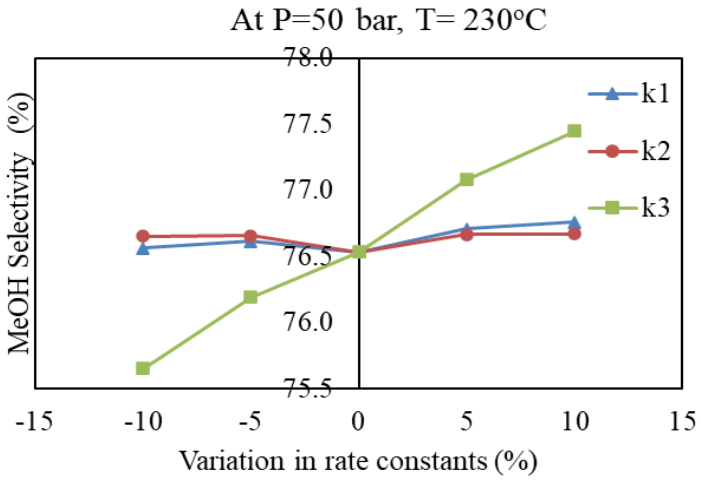
At P=50 bar, T= 230°C
MeOH Selectivity (%)
78.0
77.5
77.0
76.5
76.0
75.5
-15
-10
-5
0
5
10
15
Variation in rate constants (%)
k1
k2
k3

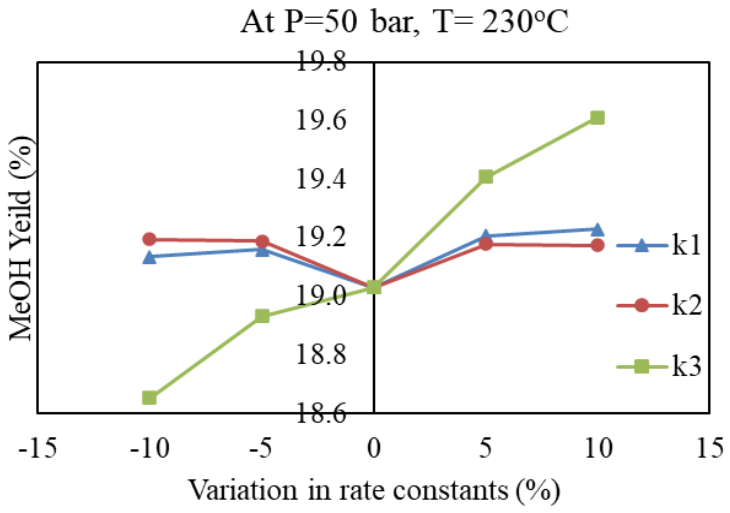

(c)

Figure 2.7 Sensitivity analysis of rate constants at 230°C at various pressures a) 10 bar b) 30 bar and c) 50 bar

2.9 Conclusions

The kinetic models developed for the synthesis of methanol from CO_2 are under high-pressure conditions that require experimental investigation for kinetic parameters evaluation. The role of CO in direct CO2 catalytic hydrogenation reactions is analysed through reverse water gas shift reactions using kinetic models in this work. Simulations are performed for increased mole ratios of H_2 to CO_2 to envisage the performance characteristics of the fixed bed reactor model. Based on modeling and simulation investigation for direct CO_2 hydrogenation, the conclusions are as follows:

i) The effect of temperature and pressure is well understood with adiabatic and isothermal model simulations.

ii) The isothermal model showed much better performance for CO_2 conversion, selectivity, and methanol yield. The result showed that the isothermal configuration converted 2.76% more methanol yield compared to the adiabatic reactor.

iii) The reaction rates showed that reverse water gas shift reaction enhanced the rate of methanol formation by 5 times via CO hydrogenation alone as CO formation favors with an increase in temperature. However, the contribution of CO_2 hydrogenation for methanol formation is much higher compared to CO hydrogenation.

iv) The higher H_2 to CO_2 ratio yielded better performance under low-pressure conditions as reported in the literature. Therefore, the model showed enhancement in the reaction rates

with improved methanol yields of 19.03%, 29.25%, and 36.41% for H_2 to CO_2 molar ratios of 3, 6, and 9, respectively.

v) A comprehensive sensitivity analysis showed <1% change in methanol yield for variations in kinetic constants (k_1, k_2, k_3) within ±5 % range.

vi) This sensitivity analysis offers valuable insights into enhancing the robustness and reliability of reaction models with implications for the design and optimization of industrial processes involving CO_2 conversion and methanol synthesis.

2.10 References

[1] Pierluigi Villa, * Plo Forzattl, Guido Buzzl-Ferraris, Guido Garone and IP. "Synthesis of alcohols from carbon oxides and hydrogen. 1. Kinetics of the low-pressure methanol synthesis." Ind Eng Chem Res 1985;24:12–9.

[2] Takagawa M, Ohsugi M. Study on reaction rates for methanol synthesis from carbon monoxide, carbon dioxide, and hydrogen. J Catal 1987;107:161–72. https://doi.org/10.1016/0021-9517(87)90281-8.

[3] Eksiri Z, Mozdianfard MR, Mirvakili A, Rahimpour MR. Two-dimensional modeling investigation of the modern methanol plate reactors. Chem Eng Res Des 2020;162:212–27. https://doi.org/10.1016/j.cherd.2020.08.009.

[4] Bisotti F, Fedeli M, Prifti K, Galeazzi A, Dell'Angelo A, Barbieri M, et al. Century of Technology Trends in Methanol Synthesis: Any Need for Kinetics Refitting? Ind Eng Chem Res 2021;60:16032–53. https://doi.org/10.1021/acs.iecr.1c02877.

[5] E.J.Stamhuis, G.H. Graaf, P.J.J.M. Sijtsema and GEHJ. Chemical equilibria in methanol synthesis 1986;41:2883–2890.

[6] Park N, Park MJ, Lee YJ, Ha KS, Jun KW. Kinetic modeling of methanol synthesis over commercial catalysts based on three-site adsorption. Fuel Process Technol 2014;125:139–47. https://doi.org/10.1016/j.fuproc.2014.03.041.

[7] Portha JF, Parkhomenko K, Kobl K, Roger AC, Arab S, Commenge JM, et al. Kinetics of Methanol Synthesis from Carbon Dioxide Hydrogenation over Copper-Zinc Oxide Catalysts. Ind Eng Chem Res 2017;56:13133–45. https://doi.org/10.1021/acs.iecr.7b01323.

[8] Skrzypek J, Lachowska M, Moroz H. Kinetics of methanol synthesis over commercial copper/zinc oxide/alumina catalysts. Chem Eng Sci 1991;46:2809–13. https://doi.org/10.1016/0009-2509(91)85150-V.

[9] Vanden Bussche KM, Froment GF. A steady-state kinetic model for methanol synthesis

and the water gas shift reaction on a commercial Cu/ZnO/Al_2O_3 catalyst. J Catal 1996;161:1–10. https://doi.org/10.1006/jcat.1996.0156.

[10] McNeil MA, Schack CJ, Rinker RG. Methanol synthesis from hydrogen, carbon monoxide and carbon dioxide over a CuO/ZnO/Al_2O_3 catalyst. II. Development of a phenomenological rate expression. Appl Catal 1989;50:265–85. https://doi.org/10.1016/S0166-9834(00)80841-6.

[11] Stangeland K, Li H, Yu Z. CO_2 hydrogenation to methanol: the structure–activity relationships of different catalyst systems. Energy, Ecol Environ 2020;5:272–85. https://doi.org/10.1007/s40974-020-00156-4.

[12] Nyári J, Izbassarov D, Toldy ÁI, Vuorinen V, Santasalo-Aarnio A. Choice of the kinetic model significantly affects the outcome of techno-economic assessments of CO_2-based methanol synthesis. Energy Convers Manag 2022;271. https://doi.org/10.1016/j.enconman.2022.116200.

[13] Al-Rowaili FN, Khalafalla SS, Al-Yami DS, Jamal A, Ahmed U, Zahid U, et al. Techno-economic evaluation of methanol production via gasification of vacuum residue and conventional reforming routes. Chem Eng Res Des 2022;177:365–75. https://doi.org/10.1016/j.cherd.2021.11.004.

[14] Nestler F, Müller VP, Ouda M, Hadrich MJ, Schaadt A, Bajohr S, et al. A novel approach for kinetic measurements in exothermic fixed bed reactors: Advancements in non-isothermal bed conditions demonstrated for methanol synthesis. React Chem Eng 2021;6:1092–107. https://doi.org/10.1039/d1re00071c.

[15] Kouzehli A, Kazemeini M, Ashrafi Moghaddam A. A robust kinetic modeling of CO_2 hydrogenation to methanol over an industrial copper–zinc oxide catalyst based on a single-active site mechanism. Int J Hydrogen Energy 2024;60:756–68. https://doi.org/10.1016/j.ijhydene.2024.02.176.

[16] Scott Fogler H. Elements of chemical reaction engineering. vol. 42. 1987. https://doi.org/10.1016/0009-2509(87)80130-6.

[17] Klier K, Chatikavanij V, Herman RG, Simmons GW. Catalytic synthesis of methanol from CO H2. IV. The effects of carbon dioxide. J Catal 1982;74:343–60. https://doi.org/10.1016/0021-9517(82)90040-9.

[18] Graaf H, Stamhuis EJ. Kinetics of low-pressure 1988;43:3185–95.

[19] G.H. Graaf, H.Scholtens, E.J.Stamhuis and AACMB. INTRA-PARTICLE diffusion limitations in low-pressure methanol synthesis. Chem Enyineeriny Sci Vol 45, No 4, Pp

773 783, 1990 Print Gt Britain CKKW 1990;45.

[20] Poto S, Vico van Berkel D, Gallucci F, Fernanda Neira d'Angelo M. Kinetic modelling of the methanol synthesis from CO2 and H2 over a CuO/CeO2/ZrO2 catalyst: The role of CO2 and CO hydrogenation. Chem Eng J 2022;435:134946. https://doi.org/10.1016/j.cej.2022.134946.

[21] Grabow LC, Mavrikakis M. Mechanism of methanol synthesis on cu through CO_2 and CO hydrogenation. ACS Catal 2011;1:365–84. https://doi.org/10.1021/cs200055d.

[22] Kunkes EL, Studt F, Abild-Pedersen F, Schlögl R, Behrens M. Hydrogenation of CO_2 to methanol and CO on Cu/ZnO/Al_2O_3: Is there a common intermediate or not? This work is dedicated to the memory and achievements of Dr. Haldor Topsøe. J Catal 2015;328:43–8. https://doi.org/10.1016/j.jcat.2014.12.016.

[23] Álvarez A, Bansode A, Urakawa A, Bavykina A V., Wezendonk TA, Makkee M, et al. Challenges in the Greener Production of Formates/Formic Acid, Methanol, and DME by Heterogeneously Catalyzed CO_2 Hydrogenation Processes. Chem Rev 2017;117:9804–38. https://doi.org/10.1021/acs.chemrev.6b00816.

[24] Ghosh S, Sebastian J, Olsson L, Creaser D. Experimental and kinetic modeling studies of methanol synthesis from CO2 hydrogenation using In_2O_3 catalyst. Chem Eng J 2021;416:129120. https://doi.org/10.1016/j.cej.2021.129120.

[25] Godini HR, Khadivi M, Azadi M, Görke O, Jazayeri SM, Thum L, et al. Multi-scale analysis of integrated c1 (Ch4 and co2) utilization catalytic processes: Impacts of catalysts characteristics up to industrial-scale process flowsheeting, part i: Experimental analysis of catalytic low-pressure CO_2 to methanol conversion. Catalysts 2020;10:1–22. https://doi.org/10.3390/catal10050505.

[26] Seidel C, Jörke A, Vollbrecht B, Seidel-Morgenstern A, Kienle A. Kinetic modeling of methanol synthesis from renewable resources. Chem Eng Sci 2018;175:130–8. https://doi.org/10.1016/j.ces.2017.09.043.

[27] Askgaard_1995.Pdf n.d.

[28] Raveesh A, Mona C, Jayveer S. Waste Management Initiatives in India for Human Well Being. Eur Sci J 2015;7881:1857–7881.

[29] Mondal U, Yadav GD. Methanol economy and net zero emissions: Critical analysis of catalytic processes, reactors and technologies. Green Chem 2021;23:8361–405. https://doi.org/10.1039/d1gc02078a.

[30] Hori H, Six C, Leitner W. Kinetic study of methanol synthesis from carbon dioxide and

hydrogen. Appl Organomet Chem 2001;15:121–6. https://doi.org/10.1002/1099-0739(200102)15.

[31] Poto S, Vico van Berkel D, Gallucci F, Fernanda Neira d'Angelo M. Kinetic modelling of the methanol synthesis from CO_2 and H_2 over a $CuO/CeO_2/ZrO_2$ catalyst: The role of CO_2 and CO hydrogenation. Chem Eng J 2022;435. https://doi.org/10.1016/j.cej.2022.134946.

[32] Kouzehli A, Kazemeini M, Moghaddam AA. International Journal of Hydrogen Energy A robust kinetic modeling of CO_2 hydrogenation to methanol over an industrial copper – zinc oxide catalyst based on a single-active site mechanism 2024;60:756–68.

[33] Arab S, Commenge J, Portha J, Falk L. Methanol synthesis from CO_2 and H_2 in multi-tubular fixed-bed reactor and multi-tubular reactor filled with monoliths Chemical Engineering Research and Design Methanol synthesis from CO_2 and H_2 in multi-tubular fixed-bed reactor and multi-tubular. Chem Eng Res Des 2014;92:2598–608.

[34] Skrzypek J, Lachowska M, Grzesik M, Słoczyński J, Nowak P. Thermodynamics and kinetics of low pressure methanol synthesis. Chem Eng J Biochem Eng J 1995;58:101–8. https://doi.org/10.1016/0923-0467(94)02955-5.

[35] Zhu J, Araya SS, Cui X, Sahlin SL, Kær SK. Modeling and design of a multi-tubular packed-bed reactor for methanol steam reforming over a $Cu/ZnO/Al_2O_3$ catalyst. Energies 2020;13. https://doi.org/10.3390/en13030610.

Chapter 3

Experimental studies for direct conversion of CO_2 to methanol production in fixed bed reactor (FBR)

3.1 Introduction

The atmosphere's content of the greenhouse gas carbon dioxide is steadily rising. Currently, several techniques are being investigated to either lower the CO_2 content or transform it into useful chemical compounds. The work aims to valorise CO_2 while reducing emissions and to meet the demand for chemicals that have applications in various chemical industries. In particular, CO_2 hydrogenation presents the most elevated possibility for industrial application with a technology readiness level (TRL) of 9 with a noteworthy capability for net CO_2 utilization[1]. However, there are challenges remain in the selective hydrogenation of CO_2 to methanol due to its thermodynamically unstable nature. Hydrogenation of carbon dioxide to methanol is an exothermic reaction with experimentally determined enthalpy change $\Delta H_{298\,K}$ = −49.4 kJ/mol. As two molecules of products form from four molecules of reactants, low temperature and high pressure the production favours methanol whereas high-temperature favours competing reverse water–gas shift (RWGS) reaction. Consequently, a compromise must be struck between high temperatures, which increase the reaction rate, and at low temperatures, which increase the conversion. We aim to investigate temperature, and pressure conditions to either shift the reaction equilibrium towards a desirable product and/or to have proper temperature control, most importantly to increase methanol yield per unit catalyst weight. Developing a highly effective catalyst that can be operated at lower temperatures is one of the ways to overcome this equilibrium limitation to reduce the energy barrier for the breaking one C–O bond from a CO_2 molecule and thus improves the reaction kinetics[2,3]. Cu-based catalyst has been widely investigated as a highly active and naturally available element in the earth's crust which makes it sustainable and economical. This catalyst is considered as model catalyst for the conversion of CO_2 to methanol production [3–7]. In an effort to enhance the process, several researchers have studied the mechanism of CO_2 hydrogenation to methanol throughout the years; nevertheless, the molecular mechanism is still hotly contested. Although the precise nature of the active site is yet unknown, its significance throughout the reaction is widely established. Apart from catalyst studies, kinetic modelling(KM) is largely used in techno-economic assessment (TEA) studies[8,9]. The following choices for KM usage during a TEA are listed in decreasing order of confidence: 1) Ideally, laboratory tests on the specified catalyst and raw materials should be carried out, and the results should be matched to a KM; 2) Comparing TEAs conducted with multiple KMs can provide an estimate of the TEA's uncertainty in place of directly relevant experimental corroboration of a KM used in a TEA study; 3) if only one KM is used, a more recent one should be chosen because it is more

likely to represent the current commercial state-of-the-art for a given catalyst composition and could predict yield and conversion with higher accuracy. A wide range of kinetic models with appropriate assumptions regarding the reaction mechanisms and their parameters have been suggested by researchers over the last few decades [10–12].

The rate expressions are developed based on a dual-site LHHW mechanism [13–19]. Although various kinetic models have developed, the CO_2 hydrogenation to methanol reaction mechanism was relatively unclear. This is due to the major thermodynamic limitations on conversion due to competing reverse water–gas shift (RWGS) reactions [20]**.** Industrially, it depends on various performance parameters such as efficiency, safety and CO_2 mitigation, etc. to adopt technology and there is a wide variety of opportunities for understanding how methanol synthesis technologies are developed by studying the reaction mechanism and its associated kinetics.

To study mechanistic approaches for the conversion of CO_2 to useful products, it is necessary to develop a kinetic equations that describe the effects and predict the temperature distribution quantitatively in industrial reactors[21]. Methanol production through the conversion of carbon dioxide route is obtained via catalytic process using three reversible reactions: (a) carbon monoxide hydrogenation (reaction 1), (b) reverse water-gas shift (RWGS) reaction (reaction 2) and (c) carbon dioxide hydrogenation (reaction 3).

$CO + 2H_2 \leftrightarrows CH_3OH$ $\Delta H_r°(298\ K) = -90.5\ kJ/mol$ *(a)*

$CO_2 + H_2 \leftrightarrows CO + H_2O$ $\Delta H_r°(298\ K) = +41.1\ kJ/mol$ *(b)*

$CO_2 + 3H_2 \leftrightarrows CH_3OH + H_2O$ $\Delta H_r°(298\ K) = -49.4\ kJ/mol$ *(c)*

Low temperature and higher pressure are considered to be the most suitable thermodynamic conditions for the synthesis of methanol according to the Le Chatlelier principle[22,23]. This allows high methanol selectivity as the RWGS reaction is endothermic and therefore, suppresses at low temperatures. It is needed to have a trade-off temperature to maximize CO_2 conversion to methanol. In this chapter, detailed modelling studies are performed using reported models for high molar H_2 to CO_2 ratios to improve the performance characteristics for conversion of CO_2 to methanol over CuZA catalyst to have proper temperature control, most importantly to increase methanol yield per unit catalyst weight.

3.2 Literature review

The direct conversion of CO_2 to methanol in a fixed bed reactor offers a promising route for CO_2 utilization, providing a sustainable pathway to produce methanol, which is widely used in energy and chemical industries. Fixed bed reactors (FBRs) are advantageous for their simple design, easy catalyst loading, and scalability. Copper (Cu) catalysts supported on zinc oxide (ZnO) and alumina (Al_2O_3) are widely used due to their high activity and selectivity towards methanol. The incorporation of promoters like ZrO_2 has been shown to improve catalytic performance, particularly by enhancing CO_2 adsorption and stabilizing active sites [16].

Methanol synthesis from CO_2 involves a multi-step hydrogenation mechanism, often following pathways that include intermediates like Formate species. Fixed bed reactor studies reveal that Cu-based catalysts facilitate CO_2 activation and hydrogenation, with reaction temperature, pressure, and gas flow rate influencing methanol selectivity and overall conversion rates [24]. Studies using advanced spectroscopy techniques, such as in-situ DRIFTS and XPS, provide insights into the surface chemistry during CO_2 hydrogenation, which helps optimize catalyst composition and operating conditions[25].

In FBRs, exothermic reactions such as CO_2 hydrogenation require effective thermal management to maintain stable temperatures and prevent hot spots. Multi-stage heating and tailored reactor designs help manage these challenges and maintain high methanol yields [26]. CO_2 to methanol reactions are sensitive to pressure, temperature, and H_2/CO_2 ratio. Optimizing these parameters in FBRs is essential to enhance methanol selectivity. Studies have shown that higher pressures favor methanol formation, while an optimal temperature range ensures efficient CO_2 conversion without undesired byproducts like CO [27].

As environmental issues have become increasingly urgent, several studies on the development of catalysts to produce methanol from CO_2 have been conducted. An experimental investigation of the CuO/ZnO catalyst for the CO_2 hydrogenation process to methanol was carried out by Fujita et al.(1998) [28]. Arena et al.(2007) then used co-precipitation under ultrasonic irradiation to create a $CuO/ZnO/ZrO_2$ catalyst and assessed its effects on conversion and reaction rate[29]. In an effort to enhance CO_2 hydrogenation processes, several researchers have recently concentrated on the effects of active metals including Pd, Au, and Ag on different catalysts. The methanol production rate on Au/ZnO catalysts was examined by Hartadi et al.(2016) who discovered that the catalyst activity for CO_2 hydrogenation in CO_2/H_2 is noticeably greater than that for CO hydrogenation in CO/H_2 synthesis gas[30]. Typically,

commercial methanol synthesis catalysts (Cu− ZnO−Al_2O_3) are prepared by a coprecipitation. Although many catalyst materials with various compositions have been found active and selective for methanol synthesis from CO_2, the Cu−ZnO system prepared by coprecipitation still remains the most investigated due to its high activity and high product selectivity besides economic advantages. As CuZA catalyst is widely used in industries due to its advantages for carrying out catalytic hydrogenation of carbon dioxide to methanol. In literature it is mentioned that 69% catalyst is prepared by coprecipitation method from last decade literature. So, we initially prepare copper zinc oxide alumina (CuZA) catalyst by using coprecipitation method. Summary of the catalysts, their preparation method, reaction parameters like temperature, pressure, gas hourly space velocity (GHSV), and its effect on the conversion of carbon dioxide, methanol selectivity and yield is given in the Table 3.1 below.

Table 3.1 Summary of the literature study of Catalyst, coprecipitation method and reaction parameters on the conversion of CO_2, methanol selectivity and yield

Catalyst	Preparation method	Temperature (^{0}C)	Pressure (bar)	Mole ratio H_2: CO_2	GHSV ($cm^3\ h^{-1}\ gcat^{-1}$)	CO_2 Conversion (%)	MEOH selectivity (%)	MEOH yield (%)	Author / Reference
Cu/ZnO/Al_2O_3 (MET1)	Co-precipitation	200	10	3	684	7.9	66.1	5.2	Hamid, et al. (2020) [31]
		230	10	3	684	16.9	33.7	5.7	
		260	10	3	684	17.1	0	0	
		200	10	6	684	14.5	77.6	11.3	
		230	10	6	684	25.4	38.8	9.9	
		260	10	6	684	24.7	0.2	0	
		200	10	9	684	18.6	77.6	14.4	
		230	10	9	684	31	43.7	13.5	
		260	10	9	684	22.6	14.6	3.3	
Cu/ZnO/Al_2O_3 (MET3)	Co-precipitation	200	10	3	684	8	80.3	6.4	
		230	10	3	684	15.2	39	5.9	
		260	10	3	684	20.6	18.8	3.9	

		200	10	6	684	11.9	76.8	9.1	
		230	10	6	684	22.8	46.5	10.6	
		260	10	6	684	26.9	15.1	4.1	
		200	10	9	684	16.8	79.2	13.3	
		230	10	9	684	29.6	44.7	13.2	
		260	10	9	684	34.3	14.9	5.1	
$Cu/ZnO/Al_2O_3$	Co-precipitation	270	50	3	4000	23.7	43.7	10.36	Wei Wei et al. (2015) [32]
$Cu/ZnO/Al_2O_3$ /ZrO2	Co-precipitation	190	50	3	4000	10.7	81.8	8.75	
Cu/ZrO_2	Co-precipitation	250	30	3	..	1.3	95	1.2	Wee et al.(2020)
$Cu/ZnO/ZrO_2$	Co-precipitation	250	50	2	..	26.8	91.7	24.6	
$Cu/ZnO/Al_2O_3$	Co-precipitation	250	30	3	..	9	17	1.5	
$Cu/ZnO/ZrO_2$	Co-precipitation	250	35	4	..	8	15	1.2	
$Cu/ZnO/ZrO_2$	Co-precipitation(Catalyst diluted by SiC)	240	30	3	..	17.5	48.4	8.5	
$Cu/ZnO/Al_2O_3$	Co-precipitation (Catalyst diluted by quartz)	250	30	3	..	21.1	50.1	10.6	
$Cu/\gamma\text{-}Al_2O_3$	Co-precipitation	260	30	3	..	15.6	10.7	1.7	
CZA-K	Co-precipitation	240	30	3	2400	14	96	13.4	Nagaraju Pasupulety et al. (2021)
$Cu/ZnO/Al_2O_3$	Co-precipitation	260	331	10	182000	65.8	77.3	7.73	Atul Bansode et al. (2017) [4]
$Cu/ZnO/Al_2O_3$	Co-precipitation	260	331	10	20000	95.7	98.2	1.58	
$Cu/ZnO/Al_2O_3$	Co-precipitation	280	442	3	100000	65.3	91.9	15.2	
30CuZn–ANIT	Co-precipitation with zinc nitrate	240	50	..	10000	6.5	59	3.83	Laetitia Angelo et al. (2015)

									[33]
	Co-precipitation with zinc nitrate	260	50	..	10000	15.5	42	6.51	
	Co-precipitation with zinc nitrate	280	50	..	10000	19.5	37	7.21	
30CuZn–Aox	Co-precipitation with zinc oxide	240	50	..	10000	12.9	46	5.93	
	Co-precipitation with zinc oxide	260	50	..	10000	20.8	39	8.11	
	Co-precipitation with zinc oxide	280	50	..	10000	24	35	8.4	
30%Cu/41%ZnO/21% Al_2O_3	Co-precipitation	210	50	2	7800	5.1	20	1.02	Portha et al.(2017) [16]
30%Cu/41%ZnO/21% Al_2O_3	Co-precipitation	210	50	3.9	7800	7.7	45	3.46	
30%Cu/41%ZnO/21% Al_2O_3	Co-precipitation	210	50	5	7800	8.8	38	3.34	
30%Cu/41%ZnO/21% Al_2O_3	Co-precipitation	210	50	6	7800	9.8	40	3.92	
30%Cu/41%ZnO/21% Al_2O_3	Co-precipitation	220	50	3.9	7800	11.1	43	4.77	
30%Cu/41%ZnO/21% Al_2O_3	Co-precipitation	230	50	3.9	7800	15.8	38	6.00	

3.3 Material and Methods

3.3.1 Catalyst

For each experiment, a commercial copper-based catalyst (CuZA) is used. Figure 3.1 shows the commercial methanol synthesis catalysts pellets and sieved particles. A commercial methanol synthesis catalyst ($Cu/ZnO/Al_2O_3$, Product No.: 45776) was purchased from Alfa Aesar. ThermoFischer Scientific (Product ID: 45776). The molar concentration of each component in $Cu/ZnO/Al_2O_3$ (CuZA)is in the range of CuO = 60 to 68 %, ZnO = 22 to 26 %, Al_2O_3 = 8 to 12%, and MgO = 1 to 3 %.

(a)

(b)

Figure 3.1 Commercial Cu/ZnO/Al_2O_3 catalyst from ThermoFischer Scientific a) Pellet form and b) Crushed form

3.2.2 Catalyst Characterization

3.2.2.1 X-ray diffraction (XRD)

The crystalline nature and phase formation of the sample was analyzed using Powder X-ray diffraction (PXRD) data were collected from a PAN analytical X'pert Pro dual goniometer equipped X-ray diffractometer using Cu Kα (1.5418 Å) radiation within a scanning angle of 2 θ from 5 to 95° and a step of 2° every 1 minute.

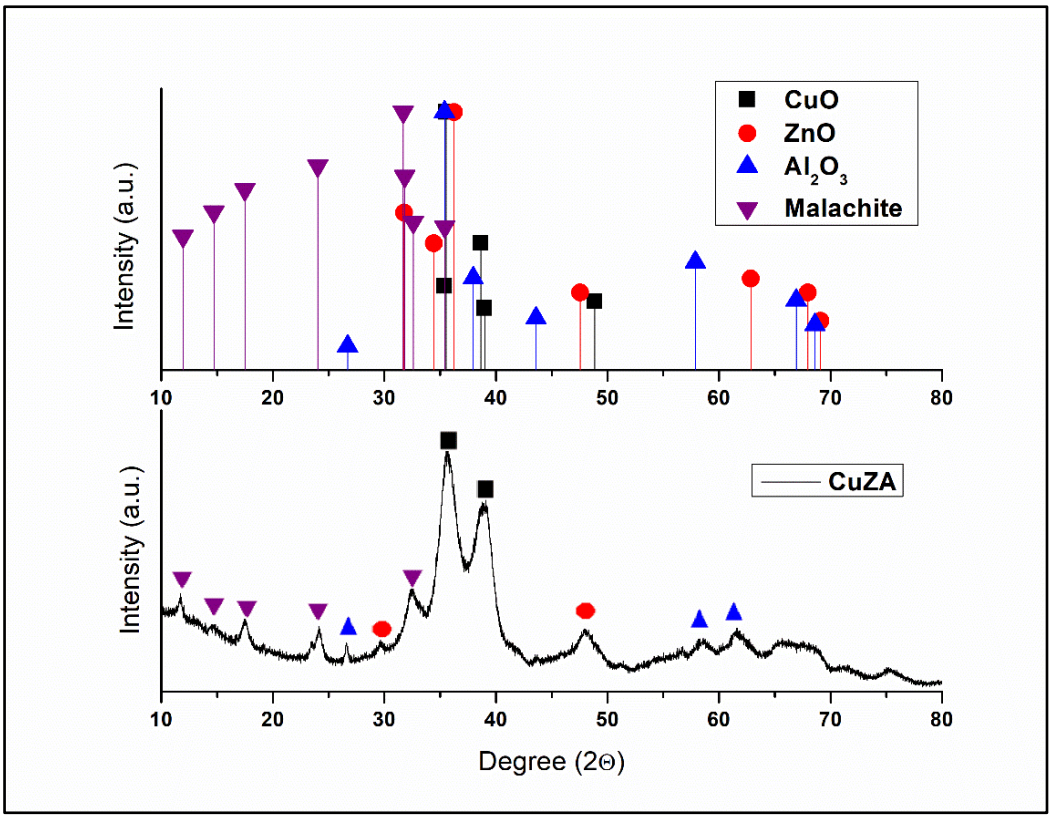

Figure 3.2 XRD pattern for CuZA catalyst

3.2.2.2 Nitrogen adsorption-desorption (BET)

Pore volume, average pore radius, and specific surface area measurements of calcined catalysts were performed by nitrogen adsorption−desorption at −76°C using the Brunauer−Emmett−Teller (BET) method on a Quantachrome BET apparatus. DFT method is used. Before analysis, all the samples were outgassed at 250 ^{o}C under vacuum for 3 h to remove adsorbed moisture. The adsorption–desorption curve shows type IV isotherm characteristics having a prominent hysteresis loop in the relative pressure (P/P_o) range of 0.2 to 1, signifying its mesoporous structure. The presence of hysteresis is due to the capillary phenomenon. Gases condense in the tiny capillary pores of the solid at pressures below the saturation pressure of the gas. Pore size distribution gives us an idea of the presence of mesoporous particles in the sample. (By IUPAC mesoporous pore diameters lies between 2 to 50 nm). Catalyst has a specific surface area of 123.129 m^2/g and a total pore volume of 0.2701 cc/g.

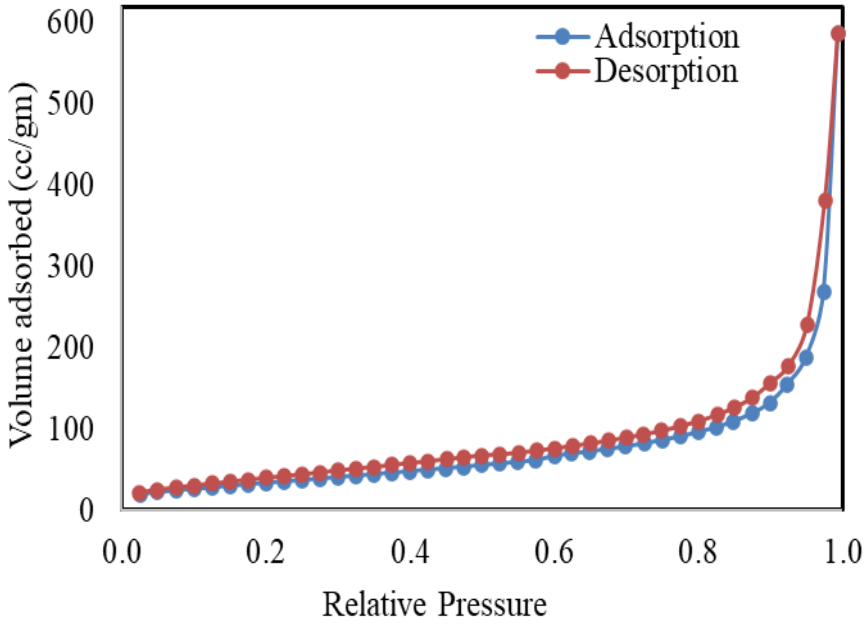

(a)

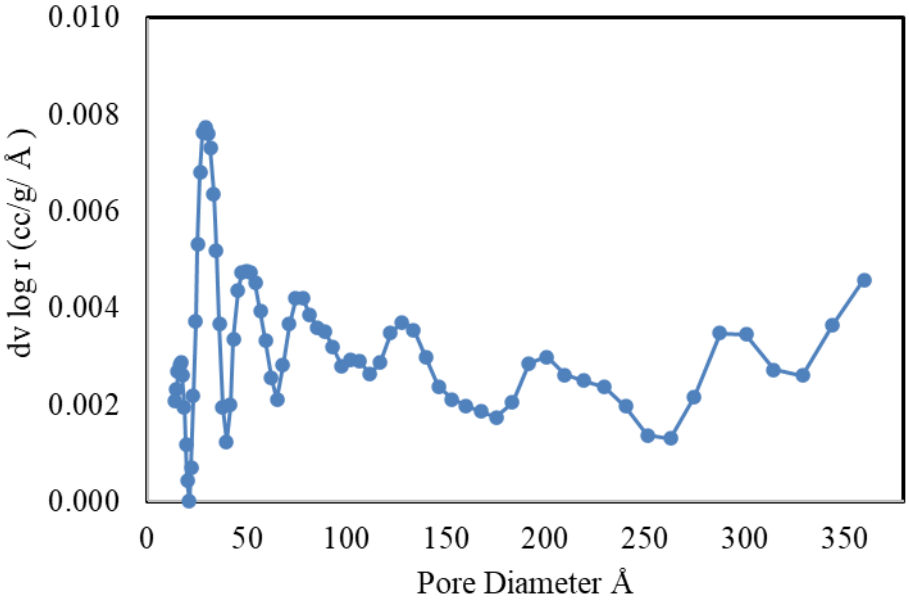

(b)

Figure 3.3 (a) BET adsorption – desorption isotherm and (b) pore size distribution of CuZA catalyst

3.3 Experimental work

3.3.1 Experimental set-up

A tubular fixed bed high-pressure reactor consisting of a stainless steel (SS316) reactor with an inner diameter of 7.5 mm, outer diameter of 14 mm and reactor length of 40 cm was placed in the temperature-controlled furnace (ATS, USA) as shown in Figure 3.4. A thermocouple (K type, Watlow) was placed along the axial direction of the reactor tube to make direct contact with the catalyst and to measure the temperature of the catalyst bed accurately. The reactor temperature was controlled using PID controller for furnace coils at three different sections. The total pressure inside the reactor system was controlled by a back pressure regulator digitally using a pressure transmitter. The feed gas flow rates were controlled using a mass flow controller (MFC, Brooks, USA) for CO_2 and H_2 gases directed from the respective gas cylinders. The reactor components comprise of condenser, high-pressure gas-liquid separator, low-pressure gas-liquid separator and wet gas meter. The experimental set-up was operated using SCADA system without manual interventions for all the experiments.

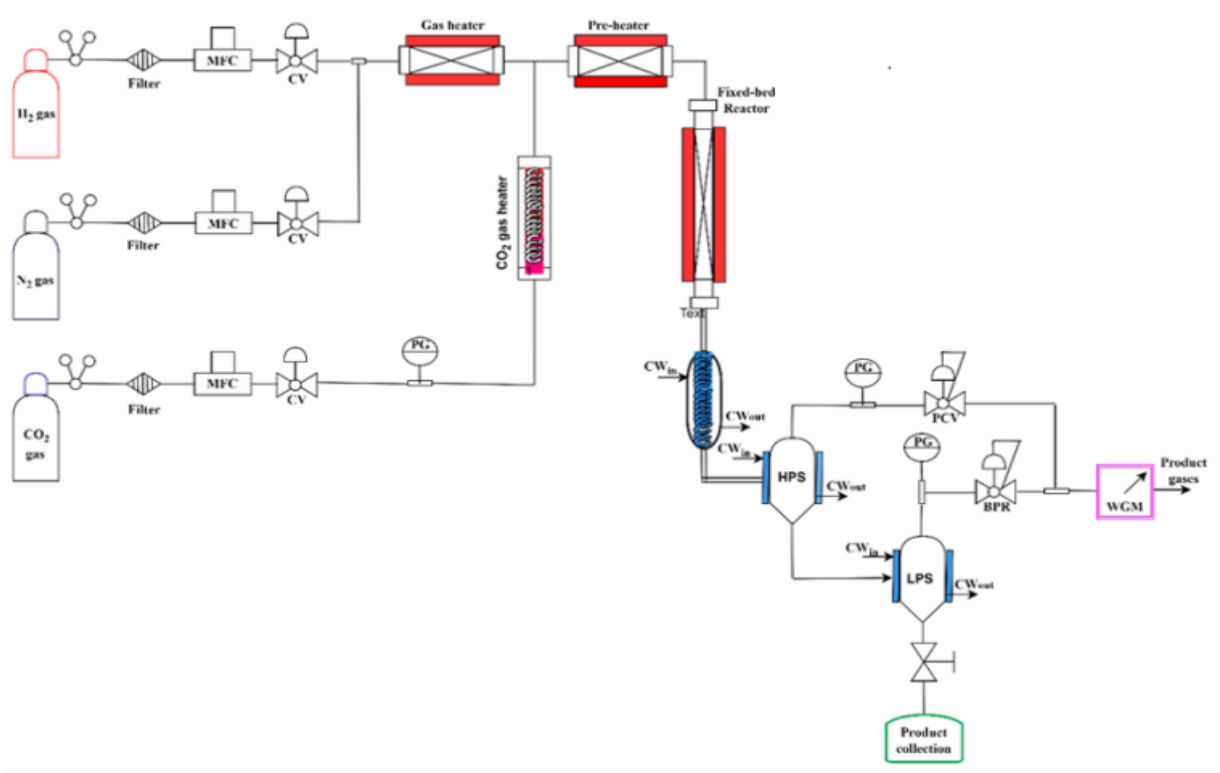

(a)

(b)

Figure 3.4 (a) Process flow diagram (b) Actual reactor set-up for conversion of CO_2 to methanol production using fixed bed reactor

3.3.1 Experimental procedure

The experiments were carried out using a commercial copper-based catalyst, $Cu/ZnO/Al_2O_3$ (CuZA) catalyst as discussed in section 3.3.1. Catalyst pellets were crushed using a mortar pestle into tiny particles in the size range of 300 to 500 microns. For the first set of experiments, a catalyst bed of length 11.3 cm with a catalyst weight of 3 g and the same weight of inert (silica gel) was placed inside the reactor. The inert material is used for dual purposes: (i) to pre-heat the feed gases and ii) to reduce outlet vapour temperature in case of hotspot generation which may decompose methanol. For the second set of experiments, a catalyst bed length of 22.6 cm long with a catalyst

weight of 6 g and the same amount of inert material was placed inside the reactor. Reactor was operated under steady condition. Initially we performed experiments at different time scales from 1h, 2h. We could not get sufficient methanol. So, we decided to collect enough methanol at the end of the reaction by keeping reaction for 5 h to ensure sufficient methanol production for analysis. Initially, the experiments were carried out at a constant pressure of 40 bar, GHSV of 720 h^{-1} and the reaction was performed for 5 hours by varying temperature, flow rate and weight of the catalyst for varying reaction conditions as given in Table 3.2 Reaction conditions and the performance results of the CuZA catalyst The bed is placed in the middle of the electrical heating element/zone. To adjust the location of the catalytic bed, quartz wool is placed between the inert material and catalyst bed which will prevent seepage of catalyst particles through inert material. The product composition at the reactor outlet estimated by calculating the CO_2 conversion, product selectivity, product yield and space-time yield is defined as follows,

$$\textbf{Selectivity}(\%) = \frac{\textbf{Molar flow rate of i species}}{\textbf{Total molar flowrate of all products}} * \textbf{100} \quad (3.1)$$

$$\textbf{Yield}\ (\%) = \frac{\textbf{Molar flowrate of desired product}}{\textbf{Molar flowrate of reactant fed}} * \textbf{100} \quad (3.2)$$

$$\textbf{STY}_{\textbf{Methanol}}\left(\frac{\textbf{mg}}{\textbf{g}_{\textbf{cat}}.\textbf{h}}\right) = \frac{\textbf{F}_{\textbf{Methanol}}}{\textbf{W}_{\textbf{cat}}} * \textbf{100} \quad (3.3)$$

Where, $F_{Methanol}$ is the methanol flowrate, mg/h

$S_{methanol}$ is methanol selectivity, %

$STY_{methanol}$ is the space-time yield of methanol, mg/g_{cat}.h

W_{cat} is the amount of catalyst, g

Table 3.2 Reaction conditions and the performance results of the CuZA catalyst

Exp. No.	P (bar)	T (°C)	Flowrate (ml/min)			Catalyst weight (g)	GHSV (h^{-1})	Amount of methanol & water (mg)
			CO_2	H_2	Total			
1	40	210	15	45	60	3	720	32.10
2	40	230	15	45	60	3	720	161.70
3	40	250	15	45	60	3	720	358.10
4	40	210	30	90	120	6	720	121.00
5	40	230	30	90	120	6	720	323.20

6	40	250	30	90	120	6	720	1261.60

3.4 Results and discussion

3.4.1 Effect of inlet flowrate and weight of catalyst on methanol yield

The experiments are carried out for H_2 to CO_2 ratio of 3 using 3 g and 6 g powdered catalyst for 60 and 120 ml/min. After the reaction protocol is set, carbon dioxide and hydrogen are passed through the preheaters at 200°C and then directed to the reactor. Mass flow controllers are used to modify the desired gas flow rates. The gas hourly space velocity (GHSV) is maintained by providing an overall gas feed flow rate to catalyst weight. Prior to it, the catalyst was reduced under H_2 flow (10 ml/ min) and N_2 flow (90 ml/ min) at atmospheric pressure from room temperature to 330°C and then maintained the reactor under isothermal for 2 h. The reduced catalyst is cooled to 100°C under the same flow conditions. The actual CO_2 hydrogenation experiments are performed at 210, 230 and 250 °C at a pressure of 40 bar for 5 h. The required gas flow rates are adjusted to 60 ml/min and 120 ml/min by keeping molar ratio of H_2 to CO_2 is 3:1. For set-1 of reactions, CO_2 hydrogenation is carried out under the flowrate of 15 ml/min of CO_2, 45 ml/min of H_2 and for set-2, CO_2 hydrogenation is carried out under the flowrate of 30 ml/min of CO_2, 90 ml/min of H_2 at 210, 230 and 250°C. Reaction products are condensed and collected from a gas-liquid separator. The concentration of reactants and products was analysed by gas chromatography (Nucon GC, 5765) equipped with manual injection functionality. The GC method is developed to detect methanol from the product mixture and water formed from the reverse water gas shift reaction. The product composition is detected by TCD (Thermal Conductivity Detector) using Helium as a carrier gas. The TCD channel is equipped with a Porapak-Q column with dimensions of 2.1 mm ID, 1/8" of OD and a length of 6 feet. The liquid phase composition is further quantified for the evaluation of performance parameters.

It is clear from the experiments that the increase in temperature increased the rate of product formation as is evident from Figure 3.5. The experimental results for space-time yield of methanol are well compared with the model predictions by Graaf et al. (1988) and Portha et al. (2017) at 250°C and 40 bar as reported in Figure 3.6(b). Therefore, further experiments are carried out at 250°C and 50 bar for higher H_2 to CO_2 molar ratios of 3, 6 and 9 under similar reaction conditions.

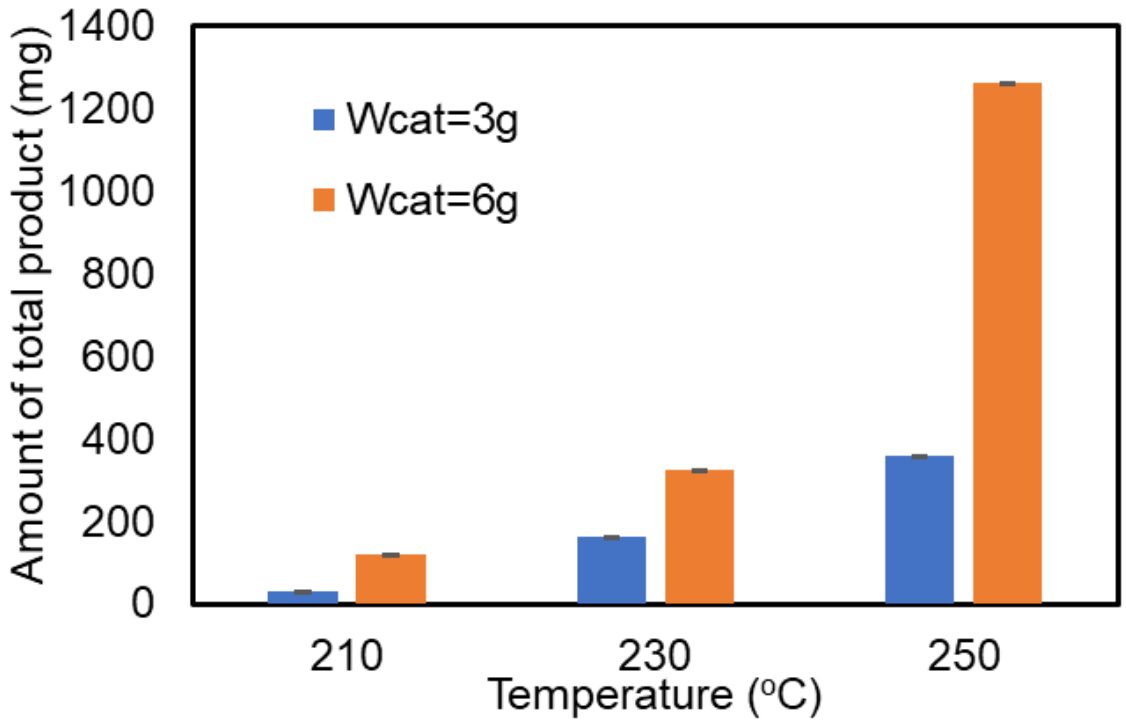

Figure 3.5 Amount of total product for different temperatures at 40 bar

Table 3.3 Case-1 Experimental data validation with reported literature

T (°C)	Flowrate (ml/min)	Model MeOH (%)		Exp. MeOH Yield (%)	Model STY MeOH (mg/g_{cat}. h)		Expt. STY MeOH (mg/g_{cat}. h)
		Graaf et al. (1988)	Portha et al. (2017)	Present Study	Graaf et al. (1988)	Portha et al. (2017)	Present Study
210	60	13.77	13.25	0.16	5.43	5.23	0.95
230	60	28.90	25.05	0.73	11.41	9.89	4.30
250	60	53.79	43.78	2.06	21.23	17.28	12.13

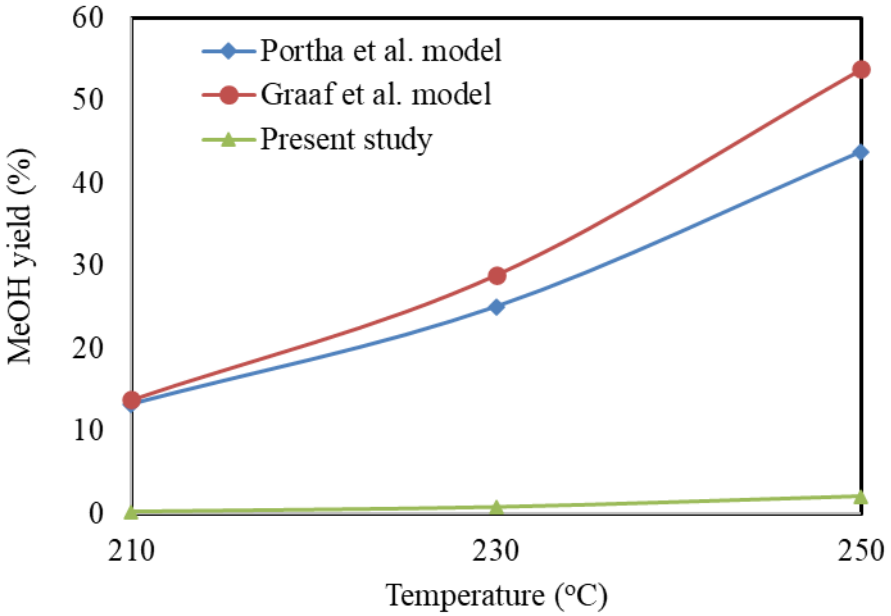

(a)

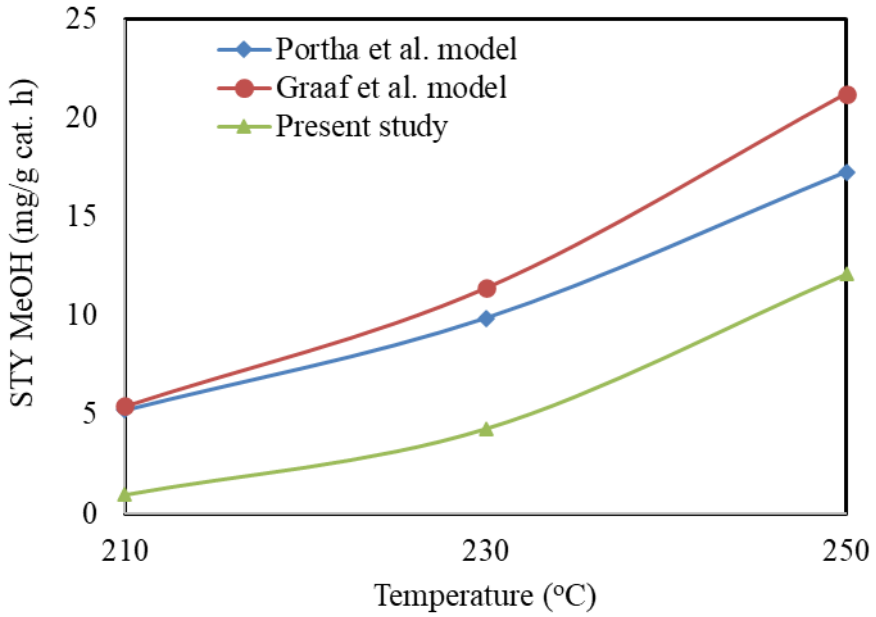

(b)

Figure 3.6 Comparison of the effect of temperature on a) Methanol yield and b) STY of MeOH with reported literature

Table 3.4 Case-2 Experimental data validation with reported literature

T (°C)	Flowrate (ml/min)	Model MeOH (%)		Exp. MeOH yield (%)	Model STY MeOH (mg/g_{cat}. h)		Expt. STY MeOH (mg/g_{cat}. h)
		Graaf et al. (1988)	Portha et al. (2017)	Present Study	Graaf et al. (1988)	Portha et al. (2017)	Present Study
210	120	13.77	13.25	0.23	2.72	5.23	1.36
230	120	28.90	25.05	0.79	5.70	9.89	4.63
250	120	53.79	43.78	3.21	10.61	17.28	18.90

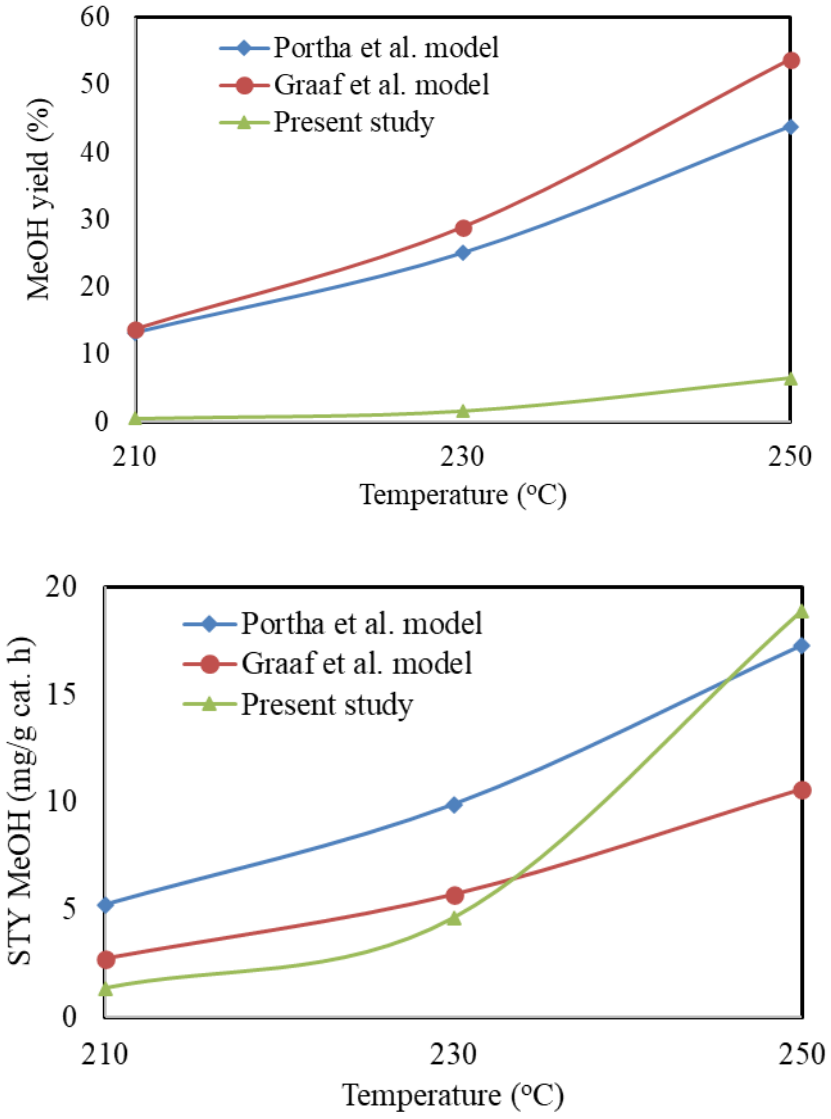

Figure 3.7 Case -2 Comparison of the effect of temperature on yield and STY of MeOH with reported literature

Table 3.5 Input conditions for simulation for experimental data validation

Parameter	Case-I	Case-II	Unit
Inlet CO_2 flowrate	15	30	ml/min
Inlet H_2 flowrate	45	90	ml/min
Total inlet flowrate	60	120	ml/min
H_2:CO_2 Molar ratio	3	3	…
CuZACatalyst ($Cu/ZnO/Al_2O_3$)	3	3	G
Particle size	400	400	Microns
Temperature	210,230 and 250	210,230 and 250	^oC
Pressure	40	40	Bar
GHSV	720	720	h^{-1}
Kinetic Model	A3B2C3	A3B2C3	…

4.5 Experimental data validation

Input conditions required for simulation studies for validating experimental results are given in below Table 3.5. From Figure 3.7, experimentally obtained results shows that methanol yield and Spacetime yield of methanol is increasing with temperature for both cases. At 250 ^oC, our present study result in terms of STY of MeOH is higher than the reported values for case II. Model A1B2C1 shows a good fit with experimental results. The residual obtained is very less for this model 7 in comparison with other models as shown in Figure 3.8. We select the A1B2C1 model for further study.

$$COs1 + Hs2 \rightleftharpoons HCOs1 + s2 \qquad (A1)$$

$$H\,CO_2s1 + Hs2 \rightleftharpoons COs1 + H_2Os2 \qquad (B2)$$

$$CO_2s1 + Hs2 \rightleftharpoons HCO_2s1 + s2 \qquad (C1)$$

Considering above A1,B2,C1 reactions the rate expressions are (A),(B) and (C) as given below,

$$r_1 = k_1 b_{CO} \left\{ \frac{P_{CO} P_{H_2}^{0.5} - (P_{CH_3OH}/(P_{H_2}^{1.5} * K_1))}{(1 + b_{CO}P_{CO} + b_{CO_2}P_{CO_2})(P_{H_2}^{0.5} + (b_{H_2O}/b_{H_2}^{0.5})P_{H_2O})} \right\} \qquad (A)$$

$$r_2 = k_2 b_{CO2} \left\{ \frac{P_{CO\,2} P_{H_2} - (P_{CO} P_{H_2O}/K_2)}{(1 + b_{CO}P_{CO} + b_{CO_2}P_{CO_2})(P_{H_2}^{0.5} + (b_{H_2O}/b_{H_2}^{0.5})P_{H_2O})} \right\} \qquad (B)$$

$$r_3 = k_3 b_{CO2} \left\{ \frac{P_{CO} P_{H_2}^{0.5} - (P_{CH_3OH} P_{H_2O}/(P_{H_2}^{2.5} K_3))}{(1 + b_{CO}P_{CO} + b_{CO_2}P_{CO_2})(P_{H_2}^{0.5} + (b_{H_2O}/b_{H_2}^{0.5})P_{H_2O})} \right\} \qquad (C)$$

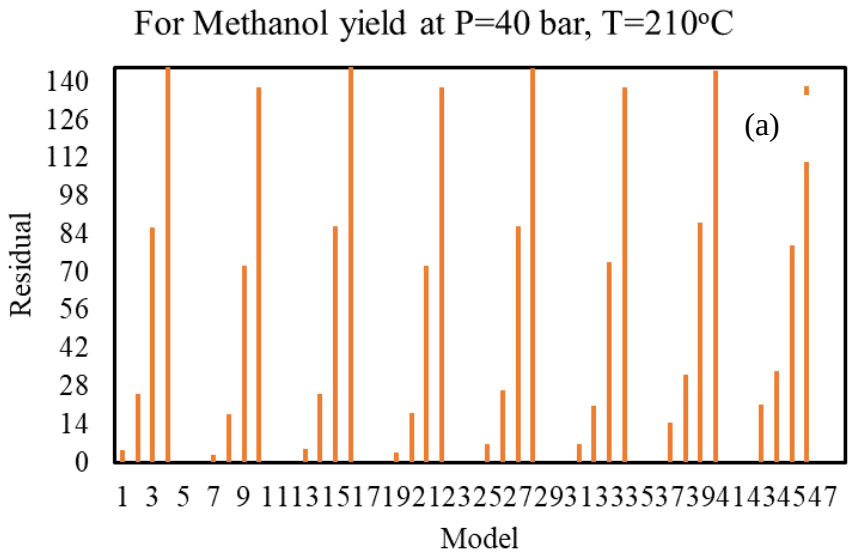
For Methanol yield at P=40 bar, T=210°C
(a)
Residual
140
126
112
98
84
70
56
42
28
14
0
1 3 5 7 9 11131517192123252729313335373941434547
Model

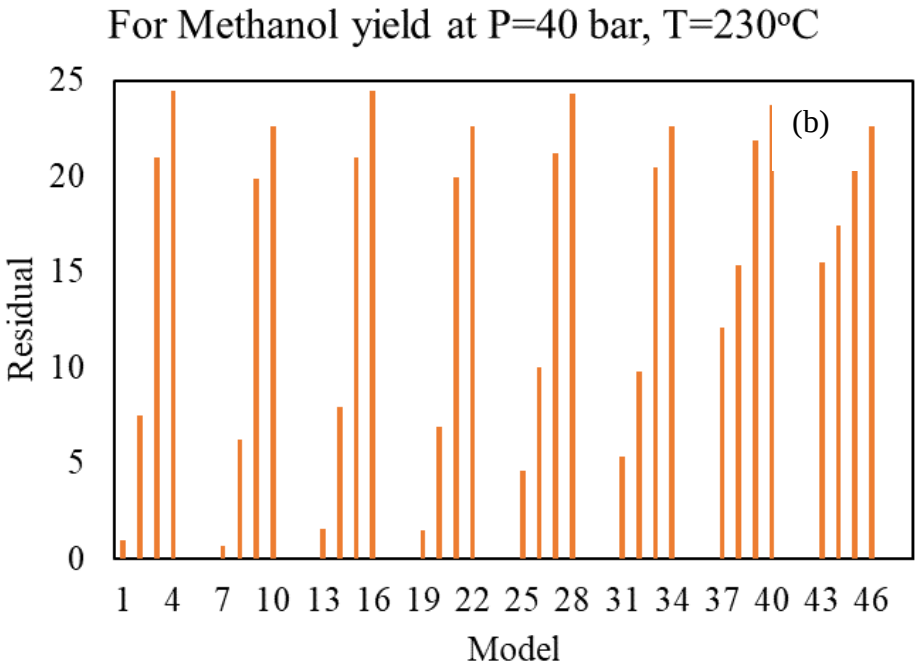
For Methanol yield at P=40 bar, T=230°C
(b)
Residual
25
20
15
10
5
0
1 4 7 10 13 16 19 22 25 28 31 34 37 40 43 46
Model

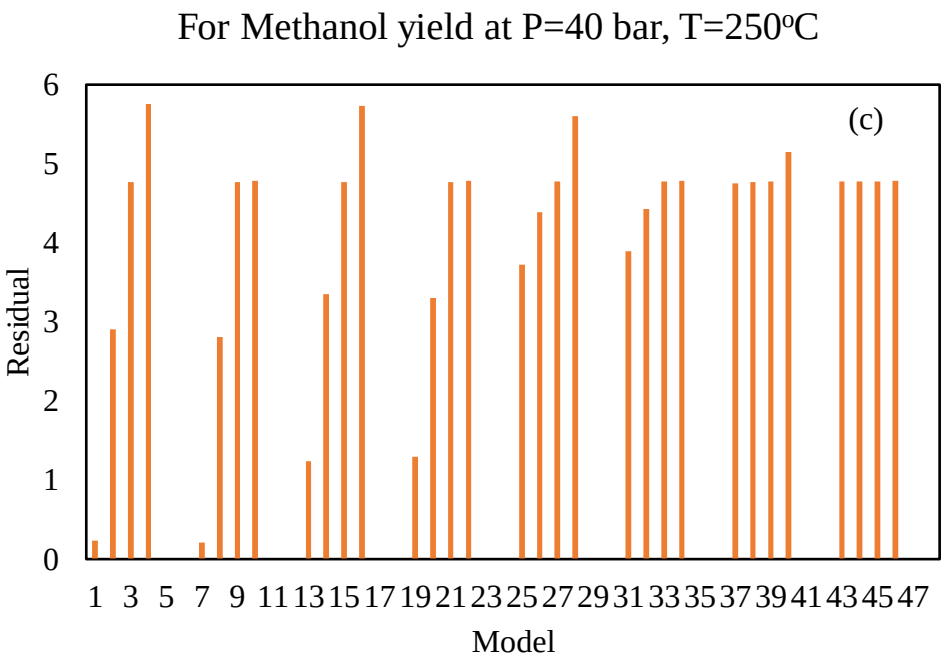

Figure 3.8 Error analysis for case I at 40 bar (a)At 210°C (b) At 230°C and (c)At 250°C

3.3.2 Effect of H_2 to CO_2 molar ratio

The results depict that the maximum methanol yield is obtained at 250°C and 40 bar for an H_2 to CO_2 ratio of 3. The experiments are performed in a high-pressure fixed-bed catalytic reactor to study the effect of H_2 to CO_2 molar ratio of 3, 6 and 9 on methanol yield. Therefore, further experiments are performed in a fixed bed reactor for catalyst particle weights of 3g and 6g with an increase in H_2 to CO_2 molar ratios of 6 and 9. The product samples are collected after the vapours are cooled in a condenser followed by a low-pressure gas-liquid separator. The circulating fluid is maintained at 3°C in the chiller throughout the reaction until the product collection. The product samples are quantified using gas chromatography (GC) using the Porapak-Q column as discussed in section 3.3.1. The experimental data is quantified in terms of product yield and space-time yield (STY) as shown in Figure 3.10. The actual samples collected from the gas-liquid separator for six experiments at 3g and 6g catalyst for H_2 to CO_2 ratios of 3, 6 and 9 are shown in Figure 3.9. The results show that there is an increase in the production of methanol with an increase in catalyst weight at optimal conditions. The maximum STY of methanol for 3 g particles is 12.41 $mg/g_{cat}.h$ and 13.59 $mg/g_{cat}.h$ was collected for 6 g catalyst at an H_2 to CO_2 ratio of 9. Therefore, it can be inferred that an increase in the H_2 to CO_2 ratio for different flowrates showed increased methanol production.

The experiments showed better reproducibility and is reported for space time yield (STY) with absolute deviation of ± 0.01 to± 0.06 for 3 g catalyst, ± 0.02 to ± 0.10 for 6 g catalyst as shown in Figure 3.5 and ± 0.09 to ± 0.32 as shown in Figure 3.10.

Table 3.6 Performance analysis for different H_2: CO_2 molar ratios of 3, 6 and 9 at 50 bar and 250°C

Exp No.	P bar	T (°C)	Flowrate (ml/min)				Catalyst weight (g)	H_2: CO_2 molar ratio	GHSV (h-1)	Amount of product (mg)	STY of MeOH (mg/gcat .h)
			CO_2	H_2	N_2	Total					
1	50	250	30	90	120	240	3	3	2880	458.10	6.03
2	50	250	30	180	120	330	3	6	3940	956.00	9.98
3	50	250	30	270	120	420	3	9	5040	942.10	12.41
4	50	250	30	90	120	240	6	3	1440	217.50	6.30
5	50	250	30	180	120	330	6	6	1980	1331.00	9.22
6	50	250	30	270	120	420	6	9	2520	990.00	13.59

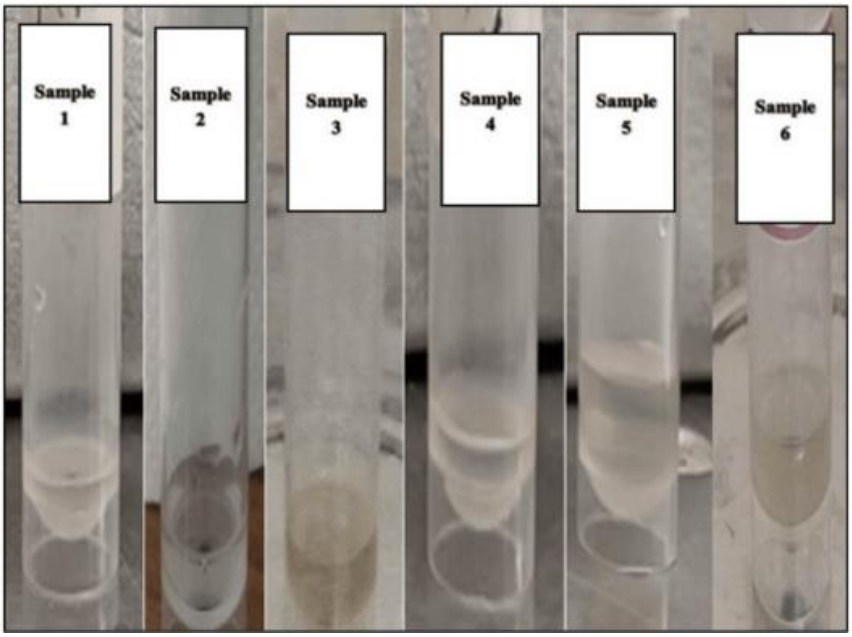

Figure 3.9 Samples collected for 50 bar experiments for H_2 to CO_2 ratios of 3, 6 and 9 for 3g and 6 g catalyst (Samples 1-3 → W cat = 3g; Samples 4-6 → W cat = 6g)

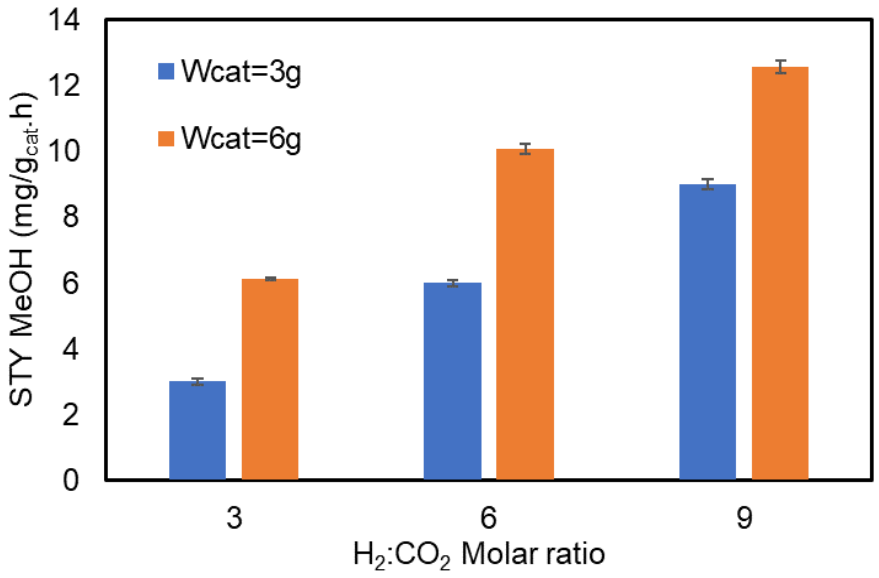

Figure 3.10 Space-time yield (STY) of methanol for different H_2:CO_2 molar ratio at 50 bar & 250ºC

3.4 Study of mass transfer limitations

Catalytic reactions with solids involve various steps that influence the rate of reaction due to internal and external mass transfer limitations. The internal mass transfer corresponds to the diffusion of reactants into the internal surface and diffusion of products from the pores to the outer surface. The external mass transfer corresponds to the transport of reactants from the bulk fluid stream to the surface of the catalyst and transport of products from the outer surface of the body to the bulk fluid. In addition to the surface reaction, internal and external mass transfer may influence the overall reaction, hence, mass transfer limitations are studied using Weisz-Prater and Mears criteria.

The Weisz-Prater criteria is used to assess if internal diffusion is restricting the reaction and Mears criteria is used to know if any external mass transfer limitation are present [34,35].

Weisz Prater parameter (C_{WP}) was calculated using the equation:

$$C_{WP} = \frac{Actual\ reaction\ rate}{A\ diffusion\ rate} \tag{3.4}$$

$$C_{WP} = \frac{-r_{A\,(obs)}\ \rho_c\ R^2}{D_e\ C_{As}} \tag{3.5}$$

$$V_{ave} = \left[\frac{8k_B T}{\Pi m}\right]^{0.5} \tag{3.6}$$

$$D_{kn} = \frac{V_{ave} * D_P}{3} \quad (3.7)$$

The Effective diffusivity D_e will be substituted by Knudsen diffusion since the pore diameter (D_p) of the catalyst is small (i.e., 9.76 nm), therefore, pore diffusion will be dominated by Knudsen diffusion (D_{Kn})[88]; $-r_{A\,(obs)}$ is the observed reaction rate (mol/kg_{cat}.s); V_{ave} is the average velocity (cm/s); k_B is Boltzmann's constant; C_{As} is the concentration of CO_2 at the reaction surface.

Mears Parameter (MP) was calculated using the equation:

$$\mathrm{MP} = \frac{-r_{A\,(obs)}\,\rho_b\,R\,n}{k_c\,C_{Ab}} \quad (3.8)$$

Moreover, the Thoenes-Kramers correlation was used to estimate the packed-bed external mass transport coefficient for the Mears Parameter. k_c is the mass transfer coefficient and R is radius of catalyst particle; m and n refers to the molecular mass of CO_2 and order of the reaction; C_{Ab} is the concentration of CO_2 at the bulk surface.

The estimations for mass transfers limitations found that for all the reaction conditions C_{WP} was significantly less than 1 and Mear's Parameter was less than 0.15 indicating that no internal diffusional limitations and no external mass transfer limitations as well. Therefore, mass transfer effects could be neglected for all the cases.

3.5 Conclusions

The kinetic models developed for the synthesis of methanol from CO_2 are under high-pressure conditions that require experimental investigation. In this work, the role of CO in direct CO_2 catalytic hydrogenation reactions is analysed through reverse water gas shift reaction using kinetic models. Simulations are performed for increased mole ratios of H_2 to CO_2 to envisage the performance characteristics of the fixed bed reactor model. Based on modelling and experimental investigation for direct CO_2 hydrogenation, the conclusions are as follows:

i. The experiments showed enhancement in the reaction rates with improved methanol STY of 6.30%, 9.22% and 13.59% for H_2 to CO_2 molar ratios of 3, 6 and 9, respectively.
ii. Model no. 7 i.e. A1B2C1 shows a good fit with experimental results. The residual obtained is very less for this model 7 in comparison with other models. We select the A1B2C1 model for further study.

iii. Weisz prater criterion: C_{WP} <<1 and Mear's Parameter: MP << 0.15

iv. It indicates that no internal diffusional limitations and no external mass transfer limitations in the reaction. Therefore, mass transfer effects could be neglected for all the cases.

v. The experiments at higher H_2-to-CO_2 molar ratios demonstrated that increase in yield and space-time yield towards methanol production and further optimized that an H_2 to CO_2 molar ratio of 9 favours higher methanol yield.

3.6 References

[1] Cordero-Lanzac T, Ramirez A, Cruz-Fernandez M, Zander HJ, Joensen F, Woolass S, et al. A CO2valorization plant to produce light hydrocarbons: Kinetic model, process design and life cycle assessment. J CO2 Util 2023;67. https://doi.org/10.1016/j.jcou.2022.102337.

[2] Arab S, Commenge J, Portha J, Falk L. Methanol synthesis from CO_2 and H_2 in multi-tubular fixed-bed reactor and multi-tubular reactor filled with monoliths Chemical Engineering Research and Design Methanol synthesis from CO_2 and H_2 in multi-tubular fixed-bed reactor and multi-tubular. Chem Eng Res Des 2014;92:2598–608.

[3] Sharma P, Sebastian J, Ghosh S, Creaser D, Olsson L. Recent advances in hydrogenation of CO_2 into hydrocarbonsviamethanol intermediate over heterogeneous catalysts. Catal Sci Technol 2021;11:1665–97. https://doi.org/10.1039/d0cy01913e.

[4] Álvarez A, Bansode A, Urakawa A, Bavykina A V., Wezendonk TA, Makkee M, et al. Challenges in the Greener Production of Formates/Formic Acid, Methanol, and DME by Heterogeneously Catalyzed CO_2 Hydrogenation Processes. Chem Rev 2017;117:9804–38. https://doi.org/10.1021/acs.chemrev.6b00816.

[5] De Oliveira Campos BL, Delgado KH, Wild S, Studt F, Pitter S, Sauer J. Surface reaction kinetics of the methanol synthesis and the water gas shift reaction on Cu/ZnO/Al2O3. React Chem Eng 2021;6:868–87. https://doi.org/10.1039/d1re00040c.

[6] Hafeez S, Harkou E, Al-Salem SM, Goula MA, Dimitratos N, Charisiou ND, et al. Hydrogenation of carbon dioxide (CO_2) to fuels in microreactors: a review of set-ups and value-added chemicals production. React Chem Eng 2022;7:795–812. https://doi.org/10.1039/d1re00479d.

[7] Mbatha S, Everson RC, Musyoka NM, Langmi HW, Lanzini A, Brilman W. Power-to-methanol process: A review of electrolysis, methanol catalysts, kinetics, reactor designs and modelling, process integration, optimisation, and techno-economics. Sustain Energy Fuels 2021;5:3490–569. https://doi.org/10.1039/d1se00635e.

[8] Nyári J, Izbassarov D, Toldy ÁI, Vuorinen V, Santasalo-Aarnio A. Choice of the kinetic model significantly affects the outcome of techno-economic assessments of CO2-based methanol synthesis. Energy Convers Manag 2022;271. https://doi.org/10.1016/j.enconman.2022.116200.

[9] Al-Rowaili FN, Khalafalla SS, Al-Yami DS, Jamal A, Ahmed U, Zahid U, et al. Techno-economic evaluation of methanol production via gasification of vacuum residue and conventional reforming routes. Chem Eng Res Des 2022;177:365–75. https://doi.org/10.1016/j.cherd.2021.11.004.

[10] Pierluigi Villa, * Plo Forzattl, Guido Buzzl-Ferraris, Guido Garone and IP. "Synthesis of alcohols from carbon oxides and hydrogen. 1. Kinetics of the low-pressure methanol synthesis." Ind Eng Chem Res 1985;24:12–9.

[11] Takagawa M, Ohsugi M. Study on reaction rates for methanol synthesis from carbon monoxide, carbon dioxide, and hydrogen. J Catal 1987;107:161–72. https://doi.org/10.1016/0021-9517(87)90281-8.

[12] Eksiri Z, Mozdianfard MR, Mirvakili A, Rahimpour MR. Two-dimensional modeling investigation of the modern methanol plate reactors. Chem Eng Res Des 2020;162:212–27. https://doi.org/10.1016/j.cherd.2020.08.009.

[13] Bisotti F, Fedeli M, Prifti K, Galeazzi A, Dell'Angelo A, Barbieri M, et al. Century of Technology Trends in Methanol Synthesis: Any Need for Kinetics Refitting? Ind Eng Chem Res 2021;60:16032–53. https://doi.org/10.1021/acs.iecr.1c02877.

[14] E.J.Stamhuis, G.H. Graaf, P.J.J.M. Sijtsema and GEHJ. Chemical equilibria in methanol synthesisG.H. Graaf, P.J.J.M. Sijtsema, E.J.Stamhuis and G.E.H.Joosten 1986;41:2883–90.

[15] Park N, Park MJ, Lee YJ, Ha KS, Jun KW. Kinetic modeling of methanol synthesis over commercial catalysts based on three-site adsorption. Fuel Process Technol 2014;125:139–47. https://doi.org/10.1016/j.fuproc.2014.03.041.

[16] Portha JF, Parkhomenko K, Kobl K, Roger AC, Arab S, Commenge JM, et al. Kinetics of Methanol Synthesis from Carbon Dioxide Hydrogenation over Copper-Zinc Oxide Catalysts. Ind Eng Chem Res 2017;56:13133–45. https://doi.org/10.1021/acs.iecr.7b01323.

[17] Skrzypek J, Lachowska M, Moroz H. Kinetics of methanol synthesis over commercial copper/zinc oxide/alumina catalysts. Chem Eng Sci 1991;46:2809–13. https://doi.org/10.1016/0009-2509(91)85150-V.

[18] Vanden Bussche KM, Froment GF. A steady-state kinetic model for methanol synthesis and the water gas shift reaction on a commercial Cu/ZnO/Al2O3 catalyst. J Catal 1996;161:1–10. https://doi.org/10.1006/jcat.1996.0156.

[19] McNeil MA, Schack CJ, Rinker RG. Methanol synthesis from hydrogen, carbon monoxide and carbon dioxide over a $CuO/ZnO/Al_2O_3$ catalyst. II. Development of a phenomenological rate expression. Appl Catal 1989;50:265–85. https://doi.org/10.1016/S0166-9834(00)80841-6.

[20] Stangeland K, Li H, Yu Z. CO2 hydrogenation to methanol: the structure–activity relationships of different catalyst systems. Energy, Ecol Environ 2020;5:272–85. https://doi.org/10.1007/s40974-020-00156-4.

[21] Nestler F, Müller VP, Ouda M, Hadrich MJ, Schaadt A, Bajohr S, et al. A novel approach for kinetic measurements in exothermic fixed bed reactors: Advancements in non-isothermal bed conditions demonstrated for methanol synthesis. React Chem Eng 2021;6:1092–107. https://doi.org/10.1039/d1re00071c.

[22] Ghosh S, Sebastian J, Olsson L, Creaser D. Experimental and kinetic modeling studies of methanol synthesis from CO2 hydrogenation using In_2O_3 catalyst. Chem Eng J 2021;416:129120. https://doi.org/10.1016/j.cej.2021.129120.

[23] Ng WL, Sripada P, Biswas S, Bhattacharya S. Experimental work and kinetic modelling of CO2 hydrogenation to methanol on CeO_2 supported In_2O_3 catalyst. Appl Catal A Gen 2022;646. https://doi.org/10.1016/j.apcata.2022.118885.

[24] Kattel S, Liu P, Chen JG. Tuning Selectivity of CO_2 Hydrogenation Reactions at the Metal/Oxide Interface. J Am Chem Soc 2017;139:9739–54. https://doi.org/10.1021/jacs.7b05362.

[25] Wang Y, Kattel S, Gao W, Li K, Liu P, Chen JG, et al. to methanol n.d. https://doi.org/10.1038/s41467-019-09072-6.

[26] Bozzano G, Manenti F. Efficient methanol synthesis: Perspectives, technologies and optimization strategies. Prog Energy Combust Sci 2016;56:71–105. https://doi.org/10.1016/j.pecs.2016.06.001.

[27] Ghosh S, Olsson L, Creaser D. Methanol mediated direct CO_2 hydrogenation to hydrocarbons: Experimental and kinetic modeling study. Chem Eng J 2022;435. https://doi.org/10.1016/j.cej.2022.135090.

[28] Fujita S, Kanamori Y, Satriyo AM, Takezawa N. Methanol synthesis from CO_2 over Cu / ZnO catalysts prepared from various coprecipitated precursors 1998;45:241–4.

[29] Arena F, Barbera K, Italiano G, Bonura G, Spadaro L, Frusteri F. Synthesis , characterization and activity pattern of Cu – ZnO / ZrO_2 catalysts in the hydrogenation of carbon dioxide to methanol 2007;249:185–94. https://doi.org/10.1016/j.jcat.2007.04.003.

[30] Hartadi Y, Widmann D, Ju R. Methanol synthesis via CO_2 hydrogenation over a Au / ZnO catalyst : an isotope labelling study on the role of CO in the reaction process † 2016:10781–91. https://doi.org/10.1039/c5cp06888f.

[31] Godini HR, Khadivi M, Azadi M, Görke O, Jazayeri SM, Thum L, et al. Multi-scale analysis of integrated C1 (CH_4 and CO_2) utilization catalytic processes: Impacts of catalysts characteristics up to industrial-scale process flowsheeting, part i: Experimental analysis of catalytic low-pressure CO_2 to methanol conversion. Catalysts 2020;10:1–22. https://doi.org/10.3390/catal10050505.

[32] Wei W, Sun Y. Science &. Catal Sci Technol 2015;5:4365–77. https://doi.org/10.1039/C5CY00372E.

[33] Angelo L, Kobl K, Marcela L, Tejada M, Zimmermann Y, Parkhomenko K. Comptes Rendus Chimie Study of CuZn M O x oxides (M = Al , Zr , Ce , CeZr) for the catalytic hydrogenation of CO_2 into methanol 2015;18:250–60.

[34] Poto S, Vico van Berkel D, Gallucci F, Fernanda Neira d'Angelo M. Kinetic modelling of the methanol synthesis from CO_2 and H_2 over a $CuO/CeO_2/ZrO_2$ catalyst: The role of CO_2 and CO hydrogenation. Chem Eng J 2022;435. https://doi.org/10.1016/j.cej.2022.134946.

[35] Infantes-Molina A, Gralberg E, Cecilia JA, Finocchio E, Rodríguez-Castellón E. Nickel and cobalt phosphides as effective catalysts for oxygen removal of dibenzofuran: Role of contact time, hydrogen pressure and hydrogen/feed molar ratio. Catal Sci Technol 2015;5:3403–15. https://doi.org/10.1039/c5cy00282f.

Chapter 4

Kinetics studies for Quinoline hydrogenation to decahydroquinoline

4.1 Introduction

The world continues to shift towards renewable energy sources with the need for efficient and cost-effective energy storage solutions becomes increasingly important. Recently, the Hydrogen Council released a report asserting that hydrogen has the potential to account for 22% of the global final energy demand by 2050, equivalent to an annual production of 660 million tonnes (MT) of hydrogen [1]. The mass-energy density of 120 MJ/kg of hydrogen is much higher than that of hydrocarbon fuel with a calorific value of 44MJ/kg for gasoline [2,3]. However, its widespread use requires economical and safe hydrogen storage with a gravimetric content of over 6.5 wt.% H_2 (>2.0 kWh/kg) and volume density over 0.04 kg/L (>1.3 kWh/L) [4]. Thermodynamic feasibility and attractiveness in terms of simplicity, safety, scalability, heat control, and economics make hydrogen storage in liquid organic heterocycles a desirable option [5]. One of the fundamental pillars of the contemporary chemical industry is a heterogeneous catalyst which offers the possibility of economically and efficiently converting raw materials into valuable chemicals and fuels as well as ecologically favorable [6]. Different technologies of storing hydrogen have been extensively studied such as compressed hydrogen, liquefied hydrogen, physisorption in porous materials or metal-organic frameworks, and metal hydrides although each technology has certain advantages and drawbacks [7]. The storage and transportation of hydrogen provide a significant challenge in developing a hydrogen-based economy due to its high specific gravity and low thermal energy density [8]. In recent years, the chemical and industrial sectors have paid a great deal of attention to the storage of hydrogen using methane, ammonia, and other materials [9]. Liquid organic hydrogen carriers (LOHCs) have emerged as one of attractive sources for the storage and transportation of hydrogen with large quantities of hydrogen can be loaded and unloaded using a reversible chemical reaction. For longer energy storage durations, LOHCs were found to be a more effective solution compared to other storage technologies [10]. Many hydrogen carriers have been examined and assessed in terms of their availability, cost, and toxicological profile. LOHC shows various advantages such as high gravimetric and volumetric density, safety to handle, longevity, good reversibility, logistics, compatibility with the existing energy infrastructure, and cost-effective, high-purity hydrogen [11,12]. The concept of LOHCs aligns with the principles of the hydrogen economy which envisions hydrogen as a versatile and clean energy carrier capable of replacing or supplementing traditional fossil fuels [13]. LOHC systems have huge demand in European countries for residential and commercial buildings where thermal losses from the

storage processes can be used for heating and cooling purposes [14]. The chemical storage of hydrogen in liquid carriers involves an exothermic process during hydrogenation, while the dehydrogenation process exhibits an endothermic release of hydrogen. Therefore, the endothermic nature poses a significant challenge due to the necessity for elevated heat input [12,15]. However, LOHC energy storage is a technology that requires research and development activities to optimize its performance to a commercially viable level. As a result, heterocyclic aromatic compounds (HACs) are being studied intensively as a future-oriented form of LOHC [16]. N-ethyl carbazole (NEC) has hydrogen storage capacity of ~5.3 wt% and the moderate conditions required for hydrogenation and dehydrogenation. The reversible storage of hydrogen in NEC has been demonstrated under practical conditions, making it a key candidate for LOHC systems. Recent studies have focused on optimizing the catalytic processes and understanding the thermodynamics involved in the hydrogenation/dehydrogenation of NEC. It can store up to 6 hydrogen atoms per molecule, with hydrogenation occurring at temperatures around 150°C and 70 bar while dehydrogenation prevails at 220°C and atmospheric conditions. The melting point of fully dehydrogenated N-ethyl-carbazole is 69.1^{o}C and it is therefore a solid at ambient temperature.These moderate conditions make NEC particularly attractive for practical applications. Studies have shown that the dehydrogenation of NEC can achieve conversion efficiencies greater than 99% under optimized conditions [14,17]. Similar to NEC, N-Propylcarbazole (NPC) is another carbazole derivative that has been investigated for hydrogen storage with a hydrogen storage capacity of approximately 5.5 wt%[18]. While it shares many properties with NEC, NPC offers a slightly different hydrogen storage capacity and reaction kinetics, which can be advantageous in specific applications. The hydrogenation of NPC typically occurs at 120-150°C, with hydrogen pressure of 70 bar over 5 wt% ruthenium on alumina[19]. Indole Series Molecules such as 2-methylindole, have been identified as promising LOHC candidates due to their ability to store hydrogen at high densities. These molecules offer a favorable balance between hydrogen content and reaction conditions, with ongoing research focusing on their stability and the optimization of dehydrogenation processes. The potential of indole-based compounds for hydrogen storage has been supported by both experimental and theoretical studies. 1-alkyl-indoles as suitable LOHC systems because of their high thermal stability and high boiling points[20]. 8-Methylquinoline is Methyl-substituted quinolines are available from petroleum, coal processing, wood preservation or they can be synthesized from aniline.8-Methylquinoline

is another material of interest in the LOHC field, known for its high hydrogen storage capacity and relatively low dehydrogenation temperatures[21]. Quinoline, a heterocyclic compound consisting of a benzene ring fused to a pyridine ring, has been the subject of extensive research owing to its diverse applications in the fields of pharmaceuticals, agrochemicals, and materials science [22–24]. There are valuable insights into the role of heteroatom within LOHC for hydrogenation and demonstrate the significance of heteroatom doping in improving hydrogen storage and transportation systems. Catalytic hydrogenation of quinoline and its derivatives are major raw materials for the production of various fine chemicals, such as agrochemicals, pharmaceuticals, and other bioactive molecules [25]. Quinoline is a byproduct of coal tar and is also produced in large quantities during the production of coal gas. Thus, much study is also focused on the mechanisms involved in quinoline's hydrodenitrogenation [26–29]. The role of quinoline as LOHC is a relatively unexplored aspect that presents exciting opportunities for the integration of quinoline-based compounds into the growing landscape of hydrogen storage and transport technologies. It has a high boiling point of 237°C thus making it suitable for use as a liquid at low temperatures. Additionally, quinoline has a high hydrogen storage capacity of 7.24 wt.% in comparison to other commonly used LOHCs such as toluene and naphthalene [30]. While quinoline shows great potential as LOHC, there are still some challenges that need to be addressed. One of the main challenges is the need for a suitable catalyst for the hydrogenation and dehydrogenation reactions. However, recent research has shown that certain metal catalysts, such as ruthenium and iron can effectively catalyze these reactions [21]. Catalytic hydrogenation of quinoline is a major organic reaction where one of the products, 1,2,3,4-tetrahydroquinoline(py-THQ), is an important intermediate for pharmaceuticals, agrochemicals, and various biologically active molecules [31]. Another intermediate is 5,6,7,8-tetrahydroquinoline (bz-THQ) and the fully hydrogenated product is decahydroquinoline (DHQ) as shown in Fig. 4.1. Hydrogenation of quinoline and its derivatives is of considerable industrial interest to produce petrochemicals, fine chemicals, and pharmaceuticals. Different metals (Pd, Ni, Rh, Pt, Cu, etc.) supported on different supports have been tested for the hydrogenation of quinoline to DHQ. This reaction is essentially carried out in two steps viz. quinoline to 1,2,3,4-tetrahydroquinoline (py-THQ) and a small amount of 5,6,7,8-tetrahydroquinoline (bz-THQ) formation in the first step while complete hydrogenation of both intermediates to DHQ occurs in the second step. The physicochemical properties of the reactant, intermediates and product are given

Table 4.1 Physicochemical properties of Quinoline and its hydrogenated products

Properties/Specifications	Quinoline	py-THQ	bz-THQ	DHQ
Chemical formula	C_9H_7N	$C_9H_{11}N$	$C_9H_{11}N$	$C_9H_{17}N$
Molecular weight (g/mol)	129.16	133.19	133.19	139.24
H_2 storage capacity (%)	7.24	4.35	4.35	NA
Boiling point (^oC)	237	251	218	201
Melting point (^oC)	−15	20	146.5	48
Density (g/ml)	1.09	1.05	1.03	0.93
Stability under process conditions	Stable	Stable	Stable	Stable
Solvent solubility	In organic solvents	In organic solvents	In organic solvents	In organic solvents
Appearance	Colourless oily liquid	Colourless oily liquid	Colourless oily liquid	White to light yellow

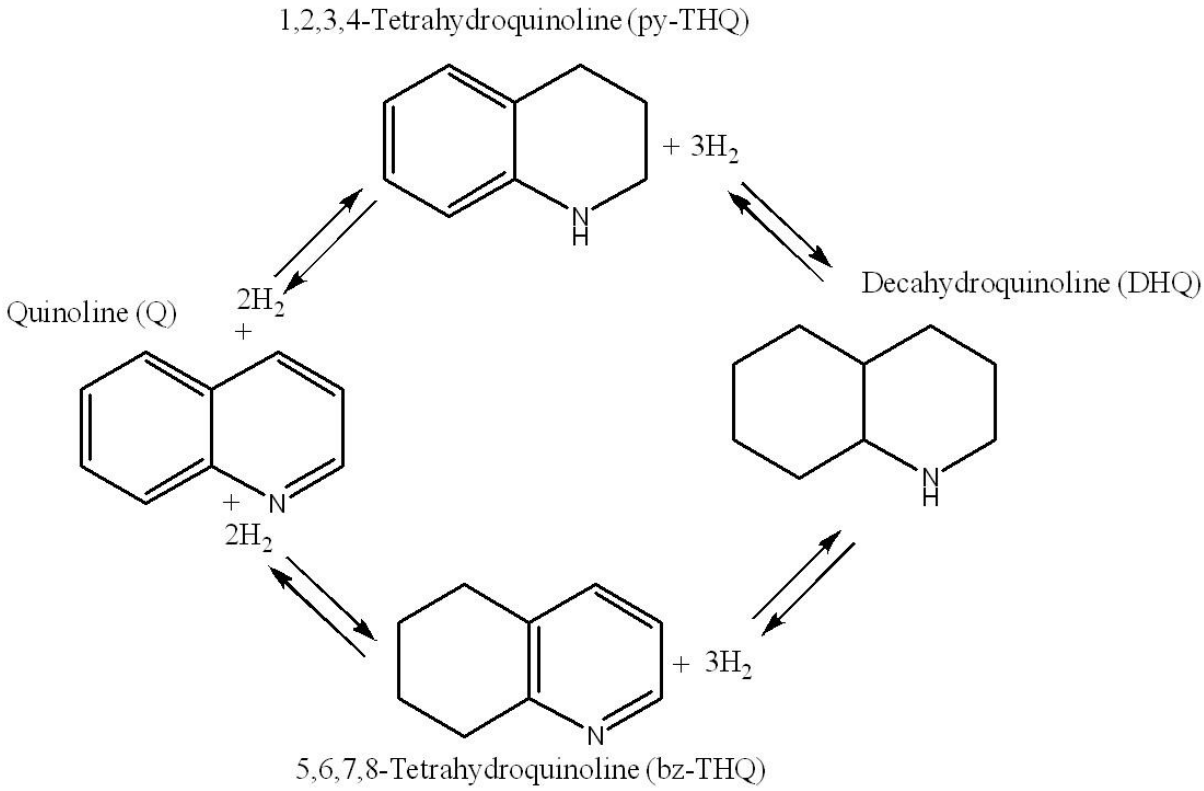

Figure 4.1 Reaction scheme for Quinoline hydrogenation

Complete hydrogenation is the most difficult step due to the need for severe reaction conditions and a longer response time and the conversion of py-THQ to DHQ is often quite challenging. Conversion of py-THQ to DHQ requires a longer reaction time and harsh reaction conditions, typically at a temperature in the range of 175–260 °C, hydrogen pressure between 110 and 210 bar[18], and the use of acid as the solvent [32,33]. The complete catalytic hydrogenation of quinoline to decahydroquinoline is a topic of significant interest as it not only provides access to valuable intermediates for various industrial processes but also aligns with the burgeoning interest in sustainable energy carriers [32]. In this study, the work is focused on hydrogenation of quinolone at various parameters such as temperature, hydrogen pressure, reaction time, solvents, reactant-to-solvent ratio, and effect of catalyst loading of 5% Pd loaded on alumina (Pd/Al_2O_3) with reaction kinetics evaluation using Markov chain Monte Carlo (MCMC) simulation tool and the route for product formation is identified.

4.2 Material and methods

4.2.1 Materials

Quinoline (AR, ≥ 98%), 1,2,3,4-tetrahydroquinoline (AR, ≥ 98%), decahydroquinoline (AR, ≥ 98%), toluene (AR, ≥ 98.0%) IPA (AR, ≥99%) are purchased from ThermoFischer scientific. Deionized water is used from an ultrapure water machine (elemental type 1820 C) from Chongqing Molecular Water System Co., ltd. A stainless-steel batch autoclave reactor with an internal capacity of 100 ml was employed for hydrogenation experiments under high-pressure conditions. A commercial Palladium-based catalyst (Pd/Al_2O_3) is used for the present experimental studies. The catalyst is procured from Alfa Aesar/Thermo Fisher Scientific in the form of powder with the composition of Pd-5 wt.%, and Al_2O_3-95 wt.% and the average particle size of the catalyst is about 2 nm.

4.2.2 Catalyst characterization

4.2.2.1 X-ray powder diffraction (XRD)

The XRD analysis is performed for the Pd/Al_2O_3 catalyst to measure the crystallinity and phase behavior of the catalyst. The crystalline nature and phase formation of the sample is analyzed using powder X-ray diffraction (PXRD) for the data taken from a PAN analytical X'pert Pro dual goniometer. It is equipped with an X-ray diffractometer using CuKα (1.5418 A^o) radiation within a scanning angle of 2θ from 20 to 80^o and a

step length of 2° every minute. The active phase formation of Palladium oxide (dark circles in Figure 4.2 and aluminium oxide (inverse triangles in Figure 4.2) is identified from the XRD analysis at different angles between 30 to 80° at intervals of 2°. The XRD analysis confirms the active deposition of PdO on the Al_2O_3 catalyst and is subjected to further surface area and TEM analysis.

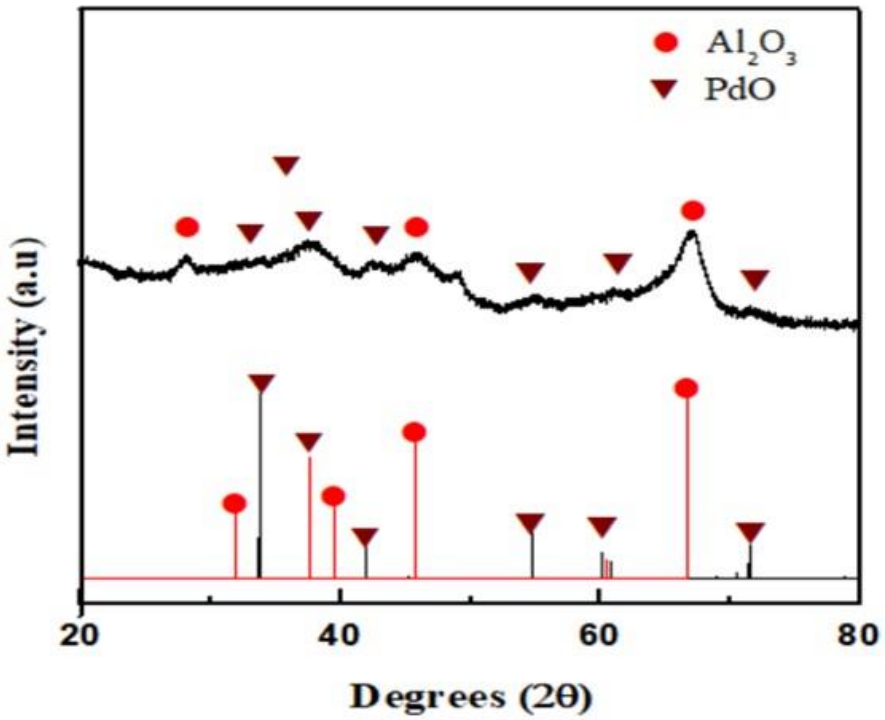

Figure 4.2 XRD analysis of the Pd/Al_2O_3 catalyst (● – PdO;▼ – Al_2O_3)

4.2.2.2 BET analysis

The surface area analysis is performed using the Braunner-Emmet-Teller (BET) method using the Quantachrome BET apparatus. The pore volume, average pore radius, and specific surface area measurements of calcined catalysts are performed using nitrogen adsorption-desorption at an analysis temperature of 77K. The method of BET surface area analysis involves the following steps: all the samples are outgassed at 120°C under vacuum for 2h to remove adsorbed moisture. Adsorption-desorption curve shows the characteristics of type IV isotherm with a prominent hysteresis loop in the relative pressure (P/P^o) range of 0.2 to 1 that denotes the presence of mesoporous structure as shown in Figure 4.3(a). The presence of hysteresis is due to the capillary phenomenon and the gases condense in the tiny capillary pores of the solid below the saturation pressure of the gas. The pore size distribution gives an idea of the presence

of mesoporous particles in the catalyst as shown in Figure 4.3(b). It can be inferred from the BET analysis that monolayers followed by multilayers formation at low pressures. Based on the monolayer adsorption capacity of the nitrogen gas, the total surface area of the catalyst sample is calculated using the BET isotherm equation. The specific surface area of 102.65m²/g and a total pore volume of 0.213 cc/g is obtained from BET surface area analysis. The reported literature shows that BET surface area is in good agreement with the measured values for the Pd/Al_2O_3[39].

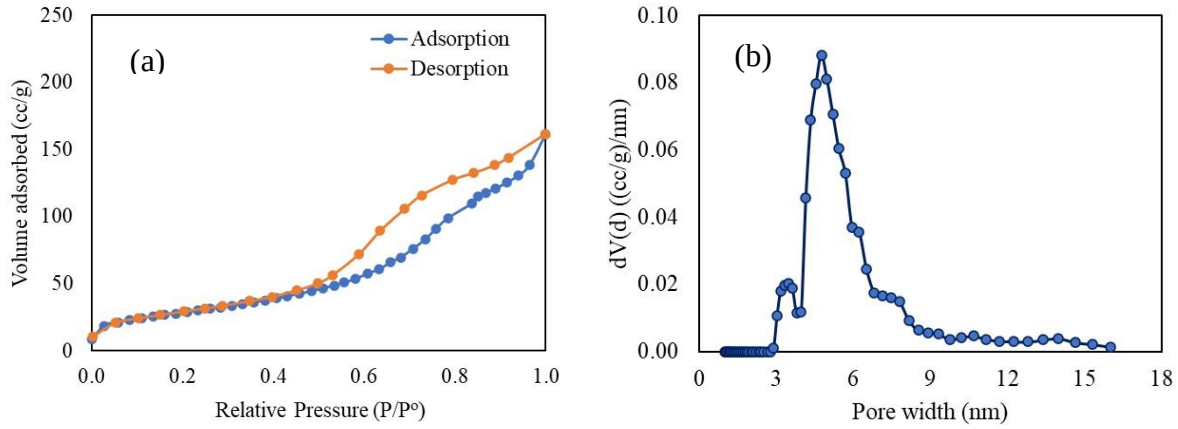

Figure 4.3 (a) BET adsorption-desorption isotherm (b) Pore size distribution

4.2.2.3 HRTEM analysis

High-resolution transmission electron microscopy (HRTEM) is a unique equipment in the investigation of local structure and chemistry of the catalyst particles dispersion. It also offers the microdiffraction pattern images and the reaction mechanisms can be derived from the TEM analysis. HRTEM analysis is carried out using a JEOL JEM F-200 microscope. Pd nanoparticles are well dispersed on the Al_2O_3 support for monometallic catalyst without any aggregate formation as shown in Figure 4.4(a). The selected area electron diffraction (SAED) pattern represents homogeneously distributed Pd particles on the support with nano-crystalline phase behavior as shown in Figure 4.4(b). The concentric ring-like structure reveals that the palladium is polycrystalline in nature. A typical HRTEM image of a fresh Pd/Al_2O_3 catalyst reveals a very narrow particle size distribution with an average particle size of 2.145 ± 0.092 nm as shown in Figure 4.4(c). The Energy dispersive X-ray spectroscopy (EDX) measurements for the Pd/Al_2O_3 of mapping image for all the elemental composition particles together are shown in Figure 4.4(d). The elemental composition of individual metal/oxide species are represented in Figure 4.4(e-g) for palladium, alumina, and oxygen for

a wavelength of 100 nm. This complete data indicates the proportional distribution of Pd particles on Al_2O_3 with homogeneous phase formation.

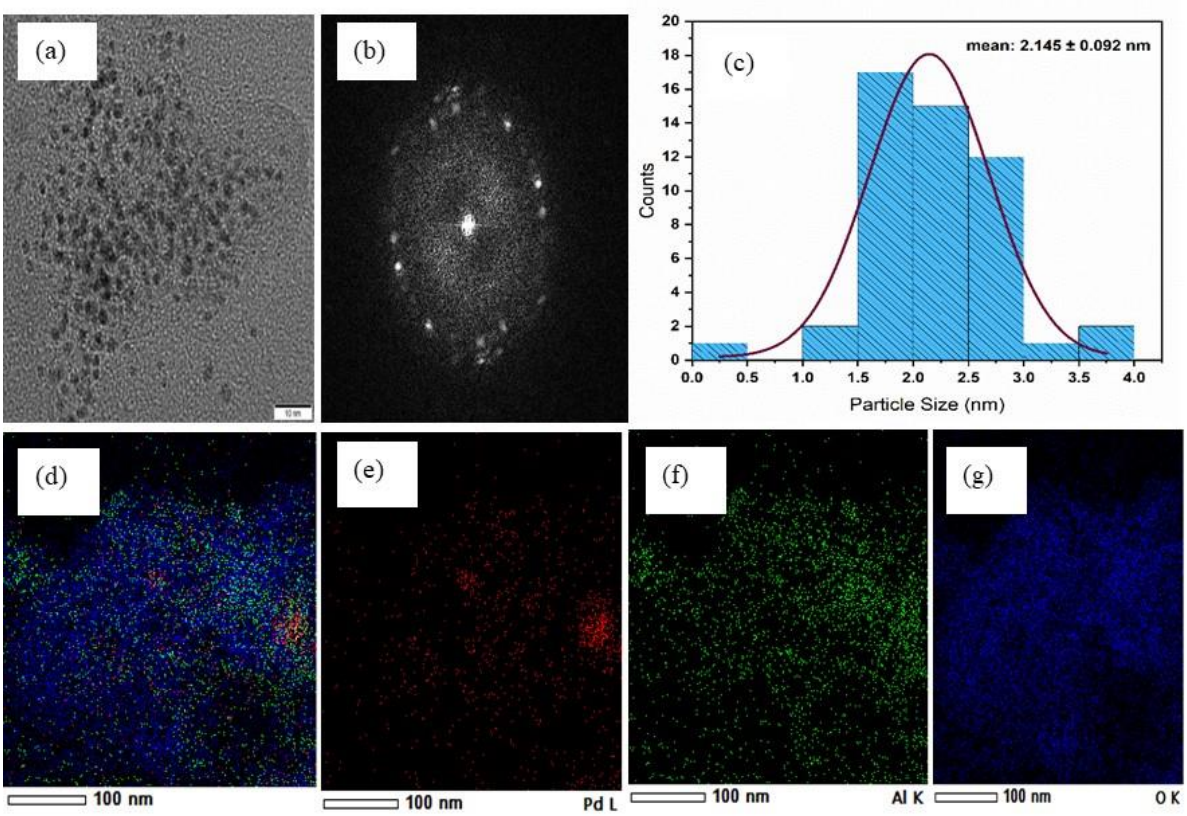

Figure 4.4 (a) HRTEM image, (b) SAED pattern, (c) particle size distribution (d) Overall energy dispersive X-ray spectroscopy (EDX) mapping image (e)-(g) EDS mapping images of a representative part of the sample containing palladium, aluminum, and oxygen

4.3 Hydrogenation experiments

4.3.1 Thermal screening unit (TSU)

Thermal screening unit (TSU) is an experimental unit extensively used for quick screening of liquids, solids, and heterogeneous systems for testing runaway conditions of the reaction. It provides data for "onset temperatures" of the reactions, temperature increase rates, and most importantly the rates and magnitudes of pressure rise in chemical systems. Reactive chemical testing includes evaluating feeds, intermediates, and products for thermal stability to precisely assess hazardous nature during storage, production, and transportation. The TSU is operated at a ramp rate of 2 °C/min from ambient to 160 °C and a pressure of 46 bar as shown in Figure 4.5. The increase in temperature and pressure with time is represented in Figure 4.5(a). Further,

experimental investigation of quinoline in isopropyl alcohol in the present reaction is safe and does not carry any hazards from TSU as evident from Figure 4.5(b). This can be justified as three is no sudden rise in temperature and pressure observed from TSU for nearly 140 minutes. This forms the basis for performing reactions at high-pressure conditions in converting the hydrogenation of quinoline to decahydroquinoline.

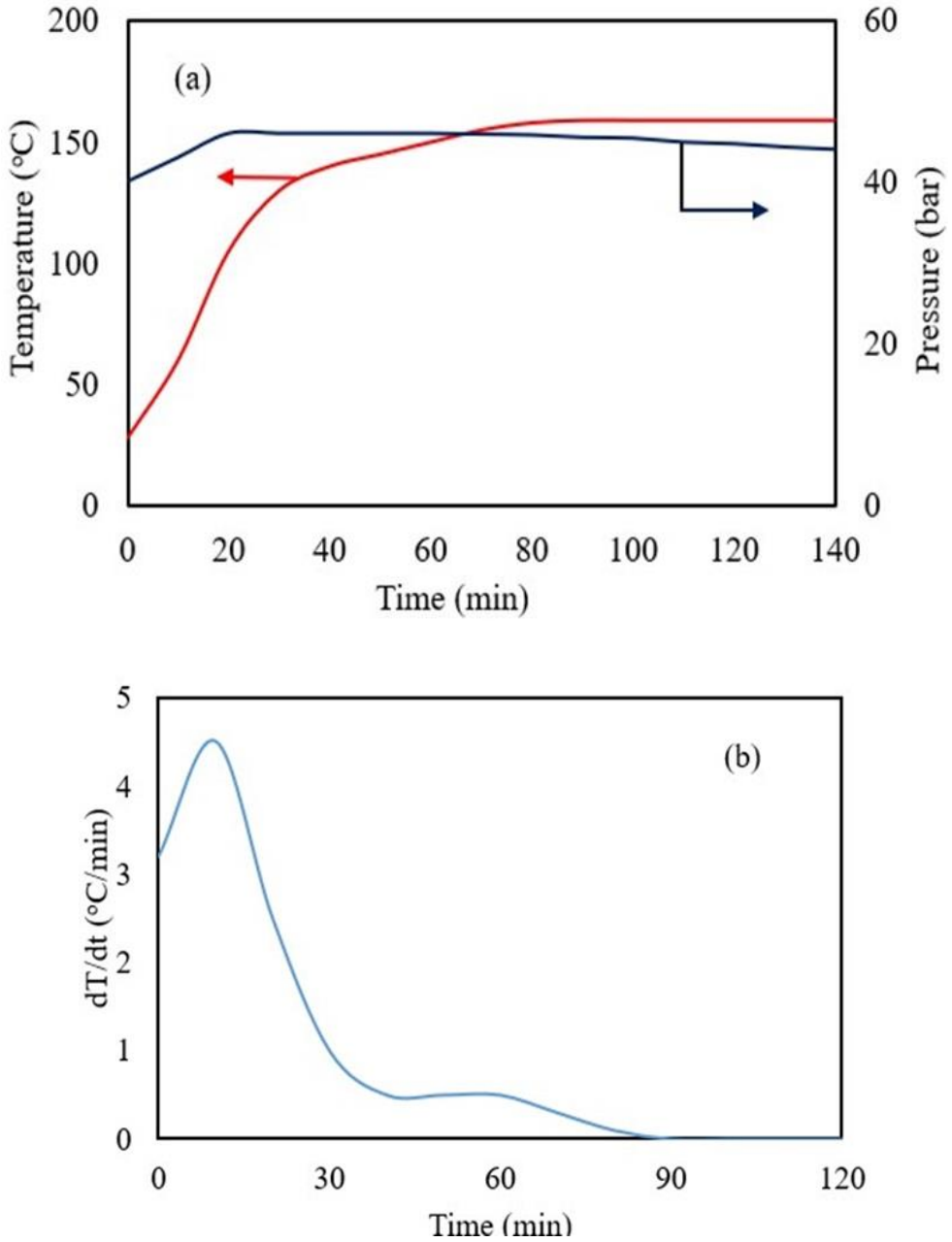

Figure 4.5 Thermal screening test for (a) temperature variation and (b) differential thermal analysis of quinoline with IPA in isothermal mode.

4.3.2 Hydrogenation in Autoclave reactor

Quinoline hydrogenation is performed for a quinoline quantity of 3 ml in 30 ml of isopropanol with 654 mg of Pd/Al_2O_3 catalyst (20wt.% Pd/Al_2O_3) using 100 ml autoclave reactor. The actual reactor set up and the schematic of the autoclave reactor set-up for high-pressure reactions along with product separation and sample analysis is shown in Figure 4.6**.** The autoclave is also purged with nitrogen followed by hydrogen from the reservoir to prevent oxide formation due to the presence of residual air in the reactor. The reactor is maintained in the pressure range from 40 to 60 bar and is operated in the temperature range from 50 to 175°C for different reaction times of 1 to 6 h. The downstream process consists of filtration followed by evaporation using rotavapor to separate the catalyst and solvent. The reaction products are analyzed by Agilent gas chromatography (GC) equipped with HP-5 capillary column (Dimensions are: 30m × 0.32mm × 0.25µm ID) using flame ionization detector maintained at 280°C with a flowrate of 0.8 ml/min using nitrogen as carrier gas. The split ratio of 1:1 and sample injection volume of 1 µL at a temperature of 250°C is used for the analysis. GC method is set as follows: The column temperature is increased from room temperature to 80ºC at a ramping rate of 5ºC/min. Further, it is increased from 80 to 280°C at a heating rate of 10°C/min with a hold time of 1 minute at 80°C.

(a)

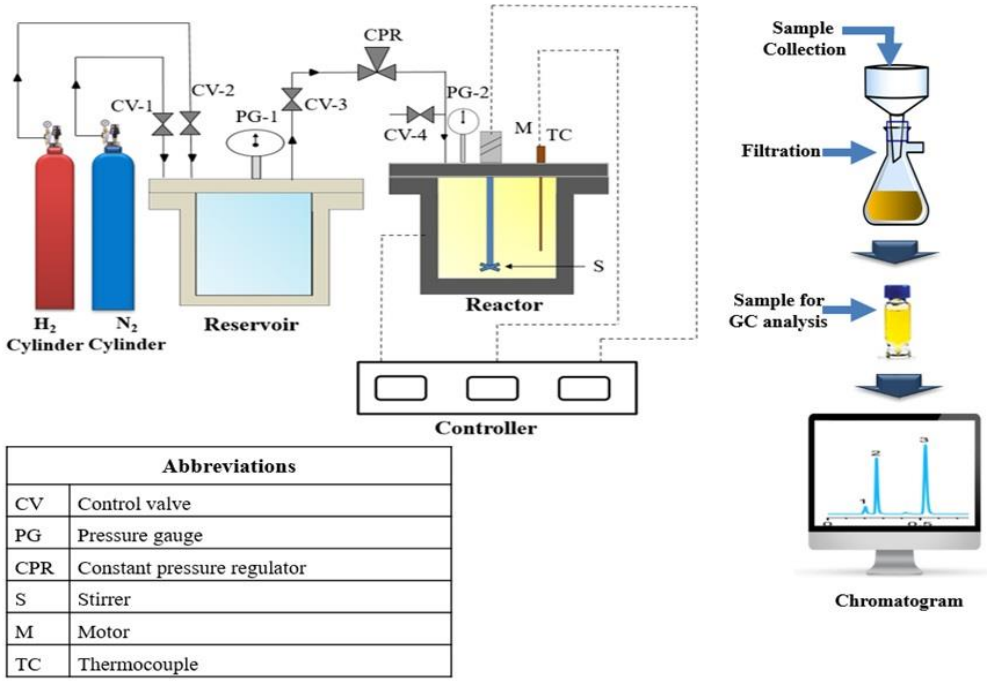

Abbreviations	
CV	Control valve
PG	Pressure gauge
CPR	Constant pressure regulator
S	Stirrer
M	Motor
TC	Thermocouple

(b)

Figure 4.6(a)Actual reactor setup (b) Schematic of the autoclave batch reactor for Quinoline hydrogenation

4.4 Results and discussion

The activated hydrogen atoms on the catalyst surface react with quinoline leading to the formation of metal-hydrogen complex. This complex involves interaction of hydrogen species with quinoline molecules. The hydrogenation of quinoline can occur at multiple positions on the aromatic ring leading to various possible hydrogenated products (py-THQ, bz-THQ and DHQ). The selectivity of the reaction is influenced by the catalyst and reaction conditions. The key factors influencing the reaction are catalyst and reaction conditions such as temperature, pressure, solvent, and time which play an important role in determining the reaction rates, yield, and selectivity towards product formation. The effect of reaction parameters is investigated and conversion of 100% is obtained under optimal conditions.

4.4.1 Effect of temperature

The effect of reaction temperature on quinoline hydrogenation is studied at temperatures of 75, 100, 125, 150 and 175°C. It is observed that complete conversion of quinoline for all

temperatures with intermediates or product formation. The catalyst and substrate molecules activates more readily at higher temperatures. It is observed that low temperature favors py-THQ formation as shown in Figure 4.7 (a). The reaction scheme shows that py-THQ and bz-THQ are intermediate products while DHQ is the final product. It is clear that there is a gradual decrease in intermediate formation and increase in DHQ formation with increase in temperature. At the reaction temperature of 175°C, the yield of DHQ is increased to nearly 99.41%. A negligible amount of bz-THQ is observed in the temperature range of 75 to 125°C. The increased amount of DHQ is equivalent to the decreased amount of py-THQ. It indicates that hydrogenation of quinoline first occurred on the N-heterocycle ring of quinoline which resulted in py-THQ and bz-THQ formation and are further hydrogenated to DHQ formation.

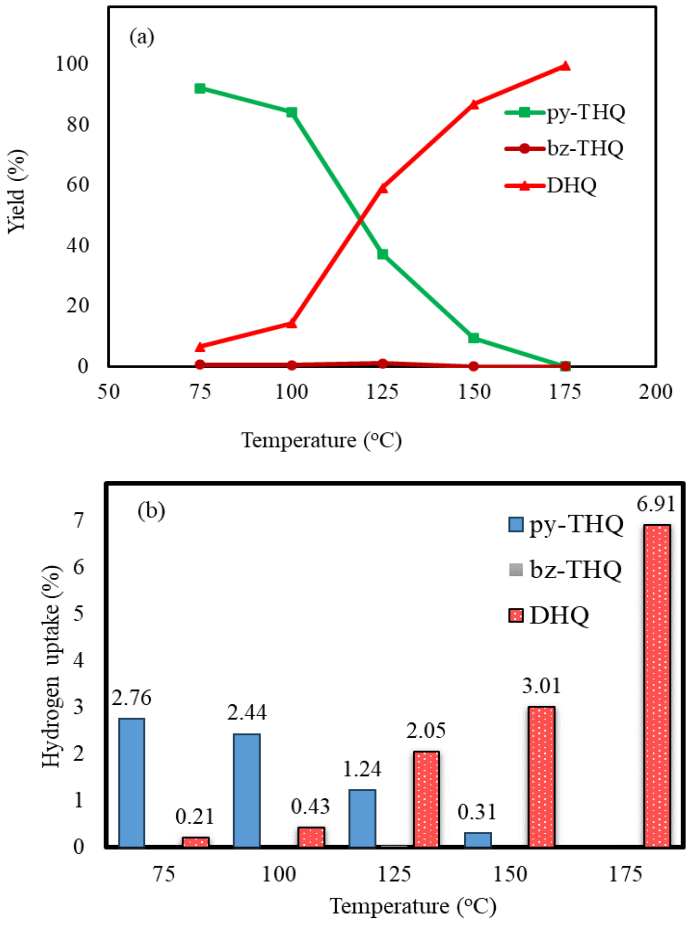

Figure 4.7 Effect of temperature at 50 bar a) on yield b) hydrogen uptake of py-THQ, bz-THQ, DHQ

The product distribution and performance analysis showed that a temperature of 175°C and pressure of 50 bar are optimized conditions to obtain more than 99% pure DHQ as the desired product. The effect of reaction temperature on hydrogen uptake is studied at temperatures from 75, 100, 125, 150, and 175°C. Low temperature favors py-THQ formation as shown in Figure 4.7 (b) hence, hydrogen uptake capacities of 2.16%, 2.76%, and 2.81% for 40 bar, 50 bar, and 60 bar pressures at 75 ^{o}C, respectively. With the increase in reaction temperature, hydrogen uptake of Quinoline increased drastically leading to the formation of DHQ. The reported literature also has a similar effect with respect to temperature on hydrogen uptake capacities [115]. Hydrogen uptake of quinoline increased to nearly 6.91% at an optimum reaction temperature of 175^{o}C and pressure of 50 bar for 5 h reaction time. A negligible amount of hydrogen uptake of quinoline via bz-THQ is observed in the temperature range from 75 to 125°C.

4.4.2 Effect of hydrogen pressure

The effect of pressure on quinoline hydrogenation is studied at different pressures of 40, 50, and 60 bar, and is observed that there is a complete conversion of quinoline for all pressures. The selectivity towards py-THQ is higher at 40 bar and 75°C with an yield of 95.97% as shown in Figure 4.8(a). The maximum formation of DHQ is observed for temperatures beyond 100°C at 50 bar as shown in Figure 4.8 (c). The py-THQ formation is higher in comparison to DHQ at low temperatures with an increase in pressures. The yield of DHQ increased to nearly 99.41% when the pressure was increased to 50 bar. Higher pressures of hydrogen gas can increase the rate of reaction, resulting in a higher yield of DHQ. This is due to an increase in pressure forces increasing the rate of reaction between hydrogen and quinoline molecules. Although the reaction rate increases with increase in pressure for py-THQ and bz-THQ formation, the rate of DHQ formation decreases at 60 bar which may be due to thermodynamic equilibrium for the desired product.

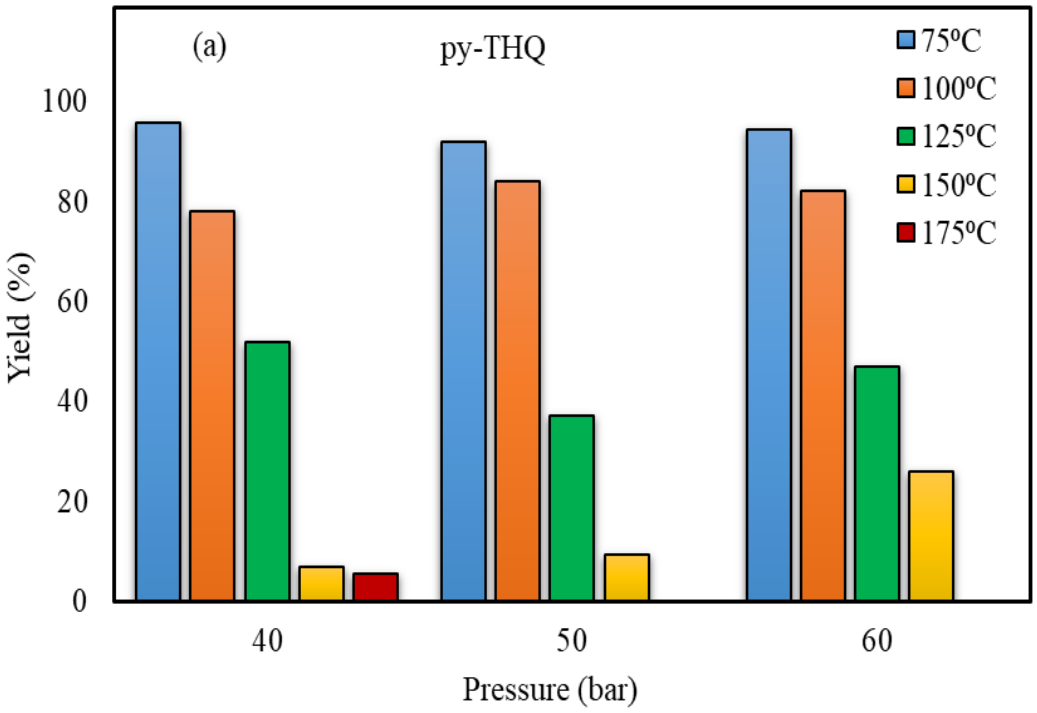
(a)
py-THQ
75°C
100°C
125°C
150°C
175°C
Yield (%)
100
80
60
40
20
0
40
50
60
Pressure (bar)

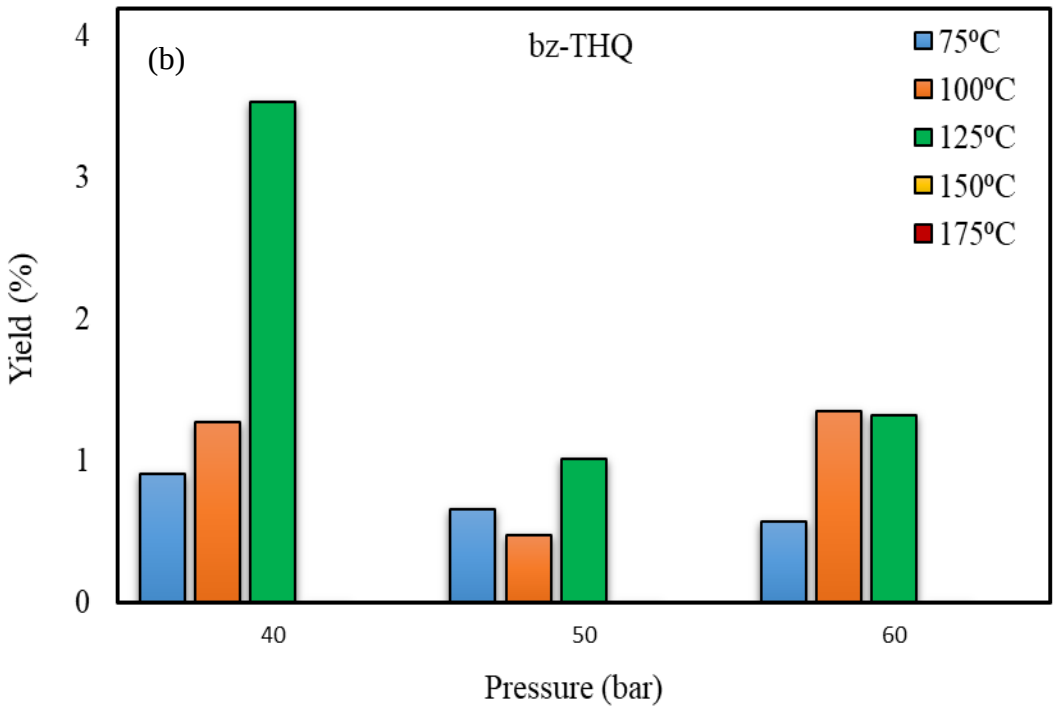
(b)
bz-THQ
75°C
100°C
125°C
150°C
175°C
Yield (%)
4
3
2
1
0
40
50
60
Pressure (bar)

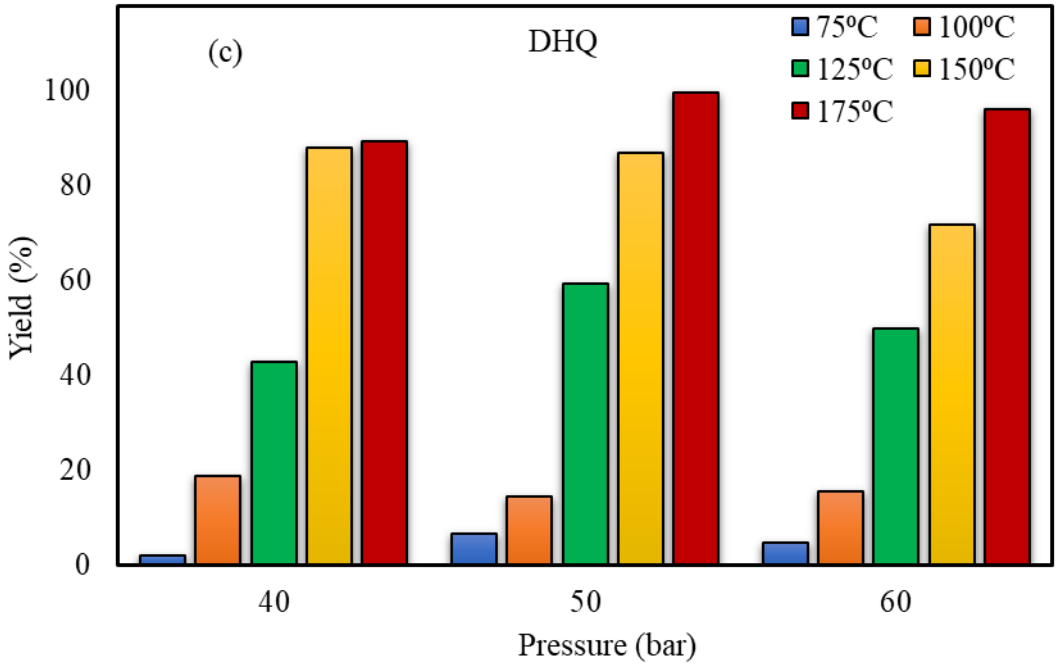

Figure 4.8 Effect of pressure on yield of (a) py-THQ (b) bz-THQ, and (c) DHQ at different reaction temperatures ranging from 75°C to 175°C

The pressure of hydrogen gas encourages the solubility of molecular hydrogen in solvent causing an increased number of reactive hydrogen atoms over palladium. Generally, LOHCs require high-pressure synthesis conditions to facilitate efficient hydrogen uptake by the LOHCs [10].

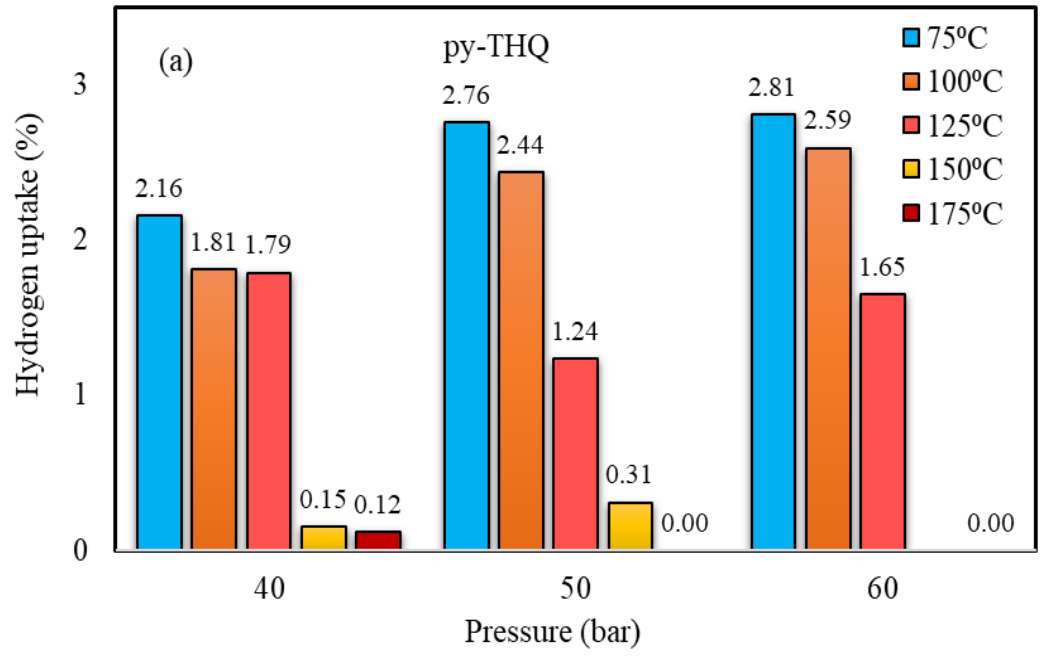

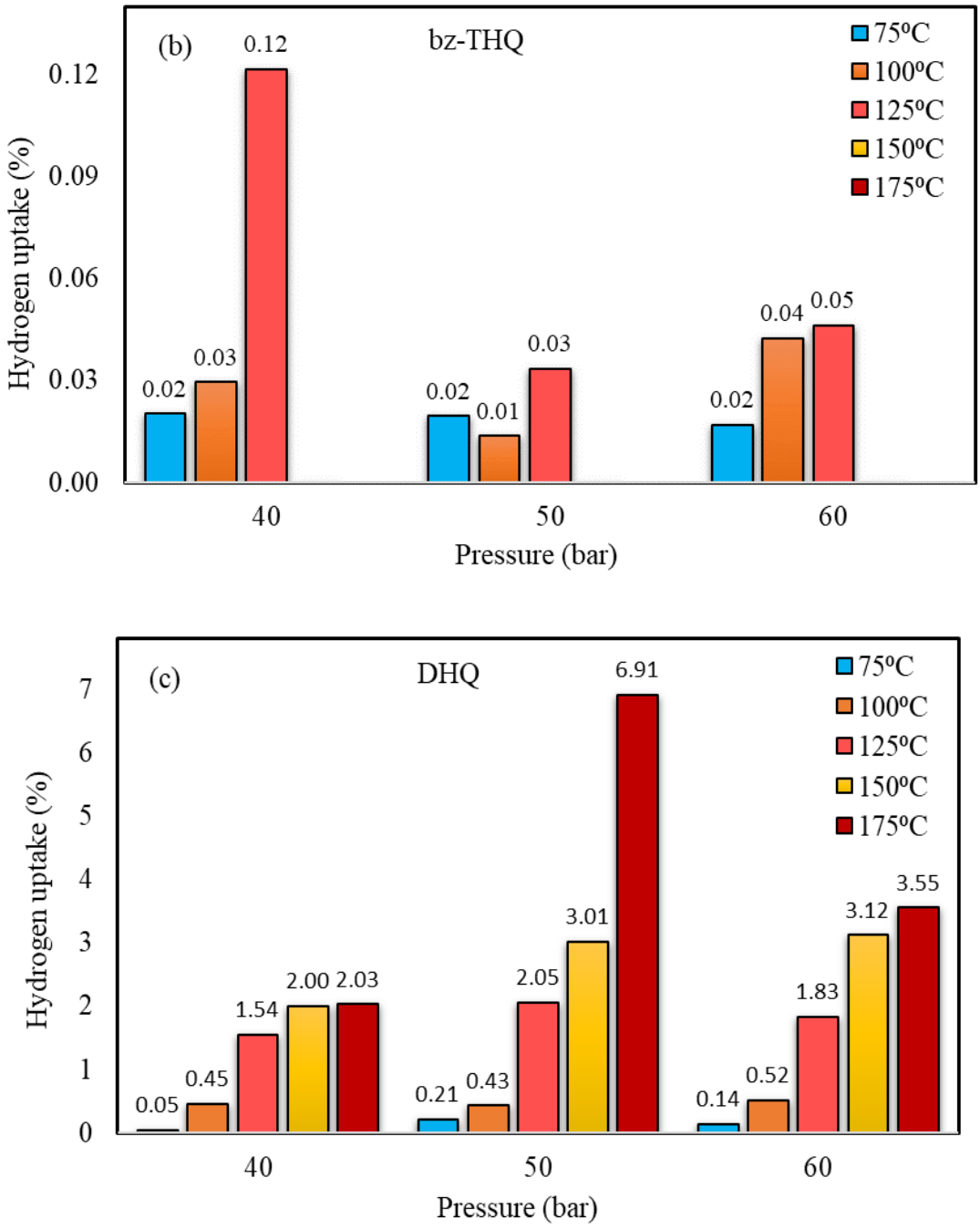

Figure 4.9 Effect of Pressure on hydrogen uptake of (a) py-THQ (b)bz-THQ, and (c) DHQ at different reaction temperature range from 75 to 175°C

Higher pressures of hydrogen gas can increase the rate of reaction, resulting in higher yield of DHQ. The hydrogen uptake of quinoline in the form of py-THQ is higher at 60 bar pressure and 75°C with hydrogen uptake of 2.81% as shown in Figure 4.9(a). It is observed that hydrogen uptake of quinoline is very negligible (< 0.1%) for almost all the conditions in the

form of bz-THQ for the temperature range of 75°C to 125°C as shown in Figure 4.9(b). The maximum hydrogen uptake of 6.91% is observed for 175°C and 50 bar as shown in Figure 4.9 (c).

4.4.3 Effect of catalyst loading

The quantity of catalyst for hydrogenation of quinoline is an important influencing factor in the process development in the context of reactor design and scale-up of the processes. Therefore, the effect of the catalyst loading on quinoline hydrogenation is studied using different loadings (5 wt.%, 10 wt.%, and 20 wt.%) at optimum temperature and pressure of 50 bar and 175°C. It is observed that with increase in the catalyst loading, py-THQ formation decreased and DHQ formation increased. The increase in catalyst loading increases the number of catalytic sites available for the quinoline hydrogenation. Therefore, it is observed that with increase in catalyst loadings from 5 to 20 wt.%, there is a huge increment in DHQ yield from 12.55 to 99.41% as shown in Figure 4.10 (a).

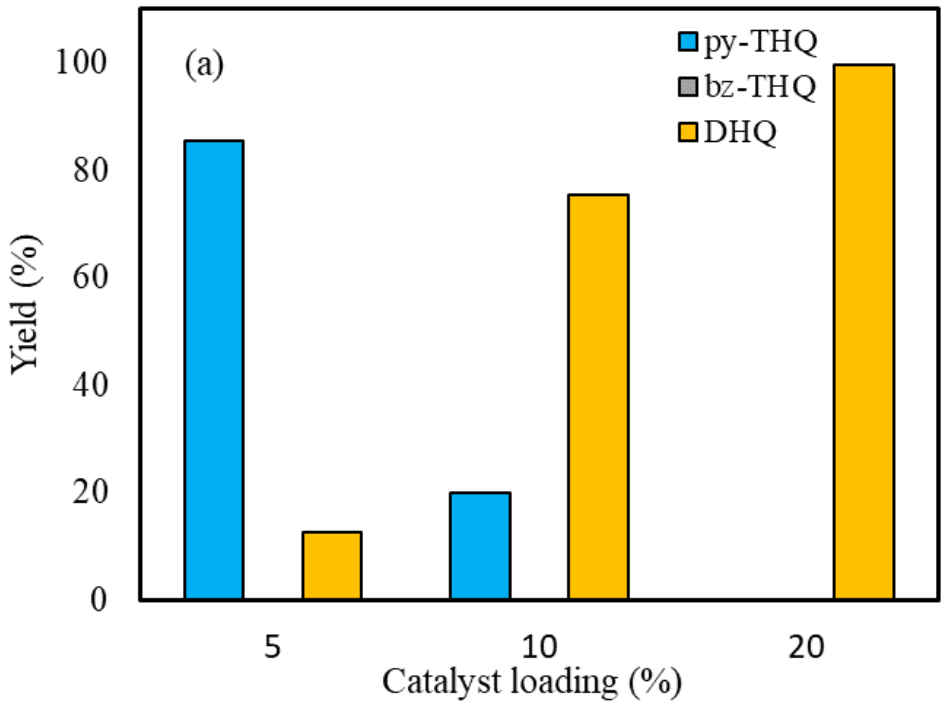

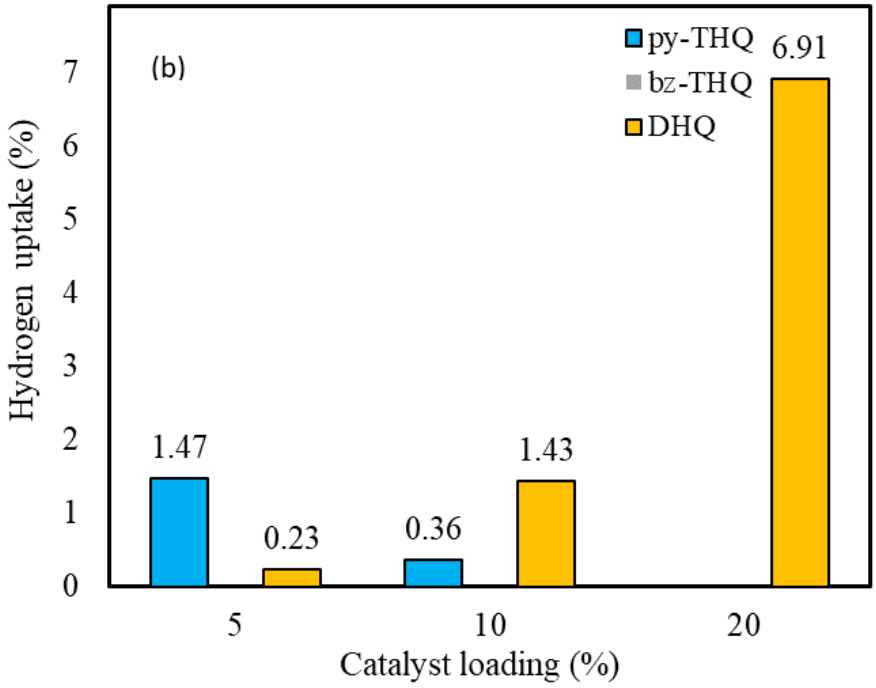

Figure 4.10 Effect of catalyst loading at 175°C and 50 bar on (a) Yield of products and (b) Hydrogen uptake

The effect of catalyst loading on hydrogen uptake at 5, 10, and 20 wt.% is studied with respect to the reactant fed to the system. It is observed that increase in the catalyst loading, the availability of active sites for the surface reaction increased. This has led to an increase in the hydrogenation of quinoline to DHQ formation. Thus, hydrogen uptake of quinoline increases with the increase in the formation of DHQ as shown in Figure 4.10(b). Hydrogen uptake of quinoline is observed to be maximum at 20 wt.% catalyst with a capacity of 6.91%.

4.4.4 Effect of Solvent

The effect of solvent on the activity of the Pd/Al_2O_3 catalyst is investigated using water, isopropyl alcohol, and toluene for quinoline hydrogenation. Since the properties of the solvents can modify reaction mechanistic features by affecting the reactant free energy states which can modify the viability of various reaction pathways [35]. As shown in Figure 4.11(a), the catalyst activity is significantly influenced by the use of solvent in the following sequence: IPA>toluene > water. The results suggest that the solvent with stronger polarity promotes the hydrogenation of quinoline over the Pd/Al_2O_3 catalyst which is consistent with the reported literature [32].

Water as a solvent is least suitable as it favors the formation of py-THQ and results in low DHQ yield of 77.28%. The highest yield of DHQ was obtained (99.52%) by using IPA as a solvent. In addition to this hydroxyl group of the polar solvent interaction with the heteroatom of the quinoline, it helps to increase the solubility and availability of the substrate in the reaction medium. Therefore, the choice of solvent plays an important role in enhancing the complete hydrogenation of quinoline to DHQ. The yield of quinoline intermediates and their product is studied for solvent effect and its effect on the product yield is represented in Figure 4.11(a). Water as a solvent is less suitable in comparison to the other two solvents with 2.68 wt.% of H_2 uptake by Quinoline whereas toluene and isopropyl alcohol shows nearly the same effect on H_2 uptake by Quinoline. It can be concluded that H_2 uptake of 6.9 % using isopropyl alcohol is the most suitable solvent for Quinoline as LOHC to DHQ formation as shown in Figure 4.11(b)

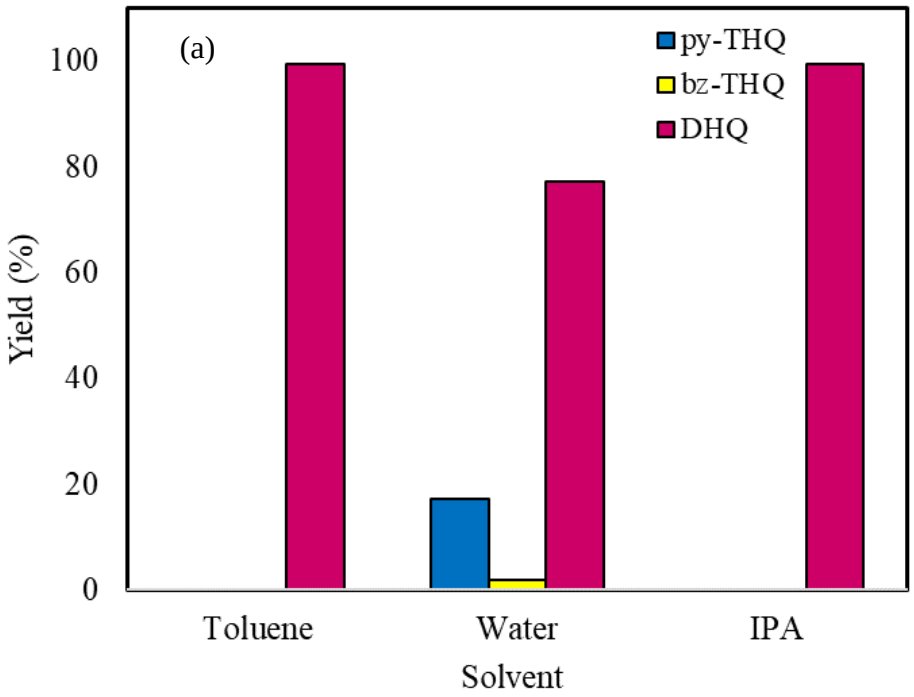

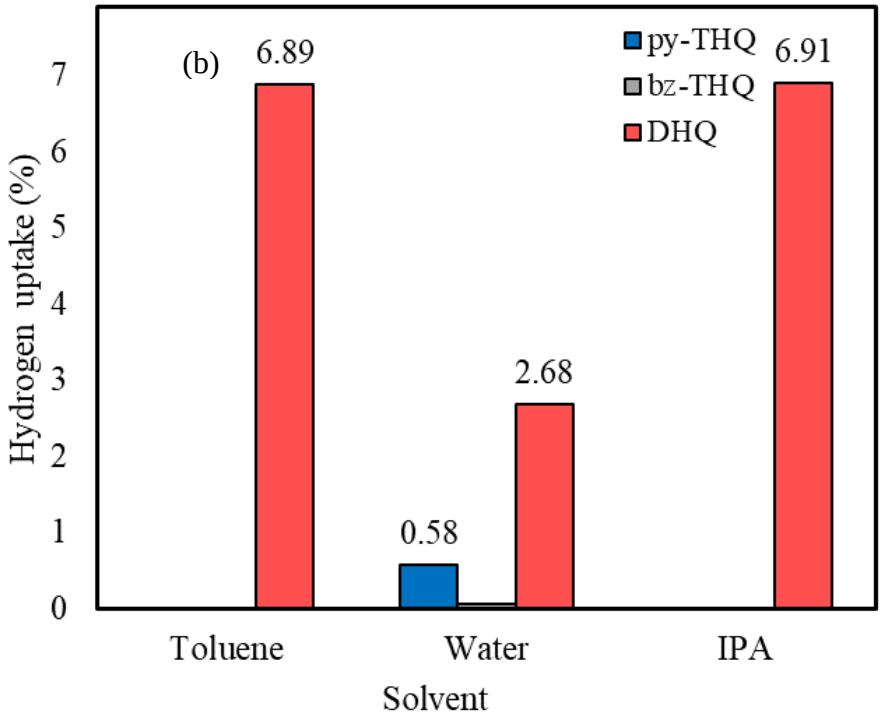

Figure 4.11 Effect of solvent reaction temperature of 175°C and 50 bar on a) Yield of DHQ b) Hydrogen uptake

4.5 Reaction mechanism

In quinoline hydrogenation, py-THQ and bz-THQ are the intermediates leading to DHQ formation through two different pathways: :(i) Quinoline to intermediates formation (1,2,3,4 tetrahydroquinoline (py-THQ)/ 5,6,7,8-tetrahydroquinoline (bz-THQ)) (ii) conversion of intermediates to product (DHQ) formation through 2 different pathways as shown in Figure 4.1 [18,32]. Heteroatom 'N' containing aromatic ring in quinoline is more prone to hydrogenation over the benzene ring because the C-N bond energy of 305 kJ/mol which is much less than the C=C bond energy of 614 kJ/mol. The molecular hydrogen already adsorbed on the active site of the catalyst is easily available for hydrogenating the pyridine ring due to the lone pair of electrons of nitrogen atom to py-THQ and the presence of the heteroatom in the ring. Hence, the hydrogenation of the heterocyclic ring is more favourable than the homocyclic benzene ring. The physical properties of the quinoline such as thermal stability, high gravimetric hydrogen densities, and high storage capacity can alter the thermodynamic driving force and hydrogenation/ dehydrogenation under reversible conditions [30]. As reported in the literature, heterocyclic compounds need low temperatures for dehydrogenation

with decreased enthalpy and faster hydrogen release ability [5,30]. Hence, the major quantity of intermediate product formed is py-THQ [36–38]. The increase in temperature can disrupt the C-N bonds of nitrogen-containing heterocyclic compounds to a great extent in the selectivity of DHQ through py-THQ via path 1 of the reaction mechanism [38]. Therefore, the reaction mechanism for the hydrogenation of quinoline to DHQ formation for the Pd/Al_2O_3 catalyst is simplified [38]. as shown in Figure 4.12.

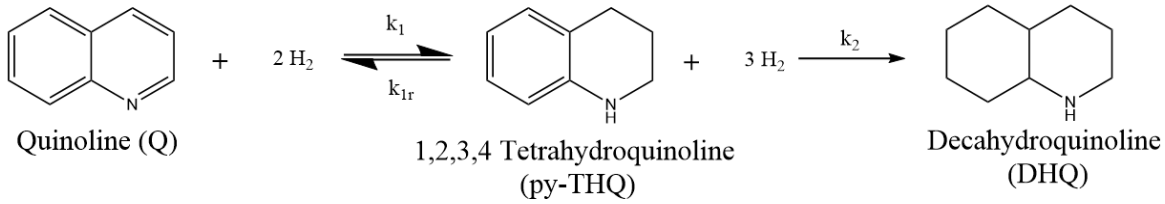

Figure 4.12 Possible reaction mechanism for hydrogenation of Quinoline to DHQ

4.6 Kinetic model development and validation

4.6.1 Power law kinetic model

The kinetic model is developed based on the reaction scheme and experimental observations for quinoline to py-THQ, bz-THQ, and DHQ formation. Although hydrogenation of heterocyclic compounds containing nitrogen has been published in the literature, the reported kinetics information for quinoline hydrogenation is not sufficient for the development of processes and scale-up of the reactors. In the present study, intermediates formed from quinoline are py-THQ and bz-THQ formation in low quantity. The absence of bz-THQ may be due to nitrogen heterocyclic rings having a higher electronic cloud density than benzene rings and are more easily adsorbed on the active sites of hydrogenation reactions. Considering the concentration of the hydrogenated species, the following assumptions are considered for the development of the power law kinetic model into the simplified form:

i) The concentration of the hydrogen is assumed to be constant as it is in excess in the reaction
ii) No Mass Transfer Limitations: It is assumed that the reactants are perfectly mixed and there are no mass transfer limitations. This implies that the rate of reaction is solely dependent on the chemical kinetics and not on the rate of mixing or diffusion.
iii) Quinoline to py-THQ reaction is assumed to be reversible [32]

iv) py-THQ to DHQ reaction is assumed to be irreversible [32]

The kinetic model was developed based on the following assumptions and the volume of the reaction mixture used for quinoline hydrogenation with the following rate expressions:

$$r_A = \frac{dC_A}{dt} = \frac{m_{cat}}{V}(-k_1 C_A + k_{1r} C_B) \quad (4.1)$$

$$r_B = \frac{dC_B}{dt} = \frac{m_{cat}}{V}(k_1 C_A - k_{1r} C_B - k_2 C_B) \quad (4.2)$$

$$r_C = \frac{dC_C}{dt} = \frac{m_{cat}}{V}(k_2 C_B) \quad (4.3)$$

Where,

r is reaction rate, mol/(m^3.min)

m_{cat} represents catalyst loading, g

k is rate constant, $m^3/(g_{cat}.\ min)$

C_A, C_B, and C_C are concentrations (mol/m^3) of reactants A, B and C, respectively

V is the volume of the reaction mixture, m^3

4.6.2 Kinetic study and validation with model

Hydrogenation experiments are performed for temperatures of 125, 150, and 175°C at a pressure of 50 bar for the reaction times of 1, 2, 3, 4, and 5 h. The concentration of the reactant, intermediate, and product species (quinoline, pz-THQ, and DHQ) are represented as C_A, C_B, and C_C, respectively. The concentration of the species for every one hour of reaction at different temperatures is shown in Figure 4.13. The quinoline concentration decreased abruptly while the formation of pz-THQ predominates simultaneously. At the same time, the rate of formation of DHQ prevails at the expense of pz-THQ hydrogenation. There is a gradual decrease in pz-THQ concentration and the increase in DHQ concentration is observed with an increase in reaction time at 125, and 150 °C as shown in Figure 4.13(a-b). On the other hand, there is a sudden decrease in pz-THQ and an increase in DHQ formation in 1 hour of reaction time as shown in Figure 4.13(c). As there is no driving force for the backward reaction to take place, the product formation suppresses the existence of reactant and intermediates. The experimental data points are used for model prediction and validated in the Figure 4.13(a-c).

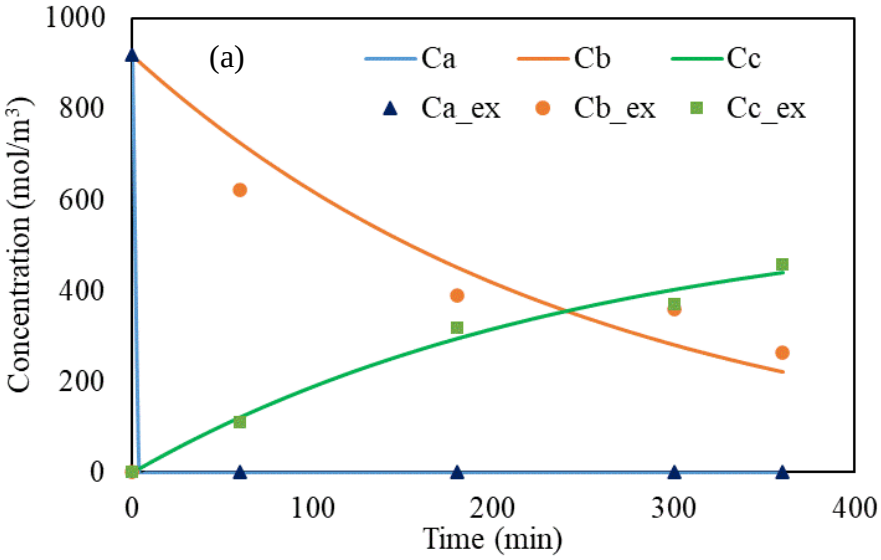
(a)
Ca
Cb
Cc
Ca_ex
Cb_ex
Cc_ex
Concentration (mol/m³)
Time (min)
0
200
400
600
800
1000
0
100
200
300
400

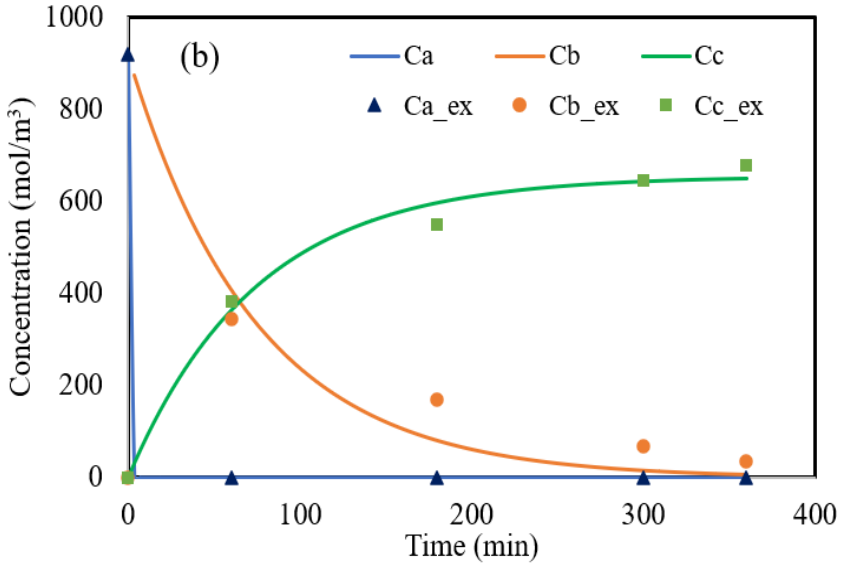
(b)
Ca
Cb
Cc
Ca_ex
Cb_ex
Cc_ex
Concentration (mol/m³)
Time (min)
0
200
400
600
800
1000
0
100
200
300
400

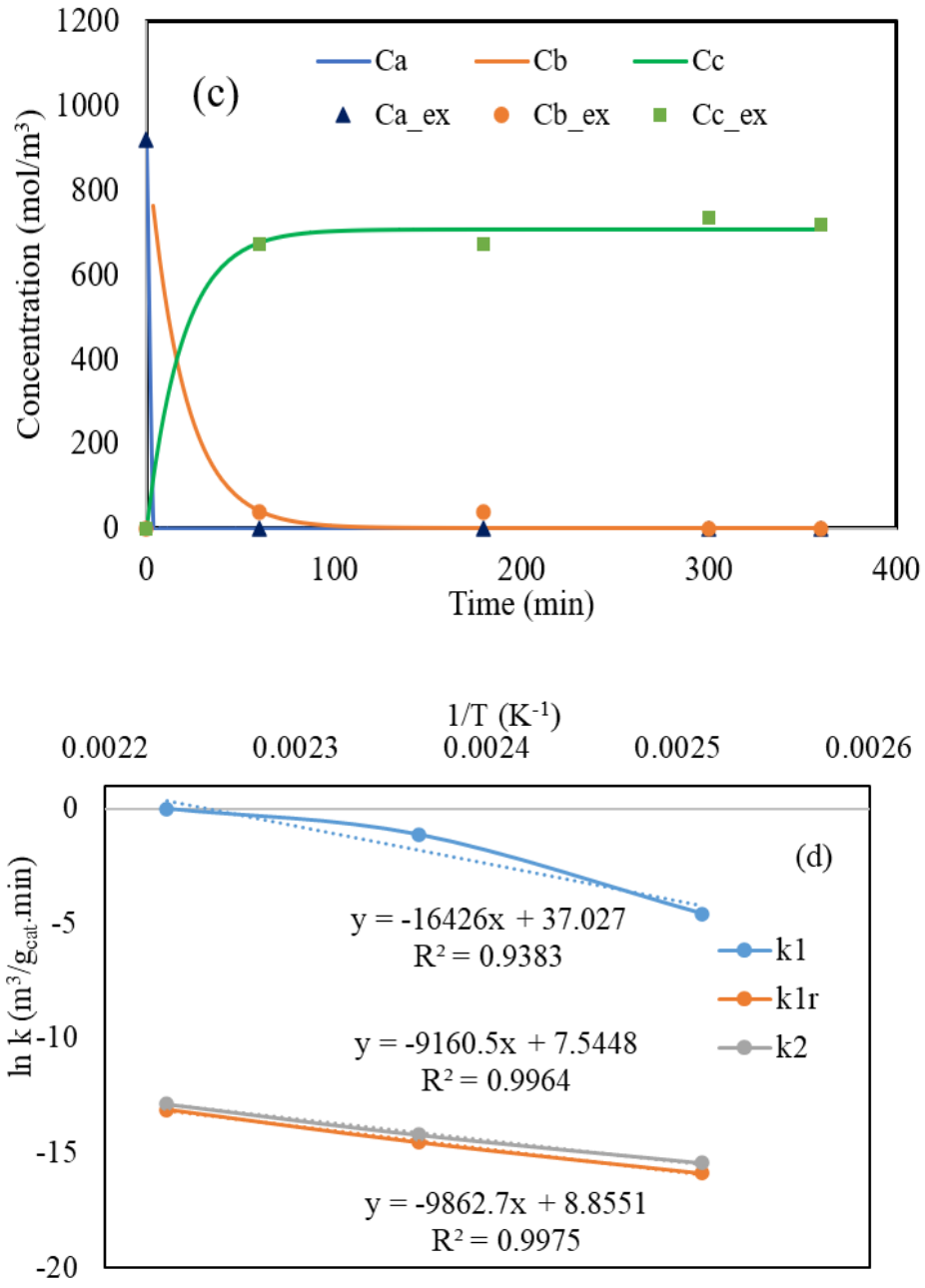

Figure 4.13 Concentration profile at 50 bar hydrogen pressure for different temperatures (a)125 ºC (b) 150 ºC and (c) 175 ºC (d) Rate constants at different temperatures

("---" represents the model and symbols represent experimental data points)

4.6.3 Parameter estimation

The kinetic parameters are estimated using experimental data points and model predictions. The models represented in the above equations (1) to (3) are used using the Markov Chain Monte Carlo (MCMC) simulation tool to solve the ordinary differential equations numerically while also estimating parameter values. Each reaction rate constant (k_1, $k_{1r,}$ and k_2) is determined as a parameter, and the best-fitting value was estimated by minimizing the sum of the square error of the concentration between the experimental data and the model calculation. The evaluated rate constants, activation energies, and pre-exponential parameters are reported in Table 2. Since every R^2 value is more than 0.99, the regression findings for the Arrhenius parameters are compelling. The changing trend of the pre-exponential factor is consistent with that of activation energy. . It is observed that the quinoline to py-THQ formation reaction had the largest activation energy of 136.57 kJ/mol and the pre-exponential factor of 1.203×10^{16}, hence, it is envisaged that quinoline to pz-THQ formation controls the rate of reaction. Indeed, Xie et al. (2022) also found the same observation as quinoline hydrogenation to py-THQ is the rate-determining step[37].

Table 4.2 Estimated rate constants and Arrhenius Parameters

Rate Constant ($m^3/(g_{cat}.min)$)	Temperature (^oC)			Activation energy, E_a (kJ/mol)	Pre-exponential factor, k_o ($m^3/(g_{cat}.min)$)	$(Residual)^2$ R^2
	125	150	175			
k1	1.0e-02	3.3e-01	3.7e-03	136.57	1.20e+16	0.99
k1r	1.3e-07	4.8e-07	2.0e-06	82.00	1890.88	0.99
K_2	1.99e-7	6.80e-7	2.6e-06	76.16	7010.05	0.99

4.7 Conclusions

Quinoline is identified as a promising and thermally stable LOHC molecule using a thermal screening unit. Hydrogenation of quinoline is investigated over a palladium supported by an alumina catalyst. The effect of temperature, hydrogen pressure, reaction time, different solvents, and catalyst loading on the hydrogenation and hydrogen uptake capacity of quinoline

in the liquid phase are studied and the optimal conditions of 175^{o}C and 50 bar for 20 wt.% of Pd/Al_2O_3 are obtained. A Hydrogen uptake capacity of 6.91 wt.% is achieved with more than 99% DHQ yield using IPA as solvent under optimal reaction conditions. Based on the experimental data, the reaction mechanism is proposed for the reaction pathway for DHQ formation. The hydrogenation of quinoline to DHQ formation is 100% and selectivity towards decahydroquinoline of 99% is achieved. The reaction kinetic model is developed for a simplified reaction path for DHQ formation and is simulated using the Monte Carlo simulation tool and validated with experimental observations. It is concluded from the kinetic study that the formation of pz-THQ is the rate-determining step in the hydrogenation of quinoline to decahydroquinoline formation.

4.8 References

[1] Sage V, Patel J, Hazewinkel P, Yasin QUA, Wang F, Yang Y, et al. Recent progress and techno-economic analysis of liquid organic hydrogen carriers for Australian renewable energy export – A critical review. Int J Hydrogen Energy 2024;56:1419–34. https://doi.org/10.1016/j.ijhydene.2023.12.269.

[2] Chen X, Gierlich CH, Schötz S, Blaumeiser D, Bauer T, Libuda J, et al. Hydrogen Production Based on Liquid Organic Hydrogen Carriers through Sulfur Doped Platinum Catalysts Supported on TiO_2. ACS Sustain Chem Eng 2021;9:6561–73. https://doi.org/10.1021/acssuschemeng.0c09048.

[3] Faye O, Szpunar J, Eduok U. ScienceDirect A critical review on the current technologies for the generation, storage , and transportation of hydrogen. Int J Hydrogen Energy 2022;47:13771–802. https://doi.org/10.1016/j.ijhydene.2022.02.112.

[4] Yadav V, Sivakumar G, Gupta V, Balaraman E. Recent Advances in Liquid Organic Hydrogen Carriers: An Alcohol-Based Hydrogen Economy. ACS Catal 2021;11:14712–26. https://doi.org/10.1021/acscatal.1c03283.

[5] Crabtree RH. Hydrogen storage in liquid organic heterocycles. Energy Environ Sci 2008;1:134–8. https://doi.org/10.1039/b805644g.

[6] Cao Y, Ding L, Qiu Z, Zhang H. Biomass-derived N-doped porous two-dimensional carbon nanosheets supported ruthenium as effective catalysts for the selective hydrogenation of quinolines under mild conditions. Catal Commun 2020;143.

https://doi.org/10.1016/j.catcom.2020.106048.

[7] Makaryan IA, Sedov I V. Hydrogenation/Dehydrogenation Catalysts for Hydrogen Storage Systems Based on Liquid Organic Carriers (A Review). Pet Chem 2021;61:977–88. https://doi.org/10.1134/S0965544121090085.

[8] Spatolisano E, Restelli F, Matichecchia A, Pellegrini LA, Angelis AR De, Cattaneo S, et al. ScienceDirect Assessing opportunities and weaknesses of green hydrogen transport via LOHC through a detailed techno-economic analysis. Int J Hydrogen Energy 2023;52:703–17. https://doi.org/10.1016/j.ijhydene.2023.08.040.

[9] Kim TWC for HS in LOHC, Jeong H, Baik JH, Suh YW. State-of-the-art Catalysts for Hydrogen Storage in Liquid Organic Hydrogen Carriers. Chem Lett 2022;51:239–55. https://doi.org/10.1246/cl.210742.

[10] Tsogt N, Gbadago DQ, Hwang S. Exploring the potential of liquid organic hydrogen carrier (LOHC) system for efficient hydrogen storage and Transport: A Techno-Economic and energy analysis perspective. Energy Convers Manag 2024;299:117856. https://doi.org/10.1016/j.enconman.2023.117856.

[11] Gianotti E, Taillades-Jacquin M, Rozière J, Jones DJ. High-Purity Hydrogen Generation via Dehydrogenation of Organic Carriers: A Review on the Catalytic Process. ACS Catal 2018;8:4660–80. https://doi.org/10.1021/acscatal.7b04278.

[12] Rao N, Lele AK, Patwardhan AW. Optimization of Liquid Organic Hydrogen Carrier (LOHC) dehydrogenation system. Int J Hydrogen Energy 2022;47:28530–47. https://doi.org/10.1016/j.ijhydene.2022.06.197.

[13] Markiewicz M, Zhang YQ, Empl MT, Lykaki M, Thöming J, Steinberg P, et al. Hazard assessment of quinaldine-, alkylcarbazole-, benzene- and toluene-based liquid organic hydrogen carrier (LOHCs) systems. Energy Environ Sci 2019;12:366–83. https://doi.org/10.1039/c8ee01696h.

[14] Teichmann D, Arlt W, Wasserscheid P. Liquid Organic Hydrogen Carriers as an efficient vector for the transport and storage of renewable energy. Int J Hydrogen Energy 2012;37:18118–32. https://doi.org/10.1016/j.ijhydene.2012.08.066.

[15] Niermann M, Beckendorff A, Kaltschmitt M, Bonhoff K. Liquid Organic Hydrogen Carrier (LOHC) – Assessment based on chemical and economic properties. Int J

Hydrogen Energy 2019;44:6631–54. https://doi.org/10.1016/j.ijhydene.2019.01.199.

[16] Safronov SP, Vostrikov S V., Samarov AA, Wasserscheid P, Müller K, Verevkin SP. Comprehensive thermodynamic study of substituted indoles/perhydro indoles as potential liquid organic hydrogen carrier system. Fuel 2023;331. https://doi.org/10.1016/j.fuel.2022.125764.

[17] Preuster P, Papp C, Wasserscheid P. Liquid organic hydrogen carriers (LOHCs): Toward a hydrogen-free hydrogen economy. Acc Chem Res 2017;50:74–85. https://doi.org/10.1021/acs.accounts.6b00474.

[18] Aakko-Saksa PT, Cook C, Kiviaho J, Repo T. Liquid organic hydrogen carriers for transportation and storing of renewable energy – Review and discussion. J Power Sources 2018;396:803–23. https://doi.org/10.1016/j.jpowsour.2018.04.011.

[19] Yang M, Dong Y, Fei S, Pan Q, Ni G, Han C, et al. Hydrogenation of N-propylcarbazole over supported ruthenium as a new prototype of liquid organic hydrogen carriers (LOHC). RSC Adv 2013;3:24877–81. https://doi.org/10.1039/c3ra44760j.

[20] Vostrikov S V., Konnova ME, Turovtsev V V., Verevkin SP. Thermodynamics of hydrogen storage: LOHC system 1-alkyl-indole/octahydro-1-alkyl-indole. Fuel 2023;344:128079. https://doi.org/10.1016/j.fuel.2023.128079.

[21] Verevkin SP, Safronov SP, Samarov AA, Vostrikov S V. Hydrogen storage: Thermodynamic analysis of alkyl-quinolines and alkyl-pyridines as potential liquid organic hydrogen carriers (LOHC). Appl Sci 2021;11. https://doi.org/10.3390/app112411758.

[22] Kokane R, Corre Y, Kemnitz E, Dongare MK, Agbossou-Niedercorn F, Michon C, et al. Palladium supported on magnesium hydroxyl fluoride: An effective acid catalyst for the hydrogenation of imines and N-heterocycles. New J Chem 2021;45:19572–83. https://doi.org/10.1039/d1nj03760a.

[23] Prajapati SM, Patel KD, Vekariya RH, Panchal SN, Patel HD. Recent advances in the synthesis of quinolines: A review. RSC Adv 2014;4:24463–76. https://doi.org/10.1039/c4ra01814a.

[24] Matada BS, Pattanashettar R, Yernale NG. A comprehensive review on the biological interest of quinoline and its derivatives. Bioorganic Med Chem 2021;32.

https://doi.org/10.1016/j.bmc.2020.115973.

[25] Timelthaler D, Topf C. Heterogeneous Hydrogenation of Quinoline Derivatives Effected by a Granular Cobalt Catalyst. Synth 2021;54:629–42. https://doi.org/10.1055/a-1654-3302.

[26] Yu CY, Hatcher WJ, Bertsch W. Hydrodenitrogenation of Quinoline with Y-Type Zeolite. Ind Eng Chem Res 1989;28:13–20. https://doi.org/10.1021/ie00085a004.

[27] Massoth FE, Kim SC. Kinetics of the HDN of quinoline under vapor-phase conditions. Ind Eng Chem Res 2003;42:1011–22. https://doi.org/10.1021/ie020390t.

[28] Nguyen MT, Tayakout-Fayolle M, Pirngruber GD, Chainet F, Geantet C. Kinetic Modeling of Quinoline Hydrodenitrogenation over a NiMo(P)/Al_2O_3 Catalyst in a Batch Reactor. Ind Eng Chem Res 2015;54:9278–88. https://doi.org/10.1021/acs.iecr.5b02175.

[29] Aboul-Gheit AK. The Kinetics of Quinoline Hydrodenitrogenation through Reaction Intermediate Products. Can J Chem 1975;53:2575–9. https://doi.org/10.1139/v75-366.

[30] Gemechu DN, Mohammed AM, Redi M, Bessarabov D, Mekonnen YS, Obodo KO. First principles-based approaches for catalytic activity on the dehydrogenation of liquid organic hydrogen carriers: A review. Int J Hydrogen Energy 2023;48:33186–206. https://doi.org/10.1016/j.ijhydene.2023.05.072.

[31] Ren D, He L, Yu L, Ding RS, Liu YM, Cao Y, et al. An unusual chemoselective hydrogenation of quinoline compounds using supported gold catalysts. J Am Chem Soc 2012;134:17592–8. https://doi.org/10.1021/ja3066978.

[32] Campanati M, Vaccari A, Piccolo O. Mild hydrogenation of quinoline 1. Role of reaction parameters. J Mol Catal A Chem 2002;179:287–92. https://doi.org/10.1016/S1381-1169(01)00401-0.

[33] Aakko-Saksa PT, Cook C, Kiviaho J, Repo T. Liquid organic hydrogen carriers for transportation and storing of renewable energy – Review and discussion. J Power Sources 2018;396:803–23. https://doi.org/10.1016/j.jpowsour.2018.04.011.

[34] Sotoodeh F, Smith KJ. Kinetics of hydrogen uptake and release from heteroaromatic compounds for hydrogen storage. Ind Eng Chem Res 2010;49:1018–26.

https://doi.org/10.1021/ie9007002.

[35] Ren Y, Wang Y, Li X, Zhang Z, Chi Q. Selective hydrogenation of quinolines into 1,2,3,4-tetrahydroquinolines over a nitrogen-doped carbon-supported Pd catalyst. New J Chem 2018;42:16694–702. https://doi.org/10.1039/c8nj04014a.

[36] Hu X, Chen Y, Huang B, Liu Y, Huang H, Xie Z. Pd-Supported N/S-Codoped Graphene-Like Carbons Boost Quinoline Hydrogenation Activity. ACS Sustain Chem Eng 2019;7:11369–76. https://doi.org/10.1021/acssuschemeng.9b01015.

[37] Xie D, Liu X, Lv H, Guo Y. Products, pathways, and kinetics for catalytic hydrodenitrogenation of quinoline in hydrothermal condition. J Supercrit Fluids 2022;182. https://doi.org/10.1016/j.supflu.2021.105509.

[38] Sheehan JD, Savage PE. Reaction pathways and kinetics of tryptophan in hot, compressed water. Chem Eng J 2020;390:124600. https://doi.org/10.1016/j.cej.2020.124600.

[39] Oh J, Bathula HB, Park JH, Suh YW. A sustainable mesoporous palladium-alumina catalyst for efficient hydrogen release from N-heterocyclic liquid organic hydrogen carriers. Commun Chem 2019;2. https://doi.org/10.1038/s42004-019-0167-7.

Chapter 5

Reaction kinetic studies for dehydrogenation of decahydroquinoline for hydrogen generation

5.1 Introduction

As global energy consumption continues to increase, there is an urgent need to develop sustainable energy storage and distribution systems. Hydrogen, a clean and efficient energy carrier, has the potential to play a significant role in meeting future energy demands while reducing greenhouse gas emissions [1,2]. The mass-energy density of hydrogen with 120 MJ/kg, is significantly higher than that of hydrocarbon fuels such as gasoline with a calorific value of 44 MJ/kg [3,4]. However, one of the primary challenges associated with hydrogen utilization is its storage and transportation [5]. Various hydrogen storage technologies have been thoroughly investigated including compressed hydrogen, liquefied hydrogen, physisorption in porous materials or metal-organic frameworks and metal hydrides. While each of these storage methods offers unique benefits, they also come with specific limitations and challenges [6]. Liquid organic hydrogen carriers (LOHCs) have emerged as a promising solution to these challenges due to their ability to reversibly store hydrogen in liquid form, facilitating safer and more efficient handling [7]. The reversible hydrogenation of an unsaturated, often aromatic molecule is the foundation of the LOHC idea. The hydrogen-rich form of the molecule known as a saturated chemical is considered in this reaction. The hydrogenated, or hydrogen-rich, form releases the hydrogen for additional use in industrial applications via dehydrogenation process [8]. LOHCs can absorb hydrogen through hydrogenation and release it via dehydrogenation, offering a feasible means to store hydrogen under ambient conditions as opposed to high-pressure or cryogenic systems typically required for hydrogen storage [9]. A key foundation of the modern chemical industry is the use of heterogeneous catalysts which enable the economical and efficient conversion of raw materials into valuable chemicals and fuels while also being environmental friendly [10]. Stephan Kiermaier et al. (2021) study demonstrates that the combination may be suitable when reduced-pressure dehydrogenation of perhydro-N-ethylcarbazole (H12-NEC) is paired with hydrogen electrification in a high-temperature polymer electrolyte membrane fuel cell (HT-PEMFC). Dehydrogenation reactions of H12-NEC were conducted within a temperature range of 160 to 200°C, using various hydrogen partial pressures in the dehydrogenation unit to simulate the effects in fuel cell operating in suction mode, which reduces hydrogen partial pressure due to fuel cell activity. The kinetic analysis reveals that a dehydrogenation temperature of 180°C combined with a hydrogen partial pressure of 500 mbar represents an effective parameter set for efficient hydrogen release [11]. Recent studies have explored various methods to enhance the dehydrogenation of various molecules including the use

of innovative catalysts, reactor designs, and alternative energy inputs such as microwave and plasma-assisted dehydrogenation. The reported literature presents reusing two primary greenhouse gases, CO 2 and CH 4 , while simultaneously creating value-added compounds (H_2 + CO). These advancements aim to reduce the activation energy of the reaction allowing for low operating temperatures and improved hydrogen release rates [12]. Among the various LOHC candidates, nitrogen-containing heterocycles like decahydroquinoline have gained attention due to their favorable hydrogen storage capacities and chemical stability [13,14]. Many studies have shown that replacing a carbon atom with nitrogen within the ring structure can decrease the dehydrogenation enthalpy [15]. Generally, nitrogen-containing cyclic molecules exhibit lower hydrogen release enthalpies, enabling the reaction to occur at reduced temperatures (140–240°C). Additionally, heterocyclic molecules are less volatile, allowing for a higher purity of the hydrogen produced. This high purity (nearly 100%) is particularly advantageous, as it can be directly used in fuel cells without the need for further purification [13].

The comparison of LOHC molecules with representation of H_2 carrying capacity are given in Table 1. Quinoline H_2 carrying capacity is higher than other molecules as well as the reaction enthalpy is 58.04 kJ/mol H_2 . Although benzene has high H_2 carrying capacity and enthalpy, it is not extensively adopting as an LOHC due to carcinogenic in nature.

Table 5.1 Comparison with other LOHC molecules

LOHC	Reaction Enthalpy (kJ/mol H_2)	Hydrogen Carrying capacity (wt%)	Reaction Temperature (^oC)	Reference
Benzene	68.6	7.2	315	[16,17]
Toluene	68.3	6.2	>300	[1]
Quinoline	7.2	58.04	250	[13]
Carbazole	51.1	6.7		[16,18]
n-ethylcarbazole	43.2	5.8	200	[11]
n-ethylcarbazole	55	5.8	220	[19]
Dibenzyltoluene	65.3	6.2	250-340	[5]
Dibenzyltoluene	71	6.2	270	[22]

N-ethylcarbazole/perhydro N-ethylcarbazole (NEC/H12-NEC) is considered one of the leading solutions for liquid organic hydrogen carriers (LOHCs), primarily due to its low dehydrogenation temperature and good stability. Additionally, it is favourable for its low reaction enthalpy[11,19]. However, the hydrogen storage capacity of the NEC system results in a lower energy density. The dibenzyltoluene/perhydro-dibenzyltoluene (DBT/H18-DBT) system gained attention following Bruckner et al. 2013 work, which reported a hydrogen capacity of 6.2 wt%. Subsequent studies have indicated a reaction enthalpy for hydrogenation and dehydrogenation ranging from 62 to 71 kJ/mol H_2. Despite its advantages, the dehydrogenation reaction of this system occurs at a relatively high temperature of approximately 270°C, which exceeds the ideal range [20–22]. Nevertheless, its considerable hydrogen carrying capacity and low cost have made it an attractive candidate for LOHC applications, despite the challenge posed by the elevated reaction temperature.

Quinoline strikes a favourable balance between reaction temperature and hydrogen carrying capacity. With an enthalpy of 58.04 kJ/kg, it is comparable to NEC while offering a higher hydrogen carrying capacity. Furthermore, when compared to the DBT system, quinoline exhibits similar hydrogen carrying capacity but operates at a lower reaction temperature than the 270°C required for DBT. Hence, Quinoline was chosen as the LOHC under study for the research.

Decahydroquinoline is a fully saturated, hydrogenated form of quinoline, capable of storing multiple hydrogen atoms within its molecular structure. Upon dehydrogenation, decahydroquinoline releases molecular hydrogen and reverts to quinoline, its unsaturated counterpart. This reversible process makes it particularly suitable for LOHC systems, where efficient hydrogen uptake and release are essential. Understanding the mechanistic pathways of decahydroquinoline dehydrogenation is also crucial as it provides insights into the molecular interactions between the LOHC and the catalyst surface. This reaction is essentially carried out in two steps viz. DHQ to 1,2,3,4-tetrahydroquinoline (py-THQ) and 5,6,7,8-tetrahydroquinoline (bz-THQ) formation in the first step while complete dehydrogenation of both intermediates to quinoline occurs in the second step as shown in Fig. 1.The dehydrogenation process, however, poses several challenges that must be addressed for practical LOHC applications [23,24]. First, the kinetics of the reaction must be optimized to ensure rapid and complete hydrogen release. The dehydrogenation of decahydroquinoline is typically an endothermic reaction, requiring high temperatures to proceed efficiently.

Therefore, understanding the thermodynamic and kinetic parameters of this reaction is crucial. Several factors influence the dehydrogenation process, including catalyst selection, reaction temperature, and pressure. However, the previous literature focused mainly on LOHC material development, catalyst development, and characterization [25–27] as can be seen in Table 1.

Catalyst selection is a critical factor in the dehydrogenation of decahydroquinoline[28,29]. Transition metal catalysts, such as palladium, platinum, and ruthenium have been extensively studied for their ability to facilitate hydrogen release from various LOHCs. The activity and selectivity of these catalysts can be tailored by modifying their composition, support material, and particle size. Additionally, the use of bimetallic catalysts has shown promise in enhancing catalytic performance by leveraging synergistic effects between different metals. For decahydroquinoline dehydrogenation, optimizing catalyst performance is essential to minimize energy input, increase in hydrogen yield, and prevention of unwanted side reactions that could degrade the LOHC[13,27,30]. The operating conditions, particularly reaction temperature and pressure, significantly impact the dehydrogenation efficiency and hydrogen release rate. Higher temperatures generally favor dehydrogenation but may also lead to increased energy consumption and potential degradation of the LOHC. Balancing these factors is essential to achieve an efficient and sustainable process [31].

In this study, the work is focused on dehydrogenation of DHQ at various parameters such as temperature, reaction time, and effect of catalyst loading of 5% Pd loaded on alumina (Pd/Al_2O_3) with reaction kinetics evaluation using Markov chain Monte Carlo simulation (MCMC) tool and the route for product formation is identified without using solvent in the process.

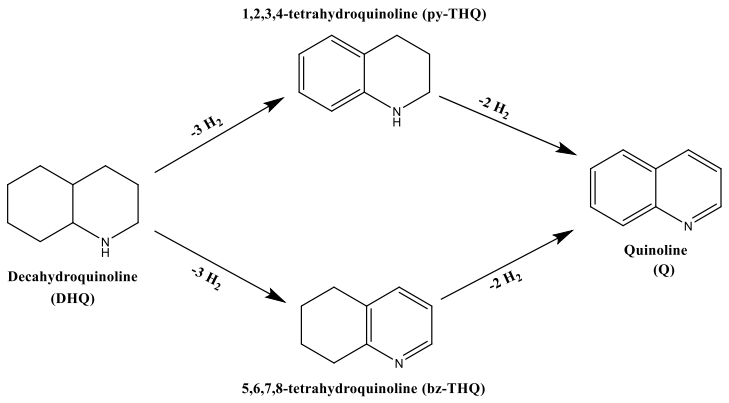

Figure 5.1 Reaction mechanism for Dehydrogenation of DHQ to Quinoline

Table 5.2 Literature on the recent dehydrogenation of LOHC molecules

S. No.	Molecule	Catalyst	Reactor details	Reaction conditions	Findings	Ref.
1.	Perhydro-dibenzyl toluene	Pt/Al_2O_3 Pt/TiO_2 Pt/C	Packed bed of U-tube reactor (L-24 cm, ID-4 mm, Wash-coated catalyst in coiled tube (L-143 cm, ID-4 mm)	(270-300 °C), 1 atm	DoD - 63%	[23]
2.	Perhydro-dibenzyl toluene	0.5% Pt-Co and 0.5% Pt-Ni catalyst	Continuous three-neck quartz reactor, 100mL, equipped with condenser	260 °C, 1 bar, (200 to 1200 rpm)	DoD - 31%	[24]
3.	Cyclohexane, Methylcyclohexane, Decalin	Pt/AC Pt/PCC	Batch reactor, Schlenk tubing (50 ml)	195, 250 to 400°C, 1 atm (N_2 environment)	Rate of H_2 formation: CH- 8.0 mmol/min MCH- 6.5 mmol/min Decalin- 5.7 mmol/min	[25]
4.	Cyclohexane, Methylcyclohexane, Decalin, Tetralin	10 wt.% Pt/CFF Pt/alumite	Continuous, Spray-pulse system	260-350 °C, 1 atm (N_2 environment)	CH- 55 mmol/min MCH- 56 mmol/min Decalin- 50 mmol/min	[26]
5.	Methylcyclohexane	Pt (0.6 wt%)/Al_2O_3	Fixed Bed reactor	300 °C 1 atm	MCH Conversion - 95%, Toluene Selectivity - 99%	[27]
6.	Methylcyclohexane (MCH), Cyclohexane (CH), Decaline, Piperidine	10 wt%, Ni-Cu/ ACC bimetallic catalyst	Continuous Spray-pulse system	350 °C 1 atm	MCH-39.45 mmol/(g.min) CH-14.51 mmol/(g.min) Decaline-93.84 mmol/(g.min) Piperidine-21.22mmol/(g.min)	[28]
7.	Decaline	Pt/C	Batch-wise catalytic reactor	240, 260, 280°C	Rate of H_2 formation: 75.8 - 400 mmol/h	[29]
8.	Mixture of bicyclohexyl and dicyclohexylmethane	Pd/C pellet (10 wt.%)	Continuous U-shaped reactor (0.45 m, 1/2" stainless steel)	300 °C, 340 °C	40% at 573 K 80% at 613K Feed rate 0.54 g/min	[30]

5.1 Materials

Quinoline (AR, ≥ 98%), 1,2,3,4-tetrahydroquinoline (AR, ≥ 98%), 5,6,7,8-tetrahydroquinoline (AR, ≥ 98%), IPA (AR, ≥99%) are purchased from ThermoFischer scientific and the manufacturer of decahydroquinoline (AR, ≥ 96%) is BLD Pharma. Deionized water is used from an ultrapure water machine (elemental type 1820 C) from Chongqing Molecular Water System Co., Ltd. A commercial Palladium-based catalyst (Pd/Al_2O_3) is used for the present experimental studies. The catalyst is procured from Alfa Aesar/Thermo Fisher Scientific in the form of powder with the composition of Pd-5wt.%, and Al_2O_3-95 wt.% and the average particle size of the palladium nanoparticles on the catalyst is about 2 nm**.**

5.2 Experimental setup and procedure

Decahydroquinoline dehydrogenation was conducted at atmospheric pressure using a two-neck round-bottom flask without solvent. A total of 3 mL of the DHQ was added to the flask along with 20 wt% of $Pd(5wt.\%)/Al_2O_3$ catalyst w.r.t DHQ weight basis. The flask was then integrated into the experimental setup, equipped with a condenser (maintained below 15 °C to prevent the loss of LOHC) and a temperature probe to monitor the LOHC temperature. The reaction was carried out in an oil bath at temperatures of 200 °C, 220 °C, and 240 °C with reaction times of 180, 300, 420, and 540 minutes on a hot plate magnetic stirrer. Stirring was carried out at different stirring rates of 150, 200, 250, and 300 rpm using a stirrer needle. Upon completion of each reaction, the flask was removed from the oil bath and allowed to cool. The reaction mixture was filtered from the catalyst particles by washing with acetone, which effectively dissolved decahydroquinoline, its intermediate dehydrogenated products, and quinoline, ensuring a homogeneous liquid phase. This prevented solidification issues, as decahydroquinoline is a solid (37-45 o C) under normal conditions. The diluted mixture was then filtered using standard methods such as vacuum filtration to separate the catalyst particles. After filtration, acetone was removed under reduced pressure, such as with a rotary evaporator, to recover the purified reaction products for GC and GC-MS analysis. This approach ensured efficient catalyst separation while maintaining sample integrity for further evaluation of the number of dehydrogenated forms of heterocycles and the hydrogen yield from the theoretical calculations. A sample of the reaction mixture was separated from the catalyst particles by filtration and analyzed with GC and GC-MS methods to evaluate the number of dehydrogenated forms of heterocycles and the hydrogen yield from the theoretical calculations.

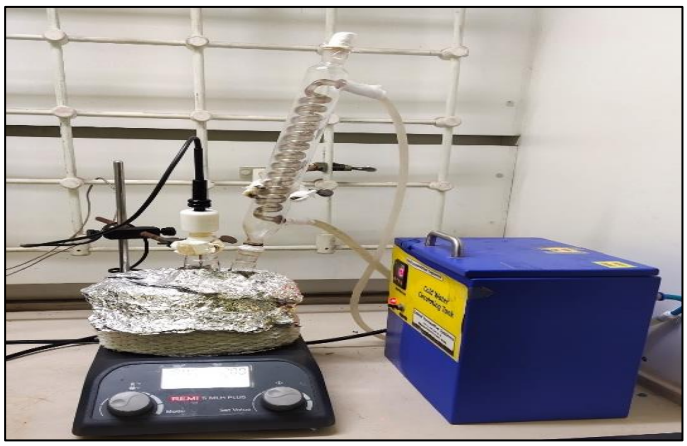

Figure 5.2 Experimental setup for dehydrogenation experiments

5.3 Result and Discussion

5.3.1 Degree of dehydrogenation (DoD)

A precise definition of the degree of hydrogenation (DoH) has replaced the conventional chemical term extent of reaction since the chemical processes of hydrogenation and dehydrogenation of the organic carrier are employed for the reversible storage of hydrogen. The ratio of the actual quantity of hydrogen (nH_2) stored to the maximum amount of hydrogen (nH_2) is known as the degree of hydrogenation. Degree of dehydrogenation (DoD) is the measure of the amount of H_2 released at a certain time in comparison to the maximum amount of H_2 that can be stored [16].

$$\text{Degree of hydrogenation, (DoH)} = \frac{n_{H2}(t)}{n_{H2,\,max}}$$

$$\text{DoH} = \frac{2n_{THQ-1} + 2n_{THQ-2} + 5n_{DHQ}}{5n_{DHQ}}$$

$$\text{Degree of dehydrogenation, (DoD)} = 1 - \text{DoH}$$

$$\text{DoD} = 1 - \frac{n_{H2}}{n_{H2,\,max}}$$

5.3.2 Effect of temperature

The effect of temperature on the degree of dehydrogenation (DoD) and DHQ conversion over time is shown in the Figure 5.3(a-b). As temperature increases from 200 to 240°C, both DoD and DHQ conversion consistently increases with the highest values observed at 240°C. At this

temperature, the reaction rate is faster, leading to higher degree of dehydrogenation and improved conversion throughout the reaction period. The maximum DoD of 82.67 % is observed at 240°C for reaction time of 9 h. The conversion of DHQ increases with an increase in reaction time at elevated temperatures. The DHQ conversion of 83.88% is obtained at 240°C for reaction time of 9 h whereas low temperatures of 200°C result in significantly low conversion values which reflects the enhanced catalytic activity and improved reaction kinetics at higher temperatures. Thus, elevated temperatures accelerate the dehydrogenation process leading to more efficient DHQ conversion.

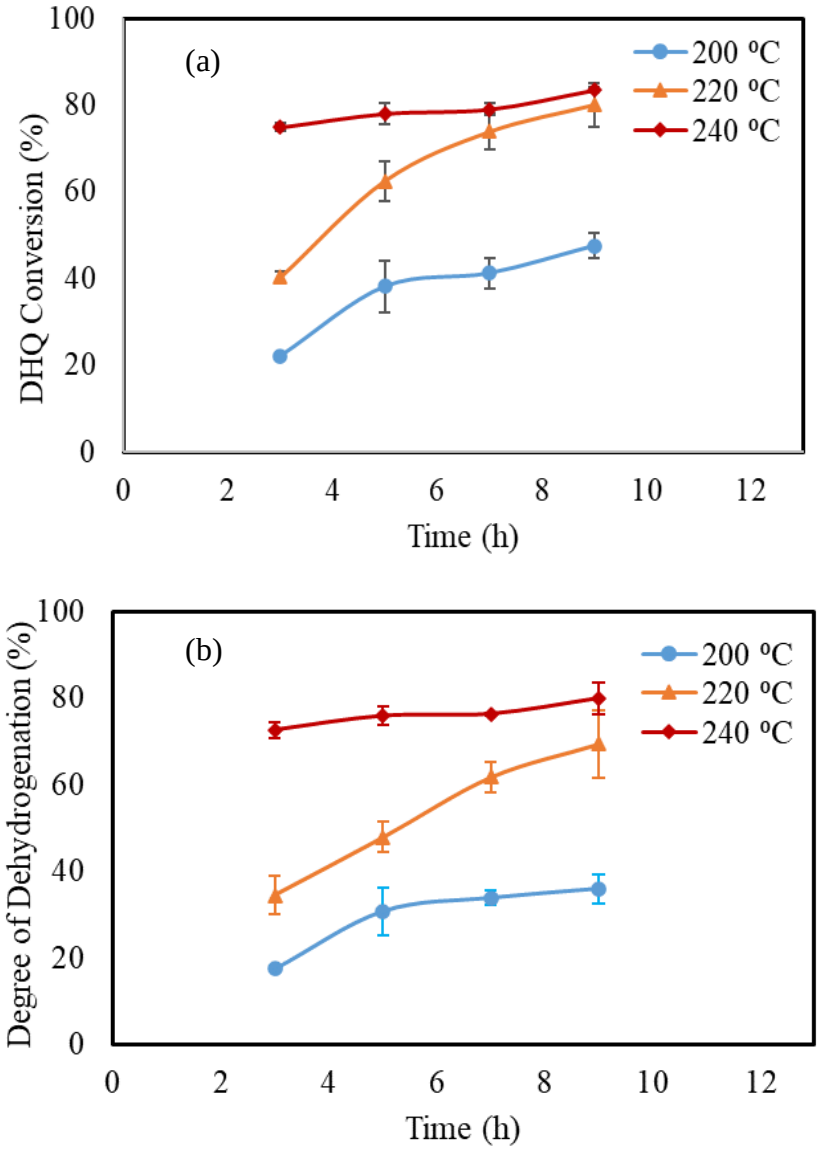

Figure 5.3 Effect of temperature on a) Degree of dehydrogenation and b) DHQ conversion

5.3.3 Effect of stirring speed

The effect of stirring speed on the conversion of DHQ and the degree of dehydrogenation (DoD) over a stirring speed range of 150 to 300 rpm at a temperature of 240°C for 5 h as shown in Fig. 4. The DHQ conversion increases initially as the stirring speed rises from 150 rpm, peaking at around 76.34% at 200 rpm. Beyond 200 rpm, the conversion begins to decrease steadily with increasing stirring speed, dropping to 18.30% at 300 rpm. The DoD also increases with stirring speed, reaching its maximum of 74.45 % close to the same stirring speed where DHQ conversion reaches its maxima (around 200 rpm). After attaining its peak dehydrogenation capacity, the DoD declines similarly to the DHQ conversion to 14.22 % at 300 rpm. The optimal stirring speed for both the DHQ conversion and the DoD is around 200 rpm. Both DHQ conversion and DoD reach their maxima suggesting that it provides the best conditions for dehydrogenation. However, higher stirring speeds beyond this optimal point likely result in diminished contact between reactants or increased turbulence, leading to reduced conversion and dehydrogenation levels.

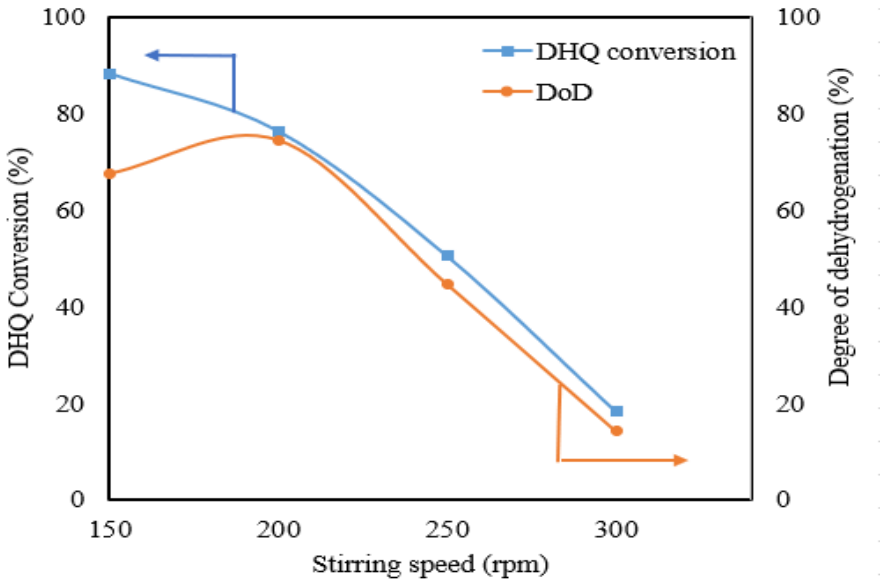

Figure 5.4 Effect of stirring speed on the degree of dehydrogenation and DHQ conversion at 240°C for 5h

The Figure 5.4 illustrates how stirring speed impacts DHQ conversion and the degree of dehydrogenation (DoD), which are both influenced by mixing and mass transfer. At low stirring speeds (150–200 rpm), increased agitation improves mass transfer by enhancing the contact between reactants and the catalyst, leading to higher conversion and dehydrogenation rates. The peak at around 200 rpm indicates an optimal balance where mixing is sufficient to

maximize reactant diffusion to the catalyst without excessive turbulence. However, beyond this point, further increases in stirring speed likely to introduce turbulence and reduce the residence time of reactants near the catalyst surface, thereby diminishing conversion and dehydrogenation rates due to disrupted mass transfer and uneven flow distribution.

5.3.4 Effect of catalyst loading

The impact of catalyst loading on DHQ conversion and the Degree of Dehydrogenation (DoD) at 240°C for 5 hours is studied as shown in Figure 5.5. Both DHQ conversion and DoD increases steadily as the catalyst loading increases from 5 wt.% to 15 wt.% which is attributed to the increased availability of active catalytic sites, enhancing reaction efficiency. However, beyond 15 wt.%**,** both curves begin to plateau in DHQ conversion and DoD. This behavior could be due to mass transfer limitations where diffusion of reactants to the catalyst surface becomes a limiting factor, catalyst site saturation, or thermodynamic equilibrium constraints that prevent further dehydrogenation. The plateau suggests that additional catalyst does not significantly improve reaction outcomes making 15 wt.% an optimal loading to achieve high DHQ conversion (~75%) and dehydrogenation efficiency (~70-75%) without excess catalyst usage. This analysis highlights the importance of balancing catalyst loading to optimize reaction efficiency, minimize material costs, and ensure practical scalability of the process.

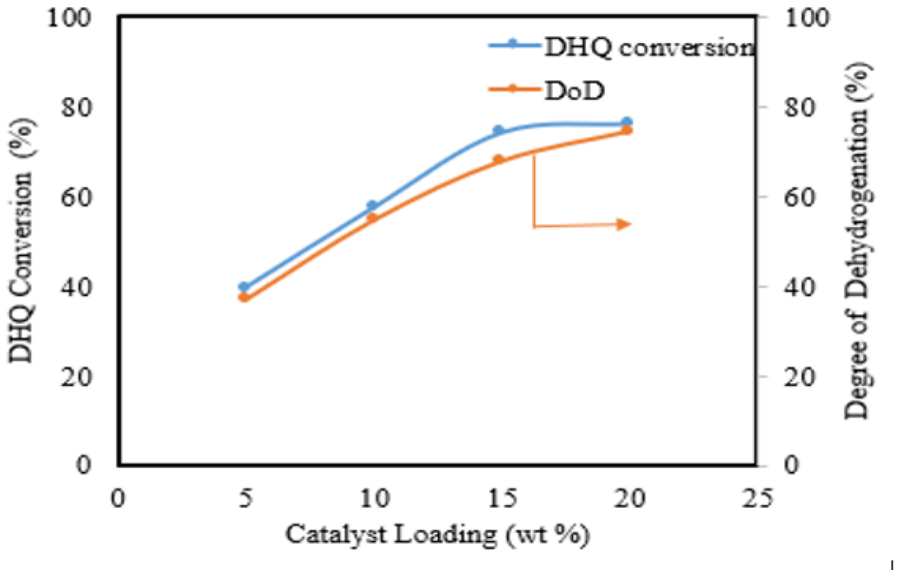

Figure 5.5 Effect of catalyst loading for 240°C and reaction time of 5 h

5.4 Development of reaction kinetic model

5.4.1 Reaction kinetics study

Experimental observations show C_a, C_b, C_c, and C_d as the concentration profiles of species DHQ, py-THQ, bz-THQ and Quinoline respectively over time during the dehydrogenation reaction at 240°C. The concentration of the reactant (C_A)starts at the highest concentration and decreases steadily, indicating its consumption. The dehydrogenated molecule (C_D), the primary product, begins at zero and increases significantly, reaching its maximum around 400 minutes. C_C, a transient intermediate, increases initially, peaks around 200–300 minutes, and then decreases slightly. In contrast, C_B remains nearly constant and negligible throughout the reaction, suggesting minimal involvement. Overall, the results highlight the progression of the reaction with C_A being converted into C_D through intermediate species like Cc. There is a very less (<10 %) formation of pz-THQ so it is not considered in the reaction mechanism as can be seen in Figure 5.6. The kinetic model is developed based on the reaction scheme and experimental observations for decahydroquinoline to bz-THQ, and Quinoline formation as shown in Figure 5.7. Although dehydrogenation of heterocyclic compounds containing nitrogen has been published in the literature, the reported kinetics information for decahydroquinoline dehydrogenation is not sufficient for the development of processes and scale-up of the reactors.

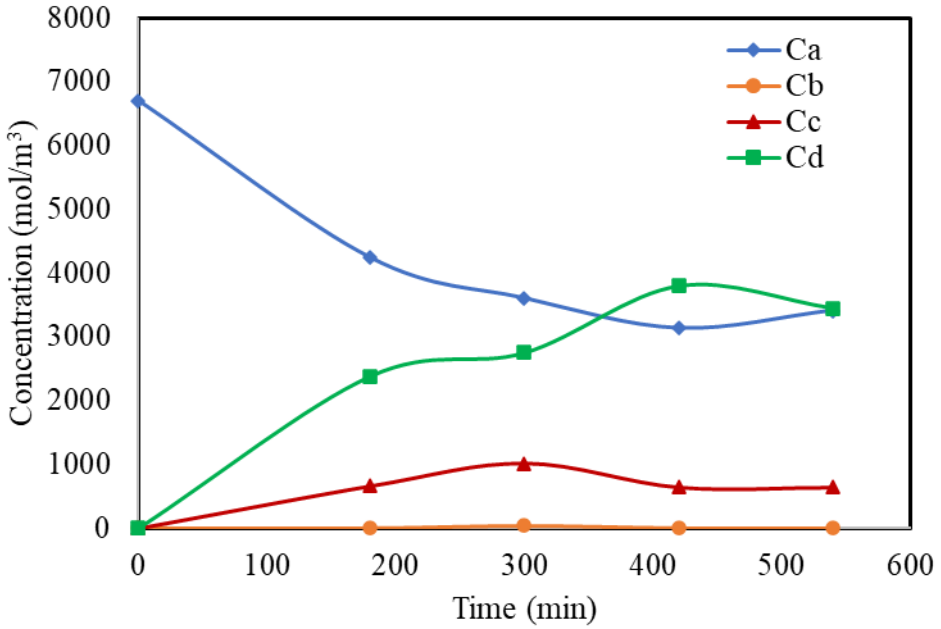

Figure 5.6 Concentration profile of DHQ, py-THQ, bz-THQ and Quinoline after dehydrogenation reaction at 240°C

5.4.2 Reaction mechanism

There are two possible routes for dehydrogenation of DHQ to Quinoline formation for the reaction scheme shown in Figure 5.1. The first dehydrogenation step removes three hydrogen atoms from the nitrogen containing cyclic ring of the DHQ, leading to the formation of py-THQ. Subsequently, two more hydrogen atoms are removed from the remaining cyclohexane ring, yielding quinoline which is considered to be route 1. In the route 2, the first dehydrogenation step removes three hydrogen atoms from the cyclohexane ring, forming bz-THQ. The second dehydrogenation step removes two more hydrogen atoms from the remaining cyclohexane ring resulting in quinoline. Nitrogen is more electronegative than many other elements commonly involved in organic molecules, such as carbon and hydrogen. Electronegativity is the ability of an atom to attract electrons toward itself in a chemical bond. Because nitrogen strongly attracts electron density, it creates a localized electronic environment around itself, affecting adjacent bonds and atoms. Dehydrogenation is a chemical reaction in which hydrogen atoms are removed from a molecule, typically involving breaking of a C-H, N-H, or other similar bonds. The pathway a molecule follows during dehydrogenation depends on:

- Electronic effects (like inductive effects from electronegative atoms).
- Transition state stabilization (the ease of forming intermediates during the reaction).
- Thermodynamic favourability (the stability of products or intermediates).

"Route 2" likely represents a dehydrogenation pathway where nitrogen's presence plays a significant role, such as activating a nearby hydrogen atom or stabilizing an intermediates can be seen in Figure 5.7.

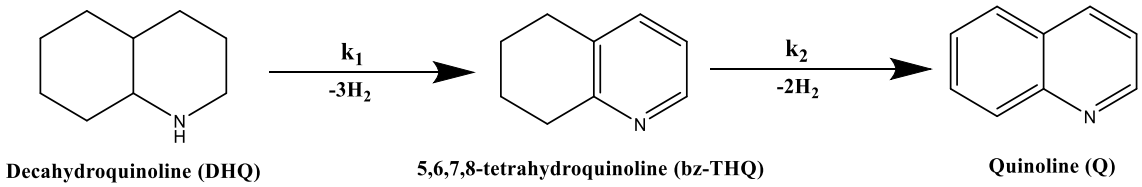

Figure 5.7 Possible reaction mechanism for dehydrogenation of DHQ to Quinoline formation

5.4.3 Development of Power law

Considering the concentration of the dehydrogenated species, the following assumptions are considered for the development of the power law kinetic model into the simplified form:

i. No Mass Transfer Limitations: It is assumed that the reactant is perfectly mixed and there are no mass transfer limitations.

ii. This implies that the rate of reaction is solely dependent on the chemical kinetics and not on the rate of mixing or diffusion.

iii. All reactions are assumed to be irreversible[13]

iv. There is a very less (<10 %) formation of pz-THQ so it is not considered in the reaction mechanism

The kinetic model was developed based on the following assumptions and the volume of the reaction mixture used for quinoline hydrogenation with the following rate expressions

$$r_1 = \frac{dC_A}{dt} = \frac{m_{cat}}{V}(-k_1 C_A) \qquad (5.1)$$

$$r_2 = \frac{dC_C}{dt} = \frac{m_{cat}}{V}(k_1 C_A - k_2 C_C) \qquad (5.2)$$

$$r_3 = \frac{dC_D}{dt} = \frac{m_{cat}}{V}(-k_2 C_C) \qquad (5.3)$$

Where, r is reaction rate, mol/(m^3.min)

m_{cat} represents catalyst loading, g

k is rate constant, $m^3/(g_{cat}.\ min)$

C_A, C_C, and C_D are concentrations (mol/m^3) of reactants A, C, and D, respectively.

V is the volume of the reaction mixture, m^3

5.4.4 Reaction kinetics validation with model

The concentration of the species for `different reaction times of 2 h intervals at different temperatures is shown in Figure 5.8. The DHQ concentration decreased abruptly while the formation of bz-THQ predominates simultaneously. At the same time, the rate of formation of quinoline prevails at the expense of bz-THQ hydrogenation. Quinoline concentration is observed with increase in reaction times at 200, 220 and 240 ^oC as shown in Fig. 7 (a-c). As

there is no driving force for the backward reaction to take place, the product formation suppresses the existence of reactants and intermediates. The concentration of the species is fitted using the kinetic parameters estimated using Markov Chain Monte Carlo (MCMC) simulation as validated in Figure 5.8 (a-c).

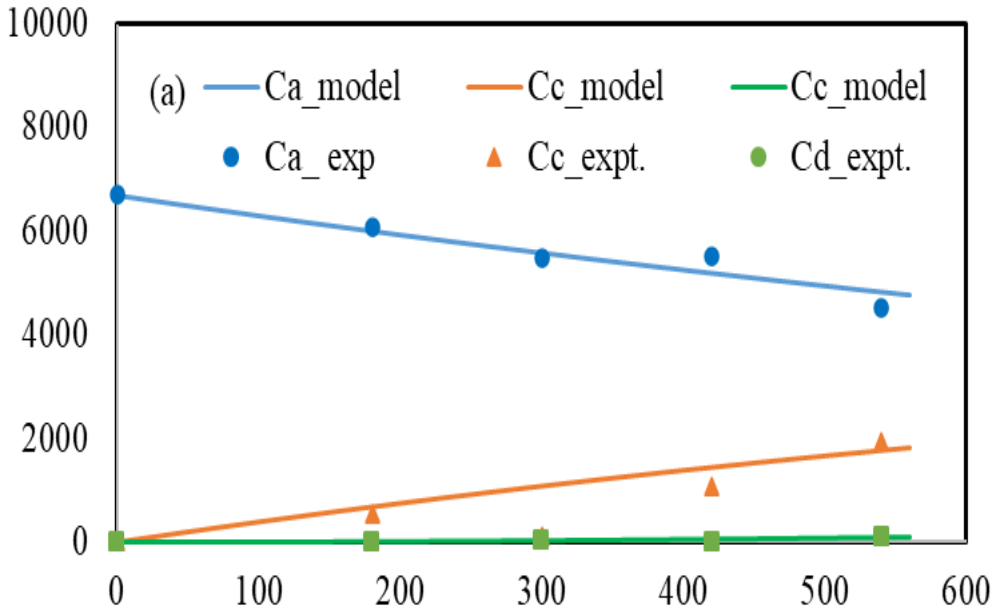

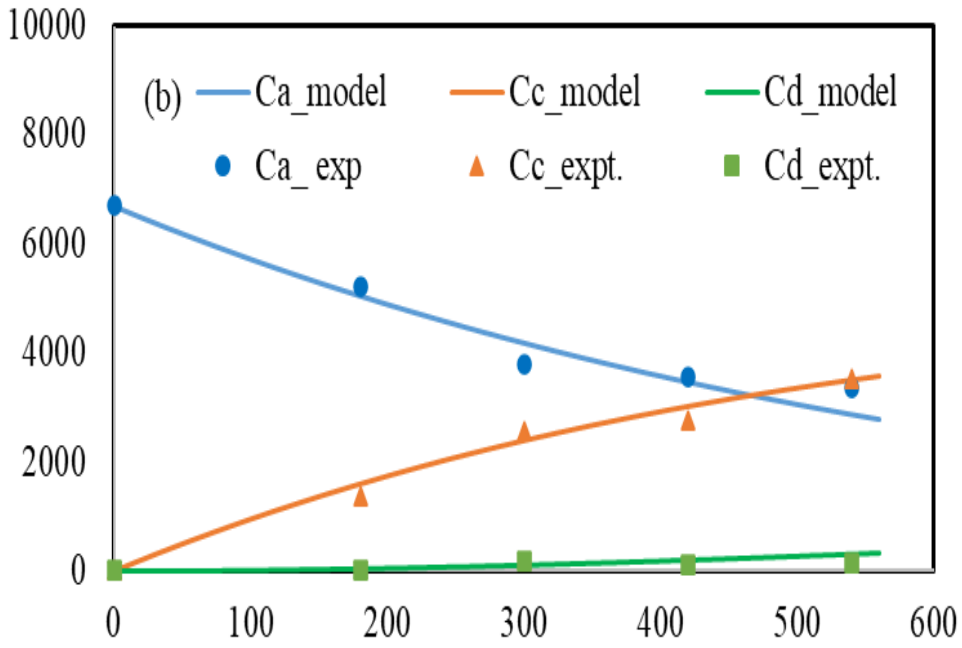

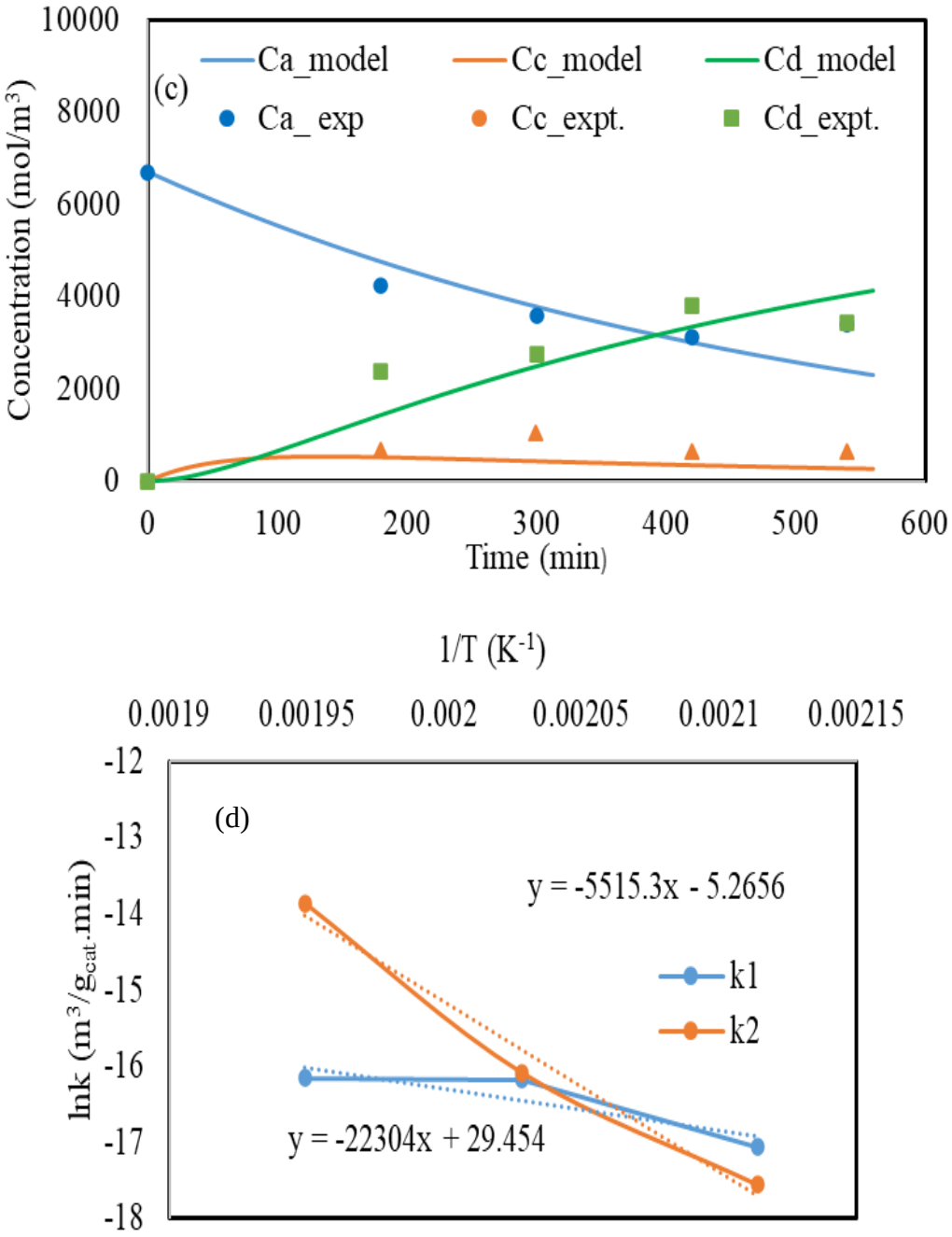

Figure 5.8 Concentration profile at 50 bar hydrogen pressure for different temperatures (a)200 ^{o}C (b) 220 ^{o}C and (c) 240 ^{o}C (d) Rate constants at different temperatures

("---" represents model and symbols represent experimental data points)

5.5 Parameter estimation

Model predictions and experimental data are used to determine the kinetic parameters. The Markov Chain Monte Carlo (MCMC) simulation tool is used to solve the ordinary differential equations numerically and estimate parameter values for the model shown in equations (1) through (3). The best fitting value for each of the reaction rate constants (k_1 and k_2) was obtained by minimizing the sum of the square errors of the concentration between the model computation and the experimental data. Table 5.2 reports the pre-exponential parameters, activation energies, and estimated rate constants using Arrhenius plot with model fitted rate constants. The variation in activation energy and pre-exponential factor show the extent of rate determining steps. Therefore, it is thought that the formation of Quinoline from bz-THQ controls the rate of reaction. The Activation energy of 185.43 kJ/mol for the conversion bz-THQ to Quinoline in the dehydrogenation process is considered to be the rate-determining step.

Table 5.3 Estimated rate constants and Arrhenius parameters for dehydrogenation of DHQ to Quinoline formation

Rate constant ($m^3/(g_{cat}.min)$)	Temperature (^oC)			Activation energy, E_a (kJ/mol)	Pre-exponential factor, k_o ($m^3/(g_{cat}.min)$)
	200	220	240		
k_1	3.9E-08	9.4E-08	9.6E-08	45.85	0.0051
k_2	2.4E-08	1.0E-07	9.5E-07	185.43	6.19E+12

5.6 Study of mass transfer limitations

5.6.1 External mass transfer effects

External mass transfer limitations have a significant impact on the overall reaction rate. In three-phase systems, these limitations are assessed using the Carberry number for the gas-liquid system, which accounts for stirring speed and liquid diffusion to the solid phase. The Carberry number (Ca) measures the degree of external mass transfer limitation, ranging from zero to one. When the Carberry number is below 0.05 which indicates that diffusion resistance due to external mass transfer can be considered negligible [31].

$$C_a = \frac{r^{,o}}{k_{ls}\frac{6w}{d_p \rho_p} C^o} < 0.05 \qquad (5.4)$$

The liquid-solid mass transfer coefficient is determined using a correlation specific to batch-stirred tank reactors [32].

$$Sh = 2.0 + 0.6\left(Re_p{}^{0.5}\right)\left(Sc^{0.33}\right) \qquad (5.5)$$

Table 5.4 Carberry number and Weisz Prater criteria for mass transfer limitations

Parameters	Values
Batch time	9
Initial rate of DHQ, r^0 (mol/(kg_{cat}.s))	0.001120067
Initial rate of DHQ, r^0 (mol/s)	1.10086E-05
Initial concentration of DHQ, C^o (mol/m^3)	699.1906475
Avg. catalyst particle radius, R (m)	2.72E-09
Weight of catalyst, w (kg)	0.000578
Molecular diffusivity, D_{AB} (m^2/s)	9.72E-02
Effective diffusivity, D_{eff} (m^2/s)	2.78E-02
Weisz-Prater modulus, ϕ	4.68E-19
Drag Coefficient, C_D	0.44
Terminal velocity, U_t (m/s)	2.47E-04
L-S Mass transfer coefficient, k_{ls}, (m/s)	3.57E+07
Carberry Number, Ca	7.60E-19

Where, Sh= $\frac{k_{Ls}d_p}{D_{AB}}$, Sc= $\frac{\mu_l}{\rho_L D_{AB}}$, $Re_{P=}$ $\frac{\rho_L v_P d_p}{\mu_L}$;

Carberry number found out using the above correlations and equations is less than 0.05 as shown in Table 5.3. Therefore, it is confirmed that the absence of liquid-solid diffusion limitations

5.6.2 Internal mass transfer effects

Internal mass transfer limitations were evaluated using the Weisz-Prater criterion, as outlined in the literature [33]. The Weisz-Prater modulus can be estimated using the following correlations.

$$\phi = \eta\emptyset^2 = \frac{\rho_{pr^o R_p^2}}{D_{ef} C^o}$$

$$\varepsilon_p = \frac{v_P}{v_{P+\frac{1}{\rho_S}}} \quad [34]$$

$$D_{ef} = \frac{D_{AB}\varepsilon_P}{\tau_P}$$

$$D_{AB} = \frac{7.4 \times 10^{-8}\left(\phi_B {M_B}^{0.5}\right) \times T \times 10^{-4}}{\mu_{AB} v_A}$$

A Weisz-Prater modulus greater than 6 indicates a regime of complete diffusional control, while the modulus less than 1 suggests that pore diffusion limitations are negligible as shown in Table 5.3. Therefore, the reactions are suggested to perform without mass transfer limitations and the reaction kinetics can be used for scale-up of the reactors.

5.7 Conclusions

A comprehensive overview of the current state of research on the reaction kinetic studies for dehydrogenation of decahydroquinoline as an LOHC is explored in the present study. It investigates the effects of reaction conditions, stirring speed and catalyst loading on DHQ conversion and degree of dehydrogenation (DoD). By addressing these key aspects, this study aims to contribute to the ongoing efforts to develop sustainable and efficient hydrogen storage solutions that can meet the demands of a hydrogen-based economy. The catalytic dehydrogenation of decahydroquinoline (DHQ) to quinoline (Q) has been comprehensively studied, demonstrating its potential as an efficient method for hydrogen generation. Using 5% Pd supported on alumina (Pd/Al_2O_3) as the catalyst, the reaction conditions were optimized to achieve maximum hydrogen release and dehydrogenation efficiency. Among the tested parameters, a reaction temperature of 240°C and reaction time of 9 h yields the maximum DHQ conversion and degree of dehydrogenation. A reaction kinetic model developed for the process, validated through Markov Chain Monte Carlo (MCMC) simulations, accurately predicted the rate constants and provided insights into the reaction mechanism. The activation energy for the dehydrogenation of bz-THQ to quinoline was determined to be 185.43 kJ/mol,

with the conversion of benzo-tetrahydroquinoline (bz-THQ) to quinoline identified as the rate-limiting step. These findings not only enhance the understanding of DHQ dehydrogenation but also offer valuable guidance for optimizing reaction parameters to improve hydrogen generation efficiency. This work establishes a foundation for further research into sustainable hydrogen production from liquid organic hydrogen carriers (LOHCs).

Notations

Φ is the dimensionless Weisz- Prater modulus

η is the effectiveness factor for catalyst particle

ρ_p is the particle density in kg/m^3

ε_p is the porosity of the catalyst particles

τ_p is the Tortuosity of the catalyst particles

r^o is the initial reaction rate per weight of the catalyst (mol/kg$_{cat}$.s)

ϕ_B is the association factor of solvent

T is the reaction temperature in K

μ_{AB} is the viscosity of mixture in kg/m s

v_A is the molar volume of DHQ

R_p is the radius of the catalyst particle in m

C^o is the Initial concentration of DHQ in (mol/m^3)

D_{AB} is the molecular diffusivity of DHQ (m^2/s)

D_{ef} is the effective diffusivity of DHQ (m^2/s) calculated using [44]

ρ_L = Liquid mixture density (kg/m^3);

μ_L = Mixture Viscosity (kg/ms);

v_p = Terminal velocity of particles (m/s);

DoH =Degree of hydrogenation;

DoD =Degree of dehydrogenation;

a is Decahydroquinoline

b is 1,2,3,4-tetrahydroquinoline (py-THQ)

c is 5,6,7,8-tetrahydroquinoline (bz-THQ)

d is Quinoline (Q)

5.8 References

[1] Sage V, Patel J, Hazewinkel P, Yasin QUA, Wang F, Yang Y, et al. Recent progress and techno-economic analysis of liquid organic hydrogen carriers for Australian renewable energy export – A critical review. Int J Hydrogen Energy 2024;56:1419–34. https://doi.org/10.1016/j.ijhydene.2023.12.269.

[2] Willer M, Preuster P, Geißelbrecht M, Wasserscheid P. Continuous dehydrogenation of perhydro benzyltoluene and perhydro dibenzyltoluene in a packed bed vertical tubular reactor – The role of LOHC evaporation. Int J Hydrogen Energy 2024;57:1513–23. https://doi.org/10.1016/j.ijhydene.2024.01.031.

[3] Mao H, Chen C, Liao X, Shi B. Catalytic hydrogenation of quinoline over recyclable palladium nanoparticles supported on tannin grafted collagen fibers. J Mol Catal A Chem 2011;341:51–6. https://doi.org/10.1016/j.molcata.2011.03.023.

[4] Faye O, Szpunar J, Eduok U. ScienceDirect A critical review on the current technologies for the generation , storage , and transportation of hydrogen. Int J Hydrogen Energy 2022;47:13771–802. https://doi.org/10.1016/j.ijhydene.2022.02.112.

[5] Rao N, Lele AK, Patwardhan AW. Optimization of Liquid Organic Hydrogen Carrier (LOHC) dehydrogenation system. Int J Hydrogen Energy 2022;47:28530–47.

https://doi.org/10.1016/j.ijhydene.2022.06.197.

[6] Makaryan IA, Sedov I V. Hydrogenation/Dehydrogenation Catalysts for Hydrogen Storage Systems Based on Liquid Organic Carriers (A Review). Pet Chem 2021;61:977–88. https://doi.org/10.1134/S0965544121090085.

[7] Sotoodeh F, Huber BJM, Smith KJ. Dehydrogenation kinetics and catalysis of organic heteroaromatics for hydrogen storage. Int J Hydrogen Energy 2012;37:2715–22. https://doi.org/10.1016/j.ijhydene.2011.03.055.

[8] Müller K, Völkl J, Arlt W. Thermodynamic Evaluation of Potential Organic Hydrogen Carriers. Energy Technol 2013;1:20–4. https://doi.org/10.1002/ente.201200045.

[9] Brigljević B, Byun M, Lim H. Design, economic evaluation, and market uncertainty analysis of LOHC-based, CO2 free, hydrogen delivery systems. Appl Energy 2020;274. https://doi.org/10.1016/j.apenergy.2020.115314.

[10] Cao Y, Ding L, Qiu Z, Zhang H. Biomass-derived N-doped porous two-dimensional carbon nanosheets supported ruthenium as effective catalysts for the selective hydrogenation of quinolines under mild conditions. Catal Commun 2020;143. https://doi.org/10.1016/j.catcom.2020.106048.

[11] Kiermaier S, Lehmann D, Bösmann A, Wasserscheid P. Dehydrogenation of perhydro-N-ethylcarbazole under reduced total pressure. Int J Hydrogen Energy 2021;46:15660–70. https://doi.org/10.1016/j.ijhydene.2021.02.128.

[12] Czylkowski D, Hrycak B, Miotk R, Dors M, Jasiński M. Microwave plasma-assisted hydrogen production via conversion of CO2–CH4 mixture. Int J Hydrogen Energy 2024;78:421–32. https://doi.org/10.1016/j.ijhydene.2024.06.313.

[13] Stepanenko SA, Shivtsov DM, Koskin AP, Koskin IP, Kukushkin RG, Yeletsky PM, et al. N-Heterocyclic Molecules as Potential Liquid Organic Hydrogen Carriers: Reaction Routes and Dehydrogenation Efficacy. Catalysts 2022;12. https://doi.org/10.3390/catal12101260.

[14] Oh J, Bathula HB, Park JH, Suh YW. A sustainable mesoporous palladium-alumina catalyst for efficient hydrogen release from N-heterocyclic liquid organic hydrogen carriers. Commun Chem 2019;2. https://doi.org/10.1038/s42004-019-0167-7.

[15] Zhu QL, Xu Q. Liquid organic and inorganic chemical hydrides for high-capacity

hydrogen storage. Energy Environ Sci 2015;8:478–512. https://doi.org/10.1039/c4ee03690e.

[16] Aakko-Saksa PT, Cook C, Kiviaho J, Repo T. Liquid organic hydrogen carriers for transportation and storing of renewable energy – Review and discussion. J Power Sources 2018;396:803–23. https://doi.org/10.1016/j.jpowsour.2018.04.011.

[17] Wang Y, Shah N, Huffman GP. Pure hydrogen production by partial dehydrogenation of cyclohexane and methylcyclohexane over nanotube-supported Pt and Pd catalysts. Energy and Fuels 2004;18:1429–33. https://doi.org/10.1021/ef049959o.

[18] Sotoodeh F, Zhao L, Smith KJ. Kinetics of H2 recovery from dodecahydro-N-ethylcarbazole over a supported Pd catalyst. Appl Catal A Gen 2009;362:155–62. https://doi.org/10.1016/j.apcata.2009.04.039.

[19] Teichmann D, Arlt W, Schlücker E, Wasserscheid P. Transport and Storage of Hydrogen via Liquid Organic Hydrogen Carrier (LOHC) Systems 2016:811–30.

[20] Ali A, G UK, Lee HJ. Parametric study of the hydrogenation of dibenzyltoluene and its dehydrogenation performance as a liquid organic hydrogen carrier 2020;34. https://doi.org/10.1007/s12206-020-0638-x.

[21] Shi L, Qi S, Qu J, Che T, Yi C, Yang B. Integration of hydrogenation and dehydrogenation based on dibenzyltoluene as liquid organic hydrogen energy carrier. Int J Hydrogen Energy 2019;44:5345–54. https://doi.org/10.1016/j.ijhydene.2018.09.083.

[22] Brückner N, Obesser K, Bçsmann A, Teichmann D, Arlt W, Dungs J, et al. Evaluation of Industrially Applied Heat-Transfer Fluids as Liquid Organic Hydrogen Carrier Systems 2020:229–35. https://doi.org/10.1002/cssc.201300426.

[23] Heublein N, Stelzner M, Sattelmayer T. Hydrogen storage using liquid organic carriers: Equilibrium simulation and dehydrogenation reactor design. Int J Hydrogen Energy 2020;45:24902–16. https://doi.org/10.1016/j.ijhydene.2020.04.274.

[24] Aakko-Saksa PT, Cook C, Kiviaho J, Repo T. Liquid organic hydrogen carriers for transportation and storing of renewable energy – Review and discussion. J Power Sources 2018;396:803–23. https://doi.org/10.1016/j.jpowsour.2018.04.011.

[25] Zhang J, Yang F, Wang B, Li D, Wei M, Fang T, et al. Heterogeneous Catalysts in N-

Heterocycles and Aromatics as Liquid Organic Hydrogen Carriers (LOHCs): History, Present Status and Future. Materials (Basel) 2023;16. https://doi.org/10.3390/ma16103735.

[26] Müller K, Stark K, Emelyanenko VN, Varfolomeev MA, Zaitsau DH, Shoifet E, et al. Liquid Organic Hydrogen Carriers: Thermophysical and Thermochemical Studies of Benzyl- and Dibenzyl-toluene Derivatives. Ind Eng Chem Res 2015;54:7967–76. https://doi.org/10.1021/acs.iecr.5b01840.

[27] Jian M, Prins R. Kinetics of the Hydrodenitrogenation of Decahydroquinoline over NiMo(P)/Al2O3 Catalysts. Ind Eng Chem Res 1998;37:834–40. https://doi.org/10.1021/ie9703292.

[28] Koskin AP, Larichev Y V., Stepanenko SA, Dubinin Y V., Ayupov AB, Saraev AA, et al. Carbonized Melamine Cyanurate as a Palladium Catalyst Support for the Dehydrogenation of N-heterocyclic Compounds in LOHC Technology. C-Journal Carbon Res 2023;9. https://doi.org/10.3390/c9030083.

[29] Koskin AP, Zhang J, Belskaya OB, Bulavchenko OA, Konovalova DA, Stepanenko SA, et al. Efficiency of high-loaded nickel catalysts modified by Mg in hydrogen storage/extraction using quinoline/decahydroquinoline pair as LOHC substrates. J Magnes Alloy 2024;12:3245–63. https://doi.org/10.1016/j.jma.2024.07.014.

[30] Mamun O, Winther KT, Boes JR, Bligaard T. High-throughput calculations of catalytic properties of bimetallic alloy surfaces. Sci Data 2019;6:1–9. https://doi.org/10.1038/s41597-019-0080-z.

[31] Preuster P, Papp C, Wasserscheid P. Liquid organic hydrogen carriers (LOHCs): Toward a hydrogen-free hydrogen economy. Acc Chem Res 2017;50:74–85. https://doi.org/10.1021/acs.accounts.6b00474.

[32] Braunschweiler A. Keywords dehydrogenation , liquid organic hydrogen carrier , platinum catalyst , hydrogen 2018.

[33] Alconada K, Barrio VL. Evaluation of bimetallic Pt–Co and Pt–Ni catalysts in LOHC dehydrogenation. Int J Hydrogen Energy 2024;51:243–55. https://doi.org/10.1016/j.ijhydene.2023.04.120.

[34] Kariya N, Fukuoka A, Ichikawa M. Efficient evolution of hydrogen from liquid

cycloalkanes over Pt-containing catalysts supported on active carbons under "wet-dry multiphase conditions." Appl Catal A Gen 2002;233:91–102. https://doi.org/10.1016/S0926-860X(02)00139-4.

[35] Kariya N, Fukuoka A, Utagawa T, Sakuramoto M, Goto Y, Ichikawa M. Efficient hydrogen production using cyclohexane and decalin by pulse-spray mode reactor with Pt catalysts. Appl Catal A Gen 2003;247:247–59. https://doi.org/10.1016/S0926-860X(03)00104-2.

[36] Okada Y, Sasaki E, Watanabe E, Hyodo S, Nishijima H. Development of dehydrogenation catalyst for hydrogen generation in organic chemical hydride method. Int J Hydrogen Energy 2006;31:1348–56. https://doi.org/10.1016/j.ijhydene.2005.11.014.

[37] Patil SP, Pande J V., Biniwale RB. Non-noble Ni-Cu/ACC bimetallic catalyst for dehydrogenation of liquid organic hydrides for hydrogen storage. Int J Hydrogen Energy 2013;38:15233–41. https://doi.org/10.1016/j.ijhydene.2013.09.115.

[38] Hodoshima S, Arai H, Takaiwa S, Saito Y. Catalytic decalin dehydrogenation/naphthalene hydrogenation pair as a hydrogen source for fuel-cell vehicle. Int J Hydrogen Energy 2003;28:1255–62. https://doi.org/10.1016/S0360-3199(02)00250-1.

[39] Jang M, Jo YS, Lee WJ, Shin BS, Sohn H, Jeong H, et al. A High-Capacity, Reversible Liquid Organic Hydrogen Carrier: H 2 -Release Properties and an Application to a Fuel Cell. ACS Sustain Chem Eng 2019;7:1185–94. https://doi.org/10.1021/acssuschemeng.8b04835.

[40] Lee SP, Chen YW. Nitrobenzene hydrogenation on Ni-P, Ni-B and Ni-P-B ultrafine materials. J Mol Catal A Chem 2000;152:213–23. https://doi.org/10.1016/S1381-1169(99)00298-8.

[41] Trubiano G, Borio D, Errazu A. Influence of the operating conditions and the external mass transfer limitations on the synthesis of fatty acid esters using a Candida antarctica lipase. Enzyme Microb Technol 2007;40:716–22. https://doi.org/10.1016/j.enzmictec.2006.06.003.

[42] Banik D, Kinage AK, Vasireddy SN. Evaluation of reaction kinetics for chemoselective

hydrogenation of citral for intensification of citral intermediates using copper-based catalysts. Indian Chem Eng 2024:1–19. https://doi.org/10.1080/00194506.2024.2390068.

[43] Kolitcheff S, Jolimaitre E, Hugon A, Verstraete J, Carrette PL, Tayakout-Fayolle M. Tortuosity of mesoporous alumina catalyst supports: Influence of the pore network organization. Microporous Mesoporous Mater 2017;248:91–8. https://doi.org/10.1016/j.micromeso.2017.04.010.

[44] Xu ZP, Chuang KT. Effect of internal diffusion on heterogeneous catalytic esterification of acetic acid. Chem Eng Sci 1997;52:3011–7. https://doi.org/10.1016/S0009-2509(97)00082-1.

Chapter 6

Mass and energy balance for 1 ton of DHQ per day

6.1 Introduction

The global climate is undergoing significant changes, largely due to decades of rising CO_2 emissions, which have steadily accumulated in the atmosphere. This increase in greenhouse gases has led to growing instability in global temperatures and weather patterns, with consequences ranging from the Arctic regions to the Equatorial belt. One of the primary drivers of these anthropogenic CO_2 emissions is the widespread reliance on fossil fuels, which are burned for industrial processes, energy production, and transportation. As a direct response to these challenges, the European Union (EU) has committed itself to transitioning away from fossil fuels, aiming for rapid decarbonization of the economy in order to mitigate climate change and reduce reliance on unsustainable energy source[1].

In an effort to lower emissions and combat the effects of climate change, various strategies have been introduced and implemented on a global scale. These strategies range from boosting energy efficiency in industries and homes to advocating for the increased use of renewable energy sources, such as wind, solar, and hydroelectric power, as well as biofuels[2,3]. However, one of the significant challenges posed by the majority of these renewable energy sources is the inherent unpredictability of their output. Solar and wind energy production is highly dependent on weather patterns and seasonal variability, making it difficult to predict and balance energy supply and demand. As a result, there has been a growing emphasis on developing advanced energy storage systems that can effectively store energy during periods of surplus generation and release it when renewable production is insufficient. These energy storage systems work by converting electrical energy into another form, such as chemical energy in batteries or mechanical energy in systems like pumped-storage hydropower or pressurized gas vessels. While these storage solutions have shown promise in many applications, they are often not well-suited to energy-intensive industries, where thermal energy is more commonly required[4–7] .

This is where hydrogen as an energy carrier presents a compelling alternative. Hydrogen offers a versatile and sustainable solution for energy storage and transport, as it can be produced using excess energy from renewable sources, particularly through the process of water electrolysis. Hydrogen, once produced, serves as a concentrated energy source that emits no pollutants when used, making it an ideal candidate for replacing fossil fuels in various sectors. The concept of green hydrogen has gained considerable attention as a critical pillar in the renewal of the global

energy system. Despite its promising potential, several challenges remain, particularly related to the cost-effectiveness of hydrogen production and its distribution. Although the process of hydrogen production through electrolysis dates back to the 1800s, and hydrogen's use as fuel in internal combustion engines was demonstrated over two centuries ago, the commercialization of hydrogen technologies has been hindered by economic and technical barriers. One of the primary challenges is hydrogen's low volumetric density, which complicates its transport and storage, especially over long distances. While hydrogen can be stored at high pressures or in its liquid form, both approaches require significant energy input, making them less viable for large-scale commercial applications. Current hydrogen transportation methods, such as Compressed Gaseous Hydrogen (CGH_2), involve compressing hydrogen gas to extremely high pressures, typically around 700 bar. This process comes with substantial energy and financial costs, both in terms of capital expenditure for the compression equipment and operational energy requirements[8].

An alternative approach is to transport hydrogen in its liquid form, which requires cooling it to cryogenic temperatures below -253°C. This method enables the transport of larger volumes of hydrogen over greater distances, facilitated by vacuum-insulated liquid tankers capable of carrying up to 4,300 kg of hydrogen [9]. However, the process of liquefying hydrogen is highly energy-intensive, with more than 10 kWh of energy required per kilogram of hydrogen, which represents over 30% of its energy content[10,11]. Despite these challenges, advancements in liquefaction and transportation technologies have been made, although the infrastructure remains costly and technologically complex[12]. To overcome these obstacles, several alternative hydrogen carriers, such as Liquid Organic Hydrogen Carriers (LOHCs), have been proposed. LOHCs are organic liquids that can absorb and release hydrogen through reversible hydrogenation and dehydrogenation cycles, making them a more practical and cost-effective option for hydrogen storage and transport. These carriers are advantageous because they are compatible with existing petroleum infrastructure, reducing the need for costly new investments[13–15].

LOHCs offer significant promise for the safe and efficient storage and transport of hydrogen. The hydrogenation process is exothermic and requires moderate temperatures, high pressures, and a catalyst to drive the reaction, while dehydrogenation, being endothermic, is typically carried out at high temperatures and low pressures, often under atmospheric conditions[16,17].

The primary advantages of LOHCs lie in their safety, ease of handling, and the ability to utilize existing infrastructure for petroleum-based fuels. These characteristics make LOHCs a compelling solution to the challenges of hydrogen transport and storage, reducing the overall cost and increasing the feasibility of a global hydrogen economy[18–20] . Additionally, LOHCs meet several key criteria required for effective hydrogen carriers, including high hydrogen storage capacity, low toxicity, stability, and ease of handling at both high and low temperatures[20].

The previous research survey shows that either hydrogenation and dehydrogenation systems have been studied separately, or combined systems studied missing either the power generation or electrolysis setup. Furthermore, the combined setup considered are experimental and they did not cover the simulation aspect, or system with simulation studies did not consider the real-time data i.e., not considering the kinetic data, and used only conversion reactors for the simulation purposes [21,22].

The aim of this work is to provide a comprehensive technical and energy analysis of hydrogen transport through LOHCs, focusing on the hydrogenation process. The study will use Aspen Plus V14® simulation software to model the hydrogenation process using quinoline as the representative LOHC. Quinoline was selected due to its novelty and potential in hydrogen storage applications. This work also aims to identify key energy drivers and effectiveness of the process in hydrogen storage, offering a optimized simulation of the hydrogenation process, which is then tested along various parameters. The energy consumed and key kinetic indicators like conversion, selectivity and yield were analysed over changes in reaction parameters i.e., pressure and temperature. These results are examined to find the optimized case for our simulation environment.

6.2 Process for hydrogenation

The Flowsheet consists of the pre-reaction stage and the post reaction stages. In the pre-reaction stage, the feedstock, comprising quinoline and isopropyl alcohol along with hydrogen gas, is initially introduced into the system at atmospheric pressure and ambient temperature. To achieve the required reaction parameters, the liquid feed components, quinoline and isopropyl alcohol, are pressurized using high-efficiency pumps, while the hydrogen gas undergoes compression through a series of multiple compressors, each operating with a compression ratio of 2. The multi-stage compression of hydrogen results in significant heat generation due to the

thermodynamic nature of the process. To optimize energy usage, the thermal energy released during gas compression is captured using a network of water-cooled heat exchangers strategically placed after each compression stage. This captured energy is then repurposed to preheat the feedstock prior to its entry into the reaction system significantly reducing the external energy required for heating and enhancing the overall energy efficiency of the process. The preheated and pressurized reactants, including the solvent, are thoroughly mixed and subsequently directed to the first continuous stirred tank reactor (CSTR). In the first CSTR, the hydrogenation of quinoline occurs resulting to py-THQ. This reaction represents the initial step in the sequential hydrogenation pathway and is facilitated by the optimized mixing and heat distribution provided by the reactor design. The partially converted stream is then transported to the second CSTR, where further hydrogenation takes place, converting py-THQ into DHQ. This two-stage reactor configuration ensures high conversion efficiency by sequentially optimizing reaction conditions for each step of the process. Upon exiting the second reactor, the product stream contains a mixture of unreacted hydrogen gas, the solvent, and the hydrogenated products. The unreacted hydrogen gas is separated from the product stream using a gas-liquid separation unit, enabling its potential recycling back into the reaction system to enhance resource efficiency.

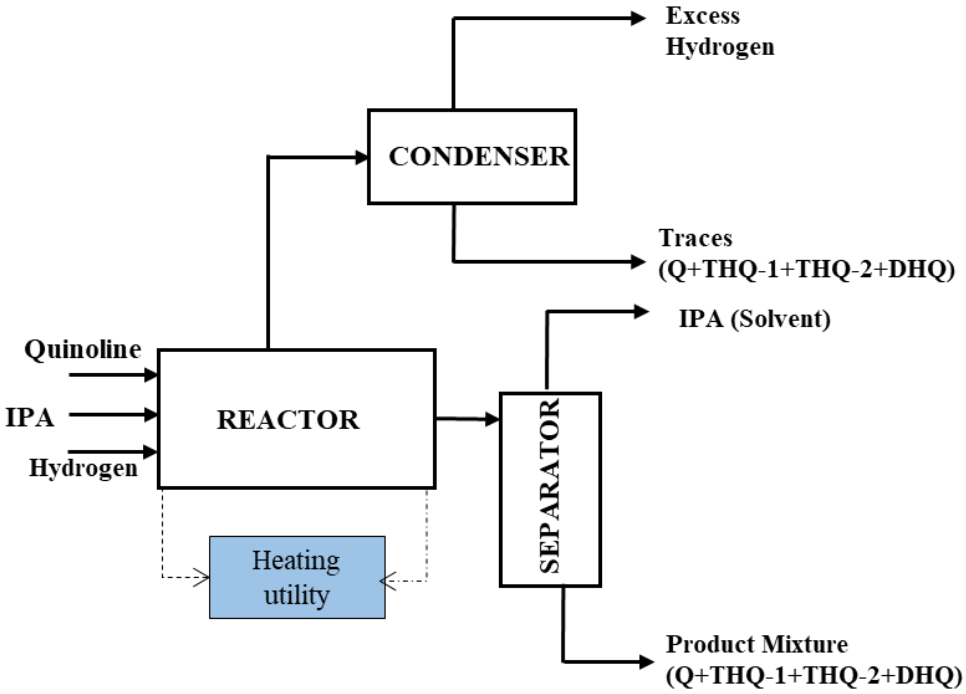

Figure 6.1 Block diagram for hydrogenation

The remaining liquid stream consisting of the solvent and hydrogenation products undergoes purification in a distillation column. During this step, the isopropyl alcohol solvent is separated using separator and recovered for potential reuse in subsequent reaction cycles. The final separation stage involves isolating the hydrogenation products, py-THQ and DHQ, from one another. This step is typically conducted using a high-precision separation unit which ensures the purity of the individual products for downstream applications or further processing. By integrating energy recovery systems, efficient reactor designs, and advanced separation techniques, the process achieves a balance between high conversion rates, energy efficiency, and resource sustainability, demonstrating its industrial applicability.

Table 6.1 Mass Balance for hydrogenation process

Component	**Mass In (kg/h)**	**Mass Out (kg/h)**
Quinoline	38.65	…
IPA	250.84	250.84
Hydrogen	4.87	1.86
DHQ	…	41.7
Total	294.36	294.36

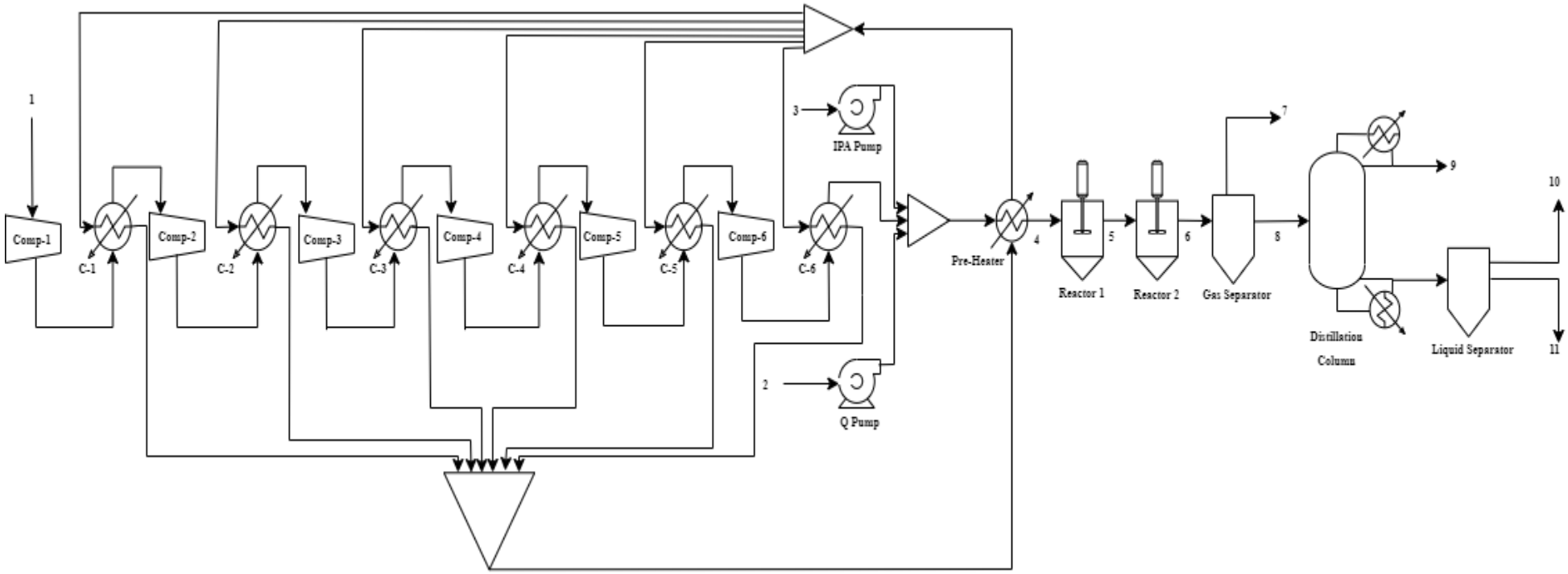

Figure 6.2 Process flow diagram for hydrogenation of quinoline to DHQ production

6.3 Simulation Methodology

The catalytic hydrogenation of quinoline was systematically modelled using Aspen Plus V14® simulation software to design a process capable of producing 1 ton per day of decahydroquinoline (DHQ). A comprehensive process simulation framework was established to replicate and optimize the reaction conditions and overall system performance. The Peng-Robinson equation of state was employed for accurate estimation of thermodynamic properties, ensuring reliability in phase behaviour and energy balance calculations across the process.

The flow rates of the reactants, including quinoline, isopropyl alcohol, and hydrogen gas, were calculated based on stoichiometric and operational requirements. These calculated flow rates were then input into the simulation to develop a process flowsheet. Hydrogen gas was intentionally fed in excess to replicate experimental conditions, ensuring complete conversion of quinoline and aligning the simulation with practical scenarios observed in laboratory-scale studies.

The simulated process underwent rigorous evaluation across a range of operating parameters, including temperature, pressure, and energy consumption. These evaluations provided insights into the relationship between reaction conditions and process efficiency, helping to identify optimal operating conditions for maximizing DHQ yield while minimizing energy demands. The simulation also facilitated the analysis of critical factors such as reactant utilization, heat integration, and overall system performance.

By leveraging the capabilities of Aspen Plus V.14, the study provided a detailed and scalable process model for the hydrogenation of quinoline. This simulation not only aligned with experimental data but also offered a foundation for industrial implementation, ensuring efficient and sustainable production of DHQ.

6.4 Process simulations using reaction kinetics

Using a mixture of continuous stirred-tank reactors (CSTRs) in Aspen Plus, the kinetic model for the hydrogenation of quinoline was developed to simulate using reaction kinetics. The simulations are carried out for various parameters using well-mixed reactor environment and the insights with reaction kinetics are studied. Quinoline hydrogenation to 1,2,3,4-Tetrahydroquinoline (py-THQ) conversion and then, py-THQ is further hydrogenated to

produce decahydroquinoline (DHQ) is modelled using series of CSTRs in the simulator. This process is carried out in two successive steps. Additionally, Iso-Propyl Alcohol (IPA) was used as a solvent in the ratio 1:9 of the substrate with two reasons: i) acts as solvent to dissolve H_2 and ii) removes heat that is being generated during hydrogenation. The underlying dynamics of the process are reflected in the distinct rate constants and activation energies that define each step.

In the first stage, Quinoline reacts reversibly with molecular hydrogen to form py-THQ. The reaction can be represented below. The forward and reverse reactions are described by their respective rate constants k_1 and k_{1r} and activation energies E as reported in Chapter 4.

$$Q + 2H_2 \leftrightarrow py - THQ$$

$$k_1 = 61.6 \times 10^{-3} \frac{m^3}{kg_{cat} \cdot sec} \; and \; E_a = 136.57 \; \frac{kJ}{mol.}$$

$$k_{1r} = 33.33 \times 10^{-6} \frac{m^3}{kg_{cat} \cdot sec} \; and \; E_a = 82 \; \frac{kJ}{mol.}$$

Where,

k_1 is the pre-exponential factor of forward Quinoline hydrogenation reaction

k_{1r} is the pre-exponential factor of backward reaction

The subsequent reaction in the hydrogenation process involves the conversion of tetrahydroquinoline-1 (py-THQ) into decahydroquinoline (DHQ) through the addition of three moles of hydrogen gas. This reaction is represented by the equation:

$$py - THQ + 3H_2 \rightarrow DHQ$$

$$k_2 = 43.33 \times 10^{-3} \frac{m^3}{kg_{cat} \cdot sec} \; and \; E_a = 76.16 \; \frac{kJ}{mol.}$$

Where,

k_2 is the pre-exponential factor of forward py-THQ hydrogenation reaction

Unlike the preceding reaction, this step is irreversible, emphasizing its directional nature under the given reaction conditions. The kinetics of this transformation are governed by a rate constant k_2 and an activation energy E_a both determined experimentally.

The lower activation energy compared to the first stage indicates that the conversion of py-THQ to DHQ proceeds more readily, provided hydrogen is available in excess and the reaction is conducted under optimized conditions.

With a total of 7.73 kg of catalyst placed into the system, the reactors were built with a catalyst bed to aid in the hydrogenation process. In order to provide a sufficient catalyst-to-reactant ratio for effective reaction kinetics, this catalyst quantity was calculated using 20 weight percent of the total quinoline loading. Additionally, the reactors had a bed voidage of 0.18, which created ideal conditions for reactant movement and hydrogen gas dispersion across the catalytic surface. These design factors were essential for guaranteeing consistent contact between the catalyst and the reactants, which increased the system's overall performance and reaction efficiency.

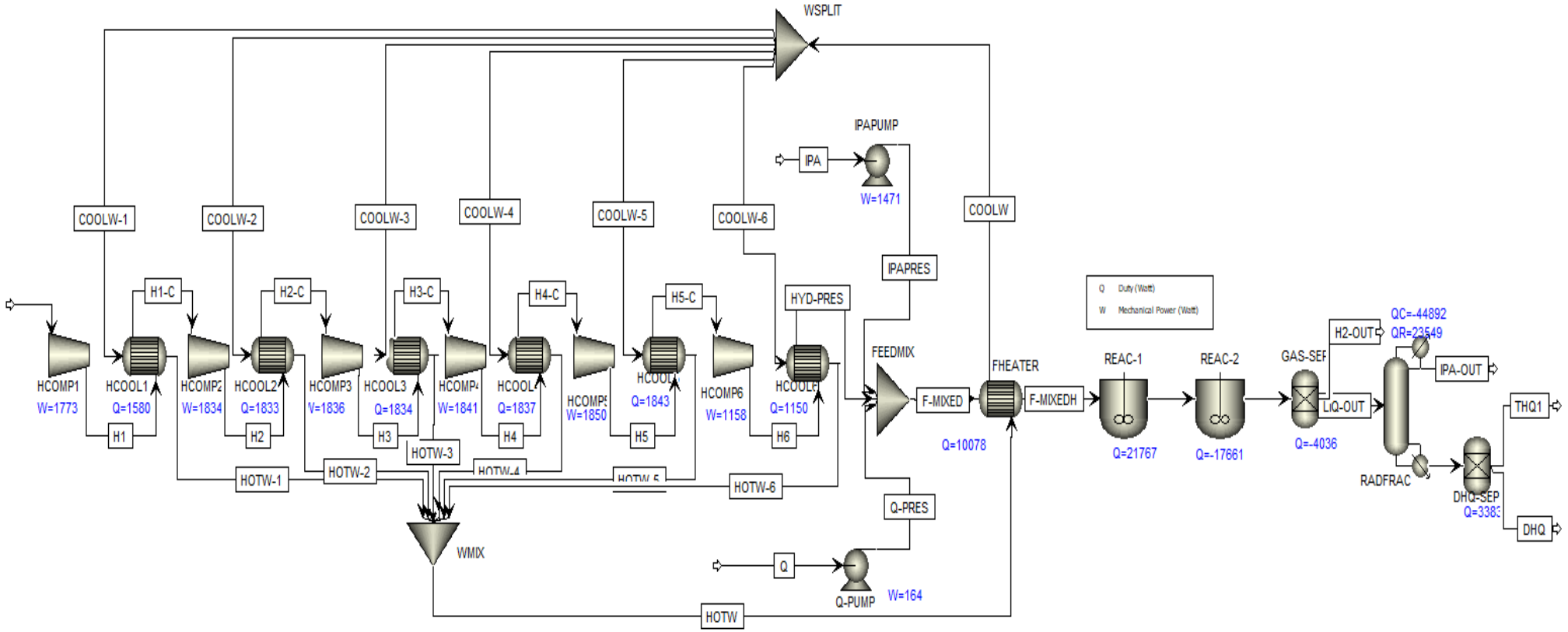

Figure 6.3 Simulation Flowsheet for hydrogenation process

6.5 Process flowsheet description

The Flowsheet consists of the pre-reaction stage and the post reaction stages. In the pre-reaction stage, the feedstock, comprising quinoline and isopropyl alcohol along with hydrogen gas, is initially introduced into the system at atmospheric pressure and ambient temperature. To achieve the required reaction parameters, the liquid feed components, quinoline and isopropyl alcohol, are pressurized using high-efficiency pumps, while the hydrogen gas undergoes compression through a series of multiple compressors, each operating with a compression ratio of 2. The multi-stage compression of hydrogen results in significant heat generation due to the thermodynamic nature of the process.

To optimize energy usage, the thermal energy released during gas compression is captured using a network of water-cooled heat exchangers strategically placed after each compression stage. This captured energy is then repurposed to preheat the feedstock prior to its entry into the reaction system, significantly reducing the external energy required for heating and enhancing the overall energy efficiency of the process. The preheated and pressurized reactants, including the solvent, are thoroughly mixed and subsequently directed to the first Continuous Stirred Tank Reactor (CSTR).

Within the first CSTR, the hydrogenation of quinoline occurs, resulting in its conversion to py-THQ. This reaction represents the initial step in the sequential hydrogenation pathway and is facilitated by the optimized mixing and heat distribution provided by the reactor design. The partially converted stream is then transported to the second CSTR, where further hydrogenation takes place, converting py-THQ into DHQ. This two-stage reactor configuration ensures high conversion efficiency by sequentially optimizing reaction conditions for each step of the process.

Upon exiting the second reactor, the product stream contains a mixture of unreacted hydrogen gas, the solvent, and the hydrogenated products. The unreacted hydrogen gas is separated from the product stream using a gas-liquid separation unit, enabling its potential recycling back into the reaction system to enhance resource efficiency. The remaining liquid stream, consisting of the solvent and hydrogenation products, undergoes purification in a distillation column. During this step, the isopropyl alcohol solvent is separated using separator and recovered for potential reuse in subsequent reaction cycles.

The final separation stage involves isolating the hydrogenation products, py-THQ and DHQ, from one another. This step is typically conducted using a high-precision separation unit, which ensures the purity of the individual products for downstream applications or further processing. By integrating energy recovery systems, efficient reactor designs, and advanced separation techniques, the process achieves a balance between high conversion rates, energy efficiency, and resource sustainability, demonstrating its industrial applicability.

6.6 Results and discussion

6.6.1 Mass and energy balance

The process energy requirement depends majorly on the reaction temperature and pressure, indicating the importance of operational and thermodynamic parameters. The energy input necessary to heat the system to the optimum reaction temperature, the energy released during the exothermic process, and the energy used to compress the hydrogen gas needed for the reaction were the main factors influencing this change. The dependence on pressure was more significant than temperature as higher pressures required more energy to compress the reactants, hence it is important to optimize reaction parameters without compromising the energy economy.

Hydrogen gas, was compressed through a series of compressors, each with a compression ratio of 2. This multi-stage compression setup was used to simulate closer to the real-world industrial conditions, providing more accurate insight into the practical energy costs associated with large-scale operation. The heat generated during the compression of hydrogen gas, was recovered and utilized within the process. This heat was repurposed to preheat the feed stream, thereby reducing the external energy demand for heating the reactants. This enhances the overall energy efficiency of the system.

Table 6.2 Mass balance of the complete hydrogenation process in terms of mass flow

Material Streams	1	2	3	4	5	6	7	8	9	10	11
Quinoline	0.00	38.65	0.00	38.65	0.01	0.01	0.00	0.01	0.00	0.01	0.00
Hydrogen	4.87	0.00	0.00	4.87	3.66	2.02	2.02	0.00	0.00	0.00	0.00
IPA	0.00	0.00	250.84	250.84	250.84	250.84	0.00	250.84	250.83	0.00	0.00
DHQ	0.00	0.00	0.00	0.00	0.00	37.84	0.00	37.84	0.00	0.00	37.83
py-THQ	0.00	0.00	0.00	0.00	39.85	3.65	0.00	3.65	0.00	3.65	0.00
bz-THQ	0.00	0.00	0.00	0.00	0.00	0.00	0.00	0.00	0.00	0.00	0.00
Total Mass (kg/hr)	4.87	38.65	250.84	294.36	294.36	294.86	2.02	292.34	250.84	3.66	37.83

Table 6.3 Mass balance of the complete hydrogenation process in terms of mass fractions

Mass Fraction	1	2	3	4	5	6	7	8	9	10	11
Quinoline	0	1.0	0.0	0.13	0.00	0.00	0.00	0.0	0.00	0.00	0.00
Hydrogen	1	0.00	0.00	0.02	0.01	0.01	1.0	0.0	0.0	0.00	0.00
IPA	0	0.00	1.00	0.83	0.85	0.85	0.00	0.86	1.00	0.00	0.00
DHQ	0	0.00	0.00	0.00	0.00	0.13	0.00	0.13	0.00	0.00	1.00
py-THQ	0	0.00	0.00	0.00	0.14	0.01	0.00	0.01	0.00	1.00	0.00
bz-THQ	0	0.0	0.00	0.00	0.00	0.00	0.00	0.00	0.00	0.00	0.00

In this present study, the recovery and utilization of compression heat were facilitated through the implementation of multiple heat exchangers. These heat exchangers operated using water as the service fluid, effectively capturing the thermal energy released after each compression cycle. The collected heat was subsequently applied to preheat the feed stream before it entered the reactor system, significantly lowering the external heating energy requirements. Furthermore, the water used in the heat exchangers was recycled back into the compression system after cooling, thereby minimizing the consumption of fresh water and contributing to energy and resource conservation. The following graphs outline the total energy that is required to operate the simulated plant and the variation in energy required based on pressure and

temperature. The following table presents an analysis of the energy transfer processes observed during the simulation is shown in Table 6.4.

Table 6.4 Energy data in the flowsheet at 175 ^{o}C and 50 bar

Block	Heat released (J/s)	Heat required (J/s)
HCOMP1	…	1773
HCOOL1	…	1580
HCOMP2	…	1834
HCOOL2	…	1833
HCOMP3	…	1836
HCOOL3	…	1834
HCOMP4	…	1841
HCOOL4	…	1837
HCOMP5	…	1850
HCOOL5	…	1843
HCOMP6	…	1158
HCOOL6	…	1150
QPUMP	…	164
IPAPUMP	…	1471
FHEATER	…	10078
REAC-1	…	21767
REAC-2	17661	…
GAS-SEP	4036	…
RADFRAC	44892	23549
DHQ-SEP	…	3383
TOTAL	**66589**	**80781**
NET ENERGY REQUIRED	**14192 J/s**	

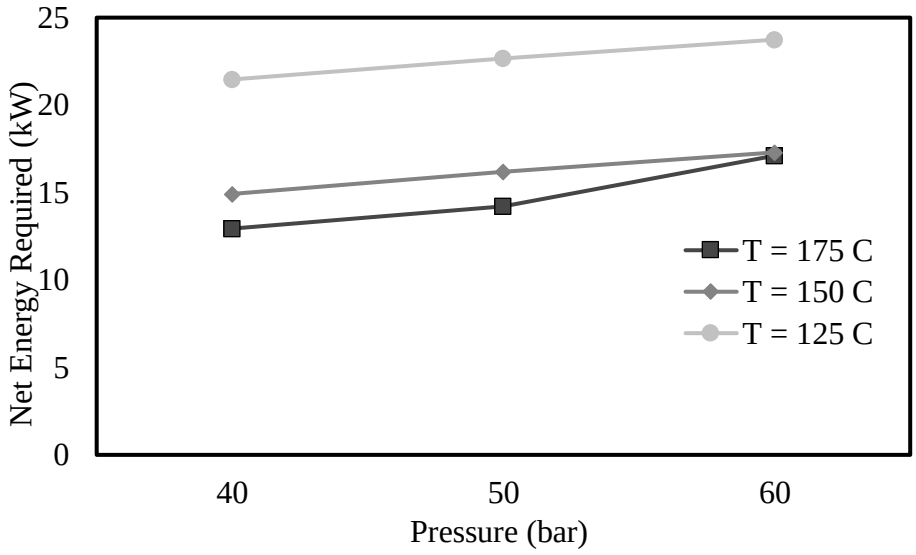

Figure 6.3 Effect of reactor pressure on energy requirement

The energy consumption across all evaluated temperatures exhibits a clear upward trend with increasing pressure. This observation aligns with the expected thermodynamic behaviour, as maintaining reactants at elevated pressures necessitates additional energy for compression. The highest energy demands are recorded at 60 bar, primarily attributable to the operational requirements of multiple compressors used for hydrogen gas and pumps for liquid feedstocks such as quinoline and isopropyl alcohol.

The energy consumption increases from 21.4 kW at lower pressures to 23.7 kW at 60 bar at 125^{o}C representing the highest energy requirement in the series. The energy consumption ranges from 14.9 kW to 17.2 kW as pressure increases at 150^{o}C while at 175 °C, the energy expenditure rises from 12.9 kW to 17.1 kW over the same pressure range. This notable decrease in energy requirements with increasing temperature is further explained.

However, the positive correlation between pressure and energy costs remains prominent. The increase in energy demand with pressure is driven by several interrelated factors. Higher pressures necessitate greater mechanical work by compressors to pressurize the hydrogen gas and by pumps to circulate liquid reactants through the system. Additionally, the thermodynamic properties of the substances under elevated pressure contribute to this trend, an increase in pressure results in a higher heat capacity of the system, requiring more energy to achieve a given temperature rise.

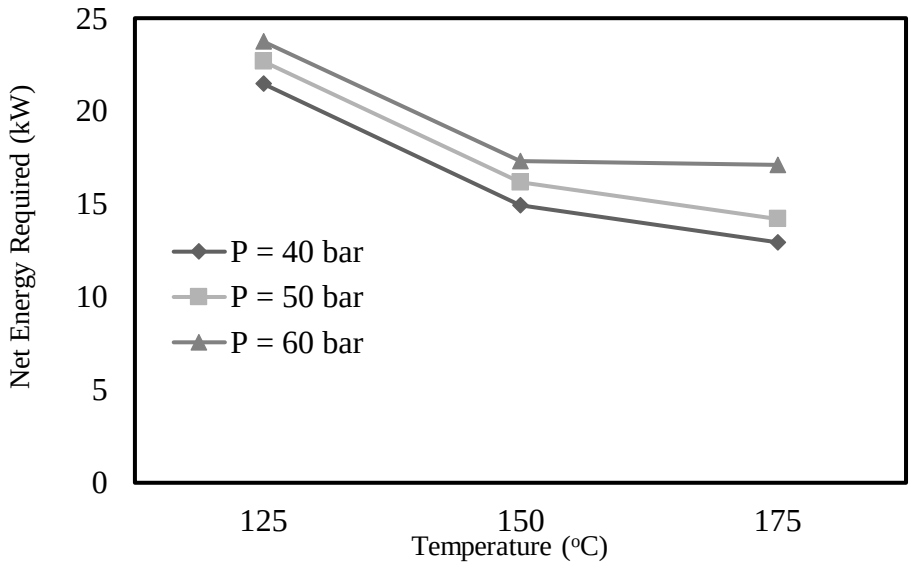

Figure 6.4 Effect of Temperature on Energy Required

The energy consumption of the system exhibits a pronounced downward trend as the reaction temperature increases, a behaviour that can be attributed to the interplay of thermodynamic and operational factors. The primary driver of this reduction is the energy released by the exothermic reaction occurring within the reactors, which offsets the energy demands of other units in the process. The reactors serve as the dominant contributors to this energy balance, given the exothermic nature of the reaction pathway.

As the reaction progresses at higher temperatures, the extent of the reaction increases, leading to a greater release of thermal energy. This increase in energy release is directly related to the temperature dependence of the reaction kinetics, where elevated temperatures enhance reaction rates and conversion efficiency. Consequently, the exothermic energy output counteracts the substantial energy requirements associated with operating compressors, pumps, and heat exchangers, resulting in a net reduction in energy consumption across the system.

For example, at a pressure of 60 bar, the total energy consumption decreases from 23.7 kW at 125 °C to 17.1 kW at 175 °C, representing the highest energy reduction observed in the series. At 50 bar, energy consumption follows a similar trend, decreasing from 22.6 kW to 14.2 kW over the same temperature range. At 40 bar, the energy requirement drops from 21.4 kW to

12.9 kW, further reinforcing the observation that higher temperatures facilitate a more energy-efficient operation.

These findings suggest that 175 °C is an optimal temperature for this reaction, not only because it minimizes the system's overall energy consumption but also due to the improved reaction extent achieved at this temperature. The results highlight the dual benefit of operating at elevated temperatures: enhanced reaction performance and a more favourable energy balance, both of which are critical for process optimization.

6.6.2 Sensitivity analysis

6.6.2.1 Effect of temperature

With the aim of assessing the impact of Temperature on the process performance, the temperature was changed from 125 °C to 175 °C and the pressure was changed from 40 to 60 bar in order to optimise the process. Throughout the experimental range, key variables such as conversion, selectivity, yield, and energy consumption were observed for the maximum performance. A thorough grasp of the process optimisation and its underlying trends is made possible by the generated data.

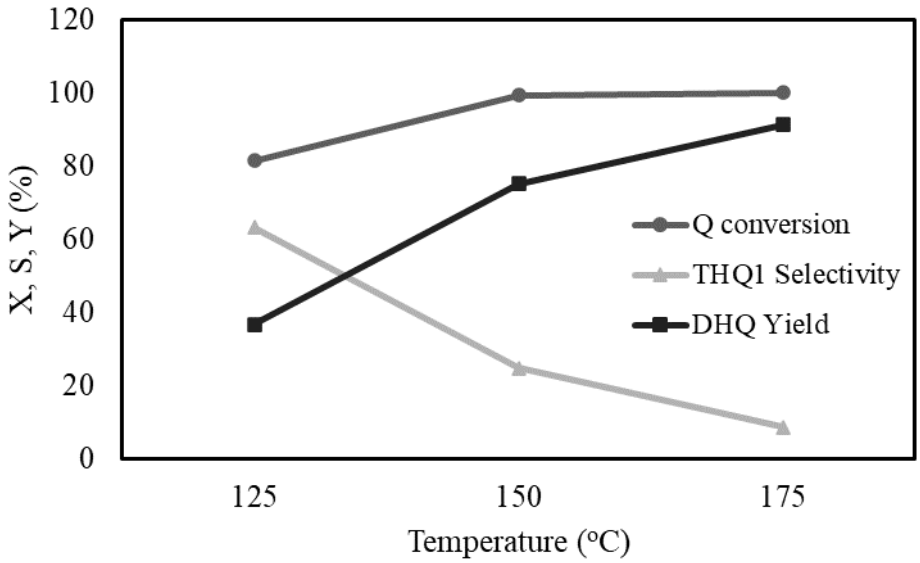

Figure 6.5 Effect of temperature on conversion, selectivity and yield at 40 bar

As the temperature is increased from 125 °C to 150 °C at a pressure of 40 bar, there is a noticeable rise in the conversion of quinoline to products. However, as the temperature is raised to 175 °C, the magnitude of this increase becomes less important. It's interesting to note that

across the same temperature range, the yield of decahydroquinoline (DHQ) increases more noticeably. The yeild of DHQ increases from 36% at 125 °C to 75% at 150 °C and 91% at 175 °C, respectively. On the other hand, Tetrahydroquinoline-1 (py-THQ) yield exhibits the opposite pattern, beginning at 64% at 125 °C and rapidly dropping to 25% at 150 °C before further lowering to 9% at 175 °C.

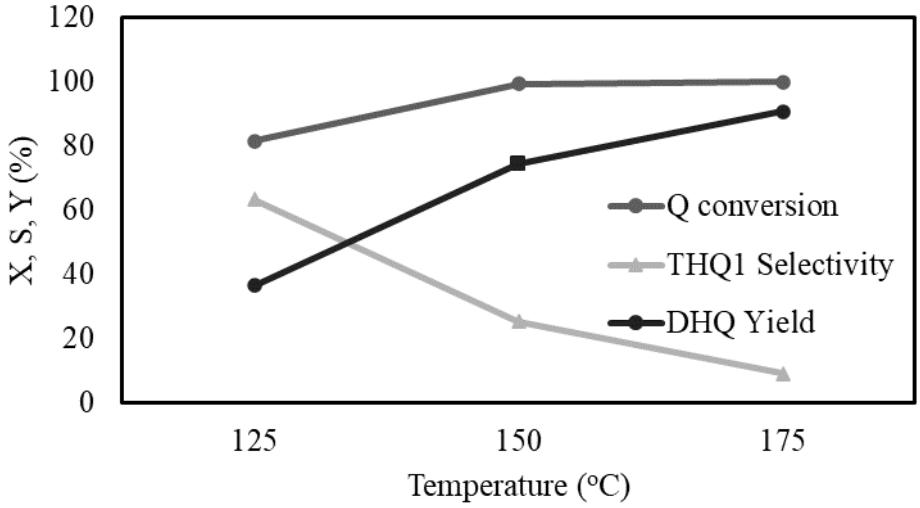

Figure 6.6 Effect of temperature on conversion, selectivity and yield at 50 bar

When the pressure is raised to 50 bar, this temperature-dependent pattern continues. The DHQ yield increases similarly at this pressure, rising from 36% at 125 °C to 75% at 150 °C and 92% at 175 °C. The conversion is rather constant over the assessed temperature range, suggesting that changes in pressure have little effect on the total conversion rates in these circumstances. The selectivity for py-THQ, on the other hand, continues to drastically decrease as the temperature rises, falling from 63% at 125 °C to only 9% at 175 °C.

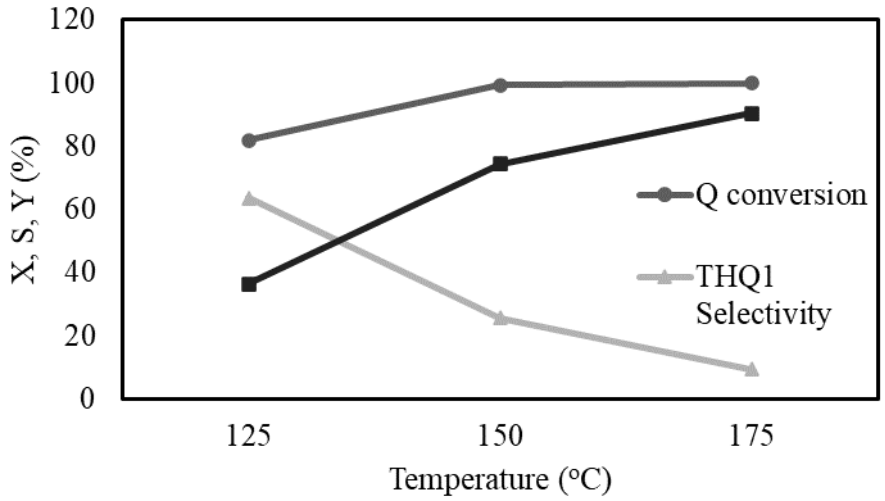

Figure 6.7 Effect of temperature on conversion, selectivity and iyeld at 60 bar

When the pressure is increased to 60 bar, Quinoline conversion increases under this pressure from 82% at 125 °C to 99.57% at 150 °C and finally to 99.98% at 175 °C. The DHQ production increases in proportion, rising from 36% at 125 °C to 74% at 150 °C and 91% at 175 °C. On the other hand, the yield of py-THQ progressively drops as the temperature rises, going from 64% at 125 °C to 26% at 150 °C and finally down to 9% at 175 °C.

There is a clear pattern across all pressures examined: the py-THQ yield sharply declines with temperature, but the DHQ yield rises noticeably. These results highlight how temperature and pressure interact to control the yield and selectivity of products throughout the quinoline dehydrogenation process.

6.6.2.2 Effect of pressure

The impact of pressure changes on crucial parameters including conversion, selectivity, and yield in the hydrogenation of quinoline is thoroughly examined in the accompanying figures.

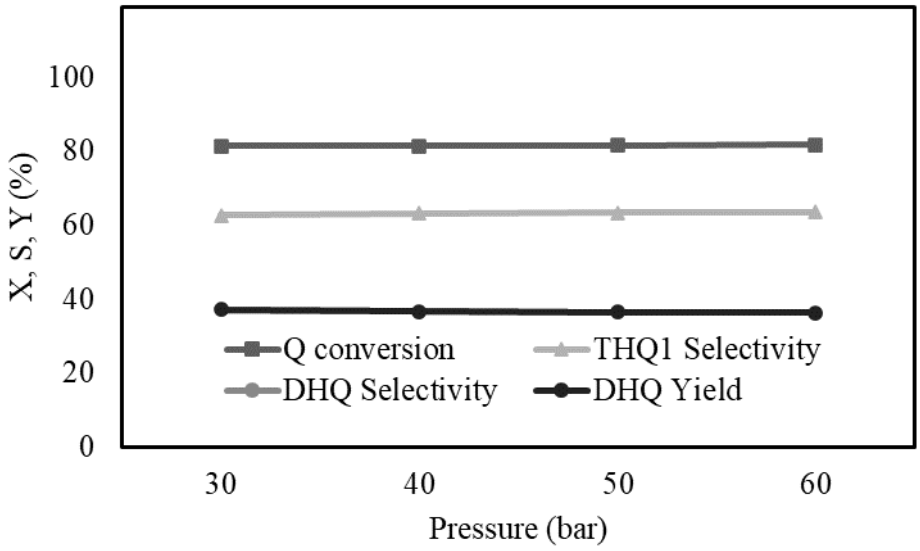

Figure 6.8 Effect of pressure on conversion, selectivity and yield at 125 ^{o}C

At 125°C, the yield of decahydroquinoline (DHQ) stayed steady at about 36%, while the conversion rate stayed steady within a small range of 81% to 82%. Likewise, the yield of py-THQ remained rather stable at 64% across the pressure range. This stability in the parameters is explained by the reaction's significant reliance on thermodynamic restrictions, which suggests that changes in pressure have little effect in these circumstances.

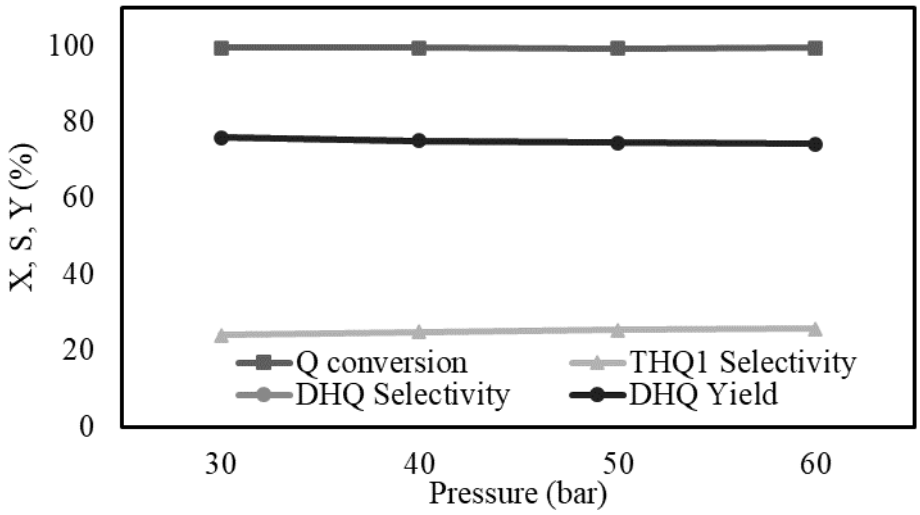

Figure 6.9 Effect of pressure on conversion, selectivity and yield at 150^{o}C

The conversion values were measured at around 99.4% at a higher temperature of 150 °C, and they showed little variation within this range under different pressures. Similar trends were

seen in the THQ-1 yield, which varied between 24% and 26%, and the DHQ yield, which varied slightly between 76% and 74%. A substantial boost in conversion is observed from 125 °C to 150 °C, or about 15%.

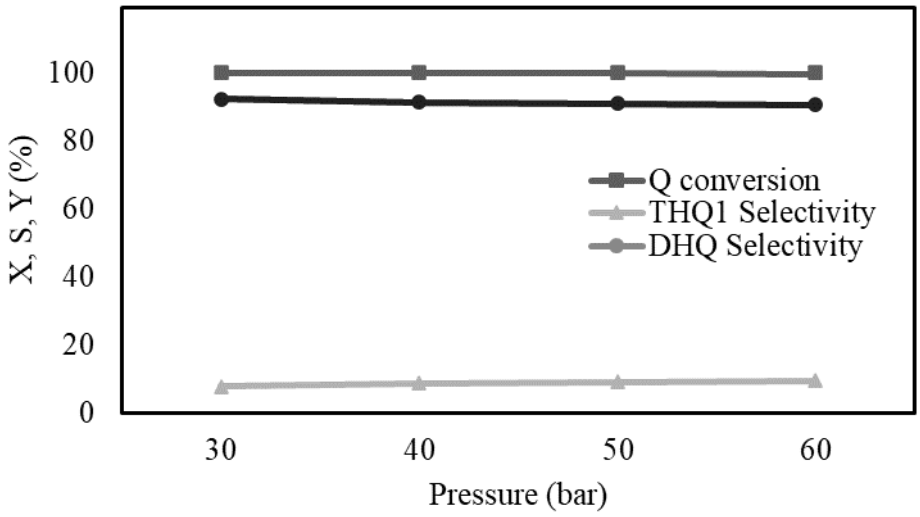

Figure 6.10 Effect of pressure on conversion, selectivity and yield at 175^{o}C

The conversion reached near-complete levels at 99.98%, and the DHQ yield similarly stabilized at high values, ranging from 92% to 91% at 175^{o}C. These findings suggest that the hydrogenation of quinoline is strongly favoured at elevated temperatures, with pressure exerting a comparatively minor influence on the reaction's outcome. Interestingly, the data indicate that lower pressures may provide slightly better DHQ yields, underscoring the complex interplay between thermodynamic and kinetic factors in optimizing product selectivity and yield.

6.7 Conclusions

The process for the catalytic hydrogenation of quinoline was effectively simulated at the industrial-scale production of 1 ton per day of decahydroquinoline (DHQ), using Aspen Plus V.14, a comprehensive analysis was carried out to optimize operating conditions, energy efficiency, and product yield. Key findings highlighted the importance of high temperature in influencing greater conversion rates and higher selectivity. Whereas, elevated pressure results in increased energy consumption. Hence, optimal conditions of 175°C and 50 bar pressure yielded the highest DHQ output while minimizing energy demands, with exothermic reactions

offsetting much of the required energy. The integration of energy recovery systems, such as multi-stage hydrogen compression and heat exchangers, significantly enhanced sustainability by repurposing heat for preheating feedstocks, this gives us a final energy requirement of 14.192 kJ/s. Sensitivity analysis confirmed the positive impact of elevated temperatures on reaction kinetics and efficiency, while higher pressures had diminishing returns on performance metrics. Overall, the simulation provided a scalable, energy-efficient process model aligned with experimental data, offering valuable insights for industrial applications. This study underscores the critical interplay between kinetics, and engineering design in optimizing chemical processes for sustainable and efficient production.

6.8 References

[1] https://www.europarl.europa.eu/factsheets/en/sheet/72/ combating-climate-change.

[2] Álvarez M, Marín P, Ordóñez S. Production of dimethyl carbonate by gas-phase oxidative carbonylation of methanol over Cu/Y zeolite: Mechanism and kinetics. Fuel Process Technol 2023;247. https://doi.org/10.1016/j.fuproc.2023.107805.

[3] Peláez R, Marín P, Ordóñez S. Direct synthesis of dimethyl ether from syngas over mechanical mixtures of $CuO/ZnO/Al_2O_3$ and Γ-Al_2O_3: Process optimization and kinetic modelling. Fuel Process Technol 2017;168:40–9. https://doi.org/10.1016/j.fuproc.2017.09.004.

[4] Stöckl F, Schill WP, Zerrahn A. Optimal supply chains and power sector benefits of green hydrogen. Sci Rep 2021;11:1–14. https://doi.org/10.1038/s41598-021-92511-6.

[5] Mah AXY, Ho WS, Hassim MH, Hashim H, Liew PY, Muis ZA. Targeting and scheduling of standalone renewable energy system with liquid organic hydrogen carrier as energy storage. Energy 2021;218:119475. https://doi.org/10.1016/j.energy.2020.119475.

[6] Liu W, Zuo H, Wang J, Xue Q, Ren B, Yang F. The production and application of hydrogen in steel industry. Int J Hydrogen Energy 2021;46:10548–69. https://doi.org/10.1016/j.ijhydene.2020.12.123.

[7] Kojima Y, Yamaguchi M. Ammonia as a hydrogen energy carrier. Int J Hydrogen Energy 2022;47:22832–9. https://doi.org/10.1016/j.ijhydene.2022.05.096.

[8] Spatolisano E, Restelli F, Matichecchia A, Pellegrini LA, Angelis AR De, Cattaneo S, et al. ScienceDirect Assessing opportunities and weaknesses of green hydrogen transport via LOHC through a detailed techno-economic analysis. Int J Hydrogen Energy 2023;52:703–17. https://doi.org/10.1016/j.ijhydene.2023.08.040.

[9] Ratnakar RR, Gupta N, Zhang K, Doorne C Van, Fesmire J, Dindoruk B, et al. ScienceDirect Hydrogen supply chain and challenges in large- scale LH_2 storage and

transportation. Int J Hydrogen Energy 2021;46:24149–68. https://doi.org/10.1016/j.ijhydene.2021.05.025.

[10] Emre M, Dincer I. Cost assessment and evaluation of various hydrogen delivery scenarios. Int J Hydrogen Energy 2017:1–11. https://doi.org/10.1016/j.ijhydene.2017.08.002.

[11] Decker KOL. The latest developments and outlook for hydrogen liquefaction technology 2014;1317:1311–7. https://doi.org/10.1063/1.4860858.

[12] Ishaq H, Dincer I, Crawford C. ScienceDirect A review on hydrogen production and utilization : Challenges and opportunities. Int J Hydrogen Energy 2021;47:26238–64. https://doi.org/10.1016/j.ijhydene.2021.11.149.

[13] Geburtig D, Preuster P, Bösmann A, Müller K, Wasserscheid P. Chemical utilization of hydrogen from fluctuating energy sources - Catalytic transfer hydrogenation from charged Liquid Organic Hydrogen Carrier systems. Int J Hydrogen Energy 2016;41:1010–7. https://doi.org/10.1016/j.ijhydene.2015.10.013.

[14] Shi L, Qi S, Qu J, Che T, Yi C, Yang B. Integration of hydrogenation and dehydrogenation based on dibenzyltoluene as liquid organic hydrogen energy carrier. Int J Hydrogen Energy 2019;44:5345–54. https://doi.org/10.1016/j.ijhydene.2018.09.083.

[15] Hurskainen M, Ihonen J. Techno-economic feasibility of road transport of hydrogen using liquid organic hydrogen carriers. Int J Hydrogen Energy 2020;45:32098–112. https://doi.org/10.1016/j.ijhydene.2020.08.186.

[16] Hamayun MH, Hussain M, Maafa IM, Aslam R. Combined dehydrogenation and hydrogen-based power generation. Int J Hydrogen Energy 2019;44:20213–22. https://doi.org/10.1016/j.ijhydene.2019.06.053.

[17] Preuster P, Papp C, Wasserscheid P. Liquid organic hydrogen carriers (LOHCs): Toward a hydrogen-free hydrogen economy. Acc Chem Res 2017;50:74–85. https://doi.org/10.1021/acs.accounts.6b00474.

[18] Niermann M, Beckendorff A, Kaltschmitt M, Bonhoff K. Liquid Organic Hydrogen Carrier (LOHC) – Assessment based on chemical and economic properties. Int J Hydrogen Energy 2019;44:6631–54. https://doi.org/10.1016/j.ijhydene.2019.01.199.

[19] Lee S, Kim T, Han G, Kang S, Yoo YS, Jeon SY, et al. Comparative energetic studies on liquid organic hydrogen carrier: A net energy analysis. Renew Sustain Energy Rev 2021;150:111447. https://doi.org/10.1016/j.rser.2021.111447.

[20] Markiewicz M, Zhang YQ, Empl MT, Lykaki M, Thöming J, Steinberg P, et al. Hazard assessment of quinaldine-, alkylcarbazole-, benzene- and toluene-based liquid organic hydrogen carrier (LOHCs) systems. Energy Environ Sci 2019;12:366–83. https://doi.org/10.1039/c8ee01696h.

[21] Firman Bagja Juangsa L, Prananto A, Mufrodi Z, Budiman A, Oda T, Muhammad Aziz. Highly energy-efficient combination of dehydrogenation of methylcyclohexane and hydrogen-based power generation. Appl Energy 2018;226:31–8. https://doi.org/10.1016/j.apenergy.2018.05.110.

[22] Prananto LA, Biddinika MK, Aziz M. Combined dehydrogenation and hydrogen-based power generation. Energy Procedia 2017;142:1603–8. https://doi.org/10.1016/j.egypro.2017.12.537.

Chapter 7

Conclusions

The first part of the thesis presents direct conversion of CO_2 to methanol as promising strategy for both mitigating climate change and meeting the growing global demand for methanol. The present work concludes that the synthesis of methanol from CO_2 under high-pressure conditions involve critical kinetic parameters that require thorough experimental investigation for accurate evaluation. The study emphasizes the role of CO in direct CO_2 catalytic hydrogenation reactions through reverse water gas shift reactions and examines the impact of varying H_2 to CO_2 mole ratios.

The reactor modelling with rate kinetics results reveals the following inferences:

i) Both temperature and pressure significantly influence the process, with detailed insights from adiabatic and isothermal model simulations

ii) The isothermal reactor configuration out performs the adiabatic model, offering 2.76% higher methanol yield, better CO_2 conversion, and selectivity

iii) Reverse water gas shift (rWGS) reactions enhance methanol formation rates by a factor of five with CO hydrogenation playing a key role, although CO_2 hydrogenation remains the primary contributor to methanol production.

Additionally, the study shows that higher H_2 to CO_2 ratios yield improved methanol yields, with the optimal molar ratios of 3, 6, and 9 providing enhancements of 19.03%, 29.25%, and 36.41%, respectively, under low-pressure conditions.

The kinetic models developed for the synthesis of methanol from CO_2 under high-pressure conditions require experimental validation for accurate assessment of kinetic parameters. The study investigates the role of CO in the direct CO_2 catalytic hydrogenation reaction via the reverse water gas shift reaction, using various kinetic models. Based on the modelling and experimental findings, the following conclusions are drawn:

i) The experiments demonstrated an increase in methanol space-time yield (STY), with improvements of 6.30%, 9.22%, and 13.59% for H_2 to CO_2 molar ratios of 3, 6, and 9, respectively.

ii) Model A1B2C1 (Model 7) showed the best fit with the experimental data, exhibiting minimal residuals compared to other models, making it the preferred choice for further study.

iii) The Weisz-Prater criterion (CWP << 1) and Mear's Parameter (MP << 0.15) indicate the absence of internal diffusional and external mass transfer limitations in the reaction, suggesting that mass transfer effects can be neglected for all cases.

iv) The results also show that higher H_2 to CO_2 molar ratios lead to improved methanol yield and space-time yield, with a molar ratio of 9 being optimal for maximizing methanol production.

The second part of the thesis presents Liquid Organic Hydrogen Carriers (LOHCs) as promising solution to the challenges of hydrogen storage and transportation. As renewable energy sources grow, the need for efficient energy storage solutions becomes increasingly urgent. The following inferences are drawn for the hydrogenation of Quinoline as LOHC molecule.

Quinoline has been successfully identified as a promising liquid organic hydrogen carrier (LOHC) molecule, offering excellent thermal stability and the potential for efficient hydrogen storage. The hydrogenation process of quinoline was studied extensively using a palladium-supported alumina (Pd/Al_2O_3) catalyst, with the effect of various parameters such as temperature, hydrogen pressure, reaction time, solvent type, and catalyst loading carefully evaluated. The optimal reaction conditions were determined to be 175°C, 50 bar hydrogen pressure, and 20 wt.% Pd/Al_2O_3 catalyst loading, which led to a hydrogen uptake capacity of 6.91 wt.% and a decahydroquinoline (DHQ) yield of over 99%. Among the solvents tested, isopropyl alcohol (IPA) was found to be the most effective, facilitating high hydrogen uptake and selectivity towards DHQ. Based on the experimental data, a reaction mechanism was proposed for the conversion of quinoline to DHQ, with the hydrogenation reaction being highly selective toward DHQ formation, achieving a 100% conversion rate and 99% selectivity. A reaction kinetic model was developed to describe the simplified reaction pathway for DHQ formation, incorporating the key reaction steps and their corresponding rate constants. The kinetic model was simulated using the Monte Carlo simulation tool and validated against the experimental results, ensuring its reliability and accuracy. The kinetic study revealed that the formation of py-THQ (pyridine-THQ) is the rate-determining step in the hydrogenation process, emphasizing the critical role of this intermediate in controlling the overall reaction rate. This insight into the reaction mechanism not only provides a deeper understanding of the hydrogenation of quinoline but also contributes valuable information for optimizing the performance of LOHC systems. Overall, the successful hydrogenation of quinoline to DHQ with high selectivity and efficiency, coupled with the development of a reliable kinetic model, underscores the potential of quinoline as a viable LOHC molecule for hydrogen storage applications. The findings from this study contribute to the growing body of knowledge in the

field of LOHCs, demonstrating quinoline's suitability as a thermally stable and efficient hydrogen carrier with significant promise for future energy storage and transportation solutions.

A comprehensive investigation into the reaction kinetics of decahydroquinoline (DHQ) dehydrogenation, offering valuable insights into its potential as a liquid organic hydrogen carrier (LOHC). The catalytic dehydrogenation of DHQ to quinoline (Q), facilitated by 5% Pd/Al_2O_3, demonstrates significant promise for efficient hydrogen generation. Key reaction parameters, including reaction temperature, time, stirring speed, and catalyst loading were systematically evaluated, with optimal conditions identified at 240°C and 9 hours for maximum DHQ conversion and degree of dehydrogenation (DoD). The development and validation of a reaction kinetic model using Markov Chain Monte Carlo (MCMC) simulations provided an accurate prediction of rate constants and mechanistic insights. Notably, the activation energy for DHQ dehydrogenation was determined to be 185.43 kJ/mol, with the conversion of benzo-tetrahydroquinoline (bz-THQ) to quinoline identified as the rate-limiting step. These findings contribute significantly to the understanding of DHQ dehydrogenation kinetics and offer practical guidance for optimizing reaction conditions to enhance hydrogen release efficiency. By addressing critical aspects of reaction kinetics and catalytic performance, this work lays a strong foundation for advancing the development of sustainable and efficient hydrogen storage solutions. The insights gained not only enrich the existing body of knowledge on LOHC systems but also underscore the potential of DHQ as a robust candidate for meeting the growing demands of hydrogen-based economy. Further research in this area could focus on scaling the process, exploring alternative catalysts, and integrating these findings into broader hydrogen production systems.

Appendix

Table A1 Experimental data validation with reported literature for H_2:CO_2=3 and 40bar

T (^oC)	Flowrate (ml/min)	Yield of CH_3OH (model) (%)		Yield of CH_3OH (exp.) (%)	STY of CH_3OH (model) ($mg/g_{cat}.h$)		STY of CH_3OH (exp.)($mg/g_{cat}.h$)
		Graaf et al.(1986)	Portha et al.(2017)	Present Study	Graaf et al.(1986)	Portha et al.(2017)	Present Study
210	60	13.77	13.25	0.16	5.43	5.23	0.95
230	60	28.90	25.05	0.73	11.41	9.89	4.30
250	60	53.79	43.78	2.06	21.23	17.28	12.13
210	120	13.77	13.25	0.23	2.72	5.23	1.36
230	120	28.90	25.05	0.79	5.70	9.89	4.63
250	120	53.79	43.78	3.21	10.61	17.28	18.90

Error Analysis:

Table A2 Error Analysis (**Case-I:** CO_2 – 15 ml/min & H_2 – 45 ml/min)

Model No.	Kinetic Model	MeOH Yield (%) at P = 40 bar and catalyst weight = 3 g					
		T= 210^{o}C	Y_{MeOH} (Residual)	T= 230^{o}C	Y_{MeOH} (Residual)	T= 250^{o}C	Y_{MeOH} (Residual)
1	A1B1C1	0.90	4.54	1.42	0.94	2.55	0.23
2	A1B1C2	4.22	24.98	6.20	7.49	8.06	2.91
3	A1B1C3	14.21	86.57	16.04	20.94	11.89	4.76
4	A1B1C4	23.74	145.29	18.61	24.46	13.93	5.75
5	A1B1C5	…	…	…	…	…	…
6	A1B1C6	…	…	…	…	…	…
7	A1B2C1	0.61	2.77	1.22	0.67	2.50	0.21
8	A1B2C2	3.01	17.52	5.31	6.26	7.85	2.81
9	A1B2C3	11.87	72.17	15.23	19.84	11.89	4.76

10	A1B2C4	22.52	137.75	17.25	22.59	11.92	4.78
11	A1B2C5	…	…	…	…	…	…
12	A1B2C6	…	…	…	…	…	…
13	A2B1C1	0.95	4.88	1.89	1.59	4.61	1.24
14	A2B1C2	4.26	25.23	6.54	7.94	8.97	3.35
15	A2B1C3.	14.22	86.63	16.08	20.99	11.89	4.77
16	A2B1C4	23.73	145.25	18.59	24.43	13.88	5.73
17	A2B1C5	…	…	…	…	…	…
18	A2B1C6	…	…	…	…	…	…
19	A2B2C1	0.71	3.38	1.83	1.51	4.72	1.29
20	A2B2C2	3.09	18.05	5.77	6.89	8.87	3.30
21	A2B2C3	11.92	72.43	15.31	19.94	11.89	4.77
22	A2B2C4	22.52	137.77	17.25	22.59	11.92	4.78
23	A2B2C5	…	…	…	…	…	…
24	A2B2C6	…	…	…	…	…	…
25	A3B1C1	1.24	6.66	4.07	4.57	9.74	3.72
26	A3B1C2	4.46	26.51	8.06	10.02	11.11	4.39
27	A3B1C3	14.27	86.93	16.25	21.23	11.91	4.77
28	A3B1C4	23.70	145.06	18.48	24.28	13.62	5.60
29	A3B1C5	…	…	…	…	…	…
30	A3B1C6	…	…	…	…	…	…

31	A3B2C1	1.23	6.57	4.63	5.33	10.09	3.89
32	A3B2C2	3.53	20.78	7.868	9.76	11.19	4.42
33	A3B2C3	12.13	73.75	15.67	20.43	11.91	4.77
34	A3B2C4	22.53	137.85	17.25	22.59	11.92	4.78
35	A3B2C5	…	…	…	…	…	…
36	A3B2C6	…	…	…	…	…	…
37	A4B1C1	2.49	14.37	9.59	12.12	11.86	4.75
38	A4B1C2	5.38	32.16	11.96	15.36	11.90	4.77
39	A4B1C3	14.50	88.34	16.69	21.83	11.91	4.78
40	A4B1C4	23.56	144.17	18.05	23.69	12.68	5.15
41	A4B1C5	…	…	…	…	…	…
42	A4B1C6	…	…	…	…	…	…
43	A4B2C1	3.58	21.08	12.06	15.50	11.91	4.77
44	A4B2C2	5.56	33.29	13.46	17.42	11.91	4.78
45	A4B2C3	13.13	79.92	16.64	21.76	11.91	4.78
46	A4B2C4	22.59	138.21	17.25	22.59	11.92	4.78
47	A4B2C5	…	…	…	…	…	…
48	A4B2C6	…	…	…	…	…	…

For Methanol yield at P=40 bar, T=210°C

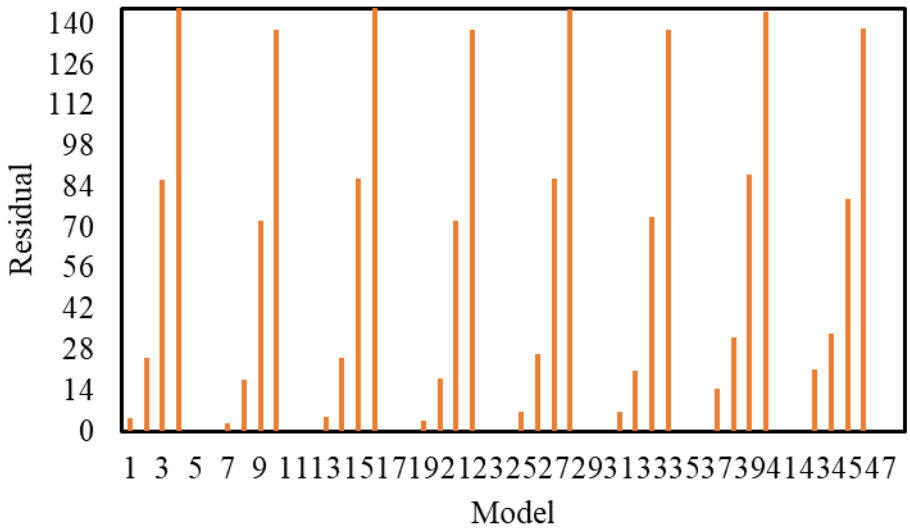

For Methanol yield at P=40 bar, T=230°C

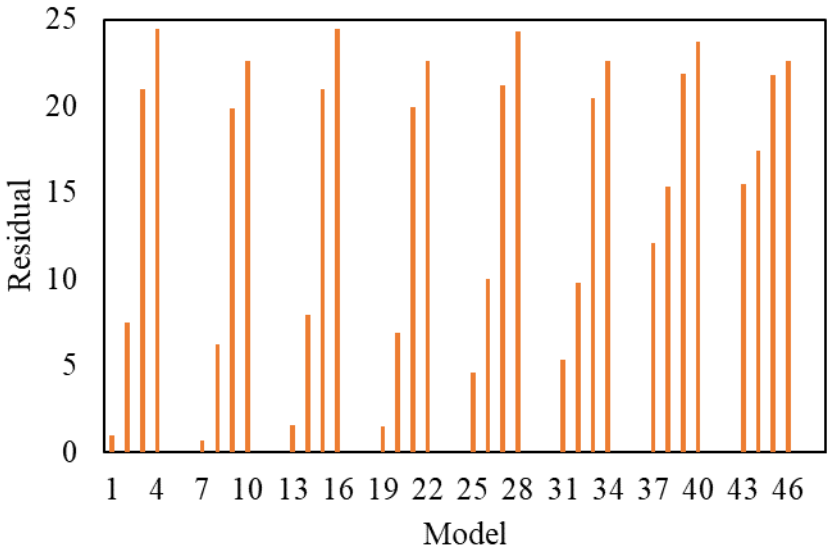

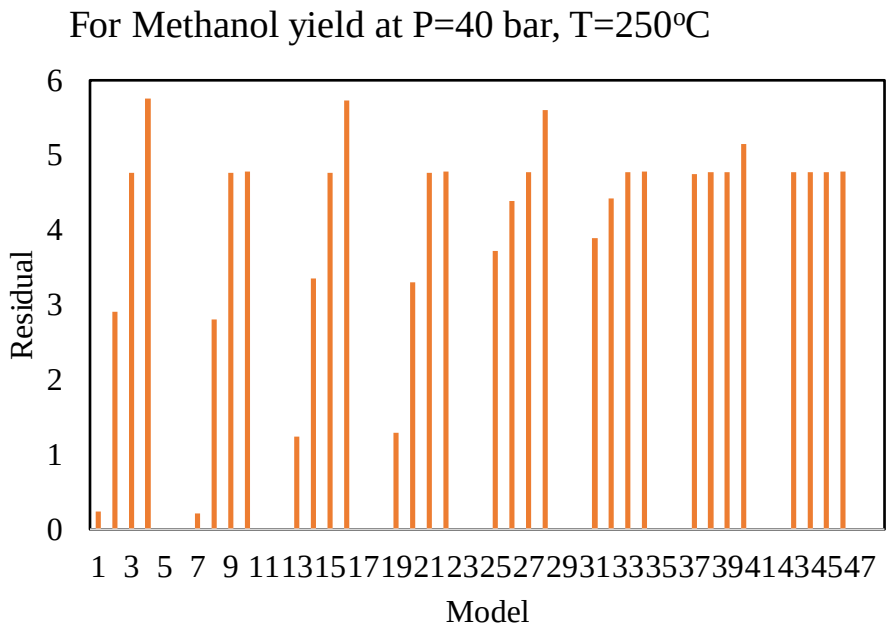

Table A3 Error analysis (**Case-II:** CO_2 – 30 ml/min & H_2 – 90 ml/min)

Model No.	Kinetic Model	MeOH Yield (%) at P = 40 bar and catalyst weight = 3 g					
		T= 210°C	Y_{MeOH} (Residual)	T= 230°C	Y_{MeOH} (Residual)	T= 250°C	Y_{MeOH} (Residual)
1	A1B1C1	0.90	0.94	1.42	-0.10	2.55	-0.60
2	A1B1C2	4.22	8.11	6.20	2.94	8.06	0.25
3	A1B1C3	14.25	29.76	16.04	9.18	11.89	0.85
4	A1B1C4	23.82	50.44	18.60	10.81	13.93	1.17
5	A1B1C5	…	…	…	…	…	…
6	A1B1C6	…	…	…	…	…	…
7	A1B2C1	0.61	0.32	1.22	-0.22	2.50	-0.61
8	A1B2C2	3.01	5.50	5.31	2.37	7.85	0.22
9	A1B2C3	11.90	24.71	15.23	8.67	11.89	0.85

10	A1B2C4	22.59	47.79	17.24	9.95	11.92	0.85
11	A1B2C5	…	…	…	…	…	…
12	A1B2C6	…	…	…	…	…	…
13	A2B1C1	0.95	1.06	1.89	0.20	4.61	-0.28
14	A2B1C2	4.26	8.19	6.54	3.15	8.97	0.40
15	A2B1C3.	14.22	29.71	16.08	9.21	11.89	0.85
16	A2B1C4	23.81	50.42	18.58	10.80	13.88	1.16
17	A2B1C5	…	…	…	…	…	…
18	A2B1C6	…	…	…	…	…	…
19	A2B2C1	0.71	0.54	1.83	0.16	4.72	-0.27
20	A2B2C2	3.10	5.69	5.77	2.66	8.87	0.38
21	A2B2C3	11.95	24.80	15.31	8.72	11.89	0.85
22	A2B2C4	22.60	47.80	17.24	9.95	11.92	0.85
23	A2B2C5	…	…	…	…	…	…
24	A2B2C6	…	…	…	…	…	…
25	A3B1C1	1.25	1.69	4.07	1.58	9.74	0.51
26	A3B1C2	4.46	8.64	8.06	4.12	11.11	0.73
27	A3B1C3	14.27	29.81	16.25	9.32	11.91	0.85
28	A3B1C4	23.70	50.18	18.47	10.73	13.61	1.12
29	A3B1C5	…	…	…	…	…	…
30	A3B1C6	…	…	…	…	…	…

31	A3B2C1	1.23	1.65	4.63	1.94	10.09	0.57
32	A3B2C2	3.53	6.63	7.87	4.00	11.19	0.74
33	A3B2C3	12.13	25.19	15.67	8.95	11.91	0.85
34	A3B2C4	22.61	47.82	17.24	9.95	11.92	0.85
35	A3B2C5	…	…	…	…	…	…
36	A3B2C6	…	…	…	…	…	…
37	A4B1C1	2.49	4.39	9.59	5.09	11.86	0.84
38	A4B1C2	5.38	10.62	11.96	6.59	11.89	0.85
39	A4B1C3	14.50	30.30	16.69	9.59	11.91	0.85
40	A4B1C4	23.56	49.87	18.03	10.45	12.68	0.97
41	A4B1C5	…	…	…	…	…	…
42	A4B1C6	…	…	…	…	…	…
43	A4B2C1	3.58	6.74	12.06	6.66	11.91	0.85
44	A4B2C2	5.56	11.01	13.46	7.55	11.91	0.85
45	A4B2C3	13.13	27.36	16.64	9.56	11.91	0.85
46	A4B2C4	22.67	47.95	17.31	9.99	11.97	0.86
47	A4B2C5	…	…	…	…	…	…
48	A4B2C6	…	…	…	…	…	…

For Methanol yield at P=40 bar, T=210^{o}C

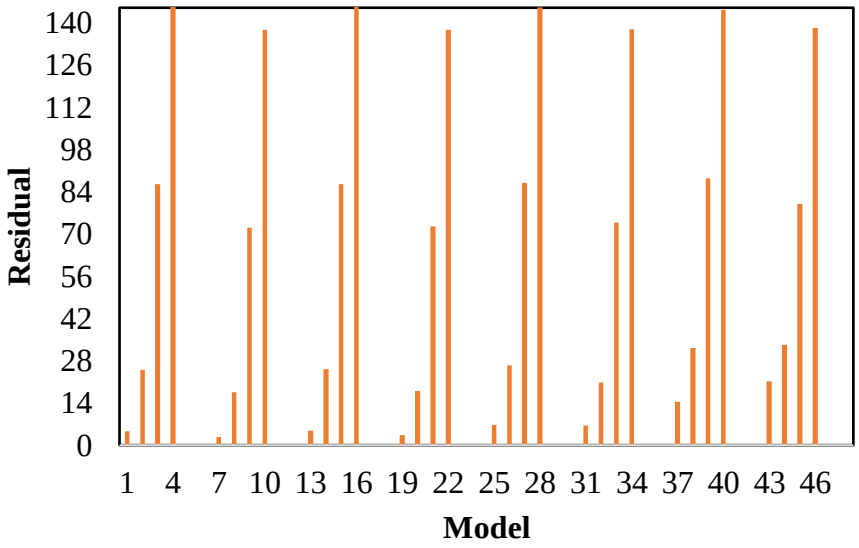

For Methanol yield at P=40 bar, T=230^{o}C

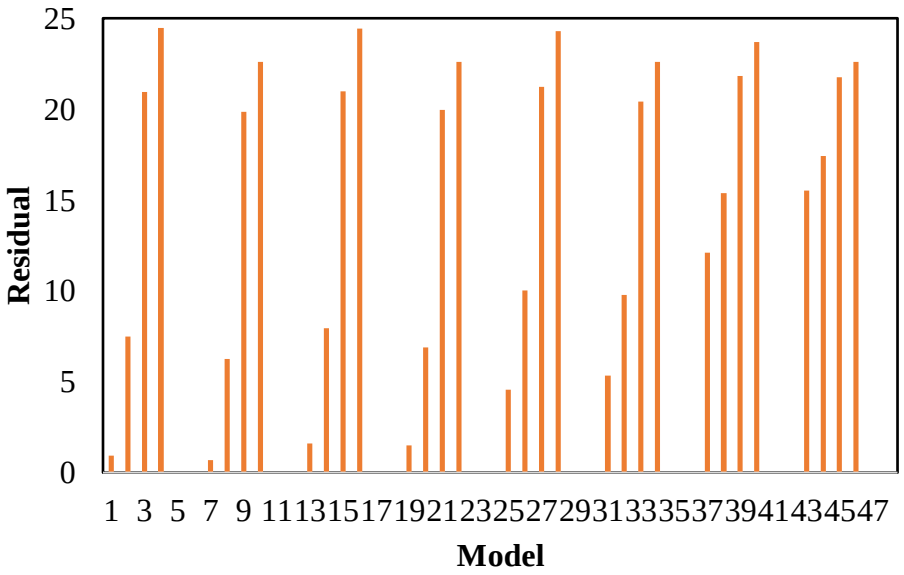

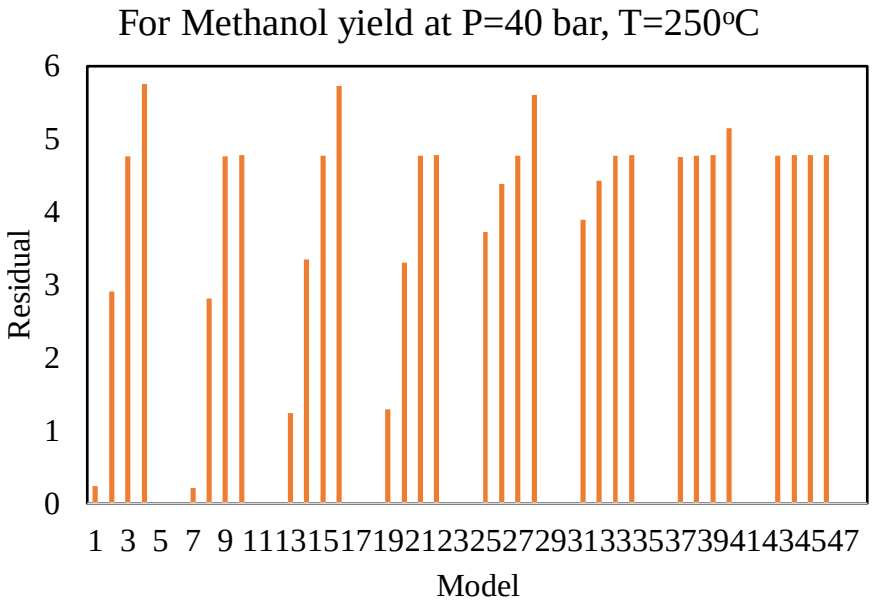

Model no. 7 i.e. A1B2C1 shows a good fit with experimental results. The residual obtained is very less for this model 7 in comparison with other models. We select the A1B2C1 model for further study.

ABSTRACT

Name of Student: Bagwan Farahanaz Mahammad Rafiq **Registration No** 20EE20A26017

Faculty of Study: Engineering Sciences **Year of Submission:** 2025

AcSIR academic centre/CSIR Lab: CSIR-NCL

Name of the Supervisor: Dr. Satyam Naidu Vasireddy

Title of the thesis: Experimental and modeling studies of catalytic hydrogenation for conversion of carbon dioxide and hydrogen storage

Direct conversion of CO_2 via hydrogenation to value added chemicals is a vital approach for utilizing CO_2 emitted into the atmosphere. Catalytic hydrogenation for conversion of CO_2 to methanol is known to be viable process to reduce CO_2 emissions. In this context, the first part of the study focuses on a critical analysis of reaction kinetic modeling in a fixed bed reactor to optimize methanol yield under different H_2 to CO_2 molar ratios, comparing adiabatic and isothermal conditions. Simulations indicate that the isothermal reactor configuration yields 2.76% more methanol compared to the adiabatic reactor. Methanol yield increases significantly from 19.03% to 36.41% as the H_2/CO_2 molar ratio rises from 3 to 9. Experimental validation using a copper-based catalyst at various temperatures and pressures corroborates the simulation results, with a maximum methanol yield of 2.53% achieved at an H_2/CO_2 ratio of 9, 250°C, and 50 bar. The second part of the study investigates the catalytic hydrogenation of quinoline to DHQ using 5% Pd/Al_2O_3 as a catalyst. Key parameters such as temperature, hydrogen pressure, reaction time, solvent type, reactant-to-solvent ratio, and catalyst loading are examined in an autoclave reactor. The optimal conditions identified include a reaction temperature of 175°C, 50 bar H_2 pressure, and a reactant-to-solvent ratio of 1:9 using isopropyl alcohol (IPA) as the solvent. Under these conditions, a hydrogen uptake of 6.89 wt.% and a DHQ yield exceeding 99% is achieved. A reaction kinetic model is developed and validated through Markov Chain Monte Carlo simulations, revealing that the hydrogenation of quinoline to pz-THQ is the rate-limiting step in DHQ formation, with an estimated activation energy of 136.57 kJ/mol. The dehydrogenation of DHQ to quinoline to identify the hydrogen release capacity of DHQ using the same catalyst is studied. The maximum DoD of 82.67 % is observed at 240°C for reaction time of 9 h. The conversion of DHQ increases with an increase in reaction time at elevated temperatures. The DHQ conversion of 83.88% is obtained at 240°C for reaction time of 9 h. The activation energy for the dehydrogenation of DHQ to quinoline was determined to be 185.43 kJ/mol, with the conversion of benzo-tetrahydroquinoline (bz-THQ) to quinoline identified as the rate-limiting step. These findings not only enhance the understanding of DHQ dehydrogenation but also offer valuable guidance for optimizing reaction parameters to improve hydrogen generation efficiency. This study provides valuable insights into the efficient conversion of CO_2 to value-added chemicals and hydrogen storage using quinoline molecule.

Keywords: CO_2 conversion, kinetic modeling, Methanol, Hydrogenation, Quinoline, Dehydrogenation, Decahydroquinoline(DHQ)

List of Publications Emanating from the Thesis Work

1. Farahanaz M Bagwan, Amol A Kulkarni, Satyam Naidu Vasireddy. Experimental and Kinetic modelling studies for the design of the fixed bed methanol reactor over CuZA catalyst. Journal of Chemical engineering research and design 205 (2024) 79-90.
2. Farahanaz M Bagwan, Anil Kinage, Satyam Naidu Vasireddy. Reaction kinetics for catalytic hydrogenation of quinoline to decahydroquinoline as liquid hydrogen carrier. International Journal of Hydrogen Energy 92 (2024) 102-112.

List of Oral/Poster Presented with Details

1. Paper presentation on "Modeling studies of hydrogenation of carbon dioxide to methanol" , in the **International Conference on Net-zero Emission Technologies for Sustainable Development: Challenges and Opportunities during 12th -13th December, 2022 at IIT Dhanbad, India.**

2. Poster presentation titled "Simulation studies on sensitivity analysis for direct conversion of CO_2 hydrogenation to methanol" in the **national conference on Catalysis for energy, environment and sustainability and 3rd CO_2 India Network Annual meeting, September 18th -20th September, 2024 at IICT Hyderabad, India**.

3. Poster presentation titled "Experimental studies of hydrogenation of carbon dioxide to methanol", in the **International Conference on Carbon Capture and Utilization-24 (ICCCU24) during 9th -13th December, 2024 at JNCASR Bangalore, India.**

Awards

1. Hindustan Platinum Award for Best Poster Presentation for the poster entitled "**Simulation studies on sensitivity analysis for direct conversion of CO2 hydrogenation to methanol**" during national conference on "**Catalysis for Energy, Environment & Sustainability (CEES)-2024"** organized on behalf of Catalysis for Society of India & CO2 India Network held at CSIR-IICT Hyderabad during 18-20 September 2024.
2. **Best Poster Prize** for the poster entitled **"Experimental studies of hydrogenation of carbon dioxide to methanol"** at the International Conference on Carbon Capture and Utilization-24 **(ICCCU24)** held during December 9-13, 2024, at JNCASR Bangalore.

International Conference on
Net-zero Emission Technologies for Sustainable Development: Challenges and Opportunities (N0ET-2022), Dec 12-13, 2022
Organized by
Department of Chemical Engineering
Indian Institute of Technology (ISM) Dhanbad, Dhanbad-826004, India

Modeling studies of hydrogenation of carbon dioxide to methanol

F. M. Bagwan[1] , A. A. Kulkarni[1*], S. N. Vasireddy[1*]
Chemical Engineering and Process Development Division, CSIR-National Chemical Laboratory (CSIR-NCL), Pune, Maharashtra 411008, India; Academy of Scientific and Innovative Research (AcSIR), Ghaziabad 201002, India
*sn.vasireddy@ncl.res.in

ABSTRACT

A rising concentration of CO_2 in the earth's atmosphere has led to concerns about global climate changes. In the last decade, the chemistry of CO_2 has received significant attention due to its potential use as an alternative and economical feedstock. Recent studies showed the CO_2 is being evolved abundantly from power plants, cement industry, steel plants, petroleum, oil & gas, and petrochemicals plants. The hydrogenation of CO_2 to alcohols or other hydrocarbon compounds is an important approach for recycling the CO_2 released to the atmosphere. Due to a continuous increase in the industrial demand for methanol, much effort is now being devoted to the conversion of CO_2 to methanol. As methanol has so many benefits as an alternative energy and in multiple applications, optimizing and enhancing its production by modeling reaction kinetics is of considerable importance. There is huge scope to develop new and effective kinetic models to improve the process which results in high methanol yield. Excessive work is done using carbon monoxide as the feed in the literature**.** In this study, no carbon monoxide only carbon dioxide is contained in the feed which corresponds to the conditions of some recent industrial applications. Also, the reaction kinetic models are simulated with varied reaction parameters in MATLAB to predict the performance of the processes. Kinetics of methanol synthesis from carbon dioxide hydrogenation is studied on a copper zinc oxide catalyst over alumina (CuZA) catalyst. Modeling is done using the kinetic laws and adsorption coefficients determined by Graaf et al. based on a Langmuir − Hinshelwood − Hougen − Watson (LHHW) mechanism. The reactor model was based on an isothermal pseudo-homogeneous plug flow model without mass-transfer limitations. The rate determining step analysis of the 48 possible combinations of Graaf model was done.

Keywords: CO_2 Conversion, Methanol, Kinetic Modeling, GHSV, LHHW mechanism

National conference on

"Catalysis for Energy, Environment & Sustainability (CEES)-2024"

organized on behalf of Catalysis for Society of India & CO_2 India Network held at CSIR-IICT Hyderabad during 18-20 September 2024.

Simulation studies on sensitivity analysis for direct conversion of CO_2 hydrogenation to methanol

Bagwan M. Farahanaz, Amol A. Kulkarni, Satyam Naidu Vasireddy*

Correspondence: Satyam Naidu Vasireddy (sn.vasireddy@ncl.res.in)
CEPD division, CSIR-NCL, Pune – 411 008

ABSTRACT

Conversion of CO_2 is critically important due to its role as a major greenhouse gas contributing to climate change. Conversion of CO_2 into valuable chemicals like methanol not only helps mitigate the environmental impact of CO_2 emissions but also contributes to the development of sustainable chemical processes. This study presents a detailed examination of reaction kinetic modeling for a fixed bed reactor aimed at enhancing methanol production. Simulations were conducted over a temperature range of 180°C to 300°C and pressures of 10, 30, and 50 bar to evaluate reactor performance in terms of CO_2 conversion, CO and methanol selectivity and methanol yield. The optimal conditions at pressure of 50 bar and temperature of 230°C were identified. A comprehensive sensitivity analysis was performed to assess the impact of variations in kinetic constants (k_1, k_2, k_3) within ±10 % range on CO_2 conversion, methanol selectivity, and methanol yield. The analysis revealed that changes in kinetic constants have minimal effect on the reaction outcomes with importance of accurate kinetic parameter estimation for process optimization. This sensitivity analysis offers valuable insights into enhancing the robustness and reliability of reaction models with implications for the design and optimization of industrial processes involving CO_2 conversion and methanol synthesis. The research advances the understanding of how variations in kinetic parameters influence catalytic reactions, providing practical guidance for improving the efficiency and reliability of CO_2 conversion and methanol production processes, thus supporting the broader objective of optimizing catalytic systems for better environmental and economic performance.

Keywords: CO_2 conversion, methanol, sensitivity analysis, simulation studies

International Conference on

Carbon Capture and Utilization-24 (ICCCU24)

December 9-13, 2024, at JNCASR Bangalore.

Experimental studies of direct conversion of carbon dioxide to methanol

Farahanaz M. Bagwan[1], Amol A. Kulkarni[1*], Satyam Naidu Vasireddy[1*]

Chemical Engineering and Process Development Division, CSIR-National Chemical Laboratory (CSIR-NCL), Pune, Maharashtra 411008, India;

Academy of Scientific and Innovative Research (AcSIR), Ghaziabad 201002, India

Correspondence:*sn.vasireddy@ncl.res.in

ABSTRACT

Conversion of CO_2 is critically important due to its role as a major greenhouse gas contributing to climate change. Conversion of CO_2 into valuable chemicals like methanol not only helps mitigate the environmental impact of CO_2 emissions but also contributes to the development of sustainable chemical processes. This work presents a detailed experimental study for a fixed-bed reactor aimed at enhancing methanol production. Kinetic Modeling is done using the Graaf et al.(1988) model based on a Langmuir − Hinshelwood − Hougen − Watson (LHHW) mechanism. Simulations were conducted over a temperature range of 180°C to 300°C and pressures of 10, 30, and 50 bar to evaluate reactor performance. Experiments are performed using commercial copper-based catalysts in the fixed bed reactor under optimal conditions of 250°C and 50 bar. The A1B2C1 kinetic model showed a good fit with experimental results. The maximum methanol yield of 2.53% and the space-time yield of 13.59 mg/gcat.h. The experiments at higher H_2 to CO_2 molar ratios demonstrated that increase in yield and space-time yield towards methanol production and further optimized that an H_2 to CO_2 molar ratio of 9 favors higher methanol yield. In addition to the surface reaction, internal and external mass transfer influences the overall reaction, hence, mass transfer limitations are studied. The estimations for mass transfer limitations found that for all the reaction conditions Weisz Prater parameter (C_{WP}) is significantly less than 1 and Mear's Parameter(MP) is less than 0.15 indicating that no internal diffusional limitations and no external mass transfer limitations influence the rate of reaction.

Keywords: CO_2 Conversion, Methanol, Kinetic Modeling, LHHW mechanism

Chemical Engineering Research and Design 205 (2024) 79–90

Contents lists available at ScienceDirect

Chemical Engineering Research and Design

journal homepage: www.elsevier.com/locate/cherd

Experimental and kinetic modelling studies for the design of fixed bed methanol reactor over CuZA catalyst

Farahanaz M. Bagwan [a,c], Pavan Dongapure [b,c], Amol A. Kulkarni [a,c], Satyam Naidu Vasireddy [a,c,*]

[a] Chem. Eng. and Proc. Dev. Div., CSIR-National Chemical Laboratory, Pune 411 008, India
[b] Cat. and Inorg. Chem. Div., CSIR, National Chemical Laboratory, Pune 411 008, India
[c] Academy of Scientific and Innovative Research (AcSIR), Ghaziabad 201 002, India

ARTICLE INFO

Keywords:
CO_2 conversion
Methanol
Kinetic modelling
CuZA catalyst
H_2 to CO_2 molar ratio

ABSTRACT

Direct conversion of CO_2 via hydrogenation to value-added chemicals is a vital approach for utilising CO_2 emitted into the atmosphere. In this paper, a critical analysis of reaction kinetic modelling studies is explored in a fixed bed reactor to improve methanol yield for different H_2 to CO_2 ratios by simulating a lab-scale reactor for adiabatic and isothermal conditions. The feed inlet temperature and pressure variations are applied to study the effect of both configurations on methanol production. The results show that the isothermal configuration yields 2.76% more methanol yield compared to the adiabatic reactor. The effect of H_2 to CO_2 molar ratios of 3, 6 and 9 on the performance of the catalyst and the influence of CO and CO_2 hydrogenation is investigated with model simulations. The overall methanol yield is increased from 19.03% to 36.41% with increase in H_2 to CO_2 molar ratio from 3 to 9. Experiments are performed using commercial copper-based catalyst for different temperatures of 210, 230 and 250 °C at a pressure of 40 bar for H_2/CO_2 of 3 and GHSV of 720 h^{-1} as well as at optimal temperature of 250 °C and 50 bar with varying H_2/CO_2 of 3, 6, 9 for 3 g and 6 g catalyst. The maximum methanol yield of 2.53% and space time yield of 13.59 $mg/g_{cat}.h$ is obtained at H_2/CO_2 ratio of 9.

1. Introduction

The world's primary source of energy non-renewable fossil fuels allowed remarkable prosperity to advance human development. The increase in energy demand to sustain industrialization and growth has led to the depletion of these finite resources. As the sources are consumed drastically, these are not renewed on the human time scale (Olah et al., 2009). However, the irreversible consumption of resources results in the accumulation of carbon dioxide in the environment which causes climate change (Gaikwad et al., 2016). Recent studies showed that CO_2 is being released abundantly from power plants, cement industries, steel plants, petroleum, oil & gas, and petrochemical plants. Currently, the CO_2 concentration in the atmosphere has reached a level of 424 ppm which represents 51% more than pre-industrial levels. The growth of CO_2 emissions in the atmosphere was 5.2 ± 0.02 GtC yr^{-1} during the decade 2012–2021 (48% of total CO_2 emissions) (Global carbon budget 2022). As GHGs lead to a great deal of problems such as global warming, the increasing concentration of GHG emissions in the atmosphere is an urgent problem that must be addressed by humanity (Hafeez et al., 2022; Olah et al., 2009). The IPCC predicted that CO_2 emissions would increase to 570 ppm by the year 2100 (Younas et al., 2016) and this is a massive and challenging task when it comes to tackling climate change (Wang et al., 2011). Thus, the recycling of CO_2 as a feedstock to produce hydrocarbons presents great economic and environmental interests (Torcida et al., 2022; Van-Dal and Bouallou, 2013). Utilization of CO_2 leads to a new carbon neutral pathway for the synthesis of precious fuels and chemicals (Atsbha et al., 2021; Van-Dal and Bouallou, 2013). Methanol is a building block material for the commercial production of various value-added chemicals, like formaldehyde (Gribovskii et al., 2017; Kropp et al., 2017), olefins (Losch et al., 2017), and biodiesel (Boffito et al., 2015; Pirola et al., 2014). Methanol is widely used as a solvent in the pharmaceutical industry and plastics sector (Machado et al., 2014). Moreover, methanol is also the source of many intermediates that are used to manufacture a broad range of products for our daily use: paints, resins, silicones, adhesives, and so on. In addition to gasoline as fuel, methanol can also be used as blended fuel

* Corresponding author at: Chem. Eng. and Proc. Dev. Div., CSIR-National Chemical Laboratory, Pune 411 008, India.
E-mail address: sn.vasireddy@ncl.res.in (S.N. Vasireddy).

https://doi.org/10.1016/j.cherd.2024.03.032
Received 15 December 2023; Received in revised form 21 March 2024; Accepted 21 March 2024
Available online 24 March 2024

in the transportation sector as per government regulations (Bozzano and Manenti, 2016). The work aims to valorise CO_2 while reducing emissions and to meet the demand for chemicals that have applications in various chemical industries. In particular, CO_2 hydrogenation presents the most elevated possibility for industrial application with a technology readiness level (TRL) of 9 with a noteworthy capability for net CO_2 utilization (Cordero-Lanzac et al., 2023). According to the Le Chatelier's principle, high pressure and low temperature favours methanol formation due to exothermic nature of the reactions. The challenge lies in the synthesis of active catalyst with sufficiently low activation energy for CO_2 hydrogenation as the CO_2 molecule is highly stable in nature. In this study, we aim to investigate temperature and pressure conditions to either shift the reaction equilibrium towards a desirable product and/or to have proper temperature control, most importantly to increase methanol yield per unit catalyst weight. Developing a highly effective catalyst that can be operated at lower temperatures is one of the ways to overcome this equilibrium limitation to reduce the energy barrier for the breaking one C–O bond from a CO_2 molecule and thus improves the reaction kinetics (Arab et al., 2014; Sharma et al., 2021a, 2021b). Cu-based catalyst has been widely investigated as a highly active and naturally available element in the earth's crust which makes it sustainable and economical. This catalyst is considered a model catalyst for the conversion of CO_2 to methanol production (Álvarez et al., 2017; De Oliveira Campos et al., 2021; Hafeez et al., 2022; Mbatha et al., 2021; Sharma et al., 2021a,b). Apart from catalyst studies, kinetic modelling is largely used in techno-economic assessment (TEA) studies (Al-Rowaili et al., 2022; Nyári et al., 2022). A wide range of kinetic models with appropriate assumptions regarding the reaction mechanisms and their parameters have been suggested by researchers over the last few decades (Eksiri et al., 2020; Villa et al., (1985); Takagawa and Ohsugi, 1987).

The rate expressions are developed based on a dual-site LHHW mechanism (Bisotti et al., 2021; Stamhuis, Graaf, Sijtsema et al. 1986; McNeil et al., 1989; Park et al., 2014; Portha et al., 2017; Skrzypek et al., 1991; Vanden Bussche and Froment, 1996). Although various kinetic models have developed, the CO_2 hydrogenation to methanol reaction mechanism is relatively unclear. This is due to the major thermodynamic limitations on conversion due to competing reverse water–gas shift (RWGS) reactions (Stangeland et al., 2020). Industrially, it depends on various performance parameters such as efficiency, safety and CO_2 mitigation, etc. to adopt technology and there is a wide variety of opportunities for understanding how methanol synthesis technologies are developed by studying the reaction mechanism and its associated kinetics.

To study mechanistic approaches for the conversion of CO_2 to useful products, it is necessary to develop a kinetic equation that describes the effect of parameters and to predict the temperature distribution quantitatively in industrial reactors (Nestler et al., 2021). Methanol production through the conversion of carbon dioxide route is obtained via a catalytic process using three reversible reactions: (a) carbon monoxide hydrogenation (reaction 1), (b) reverse water-gas shift (RWGS) reaction (reaction 2) and (c) carbon dioxide hydrogenation (reaction 3).

$$CO + 2H_2 \leftrightarrows CH_3OH\ \Delta H_r^\circ(298\ K) = -\ 90.50\ kJ/mol \quad (1)$$

$$CO_2 + H_2 \leftrightarrows CO + H_2O\ \Delta H_r^\circ(298\ K) = +\ 41.10\ kJ/mol \quad (2)$$

$$CO_2 + 3H_2 \leftrightarrows CH_3OH + H_2O\ \Delta H_r^\circ(298\ K) = -\ 49.40\ kJ/mol \quad (3)$$

Low temperature and higher pressure are considered to be the most suitable thermodynamic conditions for the synthesis of methanol according to the Le Chatelier principle (Ghosh et al., 2021; Ng et al., 2022). These conditions allow rate of CO formation in high quantities due to RWGS reaction and utilization of exothermic heat from CO and CO_2 hydrogenation. Therefore, it is needed to have a trade-off temperature to maximize the CO_2 conversion to methanol (Fogler, 1987).

In this study, detailed modelling studies are performed using reported models for high molar H_2 to CO_2 ratios to improve the performance characteristics for conversion of CO_2 to methanol over CuZA catalyst to have proper temperature control, most importantly to increase methanol yield per unit catalyst weight.

2. Material and methods

2.1. Catalyst

A commercial copper-based catalyst ($Cu/ZnO/Al_2O_3$ denoted as CuZA) is used for the present experimental and modelling studies. The catalyst is procured from Alfa Aesar/ThermoFischer Scientific in the form of pellets with the composition of CuO – 60–68%, ZnO – 22–26%, Al_2O_3 – 8–12% and MgO – 1–3%. The catalyst is crushed, grounded and further sieved to particles of 400-micron size to make sure that diffusional effects are minimal between gas and particles during the reaction.

2.2. Catalyst characterization

2.2.1. BET analysis

The surface area analysis is performed using the Braunner-Emmet-Teller (BET) method using the Quantachrome BET apparatus. The pore volume, average pore radius, and specific surface area measurements of calcined catalysts are performed using nitrogen adsorption-desorption at −76 °C. The method of BET surface area analysis involves as follows: all the samples are outgassed at 250 °C under vacuum for 3 h to remove adsorbed moisture.

The adsorption-desorption curve shows characteristics of type IV isotherm with a prominent hysteresis loop in the relative pressure (P/P°) range of 0.20–1 which denotes the presence of the mesoporous structure as shown in Fig. 1a. The presence of hysteresis is due to the capillary phenomenon and the gases condense in the tiny capillary pores of the solid below the saturation pressure of gas. The pore size distribution gives an idea of the presence of mesoporous particles in the catalyst as shown in Fig. 1b. The specific surface area of 123.13 m^2/g and a total pore volume of 0.27 cc/g is obtained from BET surface area analysis.

2.2.2. X-ray powder diffraction (XRD)

The XRD analysis is performed for the CuZA catalyst to measure the crystalline and phase behaviour of the catalyst. The crystalline nature and phase formation of the sample are analysed using Powder X-ray diffraction (PXRD) for the data taken from a PAN analytical X'pert Pro dual goniometer. It is equipped with an X-ray diffractometer using Cu Kα (1.5418 A°) radiation within a scanning angle of 2θ from 10 to 80° and a step length of 2° every minute. The active phase formation of copper oxide, zinc oxide, aluminium oxide and malachite phase formation is observed as shown in Fig. 2. The malachite phase is favourable for methanol formation as reported in the literature (Álvarez et al., 2017; Baltes et al., 2008).

3. Reactor model

3.1. Modelling of reactions

Various kinetic models are reported to describe methanol synthesis using copper-based catalysts. The modelling studies involve different reaction conditions, i.e., temperature, pressure, feedstock composition and catalysts. Different kinetic rate expressions are deduced depending on the rate-determining step. Generally, the LHHW kinetic model is constituted by the kinetic factor (mostly rate constant), driving force expression (depending on the reactants available in the reaction medium) and adsorption term. The rate of reaction is expressed as follows:

$$\text{Rate of reaction} = \left[\frac{\text{Kinetic factor} * \text{driving force}}{\text{Adsorption term}}\right]$$

The following three reactions are the basis for kinetic rate expressions:

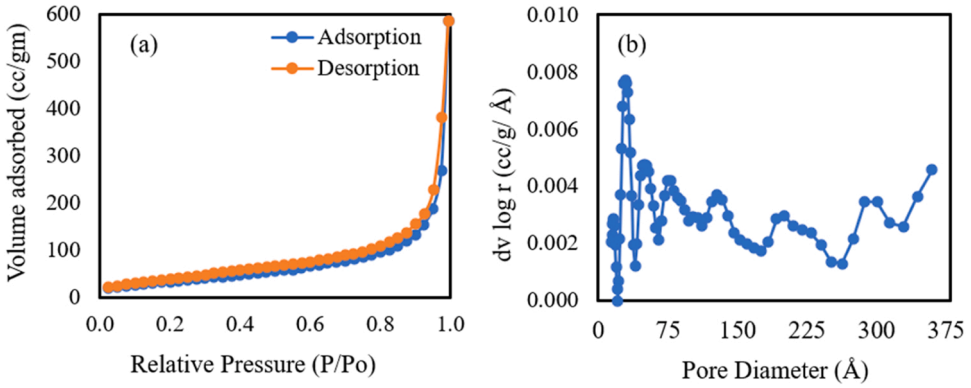

Fig. 1. (a) BET adsorption-desorption isotherm (b) pore size distribution.

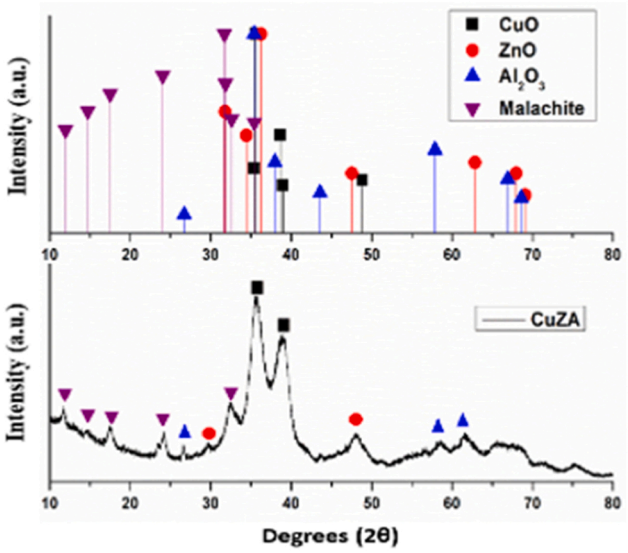

Fig. 2. XRD analysis of CuZA catalyst.

$$CO + 2H_2 \rightleftharpoons CH_3OH \quad (A)$$

$$CO_2 + H_2 \rightleftharpoons CO + H_2O \quad (B)$$

$$CO_2 + 3H_2 \rightleftharpoons CH_3OH + H_2O \quad (C)$$

The elementary reactions for the above three reactions are represented for each species on the catalyst site is as follows:

Reaction (A)

$$COs1 + Hs2 \rightleftharpoons HCOs1 + s2 \quad (A1)$$

$$HCOs1 + Hs2 \rightleftharpoons H_2COs1 + s2 \quad (A2)$$

$$H_2COs1 + Hs2 \rightleftharpoons H_3COs1 + s2 \quad (A3)$$

$$H_3COs1 + H\ s2 \rightleftharpoons CH_3OH + s1 + s2 \quad (A4)$$

Reaction (B)

$$CO_2s1 + Hs2 \rightleftharpoons HCO_2s1 + s2 \quad (B1)$$

$$H\ CO_2s1 + Hs2 \rightleftharpoons COs1 + H_2Os2 \quad (B2)$$

Reaction (C)

$$CO_2s1 + Hs2 \rightleftharpoons HCO_2s1 + s2 \quad (C1)$$

$$HCO_2s1 + Hs2 \rightleftharpoons H_2CO_2s1 + s2 \quad (C2)$$

$$H_2CO_2s1 + Hs2 \rightleftharpoons H_3CO_2s1 + s2 \quad (C3)$$

$$H_3CO_2s1 + Hs2 \rightleftharpoons H_2COs1 + H_2Os2 \quad (C4)$$

$$H_2COs1 + Hs2 \rightleftharpoons H_3COs1 + s2 \quad (C5)$$

$$H_3COs1 + Hs2 \rightleftharpoons CH_3OH + s1 + s2 \quad (C6)$$

There are 48 combinations of different kinetic rate expressions that can be derived, and these are referred to as kinetic models. This is predicated on the idea that only the surface reaction is the rate-controlling step and all other elementary reactions are in equilibrium. The driving-force groups are the sole variations among the kinetic rate expressions. Table 1 lists these driving-force categories. Here, we have considered all 48 combinations of the kinetic model that could be used for simulation studies. The kinetic parameters, adsorption, and equilibrium constants are taken from Portha et al. (2017).

The rate of reaction for each reaction is based on the dual-site Langmuir–Hinshelwood-Hougen-Watson (LHHW) mechanism with dissociative hydrogen adsorption. The LHHW A3B2C3 model rate expressions for three reactions are expressed as follows (Portha et al., 2017):

$$r_1 = k_1 b_{CO}\left\{\frac{P_{CO}P_{H2}^{1.5} - (P_{CH3OH}/(P_{H2}^{0.5}K_1))}{(1 + b_{CO}P_{CO+}b_{CO2}P_{CO2})(P_{H2}^{0.5} + (b_{H2O}/b_{H2}^{0.5})P_{H2O})}\right\} \quad (4)$$

$$r_2 = k_2 b_{CO2}\left\{\frac{P_{CO2}P_{H2} - (P_{CO}P_{H2O}/K_2)}{(1 + b_{CO}P_{CO+}b_{CO2}P_{CO2})(P_{H2}^{0.5} + (b_{H2O}/b_{H2}^{0.5})P_{H2O})}\right\} \quad (5)$$

$$r_3 = k_3 b_{CO2}\left\{\frac{P_{CO}P_{H2}^{1.5} - (P_{CH3OH}P_{H2O}/(P_{H2}^{1.5}K_3))}{(1 + b_{CO}P_{CO+}b_{CO2}P_{CO2})(P_{H2}^{0.5} + (b_{H2O}/b_{H2}^{0.5})P_{H2O})}\right\} \quad (6)$$

In addition to the following rates, further simulations are performed using driving force terms as given in Table 1 for all the 48 model combinations to verify the best model fit for the experimental data. The residual of experimental and model data is shown for all the models in

Table 1
Driving force terms of rate expressions for reactions.

Rate controlling step	Driving force group
A1	$P_{CO}P_{H2}^{0.5} - (P_{CH3OH}/P_{H2}^{1.5}K_1)$
A2	$P_{CO}P_{H2} - (P_{CH3OH}/P_{H2}K_1)$
A3	$P_{CO}P_{H2}^{1.5} - (P_{CH3OH}/P_{H2}^{0.5}K_1)$
A4	$P_{CO}P_{H2}^{2} - (P_{CH3OH}/K_1)$
B1	$P_{CO2}P_{H2}^{0.5} - P_{CO}P_{H2O}/(P_{H2}^{0.5}K_2)$
B2	$P_{CO2}P_{H2} - P_{CO}P_{H2O}/K_2$
C1	$P_{CO2}P_{H2}^{0.5} - P_{CH3OH}P_{H2O}/(P_{H2}^{2.5}K_3)$
C2	$P_{CO2}P_{H2} - P_{CH3OH}P_{H2O}/(P_{H2}^{2}K_3)$
C3	$P_{CO2}P_{H2}^{1.5} - P_{CH3OH}P_{H2O}/(P_{H2}^{1.5}K_3)$
C4	$P_{CO2}P_{H2}^{2} - P_{CH3OH}P_{H2O}/(P_{H2}K_3)$
C5	$P_{CO2}P_{H2}^{2.5}/P_{H2O} - P_{CH3OH}/(P_{H2}^{0.5}K_3)$
C6	$P_{CO2}P_{H2}^{3}/P_{H2O} - P_{CH3OH}/K_3$

Supplementary information.

3.2. Adiabatic model development

An adiabatic system is described as no substantial loss or gain of heat with the surroundings taking place during the reaction. A detailed mathematical model is developed to assess the effectiveness of the catalyst in one single tubular adiabatic reactor. The following assumptions are considered to simplify the mathematical model.

i) Steady-state conditions
ii) Ideal gas behaviour
iii) Radial heat and mass transfer effects are negligible
iv) No mass transfer limitations

A one-dimensional pseudo-homogeneous model is assumed since the particles in the two phases are so tiny that gradients between them are not taken into account. Steady-state conditions are considered because the time scales of the processes involved are much larger than the time scale of any transient effects. For adiabatic fixed-bed reactors, steady-state conditions are commonly assumed because the system reaches a stable operating condition over time, and the variations in temperature, pressure, and concentration along the reactor bed become negligible compared to the overall operating conditions. In this process, gas molecules behave closely to the predictions of the ideal gas law. This assumption is justified as the compressibility factor Z for the gas mixture at high pressure and temperature is estimated using the Soave–Redlich–Kwong equation of state (SRK) and is found to be near to unity (Arab et al., 2014; Skrzypek et al., 1995). Assuming no mass transfer limitations, the reactor model is simplified to focus solely on the kinetics of the catalytic reaction (Ghosh et al., 2021; Poto et al., 2022).

The steady-state energy balance for the adiabatic catalytic reactor is given by the following equation,

$$\Delta Q - W_s + \sum_{i=1}^{i=3} F_i H_i|_{in} - \sum_{i=1}^{i=3} F_i H_i|_{out} = 0 \tag{7}$$

As there is no shaft work involved in the process, work done (W_s) = 0;

Heat removed or generated due to cooling,

$$\Delta Q = U\ \Delta A\ (T_a - T) = \frac{Ua}{\rho_b}\Delta W(T_a - T) \tag{8}$$

The final expression for differential element in a packed-bed reactor can be represented as,

$$\frac{dT}{dW} = \frac{\frac{Ua}{\rho_b}\Delta W(T_a - T) - \sum_{i=1}^{i=3} r_i \Delta H_{ri}}{\sum_{i=1}^{n} F_i C_{pi}} \tag{9}$$

For adiabatic reactor operation, (T_a-T) = 0,

$$\frac{dT}{dW} = \frac{\sum_{i=1}^{i=3} r_i \Delta H_{ri}}{\sum_{j=1}^{5} F_j C_{pj}} \tag{10}$$

Where,

T is the reactor temperature, K

T_a is ambient temperature, K

W is the weight of the catalyst, g

ΔH_{ri} is the heat of reaction in J/mol of i^{th} reaction, J/(mol.K)

F_j is the molar flow rate of species, j, mol/h.

C_{pj} is the specific heat capacity of species j, J/ (mol. K) (Zhu et al., 2020)

The reactor simulations are performed using MATLAB® by varying inlet temperature in an adiabatic fixed-bed catalytic reactor and the effect of parameters on CO_2 conversion, methanol selectivity, methanol yield and rate of reactions are studied. Inlet conditions along with feed composition and catalyst are specified in Table 2.

3.2.1. Effect of feed temperature

The effect of feed temperature on CO_2 conversion, methanol selectivity and yield are simulated for a reactor pressure of 50 bar. The increase in feed temperature influences CO_2 conversion, methanol selectivity and yield for the reactor as shown in Fig. 3a. At 100°C, the CO_2 conversion is minimal (<1%); at 200°C, it reached a maximum of 24.54%, with a methanol yield of 16.42% at 200 °C and thereafter remained constant with increase in feed temperatures (210 °C, 230 °C, 250 °C and 300 °C). The rate of CO_2 hydrogenation favours the yield of methanol formation over CO hydrogenation as the reverse water gas shift reaction reaches its thermodynamic equilibrium condition to proceed with the reaction. As the CO and CO_2 hydrogenation reactions are highly exothermic in nature, the catalyst bed temperature along the bed length increases for an adiabatic reactor until optimum feed temperature of 210 °C. Therefore, the temperature profile shows an increase in temperature for different inlet feed temperatures along the length of the catalyst bed as shown in Fig. 3b. The optimum feed temperature to operate the adiabatic reactor is between 190 and 210 °C so as to limit the catalyst bed temperature to 250 °C as the increase in reactor temperature may favour reverse water gas shift reaction. The effect of feed temperature showed an increase in conversion from 0.17% at 100 °C to 24.23% at 200 °C. However, selectivity towards methanol decreased with an increase in temperature from 99.80% to 31.18%, hence, the maximum methanol yield of 16.42% is obtained for the feed temperature of 200 °C.

3.2.2. Effect of pressure

The effect of pressure is studied to predict the performance parameters of the adiabatic reactor model in the range from 10 to 50 bar. The performance parameters with respect to the effect of temperature and pressure are represented in Supplementary information for an optimum feed temperature of 200 °C. The CO_2 conversion increased from 9.38% to 24.53% with a decrease in rate from 10 bar to 50 bar. The selectivity towards methanol increased from 40.26% to 66.93%, eventually, the yield of methanol increased from 3.78% to 16.42%. It is observed that high pressure reaction conditions are favourable to achieve an increase in CO_2 conversion, methanol selectivity and yield. The maximum CO_2 conversion of 24.53% and methanol yield of 16.42% are observed at a pressure of 50 bar as shown in Fig. 3c. The rise in reactor outlet temperature with respect to pressure is modelled along the catalyst bed length as shown in Fig. 3d. The maximum temperature of 246 °C is obtained for a pressure of 50 bar and approaches the plateau along the bed length.

Table 2
Comparison of inlet conditions and performance parameters for adiabatic and isothermal reactor models for H_2 to CO_2 ratio = 3 and P = 50 bar.

Parameter	Adiabatic model	Isothermal model
CO_2 inflow (ml/min)	15	15, 30, 45
H_2 inflow (ml/min)	45	45, 90, 135
Total flow rate (ml/min)	60	60, 120, 180
H_2 to CO_2 molar ratio	3	3, 6, 9
CuZA catalyst (g)	3	3
Particle size (μm)	400	400
GHSV (h^{-1})	720	720, 1260, 1800
CO_2 conversion (%)	24.54	25.02
Temperature (°C)	190–300	180–300
Pressure (bar)	10–50	10–50
Performance parameters at 230 °C, 50 bar, WHSV = 720 h^{-1}; H_2/CO_2 = 3		
Methanol selectivity (%)	66.93	76.66
CO selectivity (%)	33.07	23.34
Methanol yield (%)	16.42	19.18
STY_{CH3OH} ($mg/g_{cat}.h$)	64.47	75.30

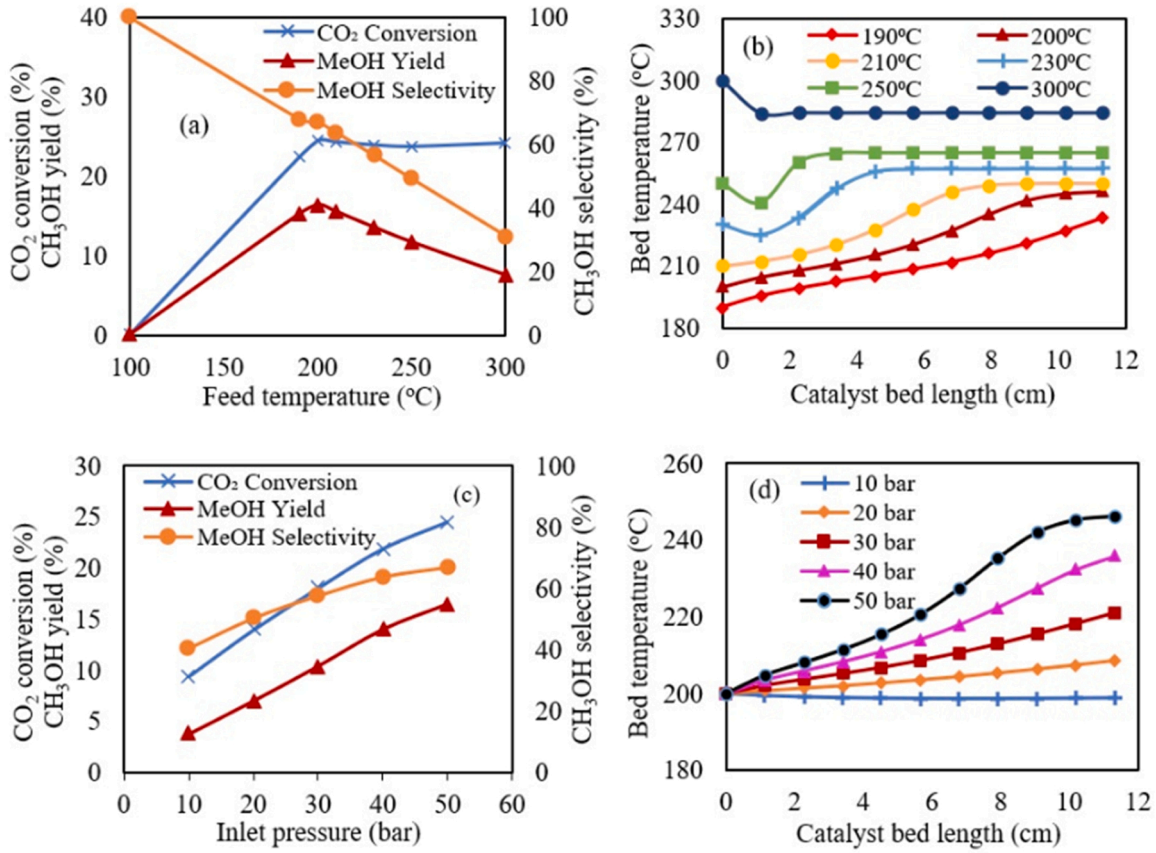

Fig. 3. Effect of feed temperature on the performance of the fixed bed reactor. (a) variation in the CO_2 conversion, MeOH selectivity and yield with feed temperature, (b) Temperature profile inside the fixed bed reactor for different feed temperatures at 50 bar pressure; (c) Effect of pressure on CO_2 conversion, MeOH selectivity and yield and (d) Effect of pressure on the resulting bed temperature at H_2:CO_2 = 3, GHSV = 720 h^{-1} and P = 10–50 bar.

3.3. Isothermal model

One-dimensional pseudo-homogenous model for an isothermal fixed-bed reactor is developed with mass balance, momentum balance and Ergun equation to predict concentration and pressure profiles. The models are simulated using MATLAB considering three chemical reactions that involve the LHHW kinetic model. The model is represented with a pseudo-homogeneous plug-flow model with the following assumptions:

i. Steady-state regime
ii. No axial dispersion
iii. No mass transfer limitations

This leads to one-dimensional model based on mole balance for multi-component species involving parallel reactions,

$$F_{jo} - F_j + (V_{ij} * r_i) * \Delta W = 0 \quad (11)$$

For a differential element in a packed bed reactor,

$$\frac{dF_j}{dW} = \sum_{i=1,j=1}^{i=3,j=5} V_{ij} r_i \quad (12)$$

Where,
Fj = molar flow rate of species
W = weight of the catalyst
V_{ij} = stoichiometric coefficient of species j in reaction i
r_i = rate of reaction for the species i

As a fluid passes through a packed bed of catalyst, it experiences pressure loss in the reactor. Specifically, when the size of catalyst particles is small, the pressure drop in the catalyst bed has to be considered. In this work, we have assumed that catalyst particles are of uniform size. The reactor simulations are performed using MATLAB® by varying inlet temperature in an adiabatic fixed bed catalytic reactor and the effect of parameters on CO_2 conversion, methanol selectivity, methanol yield and the rate of reactions are studied. Inlet conditions along with feed composition and catalyst are specified in Table 2.

3.3.1. Effect of temperature and pressure

The isothermal model simulations are performed in the temperature range from 180 to 300 °C for different pressures of 10, 30 and 50 bar. It is observed that CO_2 conversion increases with increase in temperature until optimum and then attains a plateau to attain thermodynamic equilibrium as shown in Fig. 4a. The maximum CO_2 conversion is attained in the temperature range from 230 to 250 °C for 50 bar to achieve maximum methanol yield. The CH_3OH and CO selectivity as a function of temperature are shown in Fig. 4b and 4c. The CH_3OH selectivity increases to its maximum and decreases gradually with an increase in temperature. On the contrary, CO selectivity decreases under optimal CO_2 conversion and increases further with increase in temperature. This may be due to favouring reverse water gas shift reaction at high temperatures leading to high CO formation whereas CO_2 and CO hydrogenation favours in the temperature range from 200 to 230 °C. The yield of methanol is calculated based on CO_2 conversion and methanol selectivity. Hence, the optimal conditions for methanol yield chosen to be 230–250 °C as shown in Fig. 4d. These conditions form the basis for operation of the reactor isothermally. The outlet product flow rates are obtained for optimal conditions at a pressure of 50 bar, H_2 to CO_2 ratio of 3 and GHSV of 720 h^{-1} as shown in Fig. 5a. The product composition comprises CO, CO_2, CH_3OH and water formation. As evident from Fig. 3, the optimal methanol formation is between 230 and

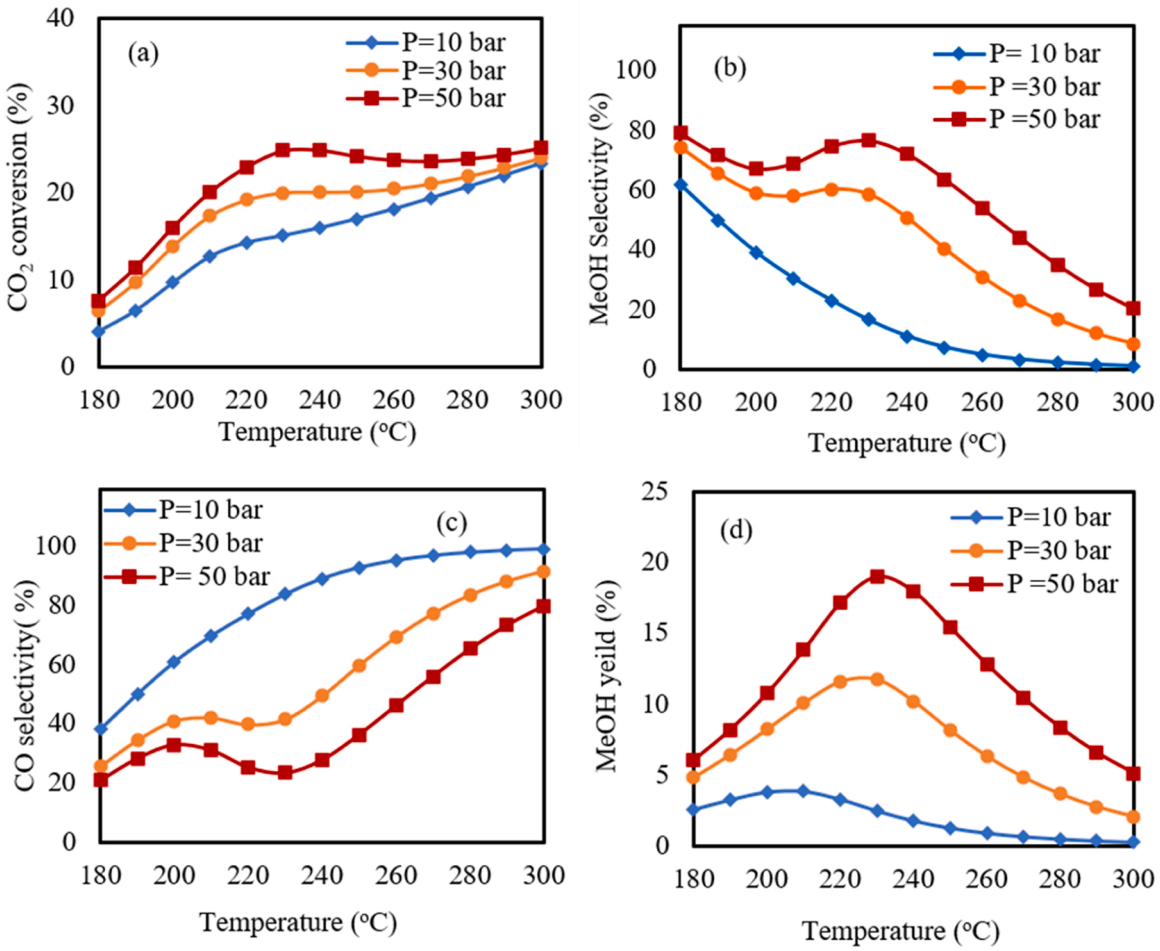

Fig. 4. Effect of temperature and pressure on (a) CO_2 conversion (b) Methanol selectivity (c) CO selectivity (d) Methanol yield for H_2 to CO_2 = 3; GHSV = 720 h^{-1}

250 °C due to CO and CO_2 hydrogenation at this temperature and a further increase in temperature favours reverse water gas shift reaction for CO and water formation. The individual reaction rates are simulated for a better understanding of in-situ reaction rates that contribute to methanol, CO and water formation. As shown in Fig. 5b, the reaction rate for reverse water gas shift reaction is much faster in comparison to CO and CO_2 hydrogenation. Therefore, the increase in CO contribution to methanol formation is further illustrated for different H_2 to CO_2 ratios to study with respect to relative reaction rates. It is clear that methanol formation increased with an increase in the H_2 to CO_2 ratio as reported in the literature (Godini et al., 2020). Hence, the simulations are carried out to demonstrate the relative rates for three reactions with increased H_2 to CO_2 ratios.

3.3.2. *Effect of H_2 to CO_2 molar ratio*

The variation in H_2 to CO_2 molar ratio has significant effect on the rate of reactions as reported in the literature (Godini et al., 2020). The effect of H_2 to CO_2 molar ratios of 3, 6 and 9 are simulated in the pressure range of 10–50 bar at an optimal temperature of 230 °C for different GHSV of 720–1800 h^{-1}.

As shown in Fig. 6, CO_2 conversion, methanol selectivity, yield and space-time yield have a direct influence on the increase in H_2 to CO_2 ratio. The effect of pressure also has a direct influence on the performance parameters of the reactor model under similar conditions. Therefore, the present simulations are performed from 10–50 bar pressure and the maximum CO_2 conversion of 44.02%, selectivity of 81.18%, the yield of 35.74% and the space-time yield of 140.28 mg/g_{cat}.h is obtained at 1800 h^{-1} for H_2 to CO_2 ratio of 9. Although CO_2 conversion, methanol yield and space-time methanol yield are increased by a significant margin, the selectivity of methanol reaches thermodynamic equilibrium beyond the H_2 to CO_2 ratio of 6 as shown in Fig. 6. Therefore, it is recommended to operate the reactor at high flow rates of H_2 to CO_2 ratio beyond stoichiometric quantities to improve the reactor performance. The model predictions compared very well with the experimental data for the H_2 to CO_2 ratio of 3, 6 and 9 for 10 bar pressure reported by Godini et al. (2020). Therefore, the simulations are extended up to 50 bar under optimal conditions and the performance parameters are compared for different ratios. The rate of enhancement in the performance parameters drastically improved for H_2 to CO_2 ratio of 3–9 from 19.03% to 36.41%. Further simulations are analysed for different reaction rates to identify the dominant reaction that contributes to methanol production. The detailed simulation results are plotted for one-to-one comparison as given in Supplementary information.

3.4. *Comparison of adiabatic and isothermal reaction conditions*

The comparative performance analysis for methanol production in adiabatic and isothermal reactors with respect to feed temperature is shown in Fig. 7a & b. It clearly indicates that as the feed temperature increases beyond 200 °C, the methanol production decreases and the reaction rate drops at a shorter reactor length in the adiabatic reactor. Since the adiabatic reactor does not remove any heat generated during the reaction, a higher feed temperature raises the temperature throughout the reactor, moving the equilibrium to the left and hastening the rate at which the generation of methanol declines. In the isothermal reactor, as shown in Fig. 7b, the effect of the temperature rise is quite the

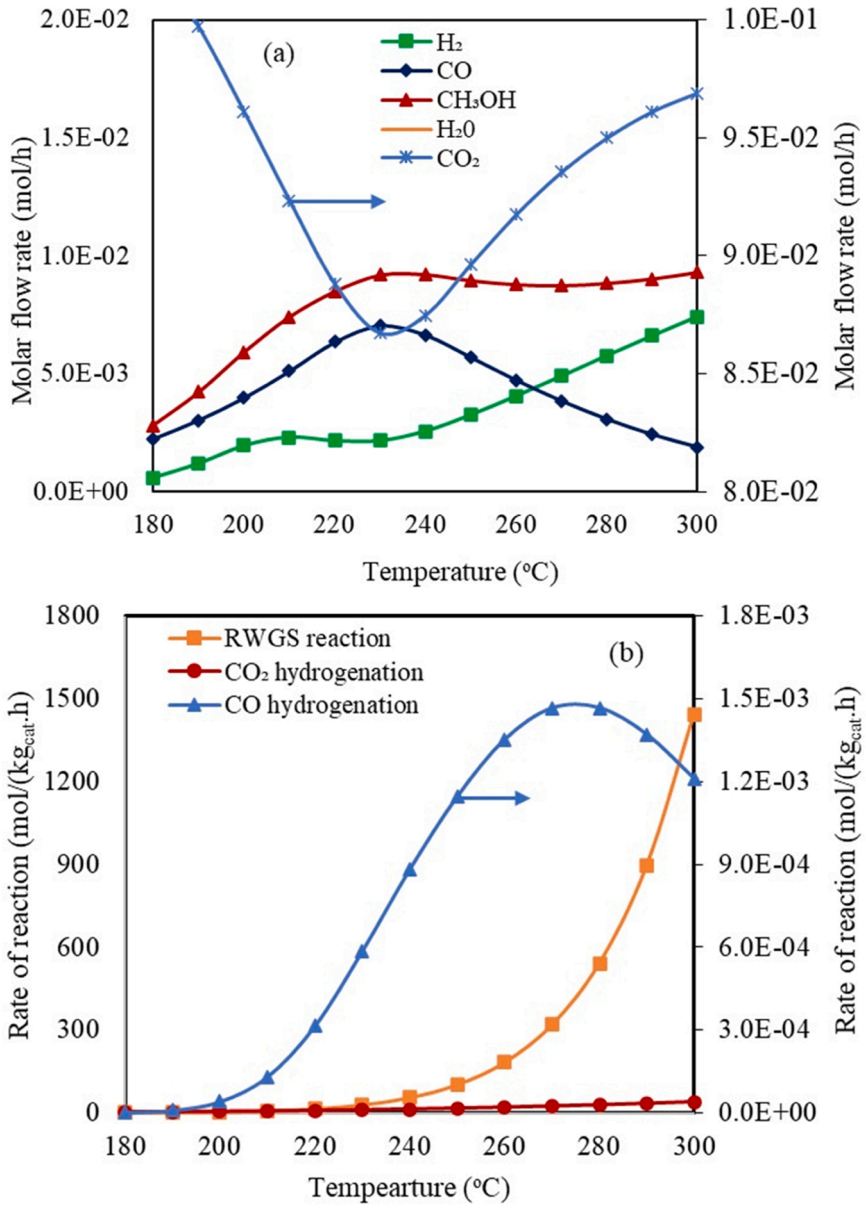

Fig. 5. Effect of temperature on (a) Outlet molar flow rate (b) Rate of reaction for H_2: $CO_2 = 3$; GHSV = 720 h^{-1} at P = 50 bar (secondary axis is given only for CO hydrogenation reaction rates representation).

opposite: although high temperature shifts the methanol production equilibrium to the left, it is compensated by the increase of methanol production rate. Moreover, the reaction equilibrium can be maintained along the reactor as the cooling system keeps the temperature constant. However, when the feed temperature increases above 230 °C, the higher reaction rate can no longer compensate for the shifted equilibrium, causing the methanol production to drop. The simulations are carried out for both adiabatic and isothermal reactor models to understand the behaviour resulting in methanol formation in each case. The temperature profile is significant factor contributing to the operation of a methanol synthesis reactor. As methanol is generated via reversible exothermic reactions (1) and (3), which benefit from low temperatures. In the adiabatic configuration, heat released inside the reactor accumulates and there is no cooling system available to take the heat out of the reactor. Consequently, the increase in temperature inhibits the exothermic reactions and eventually suppresses the methanol production. Contrary to the adiabatic case, the constant temperature can be achieved by providing a cooling system which takes out the heat produced from the exothermic reaction, keeping the temperature constant. This maintains the reaction equilibrium in favour of the methanol production, eventually leading to a higher methanol yield at the end of the isothermal reactor. It is also worth noting that methanol production in an isothermal reactor does not level off until the end of the reactor length, indicating the possibility of obtaining an even higher methanol yield along the length of the reactor. The comparison between adiabatic and isothermal reaction operation can also be explained using equilibrium constants data. It is evident that equilibrium rate constants favor isothermal conditions with increase in feed temperature for RWGS and CO, CO_2 hydrogenation reactions.

4. Experimental work

4.1. Experimental set-up

A tubular fixed bed high-pressure reactor consisting of a stainless steel (SS316) reactor with an inner diameter of 7.5 mm, outer diameter of 14 mm and reactor length of 40 cm is placed in the temperature-controlled furnace (ATS, USA) as shown in Fig. 8. A thermocouple (K

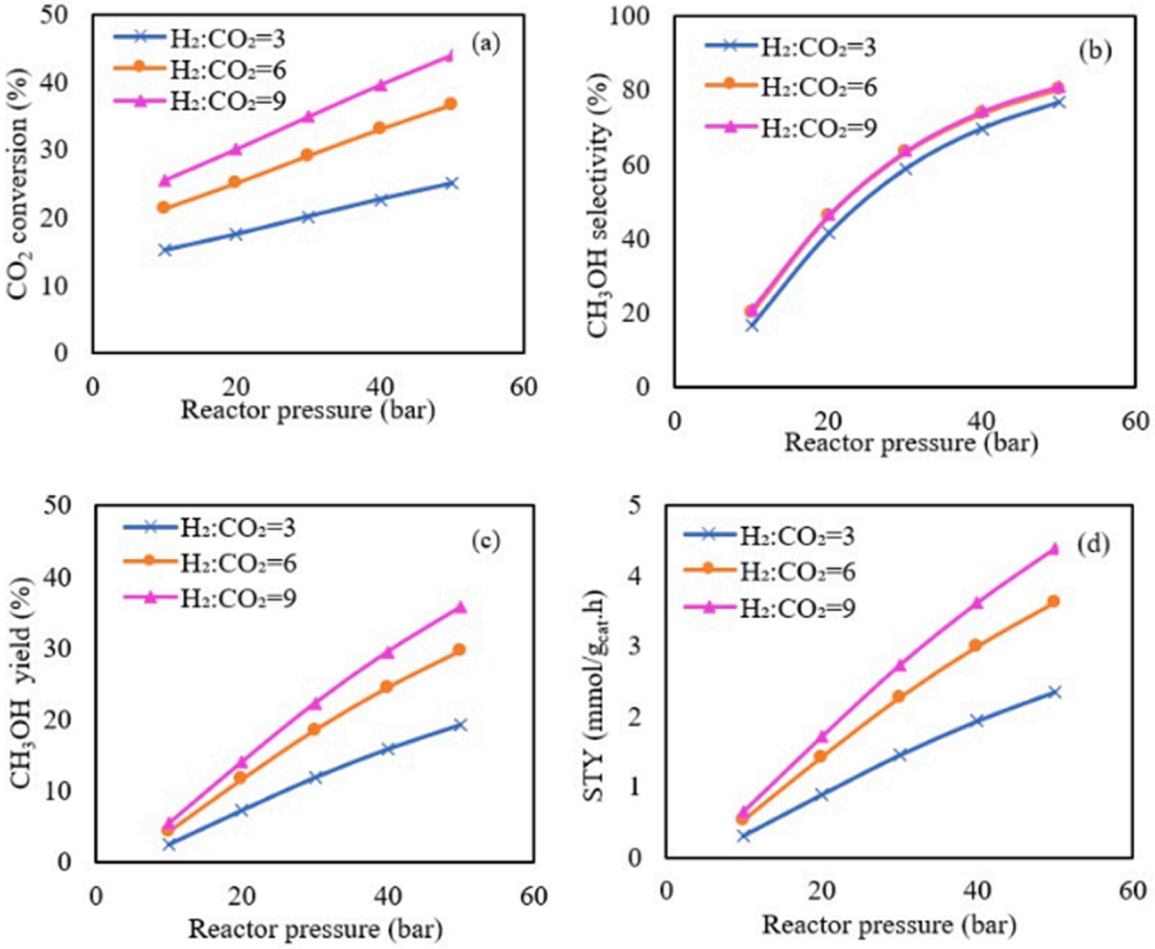

Fig. 6. Effect of H_2/CO_2 ratio on a) CO_2 conversion b) CH_3OH selectivity c) CH_3OH yield d) Space time yield (STY) of methanol as a function of H_2/CO_2 molar ratios on CuZA catalyst at T = 230 °C.

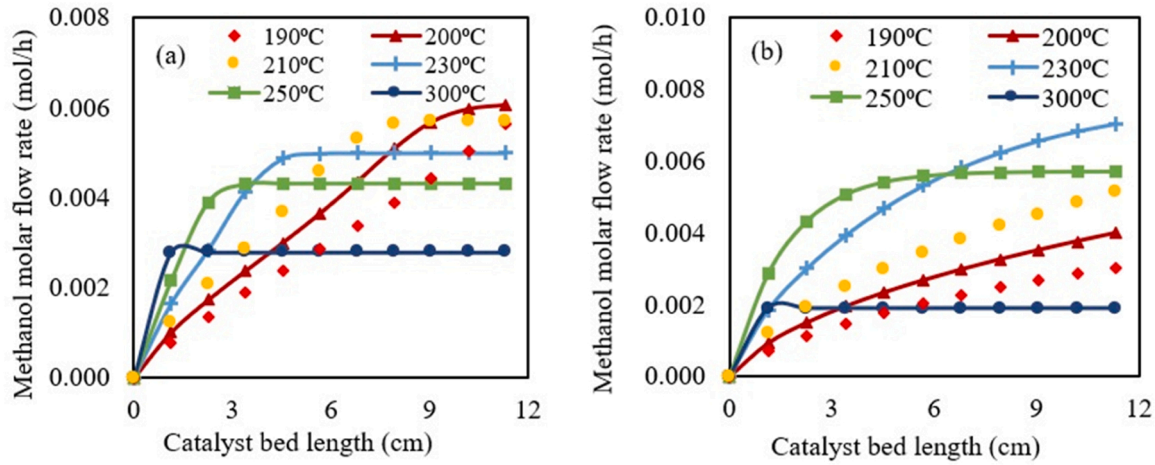

Fig. 7. Effect of feed temperature on molar flow rate of methanol for a) adiabatic and b) Isothermal reactor.

type, Watlow) is placed along the axial direction of the reactor tube to make direct contact with the catalyst and to measure temperature of the catalyst bed accurately. The reactor temperature is controlled using PID controller for furnace coils at three different sections. The total pressure inside the reactor system is controlled by a back pressure regulator digitally using a pressure transmitter. The feed gas flow rates are controlled using a mass flow controller (MFC, Brooks, USA) for CO_2 and H_2 gases directed from the respective gas cylinders. The reactor components comprise of condenser, high-pressure gas-liquid separator, low-pressure gas-liquid separator and wet gas meter. The experimental set-up is operated using a SCADA system without manual interventions for all the experiments.

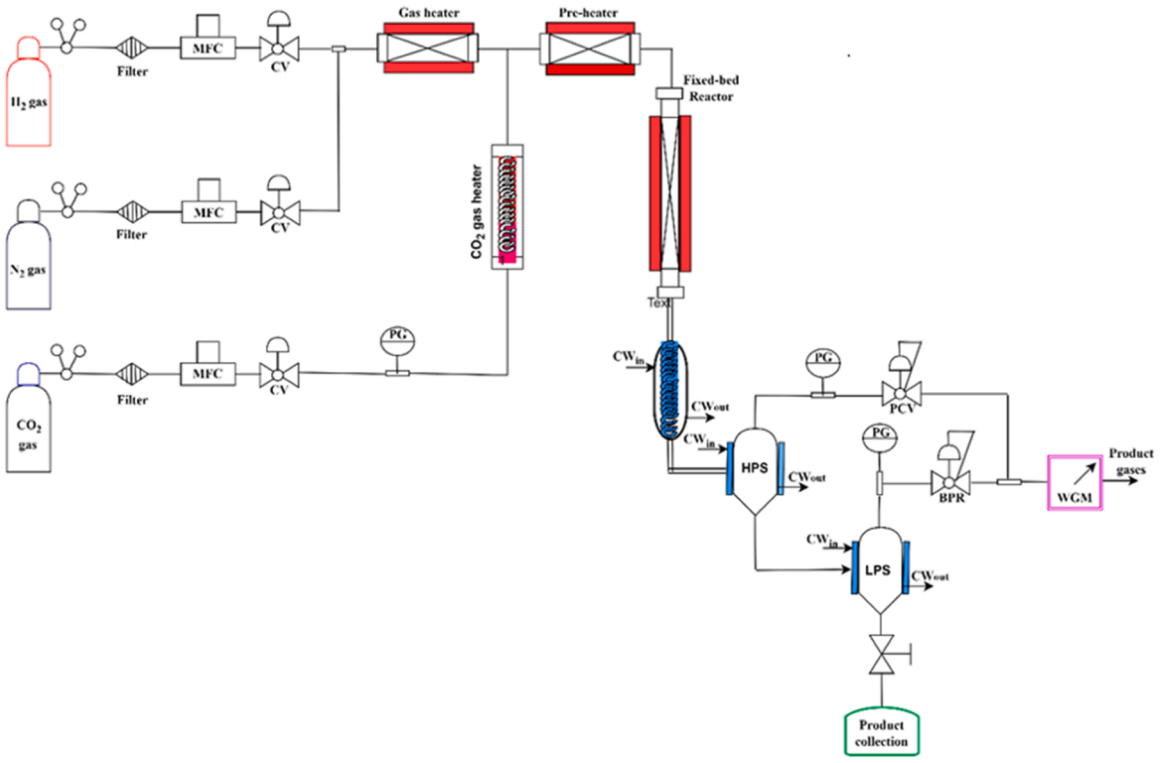

Fig. 8. Process flow diagram for conversion of CO_2 to methanol production using fixed bed reactor.

4.2. Experimental procedure

The experiments are carried out using commercial copper-based catalyst, $Cu/ZnO/Al_2O_3$ (CuZA) catalyst as discussed in Section 2.1. Catalyst pellets are crushed using a mortar pestle into tiny particles in the size range of 300–400 microns. For the first set of experiments, a catalyst bed of length 11.3 cm with a catalyst weight of 3 g and the same weight of inert (silica gel) is placed inside the reactor. The inert material is used for dual purposes: (i) to pre-heat the feed gases and ii) to reduce outlet vapour temperature in case of hotspot generation which may decompose methanol. For the second set of experiments, catalyst bed length of 22.6 cm long with a catalyst weight of 6 g and the same amount of inert material is placed inside the reactor. Initially, the experiments are carried out at a constant pressure of 40 bar, GHSV of 720 h^{-1} and the reaction is performed for 5 hours by varying temperature, flow rate and weight of the catalyst for varying reaction conditions as given in Table 3. The bed is placed in the middle of the electrical heating element/zone. To adjust the location of the catalytic bed, quart wool is placed between the inert material and catalyst bed which will prevent seepage of catalyst particles through inert material.

The product composition at the reactor outlet is estimated by calculating the CO_2 conversion, product selectivity, product yield and space-time yield defined as follows (Eqs. 13–15)

$$Selectivity\ (\%) = \frac{Molar\ flow\ rate\ of\ i\ species}{Total\ molar\ flow\ rate\ of\ all\ products} * 100 \tag{13}$$

$$Yield\ (\%) = \frac{Molar\ flow\ rate\ of\ desired\ product}{Molar\ flow\ rate\ of\ reactant\ fed} * 100 \tag{14}$$

$$STY_{Methanol}\left(\frac{mg}{g_{cat}.h}\right) = \frac{F_{Methanol}}{W_{cat}} * 100 \tag{15}$$

Where,

$F_{Methanol}$ is the methanol flow rate, mg/h
$S_{methanol}$ is methanol selectivity, %
$STY_{methanol}$ is the space-time yield of methanol, mg/g_{cat}.h
W_{cat} is the amount of catalyst, g

5. Results and discussion

5.1. Effect of inlet flow rate and weight of catalyst on methanol yield

The experiments are carried out for H_2 to CO_2 ratio of 3 using 3 g and 6 g powdered catalyst for 60 and 120 ml/min. After the reaction protocol is set, carbon dioxide and hydrogen are passed through the preheaters at 200 °C and then directed to the reactor. Mass flow controllers can be used to modify the desired gas flow rates. The gas hourly space

Table 3
Reaction conditions and the performance results of CuZA catalyst.

Exp. No.	P (bar)	T (°C)	Flow rate (ml/min)			Catalyst weight (g)	GHSV (h^{-1})	Amount of product (mg)
			CO_2	H_2	Total			
1	40	210	15	45	60	3	720	32.10
2	40	230	15	45	60	3	720	161.70
3	40	250	15	45	60	3	720	358.10
4	40	210	30	90	120	6	720	121.00
5	40	230	30	90	120	6	720	323.20
6	40	250	30	90	120	6	720	1261.60

velocity (GHSV) of 720 h^{-1} is maintained by providing an overall gas feed flow rate to catalyst weight. Prior to it, catalyst is reduced under H_2 flow (10 ml/ min) and N_2 flow (90 ml/ min) at atmospheric pressure from room temperature to 330 °C for 2 h and then the reduced catalyst is cooled to 100°C under the same flow conditions. The actual CO_2 hydrogenation experiments are performed at 210, 230 and 250 °C at a pressure of 40 bar for 5 h. The required gas flow rates are adjusted to 60 ml/min and 120 ml/min by keeping the molar ratio of H_2 to CO_2 is 3:1, respectively. For set-1 of reactions, CO_2 hydrogenation is carried out under the flow rate of 15 ml/min of CO_2, 45 ml/min of H_2 and for set-2, CO_2 hydrogenation is carried out under the flow rate of 30 ml/min of CO_2, 90 ml/min of H_2 at 210, 230 and 250 °C. Reaction products are condensed and collected from a gas-liquid separator. The concentration of reactants and products is analysed by gas chromatography (Nucon GC, 5765) equipped with manual injection functionality. The GC method is developed to detect methanol from the product mixture and the remaining species is majorly of water formed from the reverse water gas shift reaction. The product composition is detected by TCD (Thermal Conductivity Detector) using Helium as carrier gas. The TCD channel is equipped with Porapak-Q column with dimensions of 2.1 mm ID, 1/8" of OD and length of 6 feet. The liquid phase composition is further quantified for evaluation of performance parameters. It is clear from the experiments that the increase in temperature increased the rate of methanol production as is evident from Fig. 9. The experimental results for space time yield of methanol are well compared with the model predictions by Graaf et al. (1988) and Portha et al. (2017) at 250 °C as reported in the Supplementary information. Therefore, further experiments are carried out at 250 °C and 50 bar for higher H_2 toCO_2 molar ratios of 3, 6 and 9 for under similar reaction conditions.

5.2. Effect of H_2 to CO_2 molar ratio

The experiments are performed in a high pressure fixed-bed catalytic reactor to study the effect of H_2 to CO_2 molar ratio of 3, 6 and 9 on methanol yield. The results depict that the maximum methanol yield is obtained at 250 °C and 40 bar for H_2 to CO_2 ratio of 3. Therefore, further experiments are performed in a fixed bed reactor for catalyst pellet weights of 3 g and 6 g with increase in H_2 to CO_2 molar ratios of 6 and 9. The product samples are collected after the vapours are cooled in a condenser followed by low-pressure gas-liquid separator. The circulating fluid is maintained at 3 °C in the chiller throughout the reaction until the product collection. The product samples are quantified using gas chromatography (GC) using Porapak-Q column as discussed in Section 5.1. The experimental data is quantified in terms of product yield and space time yield (STY) as shown in Table 4. The actual samples collected from the gas-liquid separator for six experiments at 3 g and 6 g pellets for H_2 to CO_2 ratios of 3, 6 and 9 are shown in Fig. 10. The results show that there is an increase in production of methanol with increase in catalyst weight at optimal conditions. The maximum methanol production of 956 mg for 3 g pellets and 1331 mg is collected for 6 g catalyst at H_2 to CO_2 ratio of 6. A further increase in H_2 to CO_2 ratio to 9 decreased methanol quantity which may be due to favouring reverse water gas shift reaction leading to CO and water formation as is discussed in the literature (Portha et al., 2017).

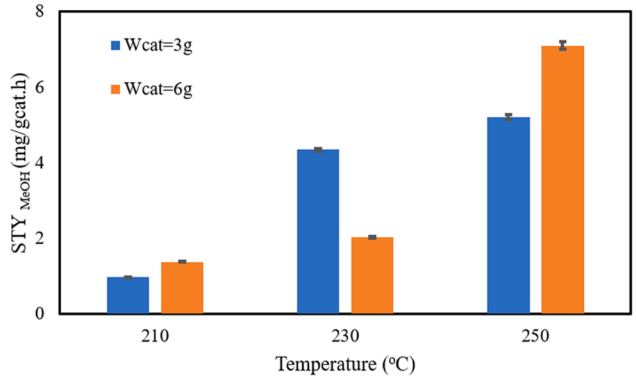

Fig. 9. Space time yield (STY) of methanol for different temperatures at 40 bar.

Therefore, it can be inferred that increase in H_2 to CO_2 ratio for different flow rates showed increased methanol production. The experiments showed better reproducibility and is reported for space time yield (STY) with absolute deviation of ± 0.01 for 3 g catalyst and ± 0.026 for 6 g catalyst as shown in Fig. 9.

5.3. Study of mass transfer limitations

Catalytic reactions with solids involve various steps that influence the rate of reaction due to internal and external mass transfer limitations. The internal mass transfer corresponds to the diffusion of reactants into the internal surface and diffusion of products from the pores to the outer surface. The external mass transfer corresponds to the transport of reactants from the bulk fluid stream to the surface of the catalyst and transport of products from the outer surface of the body to the bulk fluid. In addition to the surface reaction, internal and external mass transfer may influence the overall reaction, hence, mass transfer limitations are studied using Weisz-Prater and Mears criteria.

The Weisz-Prater criteria is used to assess if internal diffusion is restricting the reaction and Mears criteria is used to know if any external mass transfer limitation are present (Infantes-Molina et al., 2015; Poto et al., 2022).

Weisz Prater parameter (C_{WP}) is calculated using the equation:

$$C_{WP} = \frac{Actual\ reaction\ rate}{Diffusion\ rate} \tag{16}$$

$$C_{WP} = \frac{-r_{A\ (obs)}\ \rho_c\ R^2}{D_e\ C_{As}} \tag{17}$$

$$V_{avg} = \left[\frac{8k_B T}{\Pi m}\right]^{0.5} \tag{18}$$

$$D_{kn} = \frac{V_{ave} * D_P}{3} \tag{19}$$

The Effective diffusivity, D_e will be substituted by Knudsen diffusion since the pore diameter (D_p) of the catalyst is small (i.e., 9.76 nm), therefore, pore diffusion will be dominated by Knudsen diffusion (D_{Kn}) (Infantes-Molina et al., 2015); $-r_{A(obs)}$is the observed reaction rate (g/(kg_{cat}.h); V_{avg} is average gas velocity (m/s) and k_B is the Boltzmann's constant; C_{As} is the concentration of CO_2 at the reaction surface.

Mears Parameter (MP) is calculated using the equation:

$$MP = \frac{-r_{A\ (obs)}\ \rho_b\ R\ n}{k_c\ C_{Ab}} \tag{20}$$

Moreover, the Thoenes-Kramers correlation is used to estimate the packed-bed external mass transport coefficient for the Mears Parameter. K_c is mass transfer coefficient (Samimi et al., 2017) and R is radius of catalyst particle; m and n refers to the molecular mass of CO_2 and order of the reaction; C_{Ab} is the concentration of CO_2 at the bulk surface.

The estimations for mass transfers limitations found that for all the reaction conditions C_{WP} is significantly less than 1 and Mear's Parameter is less than 0.15 indicating that no internal diffusional limitations and no external mass transfer limitations as well influences the rate of reaction. Therefore, mass transfer effects could be neglected for all the cases.

6. Conclusions

The kinetic models developed for the synthesis of methanol from CO_2 are under high-pressure conditions that require experimental investigation for kinetic parameters evaluation. In this work, the role of CO in

Table 4
Performance analysis for different H_2 to CO_2 molar ratios of 3, 6 and 9 at 50 bar and 250 °C.

Exp. No.	P (bar)	T (°C)	Flow rate (ml/min)				Catalyst weight (g)	H_2 to CO_2 molar ratio	GHSV (h^{-1})	Amount of product (mg)	STY of MeOH (mg/gcat. h)
			CO_2	H_2	N_2	Total					
1	50	250	30	90	120	240	3	3	2880	458.10	6.03
2	50	250	30	180	120	330	3	6	3940	956.00	9.98
3	50	250	30	270	120	420	3	9	5040	942.10	12.41
4	50	250	30	90	120	240	6	3	1440	217.50	6.30
5	50	250	30	180	120	330	6	6	1980	1331.00	9.22
6	50	250	30	270	120	420	6	9	2520	990.00	13.59

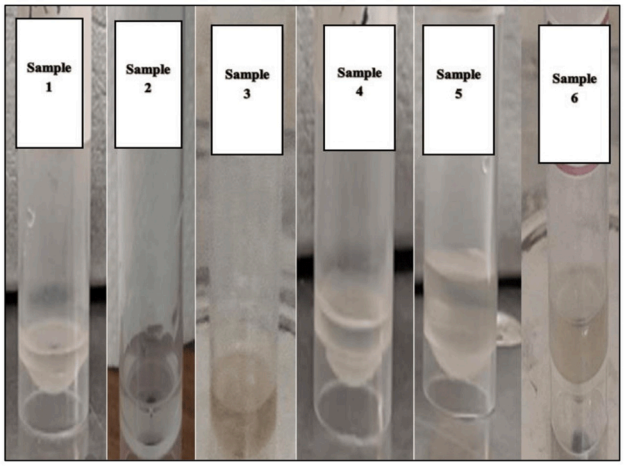

Fig. 10. Samples collected for 50 bar experiments for H_2 to CO_2 ratios of 3, 6 and 9 for 3 g and 6 g pellet catalyst (Samples 1–3 → W_{cat} = 3 g; Samples 4–6 → W_{cat} = 6 g).

direct CO_2 catalytic hydrogenation reactions is analysed through reverse water gas shift reaction using kinetic models. Simulations are performed for increased mole ratios of H_2 to CO_2 to envisage the performance characteristics of the fixed bed reactor model. Based on modelling and experimental investigation for direct CO_2 hydrogenation, the conclusions are as follows:

i) The effect of temperature and pressure is well understood with adiabatic and isothermal model simulations. The isothermal model showed much better performance for CO_2 conversion, selectivity, and methanol yield. The result showed that the isothermal configuration converted 2.76% more methanol yield compared to the adiabatic reactor.
ii) The reaction rates showed that reverse water gas shift reaction enhanced the rate of methanol formation by 5 times via CO hydrogenation alone as CO formation favours with increase in temperature. However, the contribution of CO_2 hydrogenation for methanol formation is much higher compared to CO hydrogenation.
iii) The higher H_2 to CO_2 ratio yielded better performance under low-pressure conditions as reported in the literature. Therefore, the model showed enhancement in the reaction rates with improved methanol yields of 19.03%, 29.25% and 36.41% for H_2 to CO_2 molar ratios of 3, 6 and 9, respectively.
iv) The experiments at higher H_2 to CO_2 molar ratios demonstrated that increase in yield and space time yield towards methanol production and further optimized that H_2 to CO_2 molar ratio of 9 favours higher methanol yield.

CRediT authorship contribution statement

Farahanaz M. Bagwan: Data curation, Formal analysis, Methodology, Software, Validation, Visualization, Writing – original draft. **Satyam Naidu Vasireddy:** Conceptualization, Data curation, Formal analysis, Investigation, Methodology, Resources, Software, Supervision, Validation, Visualization, Writing – review & editing. **Amol A. Kulkarni:** Conceptualization, Methodology, Project administration, Supervision, Writing – review & editing. **Pavan Dongapure:** Formal analysis, Resources, Visualization.

Declaration of Competing Interest

The authors declare that they have no known competing financial interests or personal relationships that could have appeared to influence the work reported in this paper.

Acknowledgements

The authors are thankful to the funding agency for sponsoring the IMPRINT project (Project code: File No. IMP/2018/001208) funded by the Department of Science and Technology (DST) and Dr. Nandini Devi, Senior Principal Scientist, Catalysis and Inorganic Chemistry division, CSIR-National Chemical Laboratory for providing the experimental facility.

Appendix A. Supporting information

Supplementary data associated with this article can be found in the online version at doi:10.1016/j.cherd.2024.03.032.

References

Álvarez, A., Bansode, A., Urakawa, A., Bavykina, A.V., Wezendonk, T.A., Makkee, M., Gascon, J., Kapteijn, F., 2017. Challenges in the greener production of formates/formic acid, methanol, and DME by heterogeneously catalyzed CO_2 hydrogenation processes. Chem. Rev. 117, 9804–9838.
Al-Rowaili, F.N., Khalafalla, S.S., Al-Yami, D.S., Jamal, A., Ahmed, U., Al-Mutairi, E.M., 2022. Techno-economic evaluation of methanol production via gasification of vacuum residue and conventional reforming routes. Chem. Eng. Res. Des. 177, 365–375.
Arab, S., Commenge, J., Portha, J., Falk, L., 2014. Methanol synthesis from CO_2 and H_2 in multi-tubular fixed-bed reactor and multi-tubular reactor filled with monoliths. Chem. Eng. Res. Des. 92, 2598–2608.
Atsbha, T.A., Yoon, T., Seongho, P., Lee, C.J., 2021. A review on the catalytic conversion of CO_2 using H_2 for synthesis of CO, methanol, and hydrocarbons. J. CO_2 Util. 44, 101413.
Baltes, C., Vukojević, S., Schüth, F., 2008. Correlations between synthesis, precursor, and catalyst structure and activity of a large set of CuO/ZnO/Al_2O_3 catalysts for methanol synthesis. J. Catal. 258, 334–344.
Bisotti, F., Fedeli, M., Prifti, K., Galeazzi, A., Dell'Angelo, A., Barbieri, M., Pirola, C., Bozzano, G., Manenti, F., 2021. Century of technology trends in methanol synthesis: any need for kinetics refitting? Ind. Eng. Chem. Res. 60, 16032–16053.
Boffito, D.C., Galli, F., Martinez, P.R., Pirola, C., Bianchi, C.L., Patience, G.S., 2015. Transesterification of triglycerides in a new ultrasonic-assisted mixing device. Chem. Eng. Trans. 43, 427–432.
Bozzano, G., Manenti, F., 2016. Efficient methanol synthesis: Perspectives, technologies and optimization strategies. Prog. Energy Combust. Sci. 56, 71–105.
Cordero-Lanzac, T., Ramirez, A., Cruz-Fernandez, M., Zander, H.J., Joensen, F., Woolass, S., Meiswinkel, A., Styring, P., Gascon, J., Olsbye, U., 2023. A CO_2 valorization plant to produce light hydrocarbons: Kinetic model, process design and life cycle assessment. J. CO_2 Util. 67, 102337.
De Oliveira Campos, B.L., Delgado, K.H., Wild, S., Studt, F., Pitter, S., Sauer, J., 2021. Surface reaction kinetics of the methanol synthesis and the water gas shift reaction on Cu/ZnO/Al_2O_3. React. Chem. Eng. 6, 868–887.

Godini, H.R., Khadivi, M., Azadi, M., Gorke, O., Jazayeri, S.M., Thum, L., Schomacker, R., Wozny, G., Repke, J.-U., 2020. Mutli-scale analysis of integrated C1 (CH_4 and CO_2) utilization catalytic processes: Impacts of Catalysts characteristics up to Industrial-Scale Process Flow sheeting, Part I: Experimental Analysis of catalytic low-pressure CO_2 to methanol conversion. Catalysts 20, 505.

Graaf, G.H., Sijtsema, P.J.J.M., Stamhuis, E.J., Joosten, G.E.H., 1986. Chemical equilibria in methanol synthesis, 41, 2883–2890.

Eksiri, Z., Mozdianfard, M.R., Mirvakili, A., Rahimpour, M.R., 2020. Two-dimensional modelling investigation of the modern methanol plate reactors. Chem. Eng. Res. Des. 162, 212–227.

Fogler, H.S., 1987. Elements of Chemical Reaction Engineering.

Gaikwad, R., Bansode, A., Urakawa, A., 2016. High-pressure advantages in stoichiometric hydrogenation of carbon dioxide to methanol. J. Catal. 343, 127–132.

Ghosh, S., Sebastian, J., Olsson, L., Creaser, D., 2021. Experimental and kinetic modeling studies of methanol synthesis from CO_2 hydrogenation using In_2O_3 catalyst. Chem. Eng. J. 416, 129120.

Graaf, G.H., Stamhuis, E.J., Beenackers, A.A.C.M., 1988. Kinetics of low-pressure methanol synthesis. Chem. Eng. Sci. 43 (12), 3185–3195.

Gribovskii, A.G., Ovchinnikova, E.V., Vernikovskaya, N.V., Andreev, D.V., Chumachenko, V.A., Makarshin, L.L., 2017. Microchannel reactor for intensifying oxidation of methanol to formaldehyde over Fe-Mo catalyst. Chem. Eng. J. 308, 135–141.

Hafeez, S., Harkou, E., Al-Salem, S.M., Goula, M.A., Dimitratos, N., Charisiou, N.D., Villa, A., Bansode, A., Leeke, G., Manos, G., Constantinou, A., 2022. Hydrogenation of carbon dioxide (CO_2) to fuels in microreactors: a review of set-ups and value-added chemicals production. React. Chem. Eng. 7, 795–812.

Infantes-Molina, A., Gralberg, E., Cecilia, J.A., Finocchio, E., Rodriguez-Castellon, E., 2015. Nickel and Cobalt phosphide as effective catalysts for oxygen-removal of dibenzofuran: Role of contact time, hydrogen pressure and hydrogen/feed molar ratio. Catal. Sci. Technol. 5, 3403–3415.

Kropp, T., Paier, J., Sauer, J., 2017. Oxidative dehydrogenation of methanol at ceria-supported vanadia oligomers. J. Catal. 352, 382–387.

Losch, P., Pinar, A.B., Willinger, M.G., Soukup, K., Chavan, S., Vincent, B., Pale, P., Louis, B., 2017. H-ZSM-5 zeolite model crystals: Structure-diffusion-activity relationship in methanol-to-olefins catalysis. J. Catal. 345, 11–23.

Machado, C.F.R., Medeiros, J.L., De, Araújo, O.F.Q., Alves, R.M.B., 2014. A comparative analysis of methanol production routes: synthesis gas versus CO_2 hydrogenation. Int. Conf. Ind. Eng. Oper. Manag. 2981–2990.

Mbatha, S., Everson, R.C., Musyoka, N.M., Langmi, H.W., Lanzini, A., Brilman, W., 2021. Power-to-methanol process: A review of electrolysis, methanol catalysts, kinetics, reactor designs and modelling, process integration, optimisation, and techno-economics. Sustain. Energy Fuels 5, 3490–3569.

McNeil, M.A., Schack, C.J., Rinker, R.G., 1989. Methanol synthesis from hydrogen, carbon monoxide and carbon dioxide over a $CuO/ZnO/Al_2O_3$ catalyst. II. Development of a phenomenological rate expression. Appl. Catal. 50, 265–285.

Nestler, F., Müller, V.P., Ouda, M., Hadrich, M.J., Schaadt, A., Bajohr, S., Kolb, T., 2021. A novel approach for kinetic measurements in exothermic fixed bed reactors: Advancements in non-isothermal bed conditions demonstrated for methanol synthesis. React. Chem. Eng. 6, 1092–1107.

Ng, W.L., Sripada, P., Biswas, S., Bhattacharya, S., 2022. Experimental work and kinetic modelling of CO_2 hydrogenation to methanol on CeO_2 supported In_2O_3 catalyst. Appl. Catal. A: Gen. 646, 118885.

Nyári, J., Izbassarov, D., Toldy, Á.I., Vuorinen, V., Santasalo-Aarnio, A., 2022. Choice of the kinetic model significantly affects the outcome of techno-economic assessments of CO_2-based methanol synthesis. Energy Convers. Manag. 271, 116200.

Olah, G.A., Goeppert, A., Prakash, G.K.S., 2009. Chemical recycling of carbon dioxide to methanol and dimethyl ether: from greenhouse gas to renewable, environmentally carbon neutral fuels and synthetic hydrocarbons. J. Org. Chem. 74, 487–498.

Park, N., Park, M.J., Lee, Y.J., Ha, K.S., Jun, K.W., 2014. Kinetic modeling of methanol synthesis over commercial catalysts based on three-site adsorption. Fuel Process. Technol. 125, 139–147.

Pirola, C., Manenti, F., Galli, F., Bianchi, C.L., Boffito, D.C., Corbetta, M., 2014. Heterogeneously catalyzed free fatty acids esterification in (monophasic liquid)/solid packed bed reactors (PBR). Chem. Eng. Trans. 37, 553–558.

Portha, J.F., Parkhomenko, K., Kobl, K., Roger, A.C., Arab, S., Commenge, J.M., Falk, L., 2017. Kinetics of methanol synthesis from carbon dioxide hydrogenation over copper-zinc oxide catalysts. Ind. Eng. Chem. Res. 56, 13133–13145.

Poto, S., van Berkel, D.V., Gallucci, F., d'Angelo, M.F.N., 2022. Kinetic modelling of the methanol synthesis from CO_2 and H_2 over a $CuO/CeO_2/ZnO_2$ catalyst: the role of CO_2 and CO hydrogenation. Chem. Eng. J. 435, 134946.

Samimi, F., Rahimpour, M.R., Shariati, 2017. Development of an efficient methanol production process for direct CO_2 hydrogenation over a $Cu/ZnO/Al_2O_3$ catalyst. Catalysts 7, 332.

Sharma, P., Sebastian, J., Ghosh, S., Creaser, D., Olsson, L., 2021a. Recent advances in hydrogenation of CO_2 into hydrocarbons via methanol intermediate over heterogeneous catalysts. Catal. Sci. Technol. 11, 1665–1697.

Sharma, S.K., Banerjee, A., Paul, B., Poddar, M.K., Sasaki, T., Samanta, C., Bal, R., 2021b. Combined experimental and computational study to unravel the factors of the Cu/TiO_2 catalyst for CO_2 hydrogenation to methanol. J. CO_2 Util. 50, 101576.

Skrzypek, J., Lachowska, M., Moroz, H., 1991. Kinetics of methanol synthesis over commercial copper/zinc oxide/alumina catalysts. Chem. Eng. Sci. 46, 2809–2813.

Stangeland, K., Li, H., Yu, Z., 2020. CO_2 hydrogenation to methanol: the structure–activity relationships of different catalyst systems. Energy, Ecol. Environ. 5, 272–285.

Takagawa, M., Ohsugi, M., 1987. Study on reaction rates for methanol synthesis from carbon monoxide, carbon dioxide, and hydrogen. J. Catal. 107, 161–172.

Torcida, M.F., Curto, D., Martín, M., 2022. Design and optimization of CO_2 hydrogenation multibed reactors. Chem. Eng. Res. Des. 181, 89–100.

Van-Dal, É.S., Bouallou, C., 2013. Design and simulation of a methanol production plant from CO_2 hydrogenation. J. Clean. Prod. 57, 38–45.

Vanden Bussche, K.M., Froment, G.F., 1996. A steady-state kinetic model for methanol synthesis and the water gas shift reaction on a commercial $Cu/ZnO/Al_2O_3$ catalyst. J. Catal. 161, 1–10.

Villa, P., Forzattl, P., Buzzl-Ferraris, G., Garone, G., Pasquon, I., 1985. Synthesis of alcohols from carbon oxides and hydrogen. 1. Kinetics of the low-pressure methanol synthesis. Ind. Eng. Chem. Res. 24, 12–19.

Wang, W., Wang, S., Ma, X., Gong, J., 2011. Recent advances in catalytic hydrogenation of carbon dioxide. Chem. Soc. Rev. 40, 3703–3727.

Younas, M., Loong Kong, L., Bashir, M.J.K., Nadeem, H., Shehzad, A., Sethupathi, S., 2016. Recent advancements, fundamental challenges, and opportunities in catalytic methanation of CO_2. Energy Fuels 30, 8815–8831.

Zhu, J., Araya, S.S., Cui, X., Sahlin, S.L., Kær, S.K., 2020. Modeling and design of a multi-tubular packed-bed reactor for methanol steam reforming over a $Cu/ZnO/Al_2O_3$ catalyst. Energies 13, 610.

International Journal of Hydrogen Energy 92 (2024) 102–112

Contents lists available at ScienceDirect

International Journal of Hydrogen Energy

journal homepage: www.elsevier.com/locate/he

Reaction kinetics for catalytic hydrogenation of quinoline to decahydroquinoline as liquid organic hydrogen carrier

Farahanaz M. Bagwan [a,b], Anil K. Kinage [a,b,**], Satyam Naidu Vasireddy [a,b,*]

[a] Chem. Eng. and Proc. Dev. Div., CSIR-National Chemical Laboratory, Pune, 411 008, India
[b] Academy of Scientific and Innovative Research (AcSIR), Ghaziabad, 201 002, India

ARTICLE INFO

Handling Editor: Dr J Lobato

Keywords:
Hydrogen uptake
Liquid organic hydrogen carrier (LOHC)
Thermal screening unit (TSU)
Markov chain Monte Carlo (MCMC) simulation tool
Decahydroquinoline (DHQ)

ABSTRACT

The catalytic hydrogenation of quinoline to decahydroquinoline (DHQ) formation is studied for various parameters such as temperature, hydrogen pressure, reaction time, solvents, reactant-to-solvent ratio, and catalyst loading over 5%Pd loaded on alumina (Pd/Al_2O_3) to obtain optimal reaction conditions. The hydrogen uptake of quinoline in the liquid phase reaction using isopropylalcohol (IPA) is studied in an autoclave reactor. The optimum reaction parameters of 50 bar H_2 pressure and 175°C with reactant to solvent ratio of 1:9 for reaction time of 5 h are observed. The effect of IPA solvent showed that hydrogen uptake of 6.91 wt% with complete hydrogenation of quinoline and DHQ yield of more than 99% is observed. The reaction kinetic model is developed for a simplified reaction mechanism and is simulated using the Markov Chain Monte Carlo (MCMC) simulation tool to predict the rate constants and the experimental observations are validated with the model predictions. The activation energy for quinoline hydrogenation to py-THQ formation is estimated to be 136.57 kJ/mol. It is envisaged that quinoline hydrogenation to pz-THQ is the rate-limiting step in the DHQ formation.

1. Introduction

The world continues to shift towards renewable energy sources with the need for efficient and cost-effective energy storage solutions becomes increasingly important. Recently, the Hydrogen Council released a report asserting that hydrogen has the potential to account for 22% of the global final energy demand by 2050, equivalent to an annual production of 660 million tonnes (MT) of hydrogen [1]. The mass-energy density of 120 MJ/kg of hydrogen is much higher than that of hydrocarbon fuel with a calorific value of 44 MJ/kg for gasoline [2,3]. However, its widespread use requires economical and safe hydrogen storage with a gravimetric content of over 6.5 wt% H_2 (>2.0 kWh/kg) and volume density over 0.04 kg/L(>1.3 kWh/L) [4]. Thermodynamic feasibility and attractiveness in terms of simplicity, safety, scalability, heat control, and economics make hydrogen storage in liquid organic heterocycles a desirable option [5]. One of the fundamental pillars of the contemporary chemical industry is a heterogeneous catalyst which offers the possibility of economically and efficiently converting raw materials into valuable chemicals and fuels as well as ecologically favorable [6]. Different technologies of storing hydrogen have been extensively studied such as compressed hydrogen, liquefied hydrogen, physisorption in porous materials or metal-organic frameworks, and metal hydrides although each technology has certain advantages and drawbacks [7]. The storage and transportation of hydrogen provide a significant challenges in developing a hydrogen-based economy due to its high specific gravity and low thermal energy density [8]. In recent years, the chemical and industrial sectors have paid a great deal of attention to the storage of hydrogen using methane, ammonia, and other materials [9]. Liquid organic hydrogen carriers (LOHCs) have emerged as one of attractive sources for the storage and transportation of hydrogen with large quantities of hydrogen can be loaded and unloaded using a reversible chemical reaction. For long durations of energy storage, LOHCs were found to be a more effective solution compared to other storage technologies [10]. Many hydrogen carriers have been examined and assessed in terms of their availability, cost, and toxicological profile. LOHC shows various advantages such as high gravimetric and volumetric density, safety to handle, longevity, good reversibility, logistics, compatibility with the existing energy infrastructure, and cost-effective, high-purity hydrogen [11,12]. The concept of LOHCs aligns with the principles of the hydrogen economy which envisions hydrogen as a

* Corresponding author. Chem. Eng. and Proc. Dev. Div., CSIR-National Chemical Laboratory, Pune, 411 008, India.
** Corresponding author. Chem. Eng. and Proc. Dev. Div., CSIR-National Chemical Laboratory, Pune, 411 008, India.
E-mail addresses: ak.kinage@ncl.res.in (A.K. Kinage), sn.vasireddy@ncl.res.in (S.N. Vasireddy).

https://doi.org/10.1016/j.ijhydene.2024.10.247
Received 26 June 2024; Received in revised form 12 September 2024; Accepted 18 October 2024
Available online 23 October 2024

versatile and clean energy carrier capable of replacing or supplementing traditional fossil fuels [13]. LOHC systems have huge demand in European countries for residential and commercial buildings where thermal losses from the storage processes can be used for heating and cooling purposes [14]. The chemical storage of hydrogen in liquid carriers involves an exothermic process during hydrogenation, while the dehydrogenation process exhibits an endothermic release of hydrogen. Therefore, the endothermic nature poses a significant challenge due to the necessity for elevated heat input [12,15]. However, LOHC energy storage is a technology that requires research and development activities to optimize its performance to a commercially viable level. As a result, heterocyclic aromatic compounds (HACs) are being studied intensively as a future-oriented form of LOHC [16]. Quinoline, a heterocyclic compound consisting of a benzene ring fused to a pyridine ring, has been the subject of extensive research owing to its diverse applications in the fields of pharmaceuticals, agrochemicals, and materials science [17–19]. The recent literature suggests has hydrogen storage capacity (~5.3 wt%) and the moderate conditions required for hydrogenation and dehydrogenation steps. The reversible storage of hydrogen in the NEC has been demonstrated under practical conditions, making it a key candidate for LOHC systems. The reported studies are focused on optimizing the catalytic processes and understanding the thermodynamics involved in the hydrogenation/dehydrogenation processes. It can store up to three hydrogen molecules with hydrogenation occurring at temperatures around 150 °C, 70 bar and dehydrogenation at 220 °C. Studies have shown that the dehydrogenation of NEC can achieve conversion efficiencies greater than 99% under optimized conditions [14,17]. Similar to NEC, N-Propylcarbazole (NPC) is another carbazole derivative that has been investigated for hydrogen storage with a hydrogen storage capacity of approximately 5.5 wt% [18]. While it shares many properties with NEC, NPC offers a slightly different hydrogen storage capacity and reaction kinetics, which can be advantageous in specific applications. The hydrogenation of NPC typically occurs at 120–150 °C, with hydrogen pressure of 70 bar over 5 wt% ruthenium on alumina [19]. Indole Series Molecules such as 2-methylindole, have been identified as promising LOHC candidates due to their ability to store hydrogen at high densities. These molecules offer a favorable balance between hydrogen content and reaction conditions with ongoing research focusing on their stability and the optimization of dehydrogenation processes. The potential of indole-based compounds for hydrogen storage has been supported by both experimental and theoretical studies. 1-alkyl-indoles as suitable LOHC systems because of their high thermal stability and high boiling points [20]. 8-Methylquinoline is Methyl-substituted quinolines are available from petroleum, coal processing, wood preservation or can be synthesized from aniline. 8-methylquinoline is another material of interest in the LOHC field, known for its high hydrogen storage capacity and relatively low dehydrogenation temperatures [21]. Quinoline, a heterocyclic compound consisting of a benzene ring fused to a pyridine ring, has been the subject of extensive research owing to its diverse applications in the fields of pharmaceuticals, agrochemicals, and materials science [22–24]. There are valuable insights into the role of heteroatom within LOHC for hydrogenation and demonstrate the significance of heteroatom doping in improving hydrogen storage and transportation systems. Catalytic hydrogenation of quinoline and its derivatives are major raw materials for the production of various fine chemicals, such as agrochemicals, pharmaceuticals, and other bioactive molecules [25]. Quinoline is a by-product of coal tar and is also produced in large quantities during the production of coal gas. Thus, much study is also focused on the mechanisms involved in quinoline hydrodenitrogenation [26–29]. The role of quinoline as LOHC is a relatively unexplored aspect that presents exciting opportunities for the integration of quinoline-based compounds into the growing landscape of hydrogen storage and transport technologies. It has a high boiling point of 237 °C thus making it suitable for use as a liquid at low temperatures. Additionally, quinoline has a high hydrogen storage capacity of 7.24 wt % in comparison to other commonly used LOHCs such as toluene and naphthalene [30]. While quinoline shows great potential as LOHC, there are still some challenges that need to be addressed. One of the main challenges is the need for a suitable catalyst for the hydrogenation and dehydrogenation reactions. However, recent research has shown that certain metal catalysts, such as ruthenium and iron can effectively catalyze these reactions [26]. Catalytic hydrogenation of quinoline is a major organic reaction where one of the products, 1,2,3,4-tetrahydroquinoline, is an important intermediate for pharmaceuticals, agrochemicals, and various biologically active molecules [31]. Another intermediate is 5,6,7,8-tetrahydroquinoline and the fully hydrogenated product is decahydroquinoline (DHQ) as shown in Fig. 1. Hydrogenation of quinoline and its derivatives is of considerable industrial interest to produce petrochemicals, fine chemicals, and pharmaceuticals. Different metals (Pd, Ni, Rh, Pt, Cu, etc.) supported on different supports have been tested for the hydrogenation of quinoline to DHQ. This reaction is essentially carried out in two steps viz. quinoline to 1,2,3,4-tetrahydroquinoline (py-THQ) and a small amount of 5,6,7,8-tetrahydroquinoline (bz-THQ) formation in the first step while complete hydrogenation of both intermediates to DHQ occurs in the second step. The physicochemical properties of the reactant, intermediates and product are given Table 1. Complete hydrogenation is the most difficult step due to the need for severe reaction conditions and a longer response time and the conversion of py-THQ to DHQ is often quite challenging. Conversion of py-THQ to DHQ requires longer reaction time and harsh reaction conditions, typically at a temperature in the range of 175–260 °C, hydrogen pressure between 110 and 210 bar [18] and the use of acid as the solvent [32,33].

The complete catalytic hydrogenation of quinoline to decahydroquinoline is a topic of significant interest as it not only provides access to valuable intermediates for various industrial processes but also aligns with the burgeoning interest in sustainable energy carriers [32]. In this study, the work is focused on hydrogenation of quinolone at various parameters such as temperature, hydrogen pressure, reaction time, solvents, reactant-to-solvent ratio, and effect of catalyst loading of 5% Pd loaded on alumina (Pd/Al_2O_3) with reaction kinetics evaluation using Markov Chain Monte Carlo simulation (MCMC) tool and the reaction path for the product formation is identified. MCMC toolbox provides tools to generate and analyse Metropolis-Hastings MCMC chains using multivariate Gaussian proposal distribution. The code iteratively generate samples from the target distribution, enabling the estimation of integrals and expectations that are otherwise computationally prohibitive. The core idea is to create a chain of samples where each sample depends only on the previous one, ensures the distribution of the samples approximates the target distribution. In this study, the reaction kinetics are evaluated using the model fitting for the experimental data and rate determining step is identified.

2. Materials and methods

2.1. Materials

Quinoline (AR, ≥98%), 1,2,3,4-tetrahydroquinoline (AR, ≥98%), 5,6,7,8-tetrahydroquinoline (AR, ≥98%), decahydroquinoline (AR, ≥98%), toluene (AR, ≥98.0%) IPA (AR, ≥99%) are purchased from ThermoFischer scientific. Deionized water is used from an ultrapure water machine (elemental type 1820 C) from Chongqing Molecular Water System Co., Ltd. A stainless-steel batch autoclave reactor with an internal capacity of 100 ml was employed for hydrogenation experiments under high-pressure conditions. A commercial palladium-based catalyst (Pd/Al_2O_3) is used for the present experimental studies. The catalyst is procured from Alfa Aesar/Thermo Fisher Scientific in the form of powder that has the composition of Pd-5 wt.%, Al_2O_3-95 wt% and the average particle size of the catalyst is about 2 nm.

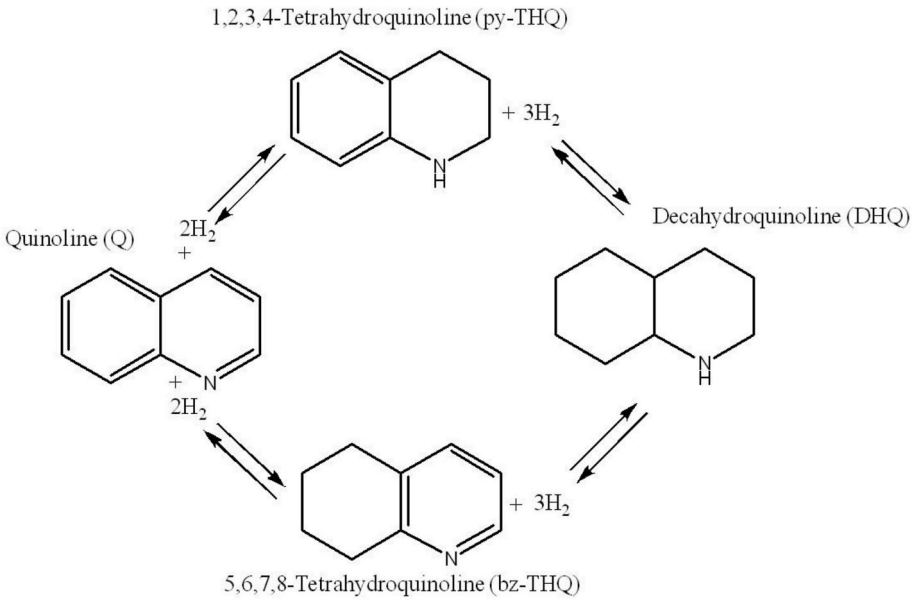

Fig. 1. Reaction scheme for Quinoline hydrogenation.

Table 1
Physicochemical properties of Quinoline and its hydrogenated products.

Properties/ Specifications	Quinoline	py-THQ	bz-THQ	DHQ
Chemical formula	C_9H_7N	$C_9H_{11}N$	$C_9H_{11}N$	$C_9H_{17}N$
Molecular weight (g/mol)	129.16	133.19	133.19	139.24
H_2 storage capacity (%)	7.24	4.35	4.35	NA
Boiling point (°C)	237	251	218	201
Melting point (°C)	−15	20	146.5	48
Density (g/ml)	1.09	1.05	1.03	0.93
Stability under process conditions	Stable	Stable	Stable	Stable
Solvent solubility	In organic solvents	In organic solvents	In organic solvents	In organic solvents
Appearance	Colourless oily liquid	Colourless oily liquid	Colourless oily liquid	White to light yellow

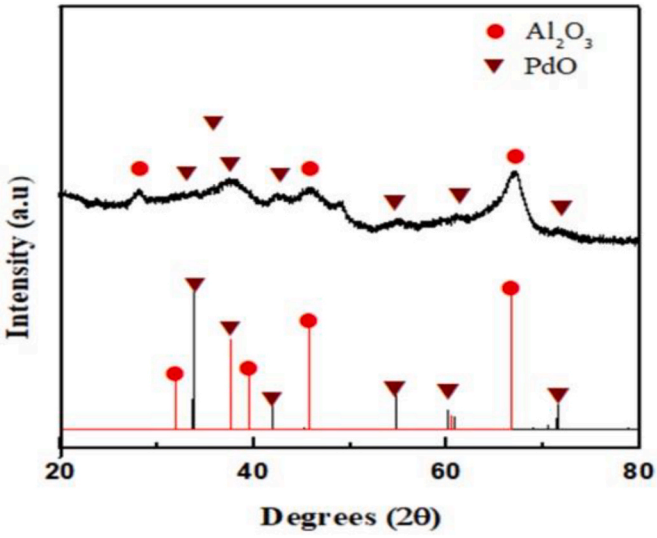

Fig. 2. XRD analysis of the Pd/Al_2O_3 catalyst (● – PdO; ▼ – Al_2O_3).

2.2. Catalyst characterization

2.2.1. X-ray powder diffraction (XRD)

The XRD analysis is performed for the Pd/Al_2O_3 catalyst to measure the crystallinity and phase behavior of the catalyst. The crystalline nature and phase formation of the sample are analyzed using powder X-ray diffraction (PXRD) for the data taken from a PAN analytical X'pert Pro dual goniometer. It is equipped with an X-ray diffractometer using CuKα (1.5418 A°) radiation with a scanning angle of 2θ from 20 to 80° and a step length of 2° every minute. The active phase formation of palladium oxide (dark circles in Fig. 2) and aluminum oxide (inverse triangles in Fig. 2) is identified from the XRD analysis at different angles between 30 and 80° at intervals of 2°. The XRD analysis cofirms the active deposition of PdO on the Al_2O_3 catalyst and is subjected to further surface area and TEM analysis.

2.2.2. BET analysis

The surface area analysis is performed using the Braunner-Emmet-Teller (BET) method using the Quantachrome BET apparatus. The pore volume, average pore radius, and specific surface area measurements of calcined catalysts are performed using nitrogen adsorption-desorption at an analysis temperature of 77K. The method of BET surface area analysis involves the following steps: all the samples are outgassed at 120°C under vacuum for 2h to remove adsorbed moisture. Adsorption-desorption curve shows the characteristics of type IV isotherm with a prominent hysteresis loop in the relative pressure (P/P^o) range of 0.2–1 that denotes the presence of mesoporous structure as shown in Fig. 3(a). The presence of hysteresis is due to the capillary phenomenon and the gases condense in the tiny capillary pores of the solid below the saturation pressure of gas. The pore size distribution gives an idea of the presence of mesoporous particles in the catalyst as shown in Fig. 3(b). It can be inferred from the BET analysis that monolayers followed by multilayers formation at low pressures. Based on the monolayer adsorption capacity of the nitrogen gas, the total surface area of the catalyst sample is calculated using the BET isotherm equation. The specific surface area of 102.65 m^2/g and a total pore volume of 0.213 cc/g is obtained from the BET surface area analysis. The reported literature shows that BET surface area is in good agreement with the measured values for the Pd/Al_2O_3 catalyst.

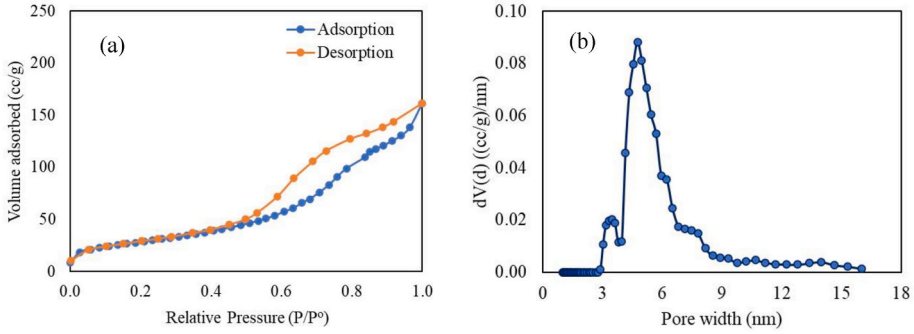

Fig. 3. (a) BET adsorption-desorption isotherm (b) Pore size distribution.

2.2.3. HRTEM analysis

High-resolution transmission electron microscopy (HRTEM) is a unique equipment in the investigation of local structure and chemistry of the catalyst particles dispersion. It also offers the microdiffraction pattern images and the reaction mechanisms that can be derived from the TEM analysis. HRTEM analysis is carried out using a JEOL JEM F-200 microscope. Pd nanoparticles are well dispersed on the Al_2O_3 support for monometallic catalyst without any aggregate formation as shown in Fig. 4 (a). The selected area electron diffraction (SAED) pattern represents homogeneously distributed Pd particles on the support with nano-crystalline phase behavior as shown in Fig. 4(b). The concentric ring-like structure reveals that the palladium is polycrystalline in nature. A typical HRTEM image of a fresh Pd/Al_2O_3 catalyst reveals a very narrow particle size distribution with an average particle size of 2.145 ± 0.092 nm as shown in Fig. 4(c). The Energy dispersive X-ray spectroscopy (EDX) measurements for the Pd/Al_2O_3 of mapping image for all the elemental composition particles together are shown in Fig. 4(d). The elemental composition of individual metal/oxide species are represented in Fig. 4(e–g) for palladium, alumina, and oxygen for a wavelength of 100 nm. This complete data indicates the proportional distribution of Pd particles on Al_2O_3 with homogeneous phase formation.

3. Hydrogenation experiments

3.1. Thermal screening test (TSU)

Thermal screening unit (TSU) is an experimental unit extensively used for quick screening of liquids, solids and heterogeneous systems for testing runaway conditions of the reaction. It provides data for "onset temperatures" of the reactions, temperature increase rates, and most importantly the rates and magnitudes of pressure rise in chemical systems. Reactive chemical testing includes evaluating feeds, intermediates, and products for thermal stability to precisely assess

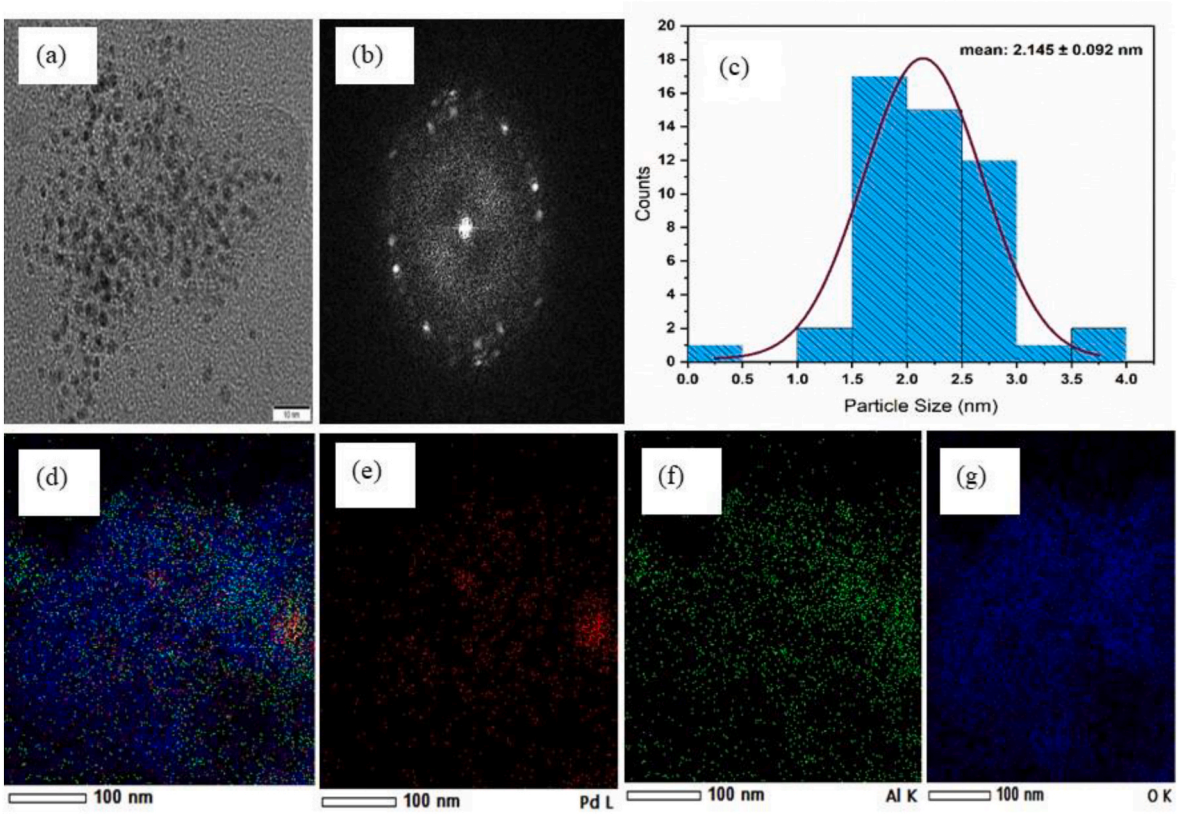

Fig. 4. HRTEM analysis for Pd/Al_2O_3 catalyst(a) HRTEM image, (b) SAED pattern, (c) particle size distribution (d) Overall energy dispersive X-ray spectroscopy (EDX) mapping image (e)–(g) EDS mapping images of a representative part of the sample containing palladium, aluminum, and oxygen.

hazardous nature during storage, production and transportation. The TSU is operated at a ramp rate of 2 °C/min from ambient to 180 °C and a pressure of 60 bar as shown in Fig. 5. As the hydrogenation takes place, the pressure decreased to 44 bar and the increase in temperature and pressure with time is represented in Fig. 5(a). Further, experimental investigation of quinoline in isopropyl alcohol in the present reaction is safe and does not carry any hazards from TSU as evident from Fig. 5(b). This can be justified as there is no sudden rise in temperature and pressure observed from TSU through out the reaction for 8 h. The dT/dt plot is represented for 150 min for better representation of change in temperature during the reaction. This forms the basis for performing reactions at high-pressure conditions in converting the hydrogenation of quinoline to decahydroquinoline.

3.2. Hydrogenation in autoclave reactor

Quinoline hydrogenation is performed for quinoline quantity of 3 ml in 30 ml of isopropanol with 654 mg of Pd/Al_2O_3 catalyst (20 wt% Pd/Al_2O_3) using 100 ml autoclave reactor. The schematic of the Autoclave reactor set-up for high pressure reactions along with product separation and sample anlaysis is shown in Fig. 6. The autoclave is also purged with nitrogen followed by hydrogen from the reservoir to prevent oxide formation due to the presence of residual air in the reactor. The reactor is maintained in the pressure range from 40 to 60 bar and is operated in the temperature range from 50 to 175 °C for different reaction times of 1–6 h. The downstream process consists of filtration followed by evaporation using rotavapor to separate the catalyst and solvent. The reaction products are analyzed by Agilent gas chromatography (GC) equipped with HP-5 capillary column (Dimensions are: 30 m × 0.32 mm × 0.25 μm ID) using flame ionization detector maintained at 280 °C with a flowrate of 0.8 ml/min using nitrogen as carrier gas. The split ratio of 1:1 and sample injection volume of 1 μL at a temperature of 250 °C is used for the analysis. GC method is set as follows: The column temperature is increased from room temperature to 80°C at a ramping rate of 5 °C/min. Further, it is increased from 80 to 280 °C at a heating rate of 10 °C/min with a hold time of 1 min at 80 °C.

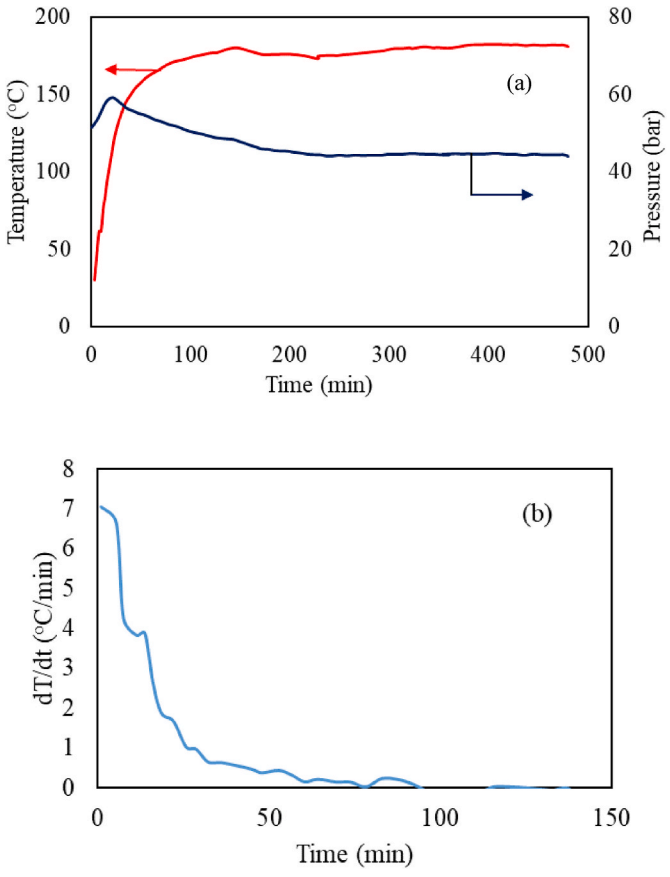

Fig. 5. Thermal screening test for (a) temperature variation (b) differential thermal analysis of quinoline with IPA in isothermal mode.

4. Results and discussion

The activated hydrogen atoms on the catalyst surface react with quinoline leading to the formation of metal-hydrogen complex. This complex involves the interaction of hydrogen species with quinoline molecules. The hydrogenation of quinoline can occur at multiple positions on the aromatic ring leading to various possible hydrogenated products (py-THQ, bz-THQ and DHQ). The selectivity of the reaction is influenced by the catalyst and reaction conditions. The key factors influencing the reaction are catalyst and reaction conditions such as temperature, pressure, solvent and time which play an important role in determining the reaction rates, yield, and selectivity towards product formation. The effect of reaction parameters is investigated and conversion of 100% is obtained under optimal conditions.

4.1. Effect of temperature

The effect of reaction temperature on quinoline hydrogenation is studied at temperatures of 75 °C, 100 °C, 125 °C, 150 °C and 175 °C at 50 bar for 5 h reaction. It is observed that complete conversion of quinoline for all temperatures with intermediates or product formation. The catalyst and substrate molecules activates more readily at higher temperatures. It is observed that low temperature favors py-THQ formation as shown in Fig. 7. The reaction scheme shows that py-THQ and bz-THQ are intermediate products while DHQ is the final product. It is clear that there is a gradual decrease in intermediate formation and an increase in DHQ formation with increase in temperature.

At the reaction temperature of 175 °C, the yield of DHQ is increased to nearly 99.41%. A little amount of bz-THQ is observed in the temperature range of 75 °C–125 °C and is negligible for 150°C and 175°C. The increase in amount of DHQ is equivalent to the decrease in amount of py-THQ approximately. It indicates that hydrogenation of quinoline first occurred on the N-heterocycle ring of quinoline which resulted in py-THQ and bz-THQ formation and are further hydrogenated to DHQ formation. The product distribution and performance analysis showed that temperature of 175 °C and pressure of 50 bar are optimized conditions for 5 h of reaction time to obtain more than 99% pure DHQ as the desired product. The effect of reaction temperature on hydrogen uptake is studied at temperatures from 75°C, 100°C, 125°C, 150°C, and 175 °C for 50 bar at 5 h reaction time. Low temperature favors py-THQ formation as shown in Fig. 7 (b), hence, hydrogen uptake capacities of 2.16%, 2.76%, and 2.81% for 40 bar, 50 bar, and 60 bar pressures at 75°C, respectively. With the increase in reaction temperature, hydrogen uptake of Quinoline increased drastically leading to the formation of DHQ. The reported literature also has a similar effect with respect to temperature on hydrogen uptake capacities [34]. Hydrogen uptake of quinoline increased to nearly 6.91 wt% at an optimum reaction temperature of 175°C and pressure of 50 bar for 5 h reaction time. A negligible amount of hydrogen uptake of quinoline via bz-THQ is observed in the temperature range from 75 °C to 125 °C as evident in Fig. 7(b).

4.2. Effect of hydrogen pressure

The effect of pressure on quinoline hydrogenation is studied at different pressures of 40, 50, and 60 bar at 175°C for 5 h reaction time and there is a complete conversion of quinoline observed for all the pressures. The selectivity towards py-THQ is higher at 40 bar and 75 °C with an yield of 95.97% as shown in Fig. 8 (a). The bz-THQ formation of less than 3.5% is observed as shown in Fig. 8(b). The maximum

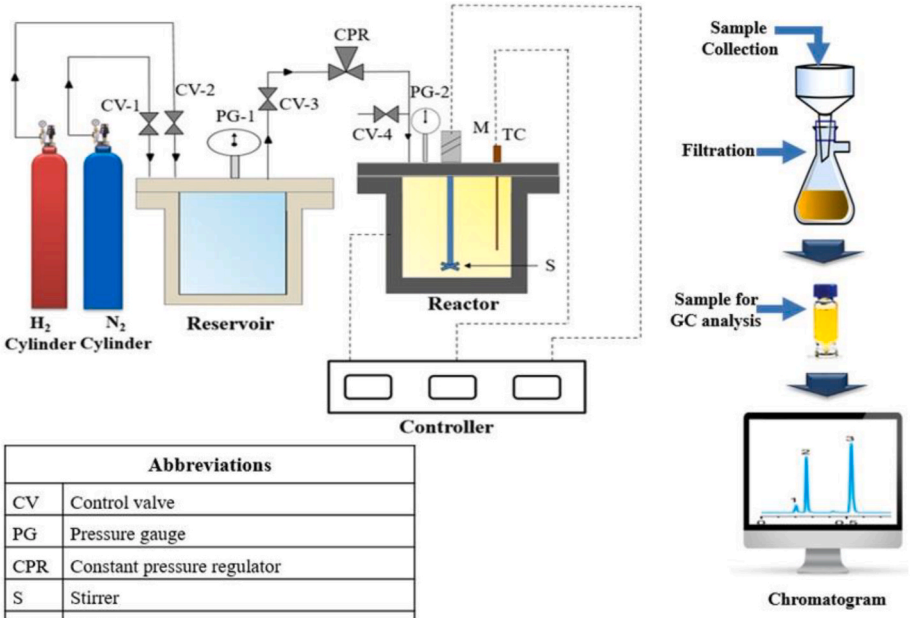

Abbreviations	
CV	Control valve
PG	Pressure gauge
CPR	Constant pressure regulator
S	Stirrer
M	Motor
TC	Thermocouple

Fig. 6. Schematic of the autoclave batch reactor for Quinoline hydrogenation.

formation of DHQ is observed for temperatures beyond 100 °C at 50 bar as shown in Fig. 8 (c). The py-THQ formation is higher in comparison to DHQ at low temperatures with an increase in pressures. The yield of DHQ increased to nearly 99.41% when the pressure was increased to 50 bar. Higher pressures of hydrogen gas can increase the rate of reaction, resulting in a higher yield of DHQ. This is due to an increase in pressure forces increasing the rate of reaction between hydrogen and quinoline molecules. Although the reaction rate increases with an increase in pressure for py-THQ and bz-THQ formation, the rate of DHQ formation decreases at 60 bar which may be due to thermodynamic equilibrium for the desired product. The pressure of hydrogen gas encourages the solubility of molecular hydrogen in solvent causing an increased number of reactive hydrogen atoms over palladium. Generally, LOHCs require high-pressure synthesis conditions to facilitate efficient hydrogen uptake by the LOHCs [10]. Higher pressures of hydrogen gas can increase the rate of reaction, resulting in a higher yield of DHQ.

The hydrogen uptake of quinoline in the form of py-THQ is increased at 60 bar and 75 °C with hydrogen uptake of 2.81% as shown in Fig. 9 (a). It is observed that hydrogen uptake of quinoline is very negligible (<0.1%) for almost all the conditions in the form of bz-THQ for the temperature range of 75 °C–125 °C as shown in Fig. 9(b). The maximum hydrogen uptake of 6.91% is observed for 175°C and 50 bar as shown in Fig. 9(c).

4.3. Effect of catalyst loading

The quantity of catalyst for hydrogenation of quinoline is an important influencing factor in the process development in the context of reactor design and scale-up of the processes. Therefore, the effect of the catalyst loading on quinoline hydrogenation is studied using different loadings (5 wt%, 10 wt%, and 20 wt%) at optimum temperature and pressure of 50 bar and 175 °C for 5 h reaction time. It is observed that with an increase in the catalyst loading, py-THQ formation decreased and DHQ formation increased. The increase in catalyst loading increases the number of catalytic sites available for the quinoline hydrogenation. Therefore, it is observed that with an increase in catalyst loadings from 5 wt% to 20 wt%, there is a drastic increment in DHQ yield from 12.55% to 99.41% as shown in Fig. 10(a).

The effect of catalyst loading on hydrogen uptake at 5 wt%, 10 wt%, and 20 wt% is studied with respect to the reactant fed to the system. It is observed that increase in the catalyst loading, increased the rate of hydrogen uptake due to favorable conditions for DHQ formation. Thus, hydrogen uptake of quinoline increases with the increase in the formation of DHQ as shown in Fig. 10(b). Hydrogen uptake of quinoline is observed to be maximum at 20 wt% catalyst with a capacity of 6.91%.

4.4. Effect of solvent

The effect of solvent on the activity of the Pd/Al_2O_3 catalyst is investigated using water, isopropyl alcohol, and toluene for quinoline hydrogenation for optimal conditions of 50 bar, 175°C and for 5 h reaction time. Since the properties of the solvents can modify reaction mechanistic features by affecting the reactant free energy states which can modify the viability of various reaction pathways [35]. As shown in Fig. 11(a), the catalyst activity is significantly influenced by the use of solvent in the following sequence: IPA > toluene > water. The results suggest that the solvent with stronger polarity promotes the hydrogenation of quinoline over the Pd/Al_2O_3 catalyst which is consistent with the reported literature [32]. Water as a solvent is least suitable as it favors the formation of py-THQ and results in a low DHQ yield of 77.28%. The highest yield of DHQ was obtained (99.52%) by using IPA as a solvent. In addition to this hydroxyl group of the polar solvent interaction with the heteroatom of the quinoline, it helps to increase the solubility and availability of the substrate in the reaction medium.

Therefore, the choice of solvent plays an important role in enhancing the complete hydrogenation of quinoline to DHQ. The yield of quinoline intermediates and their product is studied for the effect of solvent and on the product yield is represented in Fig. 11(a). Water as a solvent is less suitable in comparison to the other two solvents with 2.68 wt% of H_2 uptake by Quinoline whereas toluene and isopropyl alcohol show nearly the same effect on H_2 uptake. It can be concluded that H_2 uptake of 6.91 % using isopropyl alcohol is the most suitable solvent for Quinoline as LOHC to DHQ formation as shown in Fig. 11(b).

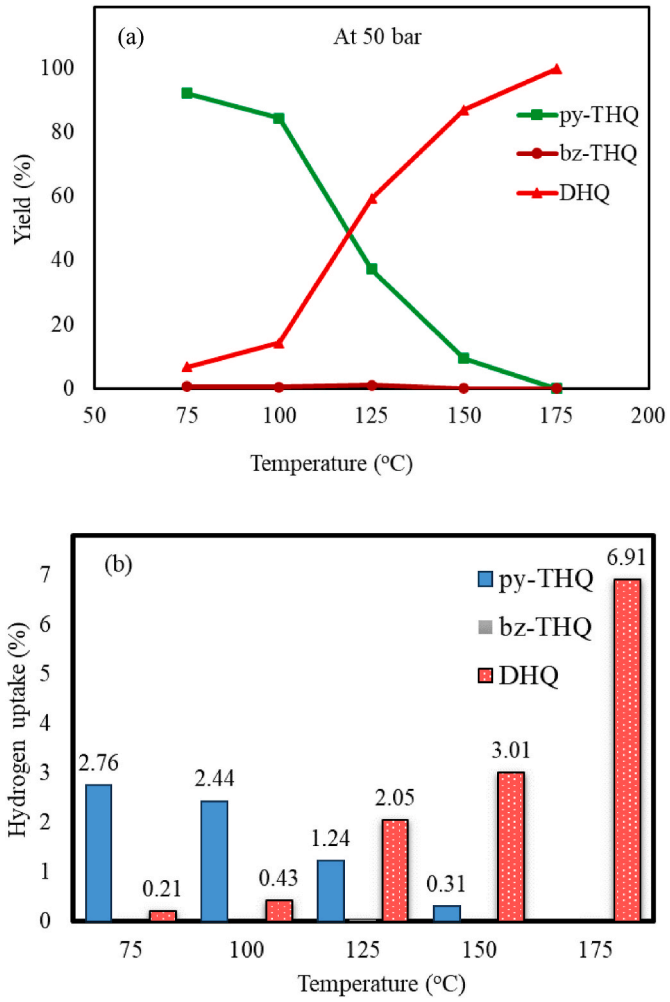

Fig. 7. Effect of temperature at 50 bar for 5 h reaction time on a) Yield b) Hydrogen uptake of py-THQ, bz-THQ, and DHQ.

4.5. Reaction mechanism

In quinoline hydrogenation, py-THQ and bz-THQ are the intermediates leading to DHQ formation through two different pathways: (i) Quinoline to intermediates formation (1,2,3,4 tetrahydroquinoline (py-THQ)/5,6,7,8-tetrahydroquinoline (bz-THQ)) (ii) conversion of intermediates to product (DHQ) formation through 2 different pathways as shown in Fig. 1 [18,32]. Heteroatom 'N' containing aromatic ring in quinoline is more prone to hydrogenation over the benzene ring because the C–N bond energy of 305 kJ/mol which is much less than the C=C bond energy of 614 kJ/mol. The molecular hydrogen already adsorbed on the active site of the catalyst is easily available for hydrogenating the pyridine ring due to the lone pair of electrons of nitrogen atom to py-THQ and presence of the heteroatom in the ring. Hence, hydrogenation of heterocyclic ring is more favorable than homocyclic benzene ring. The physical properties of the quinoline such as thermal stability, high gravimetric hydrogen densities, high storage capacity can alter the thermodynamic driving force and hydrogenation/dehydrogenation under reversible conditions [30]. As reported in the literature, heterocyclic compounds need low temperatures for dehydrogenation with decreased enthalpy and faster hydrogen release ability [5,30]. Hence, major quantity of primary intermediate (py-THQ) product is formed [32–38]. The increase in temperature can disrupt the C–N bonds of nitrogen-containing heterocyclic compounds to a great extent in selectivity of DHQ through py-THQ via path 1 of the reaction mechanism [38]. Therefore, the reaction mechanism for hydrogenation of quinoline

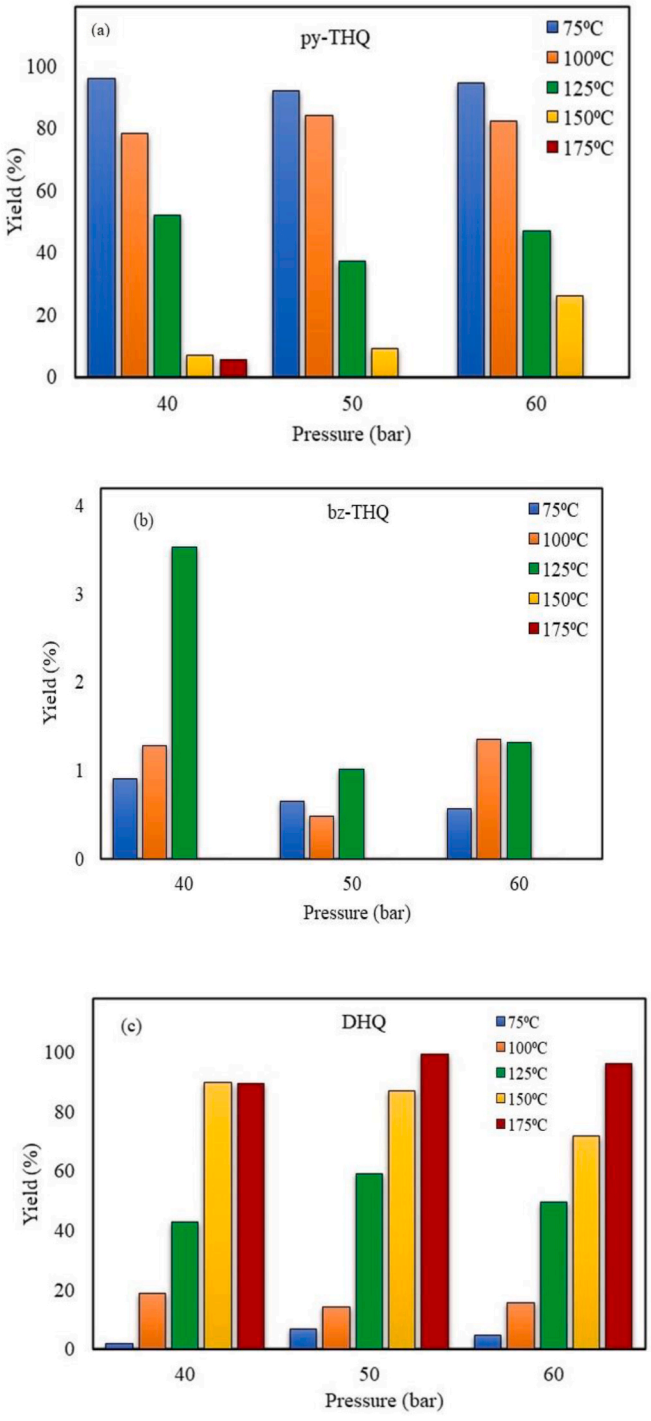

Fig. 8. Effect of pressure on yield of (a) py-THQ (b) bz-THQ, and (c) DHQ at different reaction temperatures ranging from 75°C to 175°C for 5 h reaction time.

to DHQ formation for Pd/Al_2O_3 catalyst is simplified [38] as shown in Fig. 12.

5. Kinetic model development and validation

5.1. Power law kinetic model

Kinetic model is developed based on the reaction scheme and experimental observations for quinoline to py-THQ, bz-THQ and DHQ formation. Although hydrogenation of heterocyclic compounds

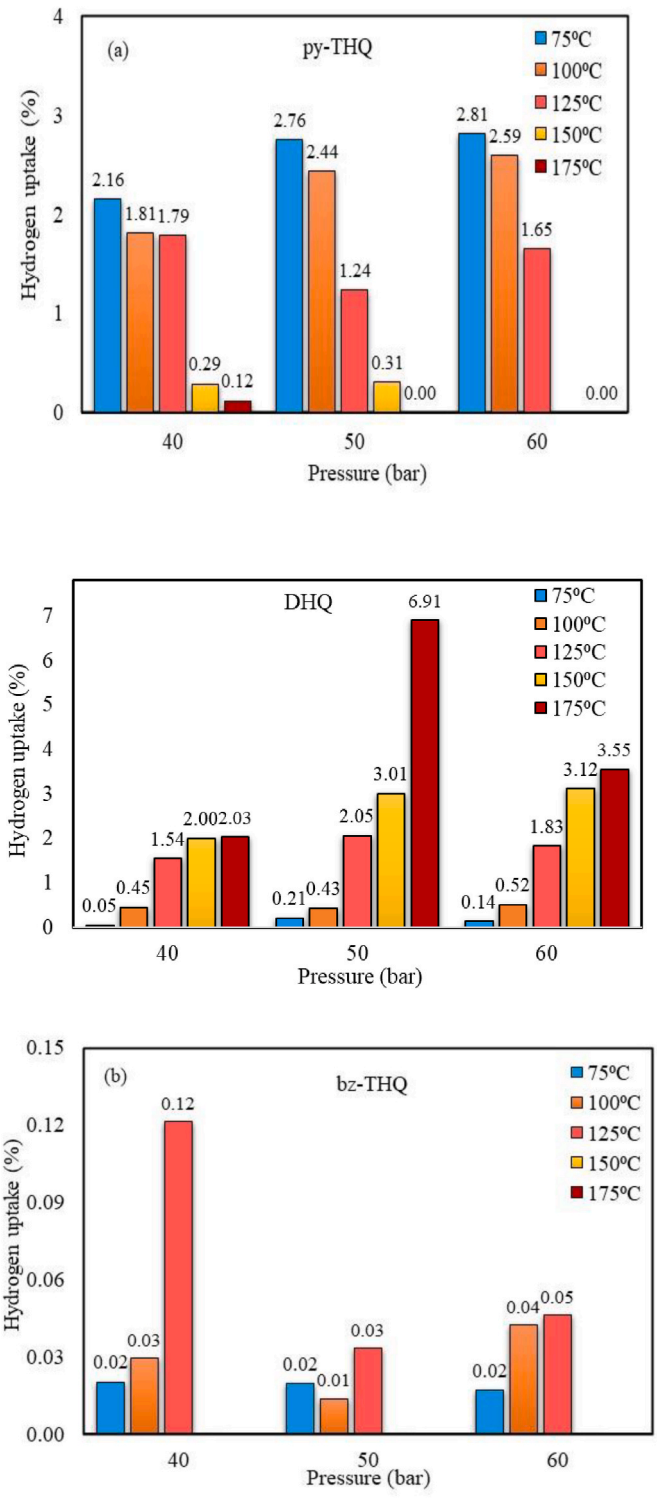

Fig. 9. Effect of pressure on hydrogen uptake of (a) py-THQ (b)bz-THQ, and (c) DHQ at different reaction temperature range from 75°C to 175°C for 5 h reaction time.

containing nitrogen have been published in literature, the reported kinetics information for quinoline hydrogenation is insufficient for development of processes and scale up of the reactors. In the present study, intermediates formed from quinoline are of py-THQ in high and bz-THQ in low quantity. The absence of bz-THQ may be due to nitrogen heterocyclic rings have a higher electronic cloud density than benzene rings and are more easily adsorbed on the active sites of hydrogenation

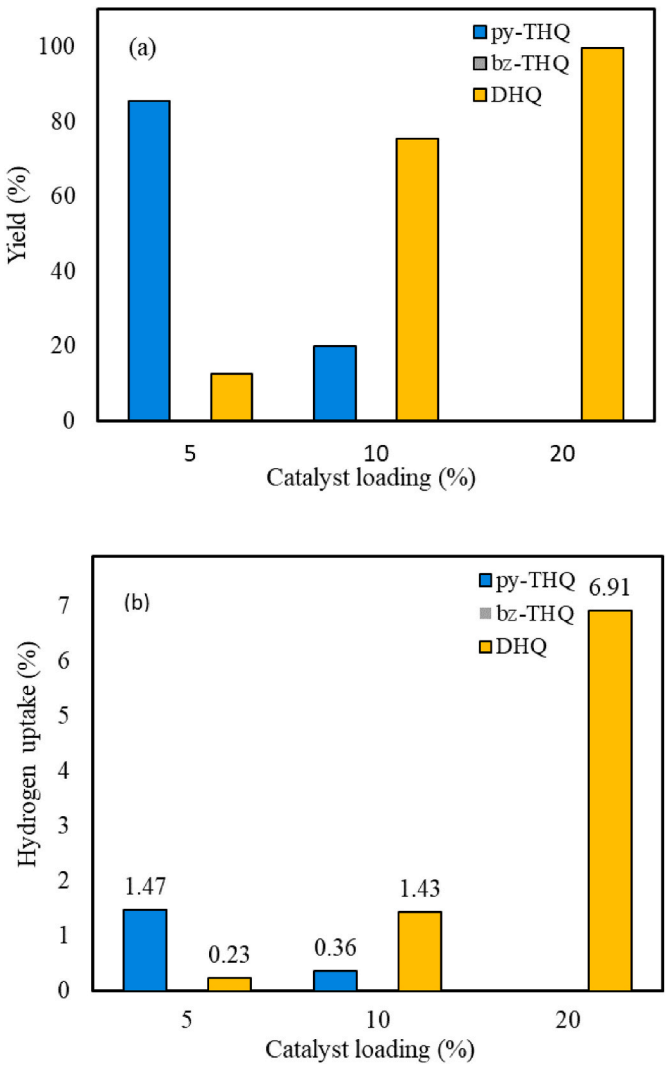

Fig. 10. Effect of catalyst loading at 175°C and 50 bar for 5 h reaction time on (a) Yield of products and (b) Hydrogen uptake.

reactions. Considering the concentration of the hydrogenated species, the following assumptions are considered for development of power law kinetic model into the simplified form.

i) Concentration of the hydrogen is assumed to be constant as it is in excess in the reaction
ii) No Mass Transfer Limitations: It is assumed that the reactants are perfectly mixed and there are no mass transfer limitations. This implies that the rate of reaction is solely dependent on the chemical kinetics and not on the rate of mixing or diffusion.
iii) Quinoline to py-THQ reaction is assumed to be reversible [37].
iv) py-THQ to DHQ reaction is assumed to be irreversible [37].

The kinetic model developed based on the following assumptions and the volume of the reaction mixture used for quinoline hydrogenation with following rate expresssions:

$$r_A = \frac{dC_A}{dt} = \frac{m_{cat}}{V}(-k_1 C_A + k_{1r} C_B) \quad (1)$$

$$r_B = \frac{dC_B}{dt} = \frac{m_{cat}}{V}(k_1 C_A - k_{1r} C_B - k_2 C_B) \quad (2)$$

$$r_C = \frac{dC_C}{dt} = \frac{m_{cat}}{V}(k_2 C_B) \quad (3)$$

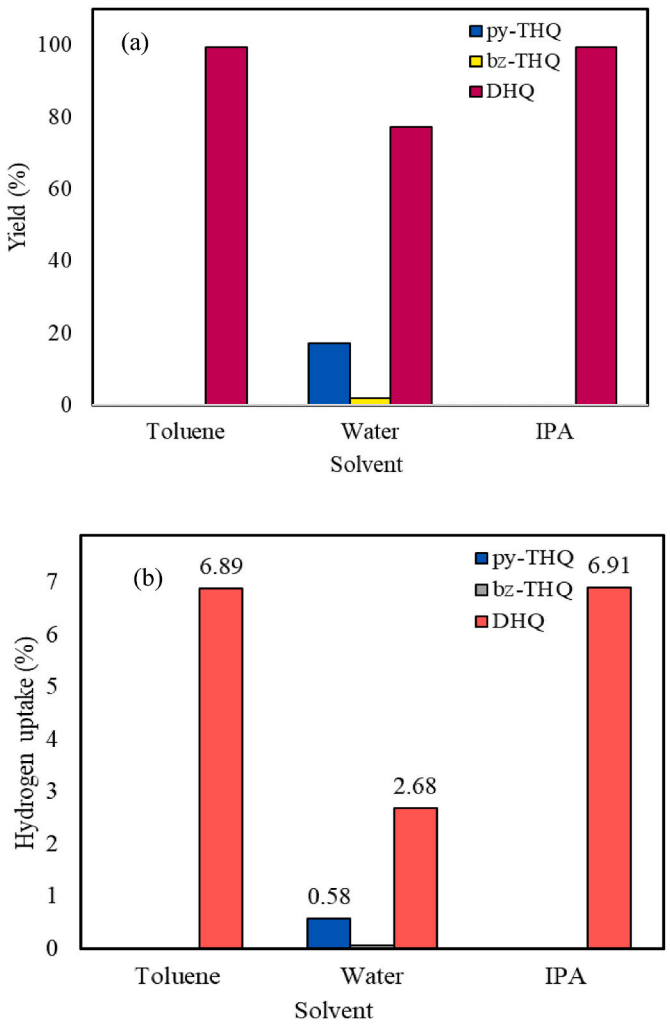

Fig. 11. Effect of solvent at 175°C and 50 bar for 5 h reaction time on a) Yield of DHQ b) Hydrogen uptake.

Where.

r is reaction rate, mol/(m^3.min)
m_{cat} represents catalyst loading, g
k is rate constant, $m^3/(g_{cat}.min)$
C_A, C_B and C_C are concentrations (mol/m^3) of reactants A, B and C, respectively
V is volume of the reaction mixture, m^3

5.2. Kinetic study and validation with model

Hydrogenation experiments are performed for temperatures of 125°C, 150°C and 175°C at a pressure of 50 bar for the reaction times of 1, 3, 5 and 6 h. The concentration of the reactant, intermediate and product species (quinoline, pz-THQ and DHQ) are represented as C_A, C_B and C_C, respectively. The concentration of the species for every 1 h of reaction at different temperatures are shown in Fig. 13. The quinoline concentration decreased abruptly while formation of pz-THQ predominates simultaneously.

At the same time, the rate of formation of DHQ prevails at the expense of pz-THQ hydrogenation. There is a gradual decrease in pz-THQ concentration and increase in DHQ concentration is observed with increase in reaction time at 125°C and 150°C as shown in Fig. 13 (a–b). On the other hand, there is a sudden decrease in pz-THQ and increase in DHQ formation in 1 h of reaction time as shown in Fig. 13(c). As there is no driving force for the backward reaction to take place, the product formation suppresses the existence of reactant and intermediates. The experimental data points are used for model prediction and validated in the same Fig. 13(a–c).

5.3. Parameter estimation

The kinetic parameters are estimated using experimental data points and model predictions. The models represented in the above equations ((1) to (3)) are used using the Markov Chain Monte Carlo (MCMC) simulation tool to solve the ordinary differential equations numerically. The kinetic parameters are estimated by fitting the experimental data with the model using Guassian distribution in the MCMC tool. Each reaction rate constant (k_1, k_{1r} and k_2) is determined as a parameter, and the best-fitting value was estimated by minimizing the sum of the square error of the concentration between the experimental data and the model calculation. The evaluated kinetic parameters, activation energy and pre-exponential factor, are estimated from Fig. 13(d) and are reported in Table 2. The regression results for the Arrhenius parameters are convincing as all the R^2 values exceed 0.99. The changing trend of the pre-exponential factor is consistent with that of activation energy. It is observed that the quinoline to py-THQ formation reaction had the largest activation energy of 136.57 kJ/mol and the pre-exponential factor of 1.203×10^{16}, hence, it is envisaged that quinoline to pz-THQ formation controls the rate of reaction. Indeed, Xie et al. (2022) also found the same observation as quinoline hydrogenation to py-THQ is the rate-determining step [37].

6. Conclusions

Quinoline is identified as a promising and thermally stable LOHC molecule using a thermal screening unit. Hydrogenation of quinoline is investigated over a palladium supported by an alumina catalyst. The effect of temperature, hydrogen pressure, reaction time, different solvents, and catalyst loading on the hydrogenation and hydrogen uptake capacity of quinoline in the liquid phase are studied and the optimal conditions of 175°C and 50 bar at 5 h reaction for 20 wt% of Pd/Al_2O_3 are obtained. The Hydrogen uptake capacity of 6.91 wt% is achieved with more than 99% DHQ yield using IPA as solvent under optimal reaction conditions. Based on the experimental data, the reaction mechanism proposed to follow via quinoline to py-THQ and to DHQ formation reaction pathway. The hydrogenation of quinoline to DHQ formation is 100% and selectivity towards decahydroquinoline of 99% is achieved. The reaction kinetic model is developed for a simplified reaction path for DHQ formation and is simulated using the Markov Chain

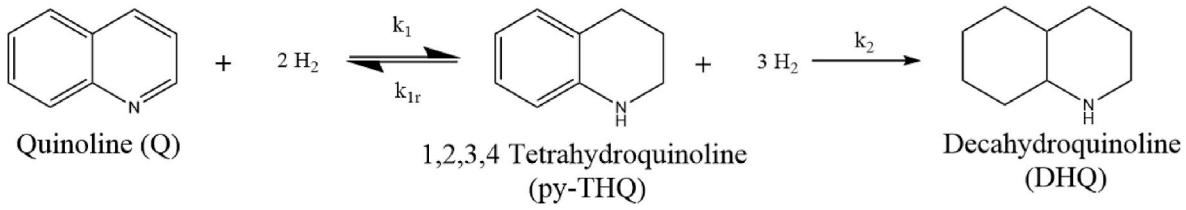

Fig. 12. Possible reaction mechanism for hydrogenation of Quinoline to DHQ.

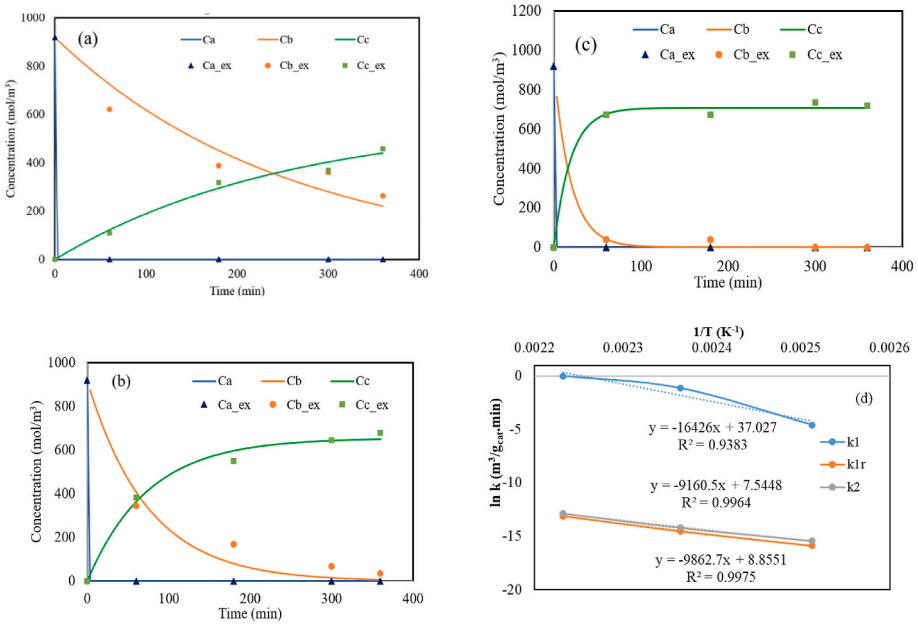

Fig. 13. Concentration profiles for hydrogen pressure at 50 bar for different temperatures (a)125°C (b) 150°C and (c) 175°C (d) Rate constants ("—" represents the model and symbols represent experimental data points).

Table 2
Estimated rate constants and Arrhenius Parameters for hydrogenation of quinoline to py-THQ and py-THQ to DHQ formation.

Rate constant (m^3/(gcat.min))	Temperature (°C)			Activation energy, E_a (kJ/mol)	Pre-exponential factor, k_o (m3/(gcat.min))	(Residual)^2 R^2)
	125	150	175			
k_1	1.0e-02	3.3e-01	3.7e-03	136.57	1.20e+16	0.99
k_{1r}	1.3e-07	4.8e-07	2.0e-06	82.00	1890.88	0.99
k_2	1.99e-7	6.80e-7	2.6e-06	76.16	7010.05	0.99

Monte Carlo (MCMC) simulation tool and validated with experimental data. It is concluded from the kinetic study that the formation of pz-THQ is the rate-determining step in the hydrogenation of quinoline to deca-hydroquinoline formation.

CRediT authorship contribution statement

Farahanaz M. Bagwan: Writing – original draft, Visualization, Validation, Software, Formal analysis, Data curation. **Anil K. Kinage:** Writing – review & editing, Visualization, Supervision, Resources, Project administration, Investigation, Funding acquisition, Conceptualization. **Satyam Naidu Vasireddy:** Writing – review & editing, Visualization, Validation, Supervision, Software, Resources, Methodology, Investigation, Formal analysis, Conceptualization.

Declaration of competing interest

The authors declare that they have no known competing financial interests or personal relationships that could have appeared to influence the work reported in this paper.

Acknowledgement

The authors are thankful to the funding agency for sponsoring for Development of versatile liquid organic hydrogen carrier (VLOHC) project (project code: HCP44-03) under the Hydrogen Technology (H_2T) mission supported by CSIR-Hqrs., Govt. of India and central analytical facility (CAF) division for providing analysis facilities at CSIR-NCL Pune.

References

[1] Sage V, Patel J, Hazewinkel P, Yasin QUA, Wang F, Yang Y, et al. Recent progress and techno-economic analysis of liquid organic hydrogen carriers for Australian renewable energy export – a critical review. Int J Hydrogen Energy 2024;56:1419–34. https://doi.org/10.1016/j.ijhydene.2023.12.269.
[2] Chen X, Gierlich CH, Schötz S, Blaumeiser D, Bauer T, Libuda J, et al. Hydrogen production based on liquid organic hydrogen carriers through sulfur doped platinum catalysts supported on TiO_2. ACS Sustain Chem Eng 2021;9:6561–73. https://doi.org/10.1021/acssuschemeng.0c09048.
[3] Faye O, Szpunar J, Eduok U. A critical review on the current technologies for the generation , storage , and transportation of hydrogen. Int J Hydrogen Energy 2022;47:13771–802. https://doi.org/10.1016/j.ijhydene.2022.02.112.
[4] Yadav V, Sivakumar G, Gupta V, Balaraman E. Recent advances in liquid organic hydrogen carriers: an alcohol-based hydrogen economy. ACS Catal 2021;11:14712–26. https://doi.org/10.1021/acscatal.1c03283.
[5] Crabtree RH. Hydrogen storage in liquid organic heterocycles. Energy Environ Sci 2008;1:134–8. https://doi.org/10.1039/b805644g.
[6] Cao Y, Ding L, Qiu Z, Zhang H. Biomass-derived N-doped porous two-dimensional carbon nanosheets supported ruthenium as effective catalysts for the selective hydrogenation of quinolines under mild conditions. Catal Commun 2020;143. https://doi.org/10.1016/j.catcom.2020.106048.
[7] Makaryan IA, Sedov IV. Hydrogenation/dehydrogenation catalysts for hydrogen storage systems based on liquid organic carriers (A review). Pet Chem 2021;61:977–88. https://doi.org/10.1134/S0965544121090085.
[8] Spatolisano E, Restelli F, Matichecchia A, Pellegrini LA, Angelis AR De, Cattaneo S, et al. Assessing opportunities and weaknesses of green hydrogen transport via LOHC through a detailed techno-economic analysis. Int J Hydrogen Energy 2023;52:703–17. https://doi.org/10.1016/j.ijhydene.2023.08.040.
[9] Kim TW, Jeong H, Baik JH, Suh YW. State-of-the-art catalysts for hydrogen storage in liquid organic hydrogen carriers. Chem Lett 2022;51:239–55. https://doi.org/10.1246/cl.210742.
[10] Tsogt N, Gbadago DQ, Hwang S. Exploring the potential of liquid organic hydrogen carrier (LOHC) system for efficient hydrogen storage and transport: a techno-economic and energy analysis perspective. Energy Convers Manag 2024;299:117856. https://doi.org/10.1016/j.enconman.2023.117856.
[11] Gianotti E, Taillades-Jacquin M, Rozière J, Jones DJ. High-purity hydrogen generation via dehydrogenation of organic carriers: a review on the catalytic process. ACS Catal 2018;8:4660–80. https://doi.org/10.1021/acscatal.7b04278.

[12] Rao N, Lele AK, Patwardhan AW. Optimization of liquid organic hydrogen carrier (LOHC) dehydrogenation system. Int J Hydrogen Energy 2022;47:28530–47. https://doi.org/10.1016/j.ijhydene.2022.06.197.
[13] Markiewicz M, Zhang YQ, Empl MT, Lykaki M, Thöming J, Steinberg P, et al. Hazard assessment of quinaldine-, alkylcarbazole-, benzene- and toluene-based liquid organic hydrogen carrier (LOHCs) systems. Energy Environ Sci 2019;12:366–83. https://doi.org/10.1039/c8ee01696h.
[14] Teichmann D, Arlt W, Wasserscheid P. Liquid Organic Hydrogen Carriers as an efficient vector for the transport and storage of renewable energy. Int J Hydrogen Energy 2012;37:18118–32. https://doi.org/10.1016/j.ijhydene.2012.08.066.
[15] Niermann M, Beckendorff A, Kaltschmitt M, Bonhoff K. Liquid organic hydrogen carrier (LOHC) – assessment based on chemical and economic properties. Int J Hydrogen Energy 2019;44:6631–54. https://doi.org/10.1016/j.ijhydene.2019.01.199.
[16] Safronov SP, Vostrikov SV, Samarov AA, Wasserscheid P, Müller K, Verevkin SP. Comprehensive thermodynamic study of substituted indoles/perhydro indoles as potential liquid organic hydrogen carrier system. Fuel 2023;331. https://doi.org/10.1016/j.fuel.2022.125764.
[17] Preuster P, Papp C, Wasserscheid P. Liquid organic hydrogen carriers (LOHCs): toward a hydrogen-free hydrogen economy. Acc Chem Res 2017;50:74–85. https://doi.org/10.1021/acs.accounts.6b00474.
[18] Aakko-Saksa PT, Cook C, Kiviaho J, Repo T. Liquid organic hydrogen carriers for transportation and storing of renewable energy – review and discussion. J Power Sources 2018;396:803–23. https://doi.org/10.1016/j.jpowsour.2018.04.011.
[19] Yang M, Dong Y, Fei S, Pan Q, Ni G, Han C, et al. Hydrogenation of N-propylcarbazole over supported ruthenium as a new prototype of liquid organic hydrogen carriers (LOHC). RSC Adv 2013;3:24877–81. https://doi.org/10.1039/c3ra44760j.
[20] Vostrikov SV, Konnova ME, Turovtsev VV, Verevkin SP. Thermodynamics of hydrogen storage: LOHC system 1-alkyl-indole/octahydro-1-alkyl-indole. Fuel 2023;344:128079. https://doi.org/10.1016/j.fuel.2023.128079.
[21] Verevkin SP, Safronov SP, Samarov AA, Vostrikov SV. Hydrogen storage: thermodynamic analysis of alkyl-quinolines and alkyl-pyridines as potential liquid organic hydrogen carriers (LOHC). Appl Sci 2021;11. https://doi.org/10.3390/app112411758.
[22] Kokane R, Corre Y, Kemnitz E, Dongare MK, Agbossou-Niedercorn F, Michon C, et al. Palladium supported on magnesium hydroxyl fluoride: an effective acid catalyst for the hydrogenation of imines and N-heterocycles. New J Chem 2021;45:19572–83. https://doi.org/10.1039/d1nj03760a.
[23] Prajapati SM, Patel KD, Vekariya RH, Panchal SN, Patel HD. Recent advances in the synthesis of quinolines: a review. RSC Adv 2014;4:24463–76. https://doi.org/10.1039/c4ra01814a.
[24] Matada BS, Pattanashettar R, Yernale NG. A comprehensive review on the biological interest of quinoline and its derivatives. Bioorganic Med Chem 2021;32. https://doi.org/10.1016/j.bmc.2020.115973.
[25] Timelthaler D, Topf C. Heterogeneous hydrogenation of quinoline derivatives effected by a granular cobalt catalyst. Synth Met 2021;54:629–42. https://doi.org/10.1055/a-1654-3302.
[26] Yu CY, Hatcher WJ, Bertsch W. Hydrodenitrogenation of quinoline with Y-type zeolite. Ind Eng Chem Res 1989;28:13–20. https://doi.org/10.1021/ie00085a004.
[27] Massoth FE, Kim SC. Kinetics of the HDN of quinoline under vapor-phase conditions. Ind Eng Chem Res 2003;42:1011–22. https://doi.org/10.1021/ie020390t.
[28] Nguyen MT, Tayakout-Fayolle M, Pirngruber GD, Chainet F, Geantet C. Kinetic modeling of quinoline hydrodenitrogenation over a NiMo(P)/Al2O3 catalyst in a batch reactor. Ind Eng Chem Res 2015;54:9278–88. https://doi.org/10.1021/acs.iecr.5b02175.
[29] Aboul-Gheit AK. The kinetics of quinoline hydrodenitrogenation through reaction intermediate products. Can J Chem 1975;53:2575–9. https://doi.org/10.1139/v75-366.
[30] Gemechu DN, Mohammed AM, Redi M, Bessarabov D, Mekonnen YS, Obodo KO. First principles-based approaches for catalytic activity on the dehydrogenation of liquid organic hydrogen carriers: a review. Int J Hydrogen Energy 2023;48:33186–206. https://doi.org/10.1016/j.ijhydene.2023.05.072.
[31] Ren D, He L, Yu L, Ding RS, Liu YM, Cao Y, et al. An unusual chemoselective hydrogenation of quinoline compounds using supported gold catalysts. J Am Chem Soc 2012;134:17592–8. https://doi.org/10.1021/ja3066978.
[32] Campanati M, Vaccari A, Piccolo O. Mild hydrogenation of quinoline 1. Role of reaction parameters. J Mol Catal Chem 2002;179:287–92. https://doi.org/10.1016/S1381-1169(01)00401-0.
[33] Aakko-Saksa PT, Cook C, Kiviaho J, Repo T. Liquid organic hydrogen carriers for transportation and storing of renewable energy – review and discussion. J Power Sources 2018;396:803–23. https://doi.org/10.1016/j.jpowsour.2018.04.011.
[34] Sotoodeh F, Smith KJ. Kinetics of hydrogen uptake and release from heteroaromatic compounds for hydrogen storage. Ind Eng Chem Res 2010;49:1018–26. https://doi.org/10.1021/ie9007002.
[35] Ren Y, Wang Y, Li X, Zhang Z, Chi Q. Selective hydrogenation of quinolines into 1,2,3,4-tetrahydroquinolines over a nitrogen-doped carbon-supported Pd catalyst. New J Chem 2018;42:16694–702. https://doi.org/10.1039/c8nj04014a.
[36] Hu X, Chen Y, Huang B, Liu Y, Huang H, Xie Z. Pd-supported N/S-codoped graphene-like carbons boost quinoline hydrogenation activity. ACS Sustain Chem Eng 2019;7:11369–76. https://doi.org/10.1021/acssuschemeng.9b01015.
[37] Xie D, Liu X, Lv H, Guo Y. Products, pathways, and kinetics for catalytic hydrodenitrogenation of quinoline in hydrothermal condition. J Supercrit Fluids 2022;182. https://doi.org/10.1016/j.supflu.2021.105509.
[38] Sheehan JD, Savage PE. Reaction pathways and kinetics of tryptophan in hot, compressed water. Chem Eng J 2020;390:124600. https://doi.org/10.1016/j.cej.2020.124600.